NASA CONTRACTOR REPORT

NASA CR-1229

BRAYTON-CYCLE TURBOMACHINERY ROLLING-ELEMENT BEARINGS

by R. Cohen, H. Means, and P. Heyl

Prepared by
UNITED AIRCRAFT CORPORATION
East Hartford, Conn.
for Lewis Research Center

NATIONAL AERONAUTICS AND SPACE ADMINISTRATION • WASHINGTON, D. C. • JANUARY 1969

BRAYTON-CYCLE TURBOMACHINERY ROLLING-ELEMENT BEARINGS

By R. Cohen, H. Means, and P. Heyl

Prepared under Contract No. NAS 3-7635 by
UNITED AIRCRAFT CORPORATION
East Hartford, Conn.

for Lewis Research Center

NATIONAL AERONAUTICS AND SPACE ADMINISTRATION

For sale by the Clearinghouse for Federal Scientific and Technical Information
Springfield, Virginia 22151 – CFSTI price $3.00

FOREWORD

This report was prepared by the Pratt and Whitney Aircraft Division of United Aircraft Corporation, East Hartford, Connecticut, to describe work conducted from July 1965 to November 1967 in fulfillment of Contract NAS3-7635, Brayton-Cycle Turbomachinery Roller-Contact Bearings. The report describes the analytical, design, fabrication and test work conducted under the contract.

Technical management was provided by Lloyd Ream of the Lewis Research Center, National Aeronautics and Space Administration. This report was originally used as Pratt & Whitney Report PWA-3277.

ABSTRACT

The National Aeronautics and Space Administration is conducting an evaluation of candidate Brayton-cycle turbomachinery configurations incorporating gas bearings. Pratt and Whitney Aircraft has conducted a development effect on a flight-type rolling element rotor support system to provide a backup to the gas bearing approach. This program included the design of two-shaft Brayton-cycle turbomachinery, the testing of critical rotor support system components and the testing of a pilot lubrication system. As a result of two successful 2500 hour endurance tests, one on a face seal only and the other on a complete pilot lubrication system, it is concluded that a rolling element support system can be developed for missions exceeding one year and the oil contamination level of the Brayton-cycle power system will not exceed one gram.

TABLE OF CONTENTS

TABLE OF CONTENTS (Cont'd)

LIST OF FIGURES

LIST OF FIGURES (Cont'd)

LIST OF FIGURES (Cont'd)

LIST OF FIGURES (Cont'd)

LIST OF FIGURES (Cont'd)

LIST OF TABLES

I. SUMMARY

Pratt & Whitney has conducted the design of an axial-flow turbine-compressor and turboalternator incorporating flight-type oil-lubricated rolling-element bearings as candidate turbomachinery for a Brayton-cycle space powerplant. Tests were conducted on the critical components of the rotor support and lubrication system. These component tests were followed by a pilot system test which included all of the functional components of the lubrication system in a closed-loop demonstration system. As a result of these tests the following was demonstrated.

1) Zero-gravity operating capability of the oil scavenge system,

2) Operation of the lubrication system on argon, krypton, and a mixture of helium-xenon over a wide range of pressure levels,

3) Bearing endurance and oil compatibility for 2500 hours at 50,000 rpm with no measurable wear,

4) Dry-face carbon seals incorporating bellows were operated for 2500 hours at 50,000 rpm with the extremely low gas leakage rate of 2 pounds per year, an oil leakage rate of 11 grams per year, and carbon wear about one-third less than predicted,

5) More than 6,000 hours of satisfactory adsorber gas cleanup performance,

6) Gas cleanup system operation for 2500 hours which limited potential oil contamination of the powerplant to less than one gram per year, and

7) Lubrication system power consumption of 1400 watts in the 50,000 rpm turbine-compressor, and 300 watts in the 12,000 rpm turboalternator.

It is concluded from this engineering program that the Brayton-cycle turbomachinery investigated can be developed with oil-lubricated rolling-element bearing rotor-support systems for extended missions lasting more than a year with no significant oil contamination of the powerplant.

II. INTRODUCTION

The National Aeronautics and Space Administration is considering two types of rotor support systems for the Brayton-cycle space powerplants currently being developed. One rotor support system utilizes gas bearings in which the main cycle gas is used in the bearings. The other support system, the subject of this contract, uses oil-lubricated rolling-element bearings. This latter concept is based upon contemporary technology with the requirement that it be a positive backup to the gas-bearing design.

The majority of existing Brayton-cycle powerplants in use for nonspace applications operate on rolling-element oil-lubricated bearings. The application of Brayton-cycle turbomachinery to space powerplants with rolling-element bearings supporting the rotor, poses several basic technical requirements. These are:

1) The rolling-element bearings must provide a lifetime of at least 10,000 hours with a high degree of reliability and acceptable power losses.

2) The lubrication system and bearing cavities must be sealed with low power consumption and low leakage.

3) The lubricant must be circulated and scavenged in a zero-gravity application.

4) The contamination of the working gas by leakage of the lubricant must be held to acceptable levels.

To evaluate these requirements, an engineering program consisting of component and system design and testing was conducted. The scope of the program included the design and component performance demonstration of rolling-element bearing systems for the turbine-compressor (50,000 rpm) and turboalternator (12,000 rpm) being developed under Contracts NAS3-4179 and NAS3-6013. The components of the rolling-element bearing system are the bearings, seals, lubrication system and gas cleanup system. The work covered four phases:

1) Design of a rolling-element bearing system that retained the components of the turbine-compressor and turboalternator with no alterations in aerodynamic design. The overall design was directed towards the achievement of low power losses, commensurate with high reliability, for the full mission life.

2) Design and fabrication of component test rigs.

3) Performance tests of bearings, seals, scavenge schemes, separators and adsorbers.

4) Completion of 2500 hours of endurance testing on a complete pilot system.

The designs of the gas-bearing turbomachinery developed under Contracts NAS3-4179 and NAS3-6013 that are shown in Figure 1 were modified to accept rolling-element bearing shaft-support systems. The associated gas cleanup and lubricant recirculation systems were also designed. A component analysis and test program was conducted to confirm and expand design information in critical areas. Several experimental rigs were designed, built and operated as a part of the component program. One rig program was designed to investigate the performance of several turbine-compressor seal designs at speeds up to 60,000 rpm. Another rig program was addressed to the lubrication, cooling and power comsumption performance of the turbine-compressor bearing. A third program was directed to the evaluation of lubricant-cooling, circulation and scavenging for use in a zero-gravity environment. A fourth rig effort investigated the practical aspects of separting gas and oil in a shaft-driven separator having high efficiency and low pressure drop. A fifth rig program evaluated several adsorber materials and column designs that would be used to perform the final gas cleanup. The experimental program was concluded by the operation of a pilot system test for 2500 hours. This system test included components which had demonstrated the most promising performance in the individual test rig programs. Also a turbine-compressor seal was operated for 2500 hours to measure gas and oil leakage and seal wear rates. Both of these test programs were completed with very successful and encouraging results.

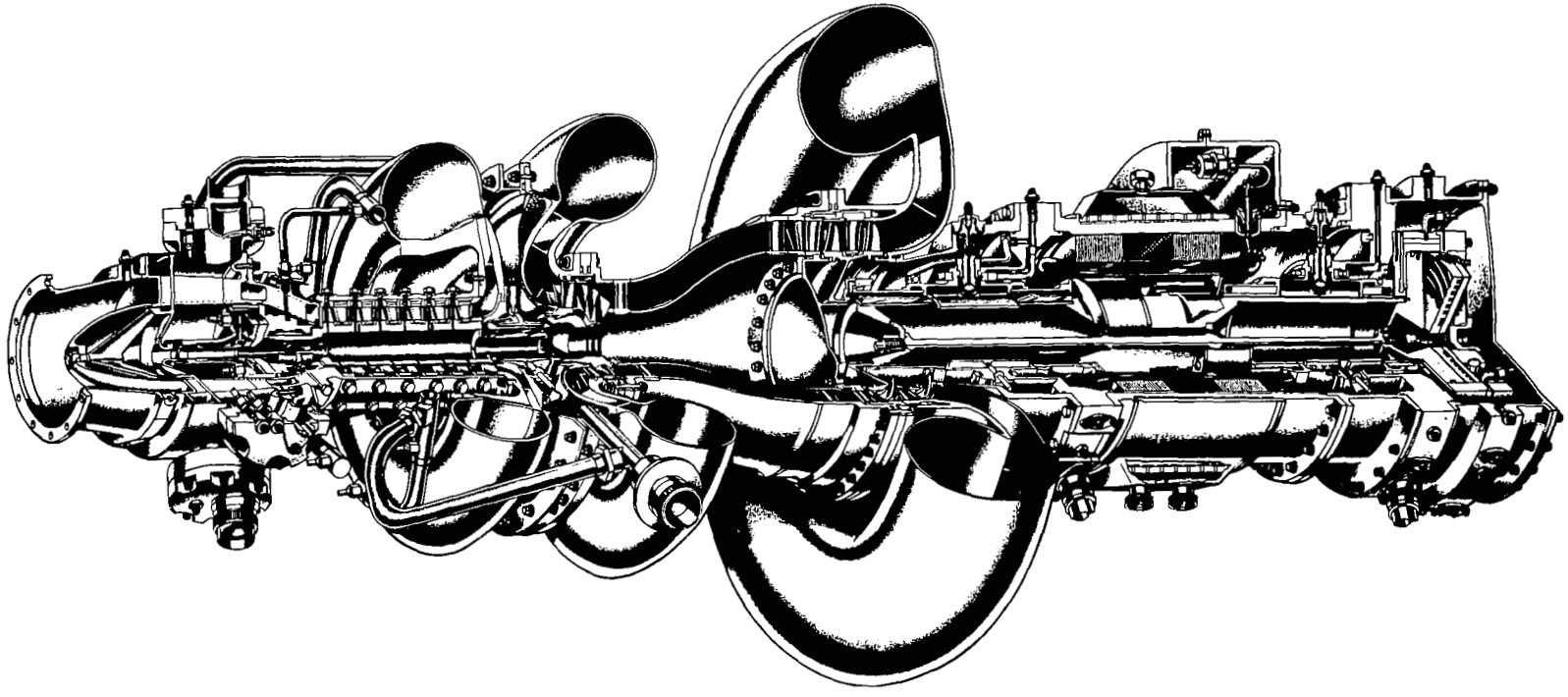

Figure 1 Brayton-Cycle Turbomachinery

III. ROLLING-ELEMENT BEARING LUBRICATION SYSTEM

A. Design

The lubrication system for Brayton-cycle turbomachinery must provide proper lubrication and cooling of the bearings and seals during development testing, prelaunch checkout, and during operation in a gravity-free space environment without contaminating the cycle gas. In addition, these requirements must be achieved with low power consumption. During development testing and prelaunch checkout, the system should be capable of operation either in a horizontal or vertical orientation.

The requirement that the powerplant be able to operate in various orientations in various gravitational fields with low power losses presents a unique requirement for the oil feed and scavenge design. An oil sump and pump system for a conventional engine is dependent upon gravity and ordinarily is not restrained by power consumption limits. In order to circumvent these two restraints, systems which depend upon rotational-centrifugal effects to circulate the oil and argon through the system are utilized. A combination of face and labyrinth seals is used to separate and restrict the leakage of oil into the cycle gas and the leakage of cycle gas into the lubrication system.

A simplified schematic diagram of the lubrication system is presented in Figure 2. Oil and gas leave the separator and enter the bearing compartments in the turboalternator. Most of the oil flows under the bearing inner race and then through the sealplate for cooling while a small amount of oil in the gas flows through the bearing for lubrication. The gas and oil mix at the discharge of the bearing compartments and the mixture flows through the turbine-compressor bearing compartments, performing the same functions of cooling and lubrication. The mixture is then cooled and returned to the separator. A small quantity of gas leaves the separator, passes through an adsorber for further purification, and then is returned to the powerplant cycle as make-up for the cycle gas leaking into the lubrication system through the face seals. An oil scoop is provided in the separator to maintain system inventory by keeping the liquid level in a rotating pool of oil in the bore of the shaft. This scoop is connected to an accumulator. A more complete system schematic is shown in Figure 3.

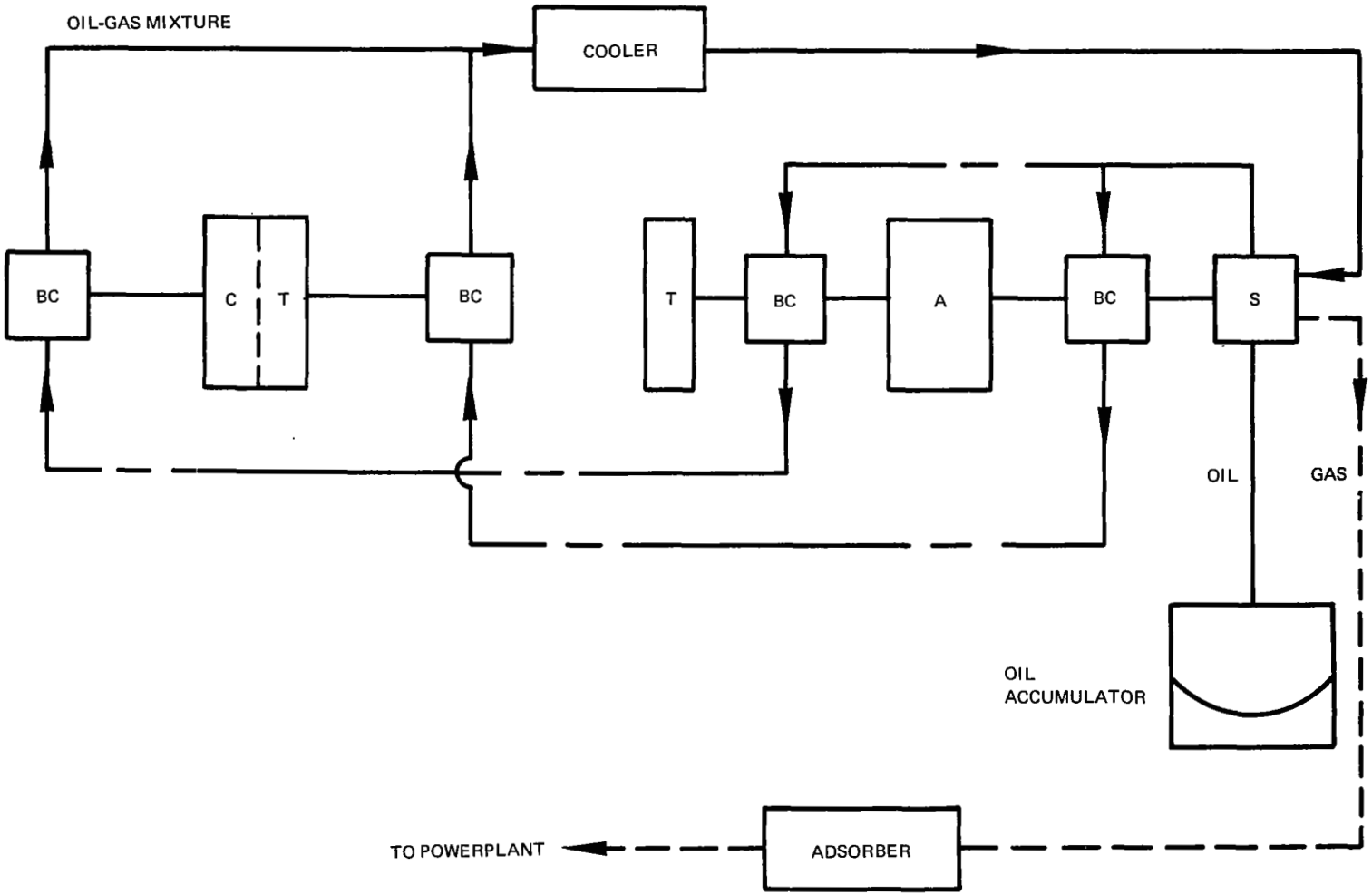

Figure 2 Simplified Lubrication System Schematic M-49741

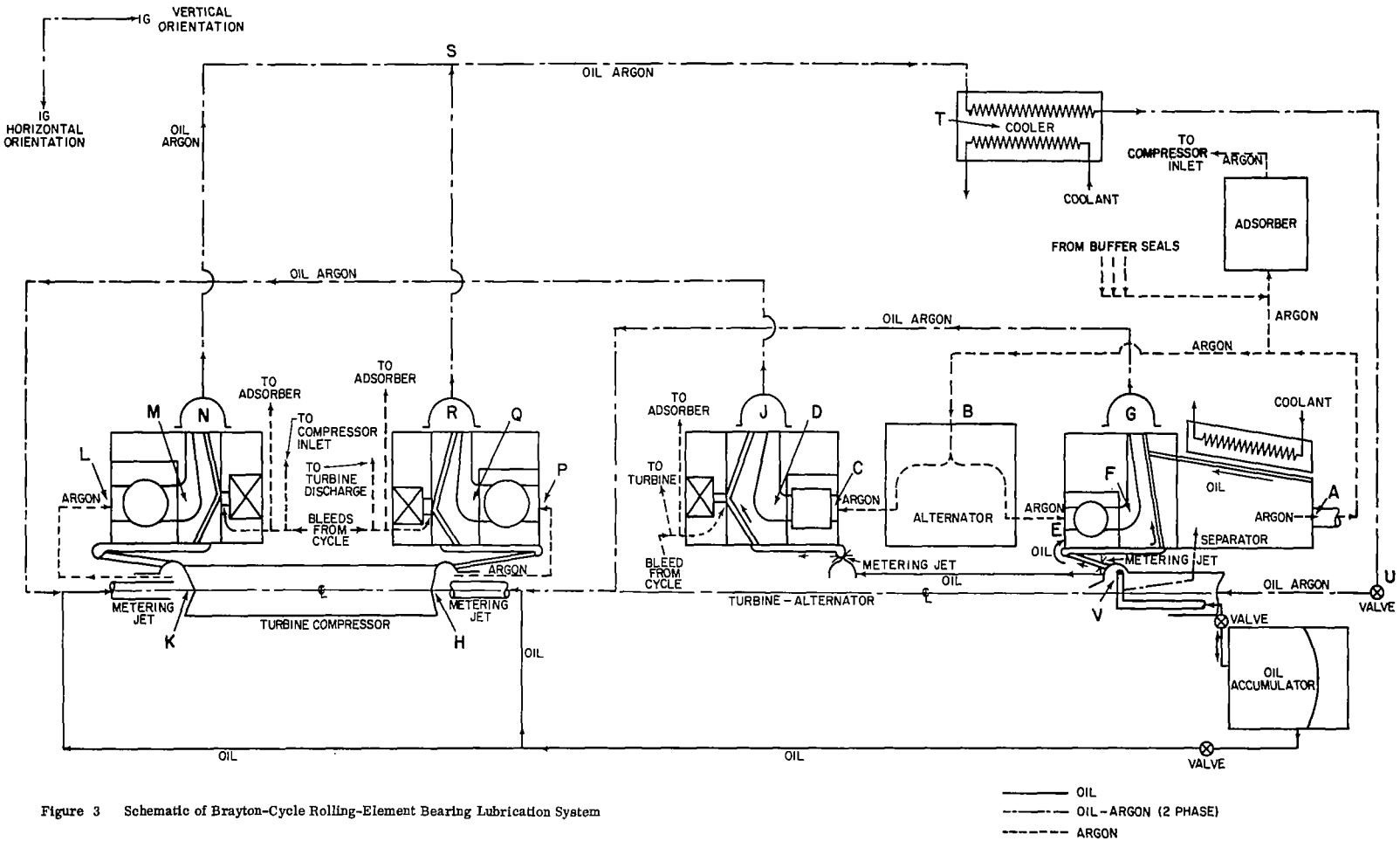

Figure 3 Schematic of Brayton-Cycle Rolling-Element Bearing Lubrication System

The oil cools the bearings by passing through slots in the inner race, and oil of various droplet sizes carried by gas in the bearing compartment provides lubrication. The oil cools the rotating sealplate after leaving the bearing. Two labyrinth seals are provided on the gas side of the face seals, and high-pressure gas is bled from the compressor and fed between these labyrinth seals. Some of this gas leaks back to the main cycle stream and some leaks into the bearing compartment. A small flow of argon is bled from the area just upstream of the face seal to the adsorber. The object of this flow is to carry to the adsorber any oil which weeps past the face seal. The side of the sealplate face adjacent to the bearing shown in Figure 3 includes vanes which form a centrifugal pump to force the argon out of the bearing compartment. The forward bearing compartment of the turbine-compressor is scavenged in a similar manner.

The pressure rise in the argon developed by the sealplate impeller is low. Therefore, the gas and oil system is connected in series so that pumping action of the turbine-compressor sealplate can be added to the turboalternator pressure rise to move the argon through the system. The oil and argon which leave the turboalternator bearing compartments are piped to the inside of the turbine-compressor shaft. The centrifugal field within the turbine-compressor shaft separates most of the oil from the argon and the oil passes under the bearing and through the sealplate as in the turboalternator. The argon flows out of the end of the shaft carrying some oil mist with it and then through the bearing to the sealplate impeller. The oil and argon are pumped out of the bearing compartment as before.

In the process of cooling the bearings and seals, the oil and argon in the bearing compartment are heated to about 375°F. As shown in Figure 3, this mixture passes through a liquid-cooled heat exchanger and is returned to the inside of the turboalternator shaft and the centrifugal separator. At this point in the lubrication system the centrifugal separator, mounted on the turboalternator shaft as shown in Figure 4, centrifuges oil from the oil-argon mixture to the outer periphery of the rotating gauze-like metallic mesh where the separated oil flows along the tapered housing to rejoin the turboalternator oil flow. The metallic mesh permits gas to pass but the oil droplets contact the mesh and acquire rotational velocity. Since the oil particles are denser than the gas they are centrifuged to the outer wall. The separator is cooled by a static cooling jacket to reduce the amount of oil vapor leaving the separator. The cool argon containing a small amount of oil passes through the adsorber column where oil retained in the argon is adsorbed and the cleaned argon is returned to the cycle. Most of the argon is recirculated through the lubrication system and the argon re-enters the system through the alternator cavity. Labyrinth seals separate the bearing compartments from the alternator, and the argon flowing through these seals limits the amount of oil that can flow into the alternator cavity.

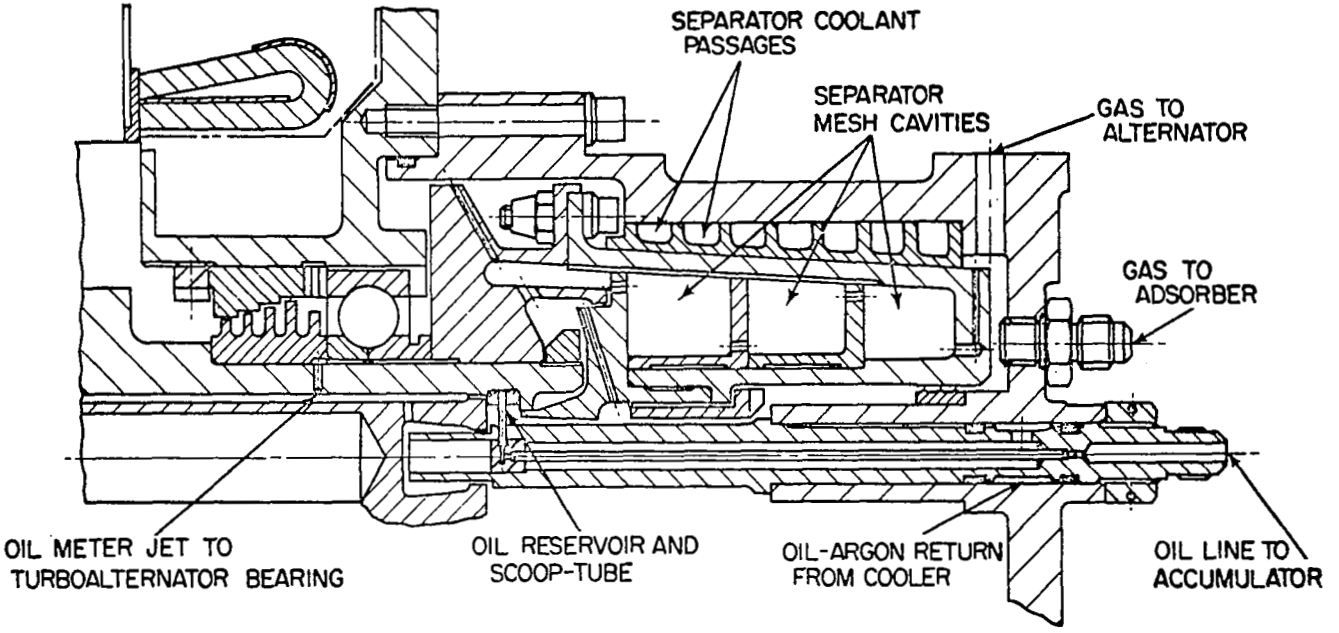

Figure 4 Arrangement of Centrifugal Separator and Oil Scoop

Oil is supplied from an accumulator which receives oil from a rotating pool of oil inside the turboalternator shaft. The oil enters the accumulator through a tube which forms a scoop in the rotating reservoir. The configuration can be visualized more readily by reference to Figure 4 which shows the mechanical arrangement of the scoop tube in relation to the turboalternator and centrifugal separator. This type of stationary scoop develops a head when totally immersed in the pool of oil rotating at a linear speed of 50 feet per second. When the scoop opening is only partially immersed in oil, the head is lost. Therefore, if the reservoir contains too little oil and the oil level is below the scoop, oil flows from the pressurized accumulator into the system. If the oil level rises above the scoop, the pumping action forces oil back into the reservoir, and the result is a rotating reservoir with essentially a constant inventory. This system permits a range of acceptable accumulator oil pressures for proper operation. Since the turboalternator speed is maintained at 12,000 rpm and since the oil level in the rotating reservoir is fixed, a given head is maintained at the bottom of the reservoir. Holes which meter oil flow to the turboalternator bearings are located at the bottom of the reservoir.

The total power loss predicted for the lubrication system is 1480 watts. A breakdown of these losses is presented in Table 1.

TABLE I

Power Losses In Brayton-Cycle Rolling-Element Bearing Lubrication System

Type of Loss and Location	Oil Flow, lb/hr	Argon Flow, lb/hr	Power Loss, watts	
Turbine-Compressor Compartment 1				
bearing heat generation	60	-	202.1	
seal heating	60	-	200.0	
oil pumping	60	-	147.5	
argon pumping	-	4	9.8	
total				559.4
Turbine-Compressor Compartment 2				
bearing heat generation	80	-	203.5	
seal heating	80	-	200.0	
oil pumping	80	-	196.8	
argon pumping	-	4	9.8	
total				610.1

Turboalternator Compartment 1

bearing heat generation	-	-	73.0	
seal heating	-	-	55.8	
oil pumping	10	-	6.2	
argon pumping	-	4	2.4	
total				137.4

Turboalternator Compartment 2

bearing heat generation	15	-	108.0	
oil pumping	15	-	10.3	
argon pumping	-	4	2.7	
separator drag	-	-	7.1	
oil probe drag	-	-	29.0	
separator pumping	-	8	16.4	
total				173.5
		Total Losses		1480.4

The buffer zones require argon bleeds through labyrinth seals for proper pressurization to prevent oil leakage. Also, there will be some gas leakage through the face seals. The summary of the predicted bleed and leakage flows is presented in Table 2.

The lubrication system shown in Figure 2 is a recirculating system with a number of single-phase and two-phase (oil and argon) flow passages. The pressure drop as a function of argon flow for each section of the system is presented in Figures 5 through 14 and the letters identifying the various locations in the circuit are shown in Figure 3. The pressure drop from the front bearing compartment in the turboalternator to the front bearing area in the turbine-compressor, Stations J to K on Figure 3, is presented as 3 curves in Figure 9. The argon-oil mixture must rise 33 inches vertically from J to K when the power system is mounted vertically in a 1 g field. The pressure loss when operating vertically consists of the sum of the basic friction loss for flow in a horizontal pipe and the equivalent head loss. In horizontal operation on the ground or in a zero-gravity environment, the pressure loss will correspond to the friction pressure loss of Figure 9 which was determined by the Lockhart-Martinelli correlation[1]. In vertical operation, the head loss based on an equiv-

[1] See Page 273 for numbered list of references

TABLE 2

Gas Leakage and Bleed Flows in
Brayton-Cycle Rolling-Element Bearing Lubrication System

Seal Location	Type	$P_{up-stream}$ psia	$P_{down-stream}$ psia	Temp., °F	Leakage, lb/hr	Per Cent of Cycle Flow
Turbine-Compressor						
front compressor seal	labyrinth	11.0	5.5	340	18.2	0.843
rear compressor front turbine	labyrinth	12.83	9.26	340	20.7	0.958
rear turbine seal	labyrinth	11.0	8.29	340	13.3	0.616
No. 1 bearing seal	carbon	9.90	-	340	0.31	0.0144
No. 2 bearing seal	carbon	10.0	-	340	0.313	0.0145
No. 1 compart. capillary bleed	capillary		6.0		1.4	0.065
No. 2 compart. capillary bleed	capillary		6.0		1.4	0.065
Turboalternator						
rear turbine seal	labyrinth	11.0	6.73	340	25.8	1.19
bearing seal	carbon	11.0	-	340	0.62	0.0287
No. 1 compart. capillary bleed	capillary	11.0	6.0	340	1.4	0.185
metered flow to front of turbine	capillary	11.0	-	340	4.00	0.185
Total					87.443	4.0446

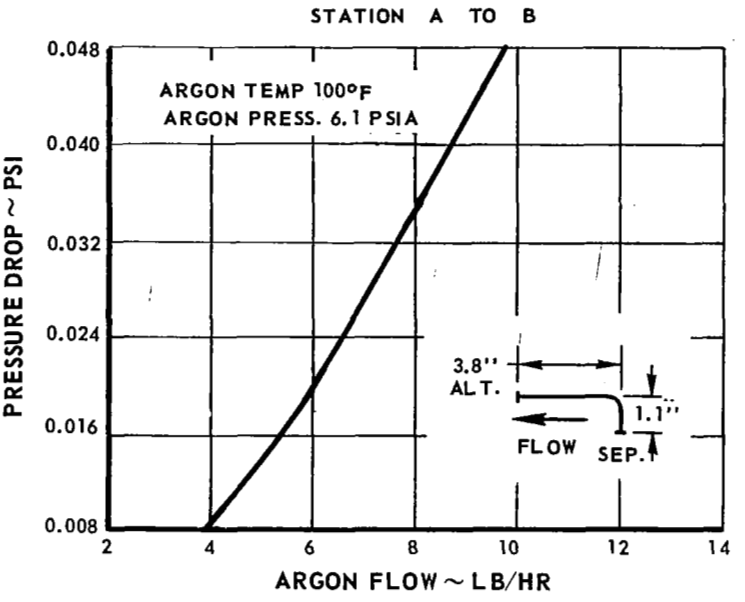

Figure 5 Pressure Drop for Tubing from Separator to Alternator

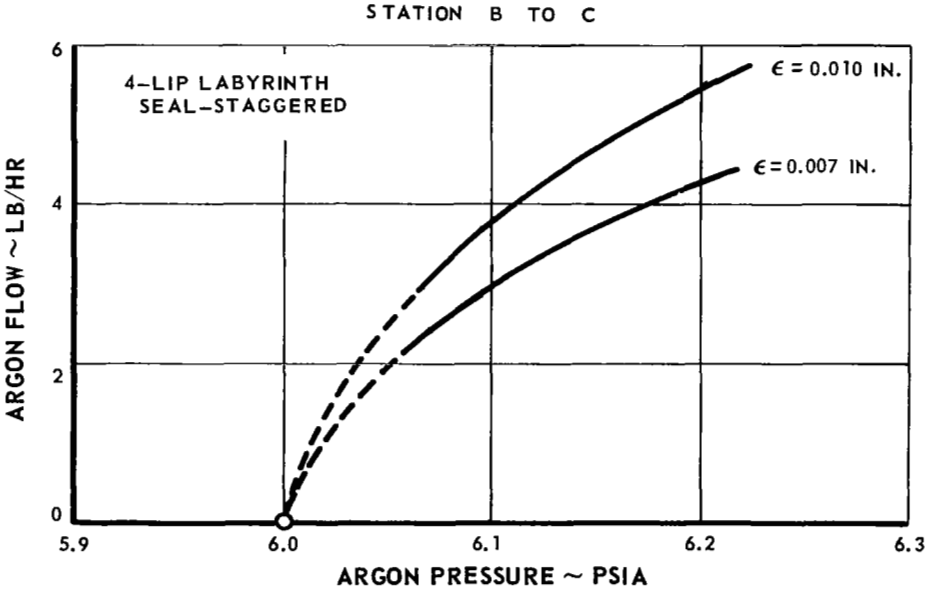

Figure 6 Turboalternator Labyrinth Seal Flow. Alternator Cavity Purge

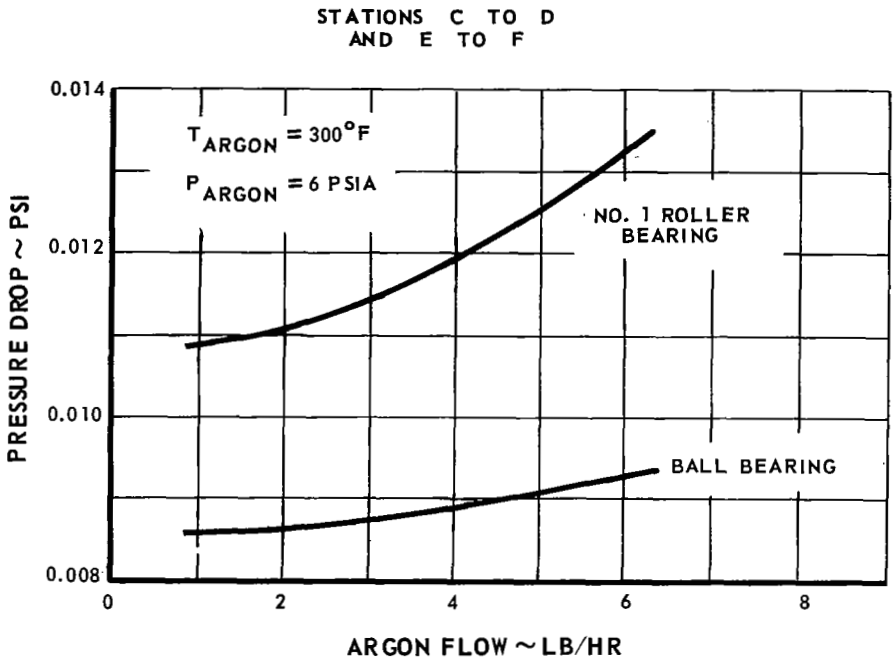

Figure 7 Turboalternator Bearing Pressure Drop vs Gas Flow Rate

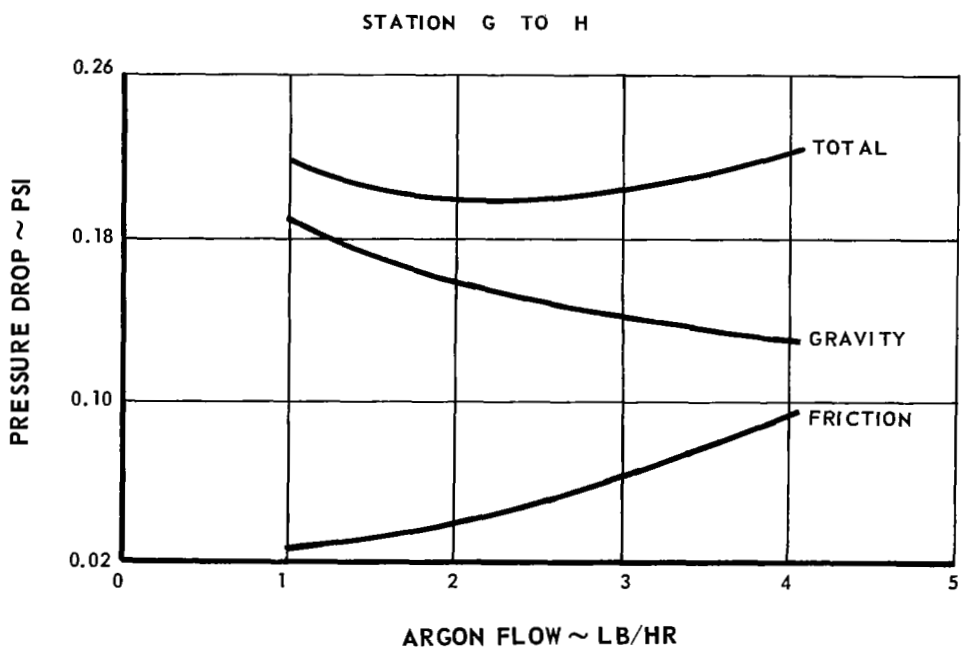

Figure 8 Pressure Drop for Tubing from Turboalternator No. 2 Area to Turbine-Compressor No. 2 Area

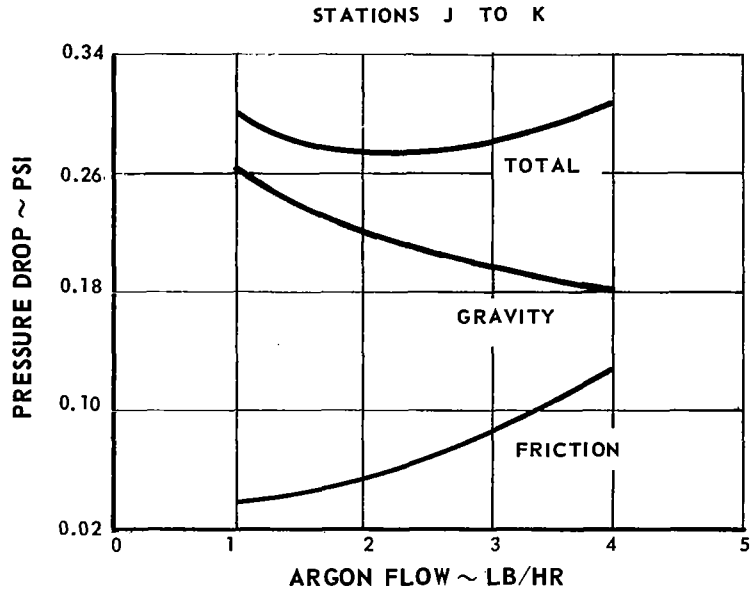

Figure 9 Pressure Drop for Tubing from Turboalternator No. 1 Area to Turbine-Compressor No. 1 Area

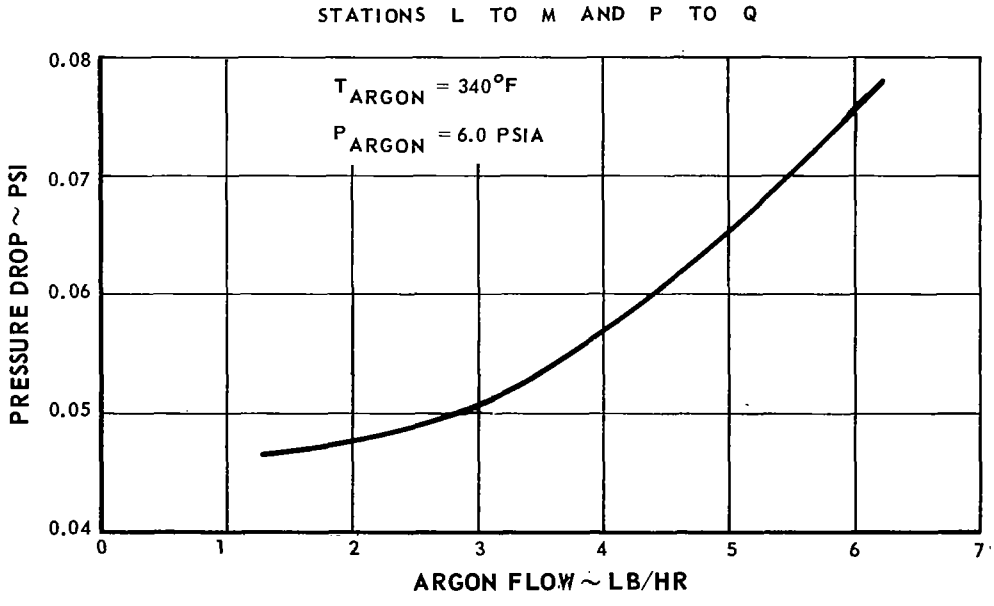

Figure 10 Turbine-Compressor Bearing Pressure Drop vs Gas Flow

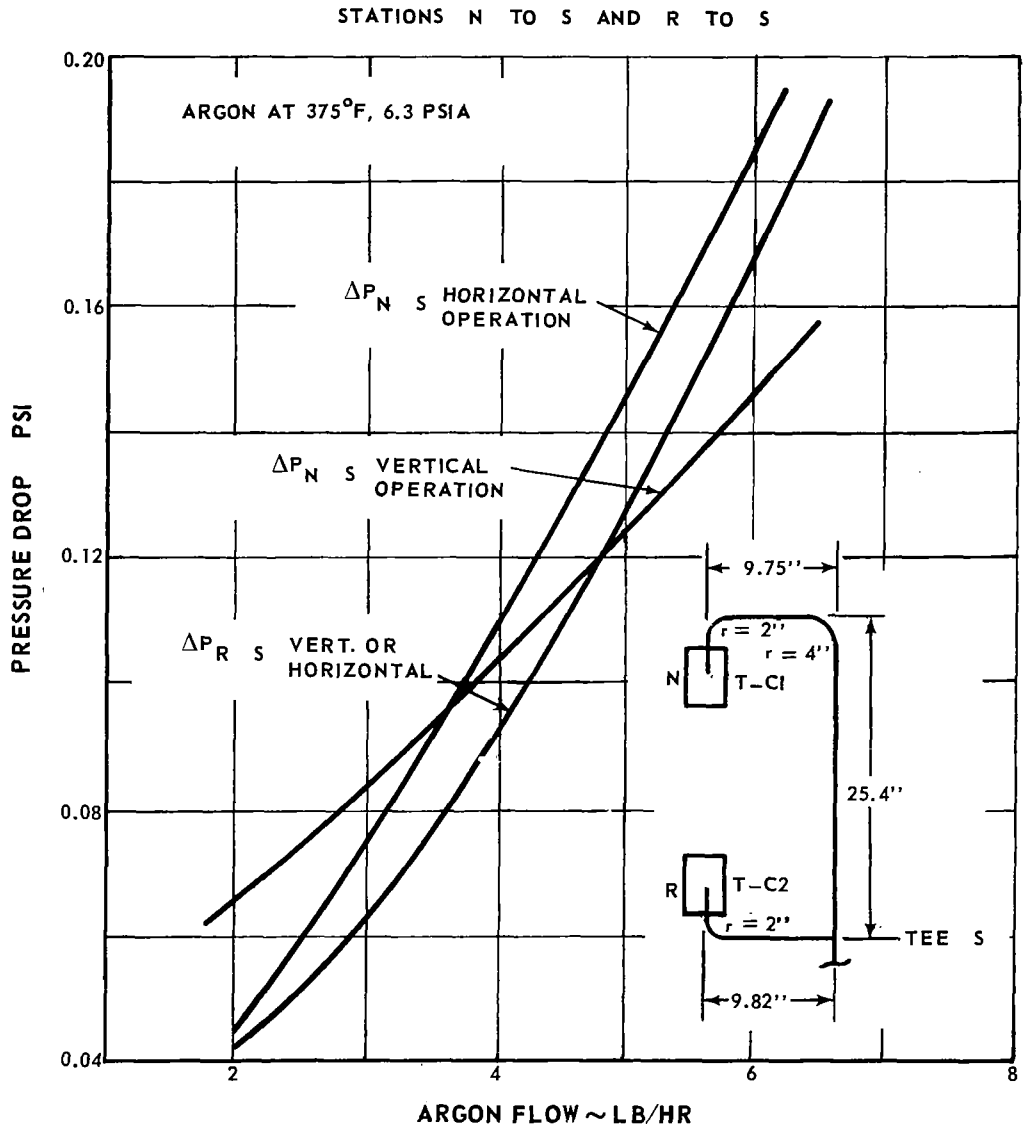

Figure 11 Pressure Drop for Tubing from Turbine-Compressor to Tee Upstream of Cooler

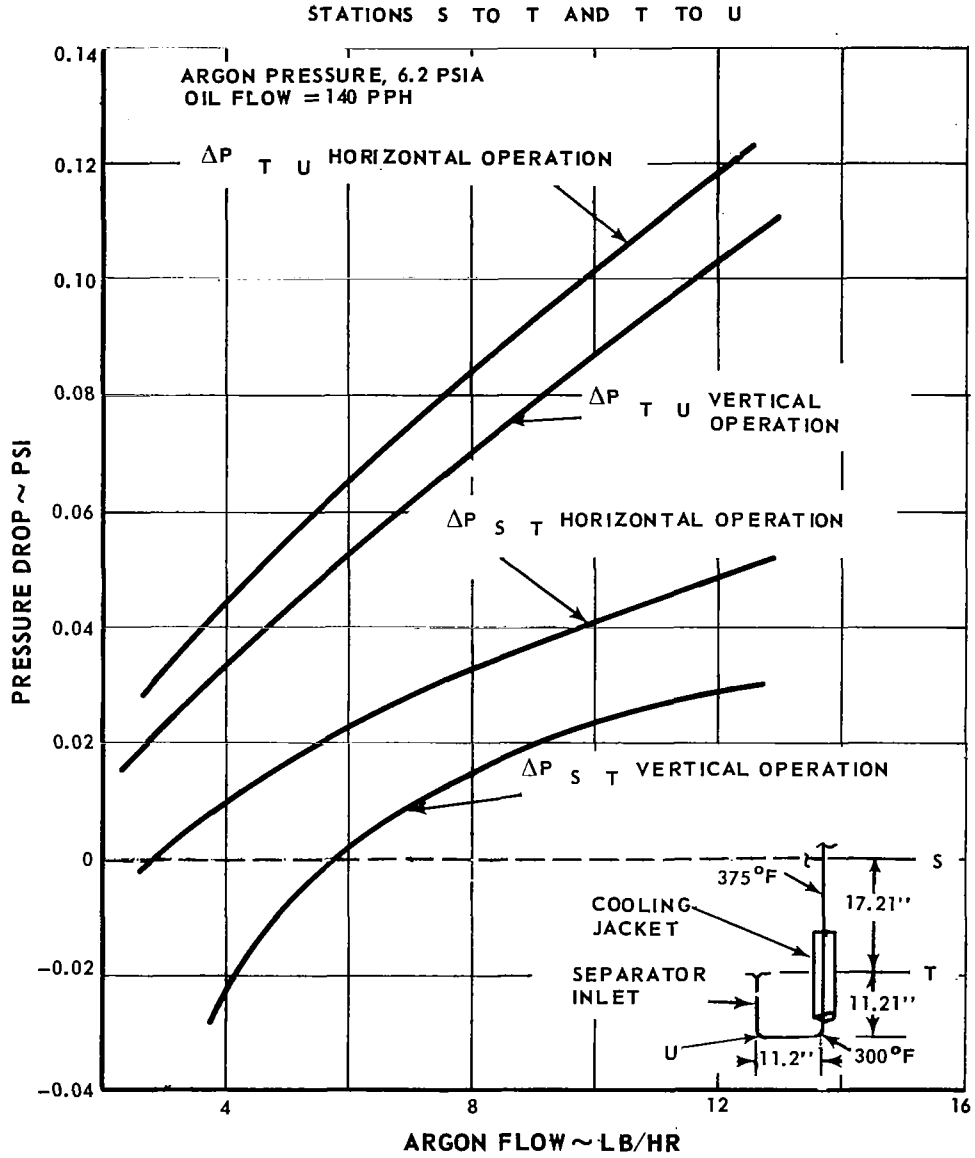

Figure 12 Pressure Drop for Tubing from Tee to Mid-Cooler, and Mid-Cooler to Separator Riser

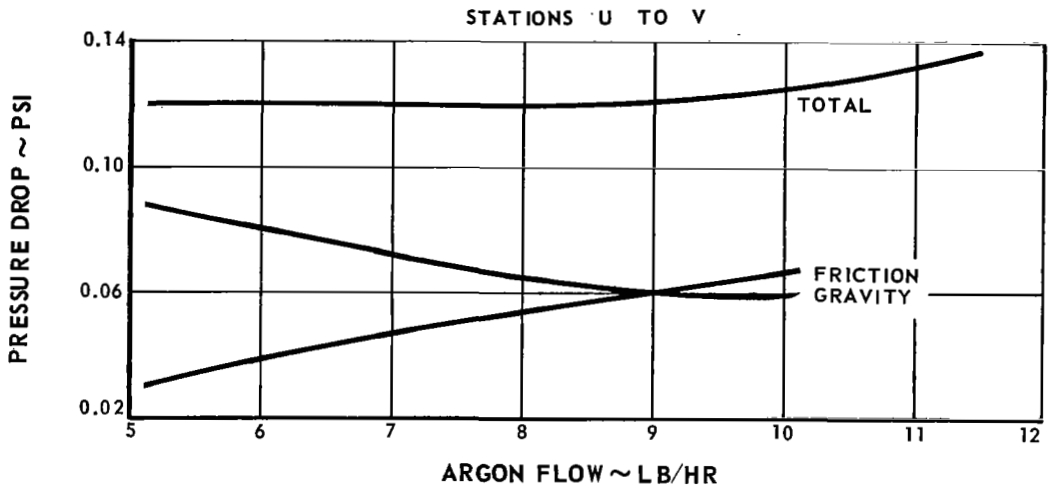

Figure 13 Vertical Lift into Separator

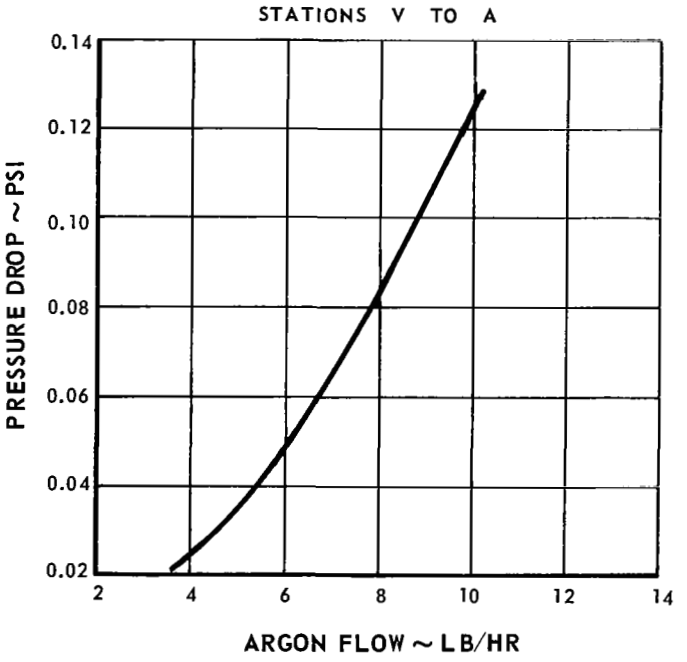

Figure 14 Pressure Drop in Separator

alent fluid density is added to produce the total pressure loss in Figure 9. The flow from the turboalternator rear bearing area to the rear compartment in the turbine-compressor, Stations G to H, involves a vertical rise of about 22 inches and the pressure loss again is dependent upon orientation, as indicated in Figure 8. Another vertical two-phase upward flow occurs in the return line from the bottom of the turboalternator to the separator. A vertical rise of 11.2 inches is involved. The pressure loss for this section, Stations U to V, is presented in Figure 13 in a manner similar to Figure 9.

The system also includes two-phase flow in the downward direction when the powerplant is oriented vertically. This flow passes through an oil cooler which consists of a single-jacketed pipe with liquid coolant circulated in the jacket. The estimated pressure losses for both vertical and horizontal operation for this return of the two-phase flow are presented in Figures 11 and 12.

The scavenge pumps located on the turbine-compressor shaft (integral with the sealplates) have a tip velocity of about 460 feet/second. Assuming the oil has no influence on the pump performance, the static pressure rise across the impeller is about 0.46 psi. The losses in the exit volute and diffuser could be in the range of 0.34 to 0.56 psi. Therefore, the conservative assumption was made that the kinetic energy at the discharge of the impeller is lost. The scavenge pumps in the turboalternator were evaluated in a similar manner. The separator contains a small impeller capable of providing some further pressure rise which just about balances the pressure losses in the separator. The estimated sum of the pressure increases provided by the scavenge pumps is 0.66 psi. Matching the various pressure losses in the system with this driving pressure indicates a system flow of 8.55 pounds per hour of argon into the separator area for operation in the horizontal or zero-gravity environment. In the vertical direction, the corresponding argon flow is 6.10 pounds per hour. A summary of the zero-gravity or horizontal operating conditions estimated for the lubrication system in Figure 3 is presented in Table 3. The corresponding conditions for vertical operation on the ground with the compressor end up are presented in Table 4.

TABLE 3

Pressure Losses for
Horizontal or Zero-Gravity Operation

Station on Figure 2	Description	Oil Flow, lb/hr	Argon Flow lb/hr	Press. Loss, psi
A-B	line from separator to alternator	-	6.75	0.024
B-C	labyrinth seal	-	3.17	0.073
C-D	roller bearing	-	3.17	0.090
J-K	line from turboalternator to turbine-compressor	10	3.77	0.116
L-M	ball bearing	10	3.77	0.055
N-S	scavenge line	60	4.07	0.111
B-E	labyrinth seal	-	3.58	0.090
E-F	ball bearing	-	3.58	0.009
G-H	line from turboalternator to turbine-compressor	15	4.18	0.102
P-Q	ball bearing	15	4.18	0.058
R-S	scavenge line	80	4.48	0.109
S-T	line to cooler	140	8.55	0.035
T-U	line from cooler	140	8.55	0.089
U-V	scavenge return	140	8.55	0.058
V-A	separator	4	8.55	0.094

TABLE 4

Pressure Losses for
Vertical Operation

Station on Figure 2	Description	Oil Flow, lb/hr	Argon Flow lb/hr	Press. Loss, psi
A-B	line from separator to alternator	-	4.30	0.009
B-C	labyrinth seal	-	1.40	0.020
C-D	roller bearing	-	1.40	0.011
J-K	line from turboalternator to turbine-compressor	10	2.00	0.273
L-M	ball bearing	10	2.00	0.048
N-S	scavenge line	60	2.30	0.072
B-E	labyrinth seal	-	2.90	0.062
E-F	ball bearing	-	2.90	0.009
G-H	line from turboalternator to turbine-compressor	15	3.50	0.214
P-Q	ball bearing	15	3.50	0.054
R-S	scavenge line	80	3.80	0.086
S-T	line to cooler	140	6.10	0.002
T-U	line from cooler	140	6.10	0.053
U-V	scavenge return	140	6.10	0.223
V-A	separator	2	6.10	0.050

An examination of the two-phase flow conditions indicates that annular flow can be expected when the system is operating horizontally or in zero gravity. Ovid Baker [2] has developed a correlation of various two-phase flow phenomena in terms of a liquid and a gas flow parameter for flow in horizontal pipes. This correlation is presented in Figure 15 with the different flow regimes marked. Actually, the demarcation between the flow regimes is not sharp, but rather the lines in Figure 15 represent transition regions. The flow conditions for the various two-phase sections in the lubrication system for horizontal operation are included in Figure 15. These points all fall in the annular flow regimes although some are close to slug flow (the line from the front turboalternator cavity to the front turbine-compressor area and the front turbine-compressor scavenge line).

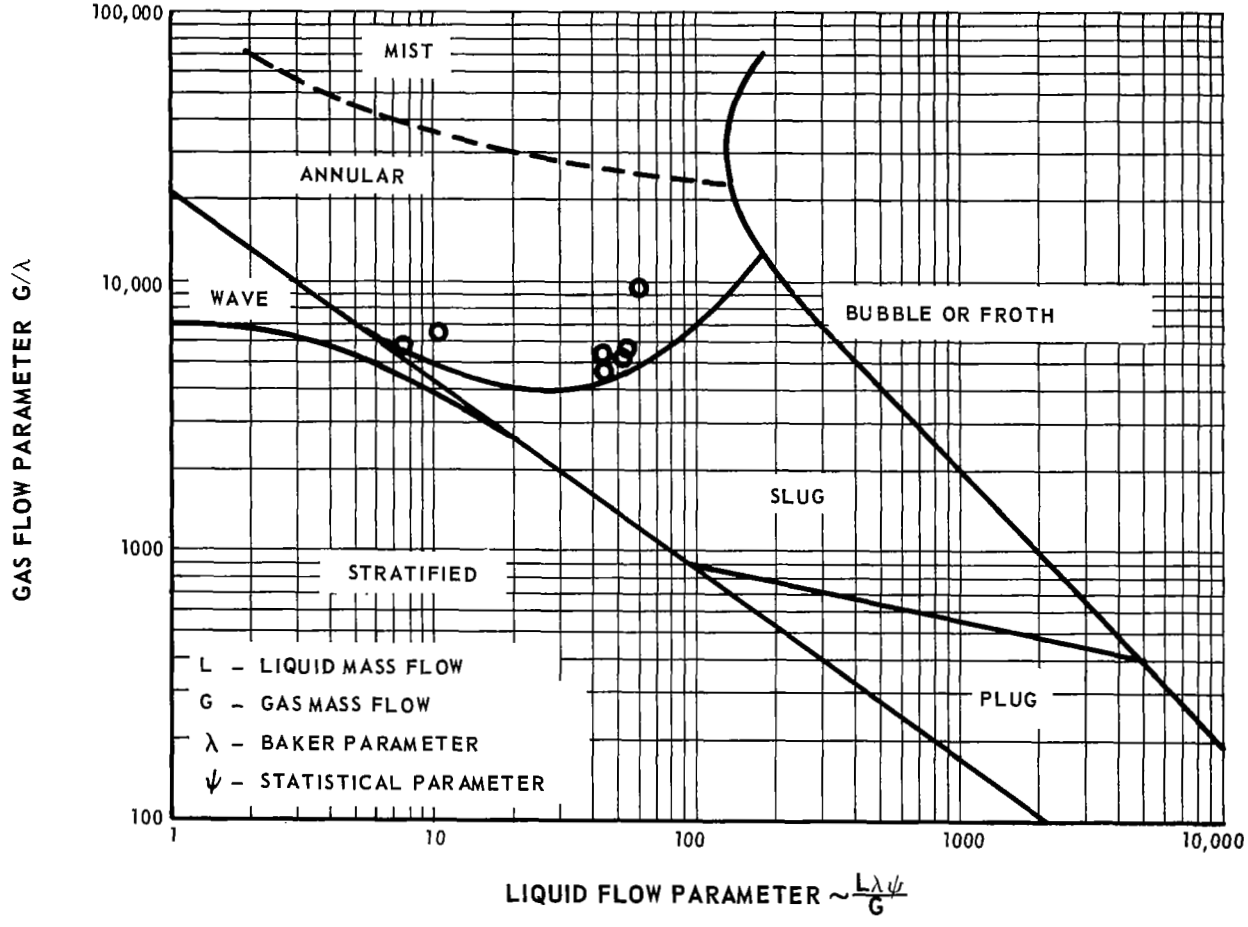

Figure 15 Flow Regime Chart for Horizontal Operation

Griffith and Wallis[3] have developed a two-phase flow regime correlation for vertical operation based on the limited vertical flow data available. This correlation is presented in Figure 16 and the three major vertical flows in the lubrication system are included in this plot. Figure 16 indicates that the vertical flows are all well within the annular or mist flow regime. There is some

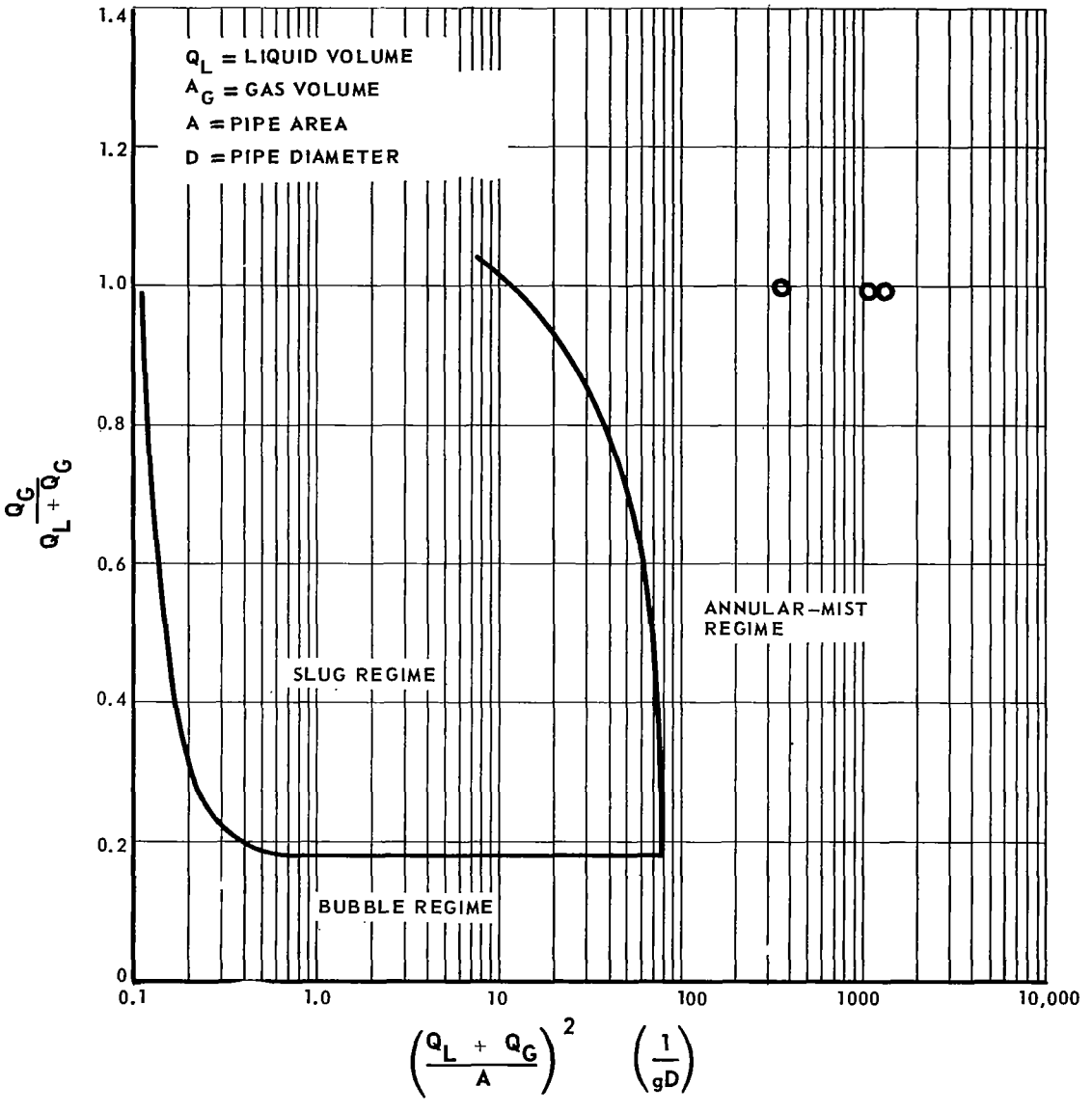

Figure 16 Flow Regime Chart for Vertical Operation

question about this result. The Baker correlation is for horizontal flow only, but if these vertical flow conditions were placed on the Baker correlation they would fall in the slug-flow regime. Two-phase flow is not a well-defined art and evidently requires experimental verification. References 4 through 17 give further background of two-phase flow phenomena.

If higher argon flows were used in the system, all of the two-phase flows, both vertical and horizontal, could fall in the annular regime on the Baker correlation. In order to achieve these higher flows higher pressure rise in the scavenge pumps would be required. Figure 17 presents the overall pressure

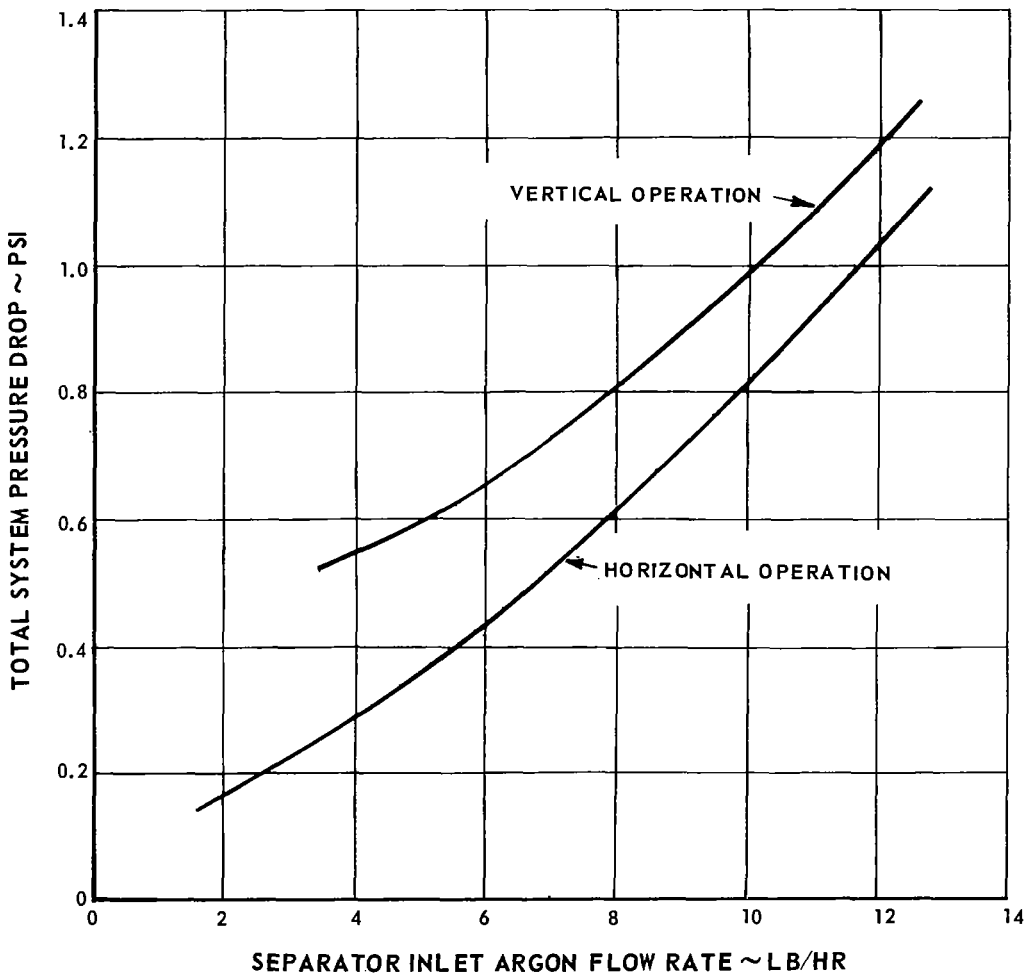

Figure 17 System Pressure Drop and Flow Characteristics

losses which must be matched by the scavenge pump pressure as a function of argon flow. Actually, the pressure rise in the pumps as designed is difficult to establish. The assumption was made that the kinetic energy added to the oil was lost and made no contribution to the pressure rise. The kinetic energy added to the oil in the scavenge pumps is many times the energy added to the argon, as indicated in Table 1. If it is a conservative assumption that the energy in the oil is lost, a higher pressure rise may be achieved. Therefore, the lubrication system may operate with increased margin from slug flow over the situation presented in Figure 15.

One alternate approach is to use a scavenge pump designed to utilize the kinetic energy in the oil rather than in the argon. This kinetic energy is 5 to 20 times that of the argon, hence significant improvements in pressure rise may be possible. Since the oil is rotated in the various grooves for cooling, no additional power loss is imposed on the system when the kinetic energy of the oil is used for pumping.

An alternate scavenge pump design was considered, based on the jet pump principle where the oil is the energizing fluid and the argon is the medium being pumped, see Figure 18. The conventional configuration of a single jet in a circular pipe is not practical for this machinery. The primary jet is replaced by a sheet of oil discharged radially from a rotating impeller. This stream of oil enters a narrow annular passage which serves as the throat of the pump. Since the passage is radial it also serves as a diffuser. The high velocity oil drags argon from the surrounding cavity into the passage, where the two fluids mix and exchange energy. This annular form of the jet pump has the inherent advantage of providing a large interface area between the primary and secondary fluids in a short throat section. The performance potential of the annular oil jet pump is very high with a pressure rise of between 1 and 5 psi, depending primarily on the width of the annular passage. Figure 19 presents the ideal pressure rise as a function of throat width. Pump performance as a function of argon flow is presented in Figures 20, 21, and 22 for various throat widths. Since the oil sheet must enter the annular passage without hitting the walls of the passage to realize proper fluid mixing, the performance is limited by the annular passage size that can be used within the limits of the mechanical arrangement. In the turbine-compressor scavenge pump a passage width between 0.045 and 0.090 inch appears practical.

If the annular jet pump were to perform as predicted in Figure 22 with a passage width of 0.090 inch (a conservative value) in the turbine-compressor, the pump pressure rise would be over 1.0 psi, providing a system pressure rise of about 1.2 psi. In the horizontal or zero-gravity environment, the argon flow

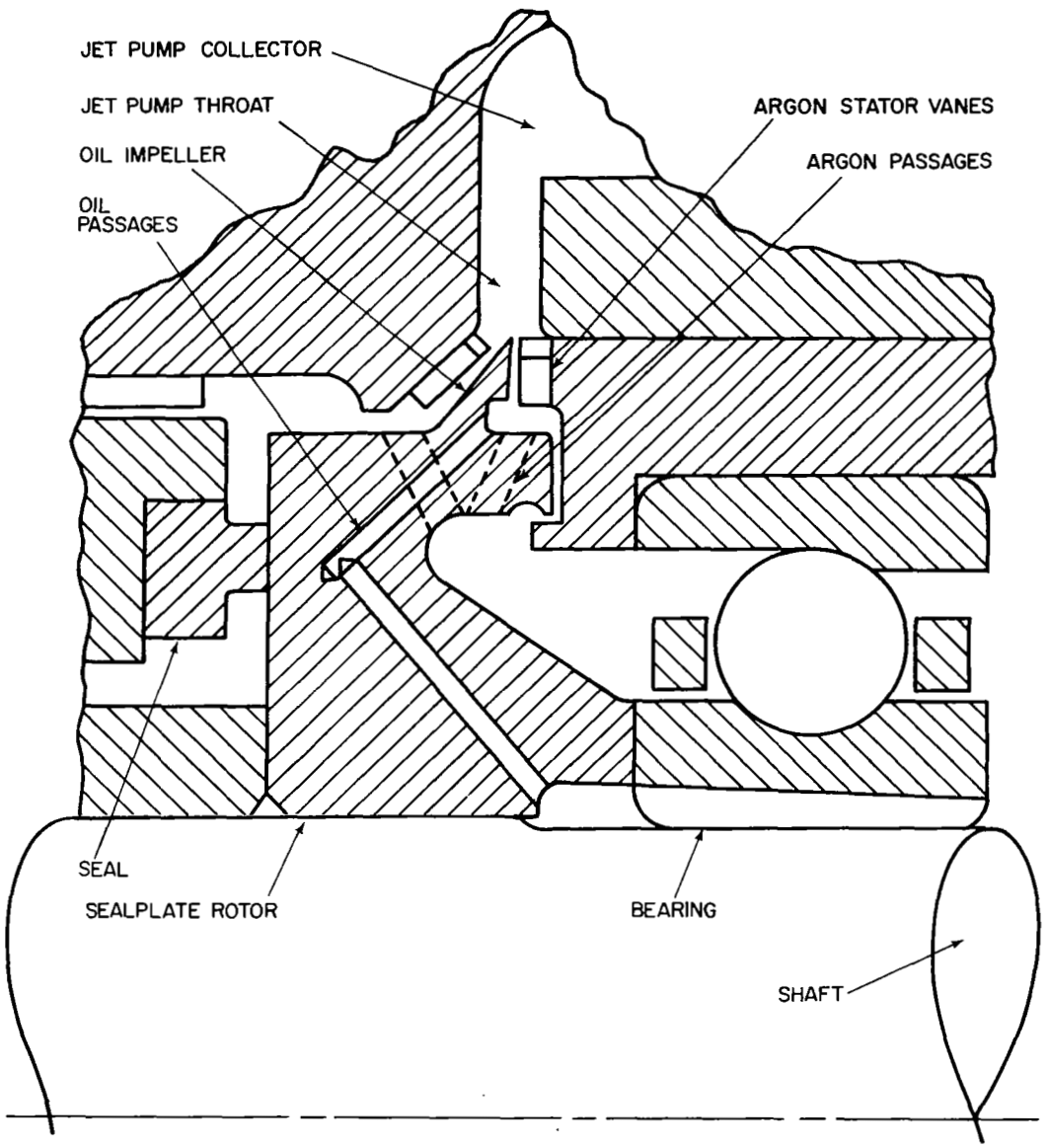

Figure 18 Annular Jet Scavenge System

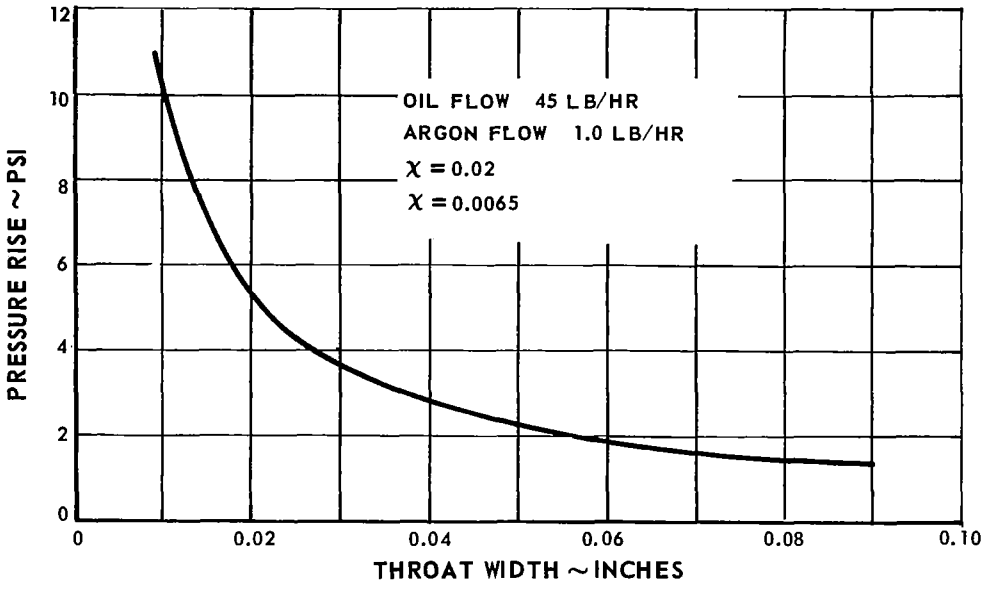

Figure 19 Annular Jet Scavenge Pump for Turbine-Compressor. Effect of Throat Width on Pressure Rise

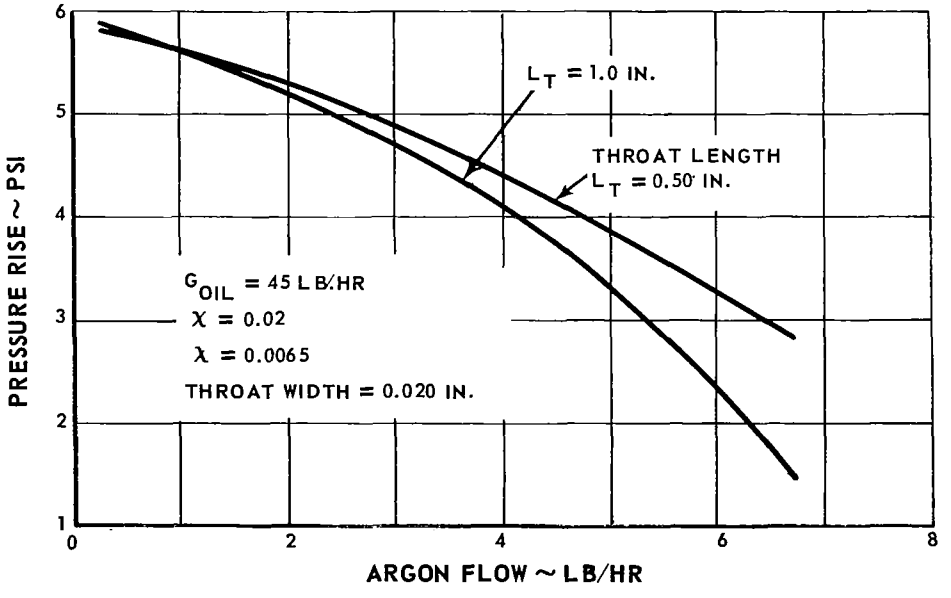

Figure 20 Pressure-Flow Characteristics of Annular Jet Scavenge Pump for Turbine-Compressor

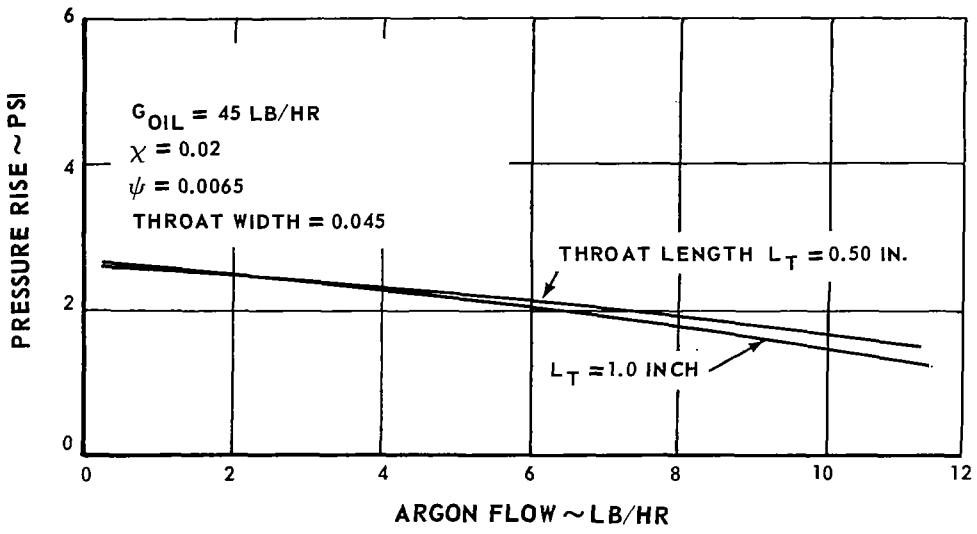

Figure 21 Pressure-Flow Characteristics of Annular Jet Scavenge Pump for Turbine-Compressor

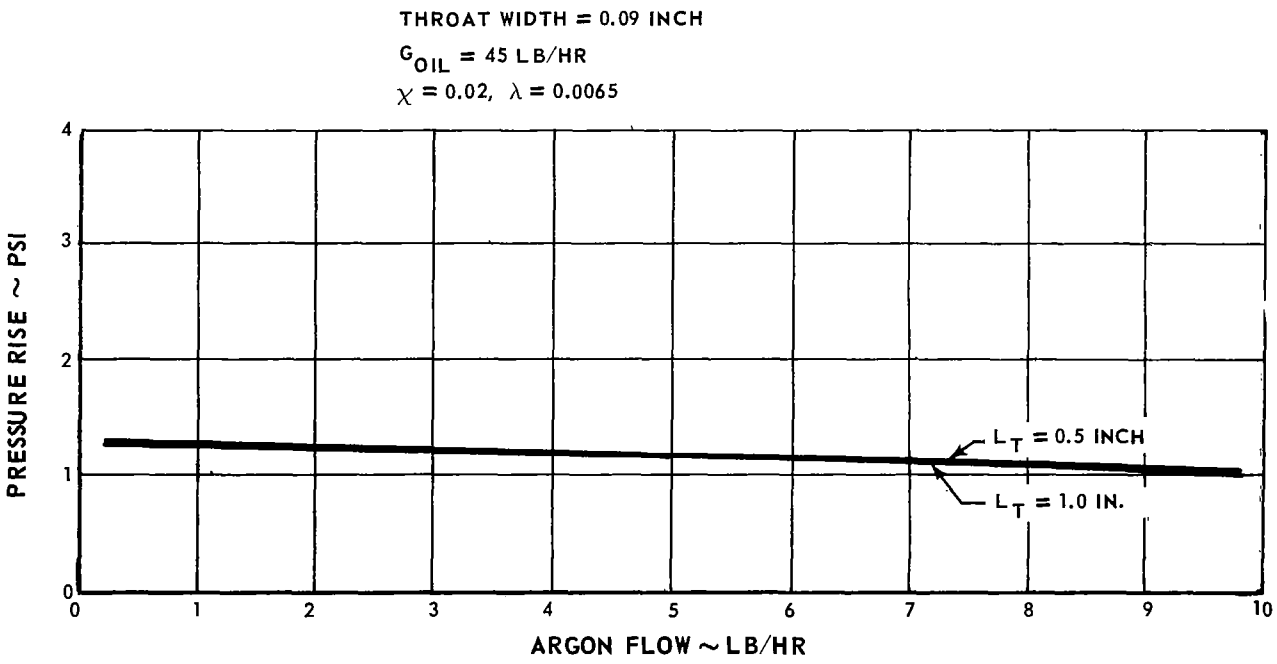

Figure 22 Pressure-Flow Characteristics of Annular Jet Scavenge Pump for Turbine-Compressor

into the separator area would be 12.9 pounds per hour. In the vertical position the corresponding flow would be about 12.1 pounds per hour. A summary of the operating conditions in the horizontal case is listed in Table 5 and the vertical operating conditions are presented in Table 6. The two-phase flow conditions for the improved scavenge pump system are in the annular regime as shown on the Baker correlation in Figure 23 and the Griffith and Wallis correlation in Figure 24. Actually, when the Baker correlation for horizontal flow is applied to vertical operation, annular flows are also indicated.

Another method of utilizing the kinetic energy imported to the oil is to scoop the oil from a rotating pool. High oil pressures can be developed in this manner, but generally at some sacrifice in losses. Such an alternate is presented schematically in Figure 25. In this case, the only two-phase vertical rise occurs from Stations U to V in Figure 25, the return line to the separator area. All of the oil returning from the turbine-compressor passes through the

TABLE 5

Pressure Losses with Oil Jet Scavenge Pumps in Turbine-Compressor Horizontal or Zero-Gravity Operation

Station on Figure 3	Description	Oil Flow, lb/hr	Argon Flow lb/hr	Press. Loss, psi
A-B	line from separator to alternator	-	11.1	0.066
B-C	labyrinth seal	-	5.3	0.186
C-D	roller bearing	-	5.3	0.013
J-K	line from turboalternator to turbine-compressor	10	5.9	0.230
L-M	ball bearing	10	5.9	0.075
N-S	scavenge line	60	6.2	0.194
B-E	labyrinth seal	-	5.8	0.226
E-F	ball bearing	-	5.8	0.009
G-H	line from turboalternator to turbine-compressor	15	6.4	0.150
P-Q	ball bearing	15	6.4	0.080
R-S	scavenge line	80	6.7	0.200
S-T	line to cooler	140	12.9	0.051
T-U	line from cooler	140	12.9	0.126
U-V	scavenge return	140	12.9	0.070
V-A	separator	2	12.9	0.220

TABLE 6

Pressure Losses with Oil Jet Scavenge Pumps in Turbine-Compressor Vertical Operation

Station on Figure 3	Description	Oil Flow, lb/hr	Argon Flow lb/hr	Press. Loss, psi
A-B	line from separator to alternator	-	10.3	0.056
B-C	labyrinth seal	-	4.8	0.152
C-D	roller bearing	-	4.8	0.012
J-K	line from turboalternator to turbine-compressor	10	5.4	0.350
L-M	ball bearing	10	5.4	0.069
N-S	scavenge line	60	5.7	0.142
B-E	labyrinth seal	-	5.5	0.200
E-F	ball bearing	-	5.5	0.009
G-H	line from turboalternator to turbine-compressor	15	6.1	0.280
P-Q	ball bearing	15	6.1	0.076
R-S	scavenge line	80	6.4	0.187
S-T	line to cooler	140	12.1	0.029
T-U	line to cooler	140	12.1	0.104
U-V	scavenge return	140	12.1	0.140
V-A	separator	2	12.1	0.192

turboalternator. The small scoop in the rear compartment of the turboalternator is replaced by a flow divider which directs the proper amount of oil to each bearing location. The oil leaving the turboalternator is not carried by argon gas to the turbine-compressor but rather it is scooped and returned to the accumulator. Argon with a small quantity of oil mist or vapor flows from the turboalternator to the turbine-compressor.

The scoops in the turboalternator (Figure 25) impose a drag loss of about 600 watts. A summary of the losses for the lubrication system employing scoop scavenge pumps in the turboalternator is presented in Table 7. The pressure losses in certain sections of the system in Figure 25 are different from the losses in the corresponding sections of Figure 4. These revised performance curves are presented in Figures 26, 27, 28, and 29. The resulting operating conditions with the system in a vertical orientation are summarized in Table 8.

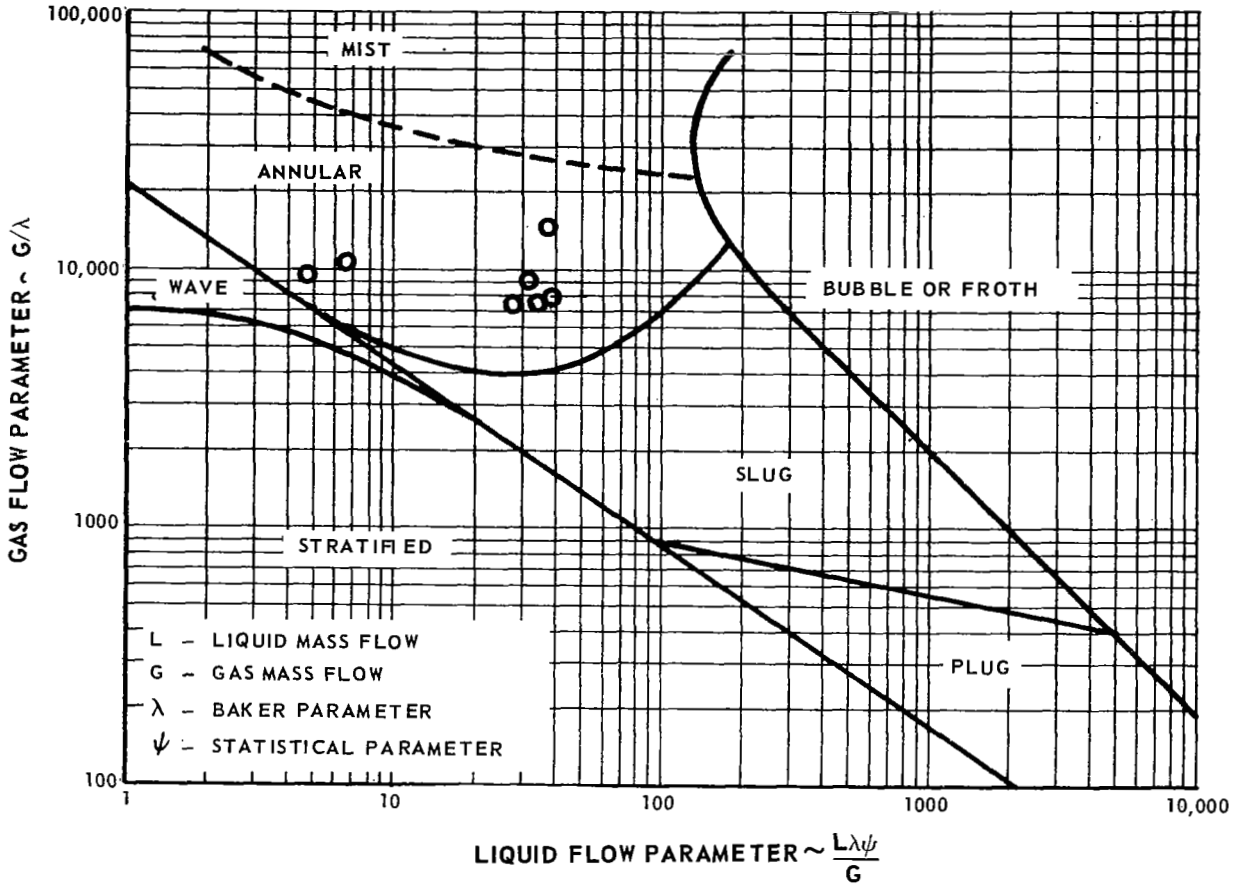

Figure 23 **Flow Regime Chart. Annular Jet Pump in Horizontal Operation**

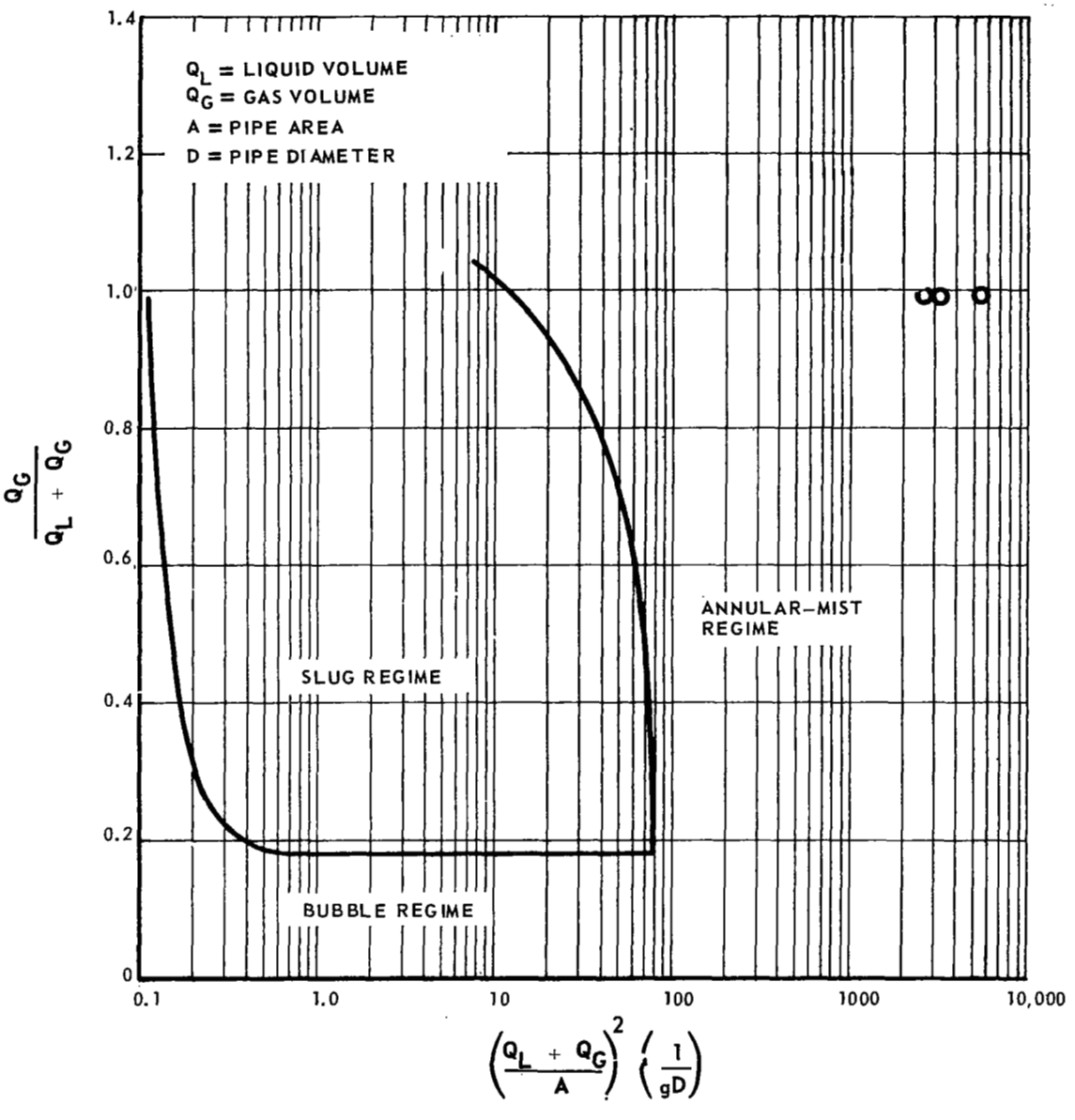

Figure 24 Flow Regime Chart. Annular Jet Pump in Vertical Operation

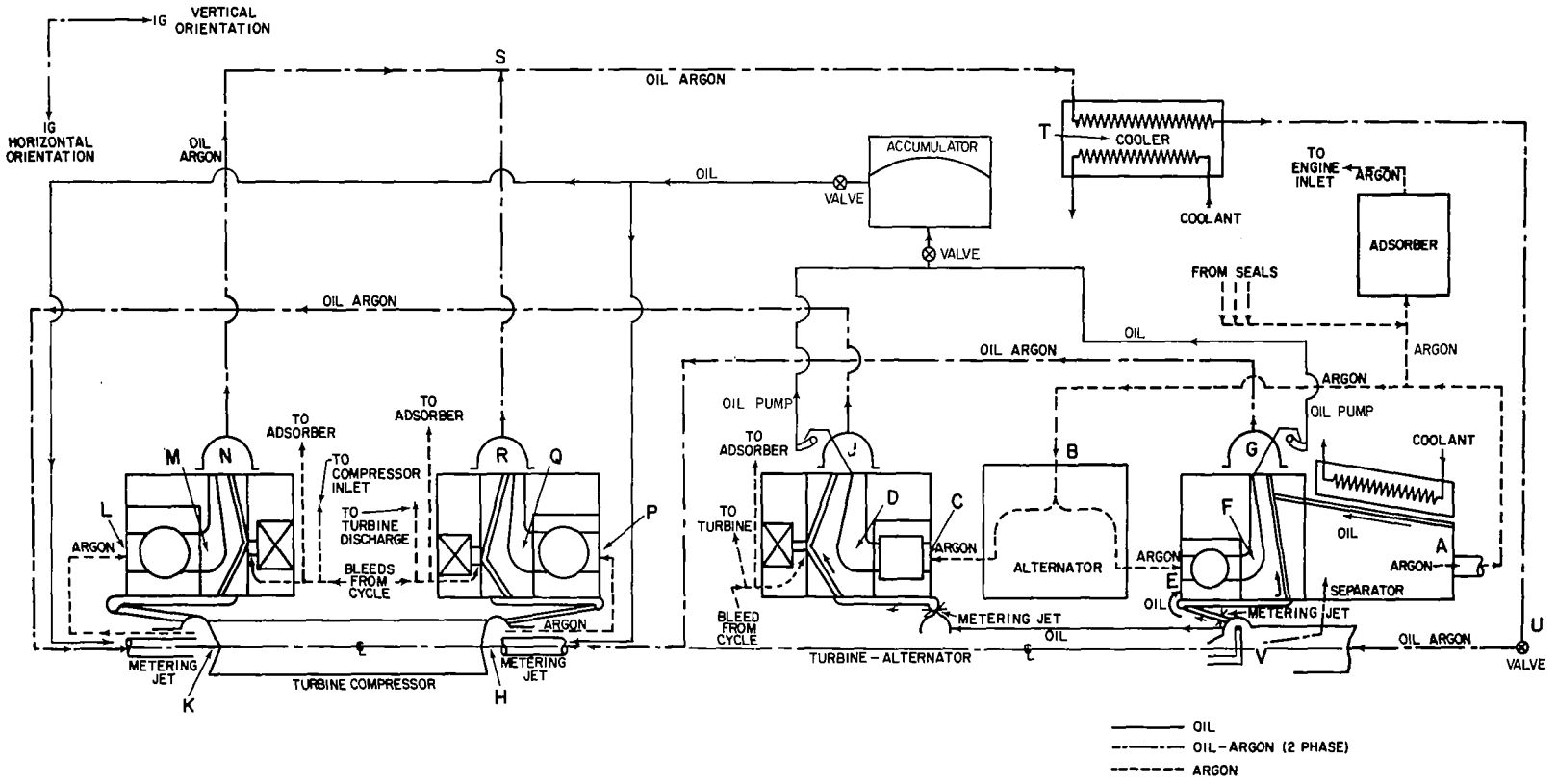

Figure 25 Schematic of Alternate Brayton-Cycle Rolling-Element Bearing System with Oil Scoop-Pump Configuration

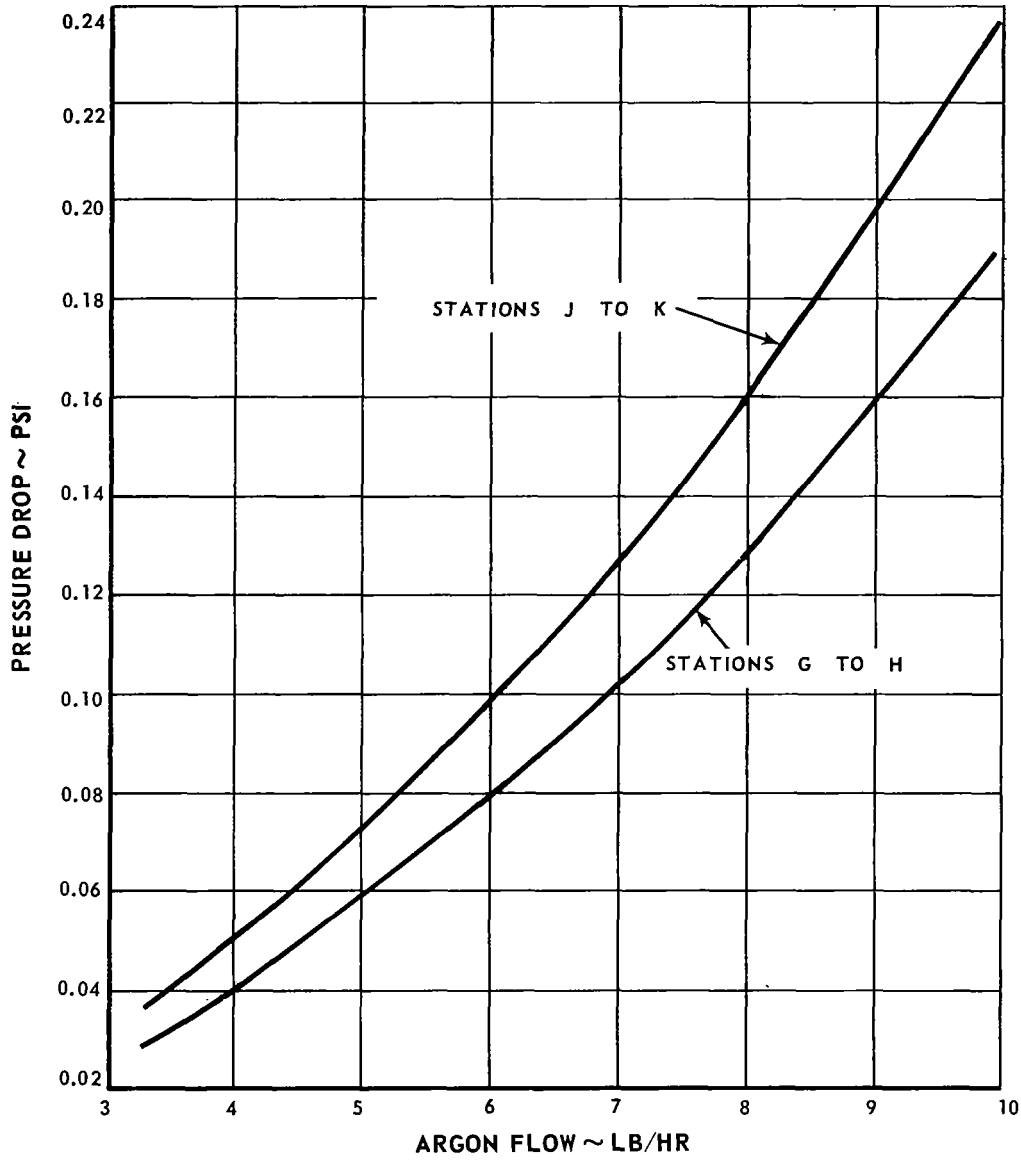

Figure 26 Scoop System. Pressure Drop from Turboalternator to Turbine-Compressor for Argon

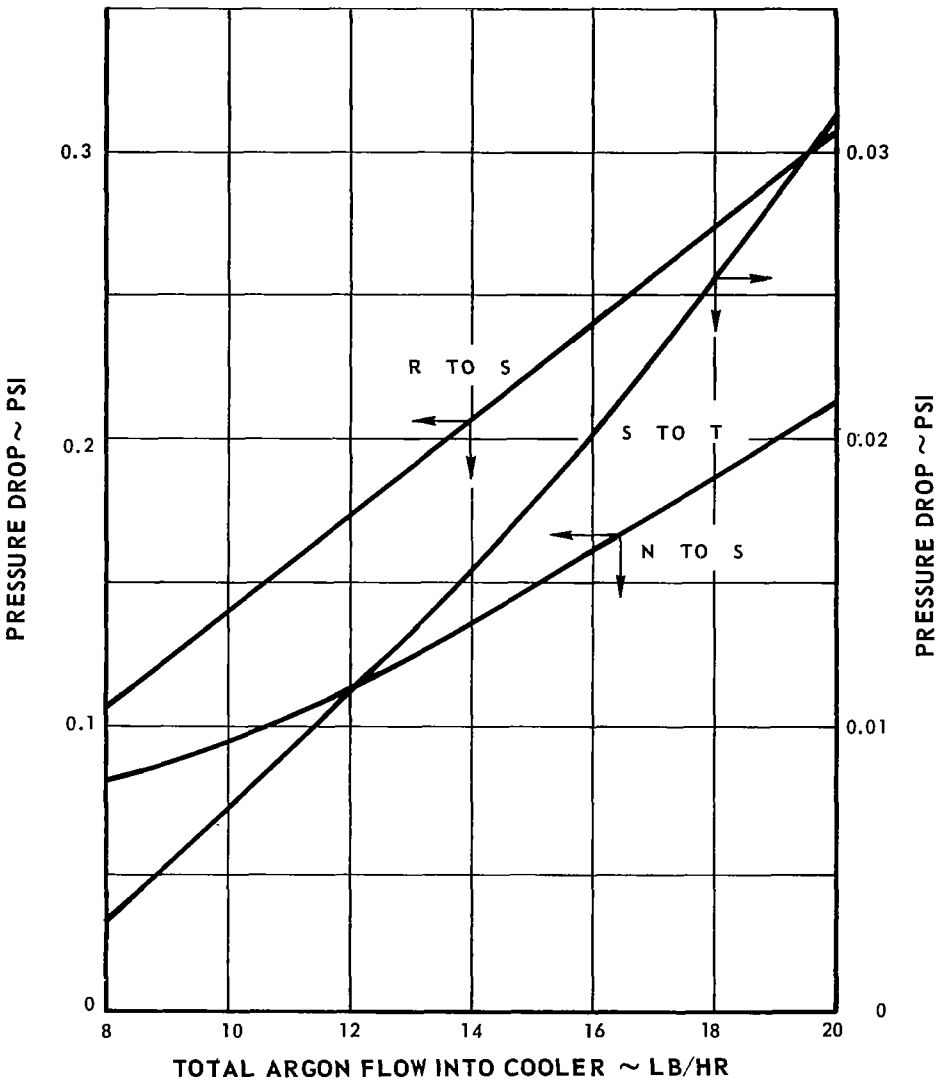

Figure 27 Scoop System. Pressure Drop from Turbine-Compressor to Cooler. Vertical Orientation

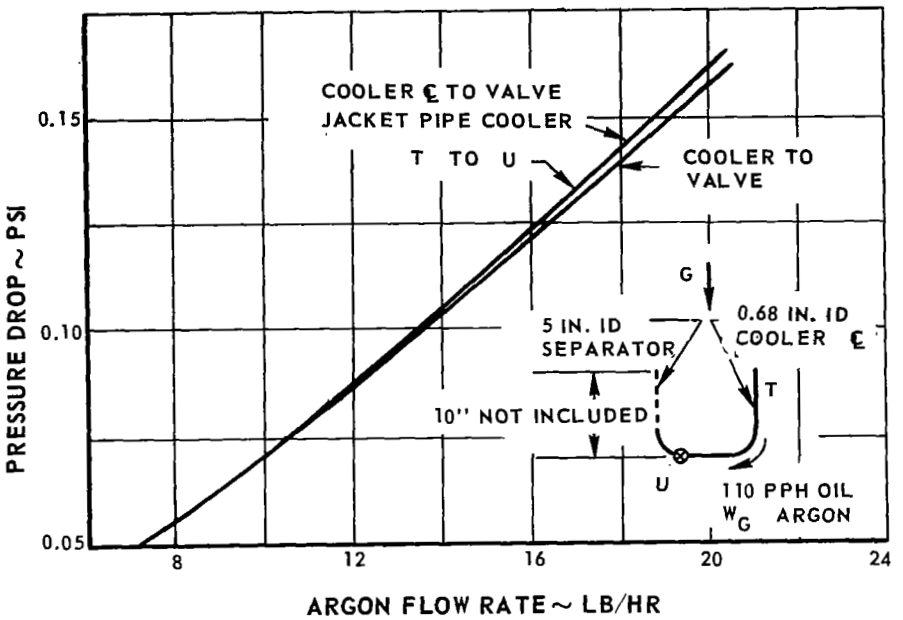

Figure 28 Scoop System. Pressure Drop from Cooler to Separator. Vertical Orientation

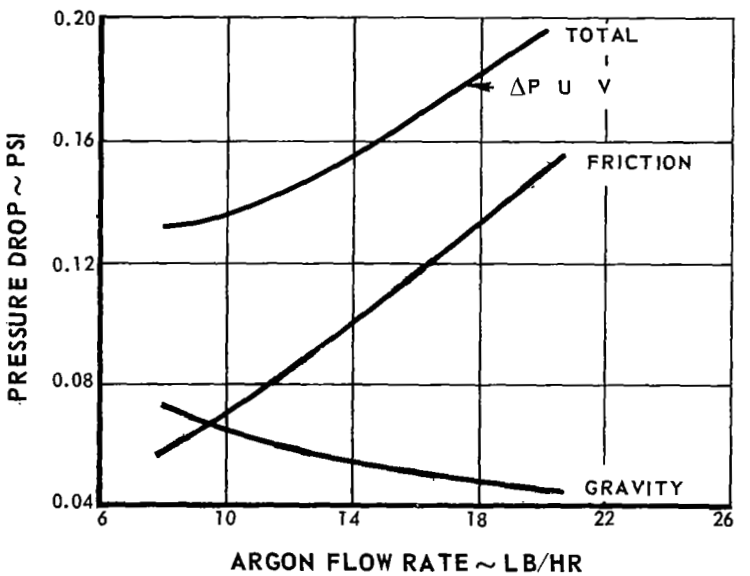

Figure 29 Scoop System. Pressure Drop for Separator Riser

TABLE 7

Power Losses with Scoop Scavenge System

Type of Loss and Location	Oil Flow, lb/hr	Power Loss, watts	
Turbine-Compressor Compartment 1			
bearing heat generation	50	202.1	
seal heat generation	50	200.0	
oil pumping	50	123.0	
argon pumping		10.0	
			535.1
Turbine-Compressor Compartment 2			
bearing heat generation	60	203.5	
seal heat generation	60	200.0	
oil pumping	60	147.5	
argon pumping		10.0	
			561.0
Turboalternator Compartment 1			
bearing heat generation	55	73.0	
seal heat generation	55	55.8	
oil pumping	55	28.8	
argon pumping		2.7	
scoop drag		310.0	
			470.3
Turboalternator Compartment 2			
bearing heat generation	22	108.0	
oil pumping	55	28.8	
argon pumping		2.7	
scoop drag		310.0	
separator drag		7.1	
separator pumping		16.4	
			473.0
Total			2039.4 watts

TABLE 8

Pressure Losses with Scoop Scavenge System
Vertical Operation

Station on Figure 25	Description	Oil Flow, lb/hr	Argon Flow, lb/hr	Pressure Loss, psi
A-B	line from separator to alternator	-	7.5	0.031
B-C	labyrinth seal	-	3.6	0.090
C-D	roller bearing	-	3.6	0.012
J-K	line from turboalternator to turbine-compressor	-	4.2	0.055
L-M	ball bearing	-	4.2	0.048
N-S	scavenge line	50	4.5	0.070
B-E	labyrinth seal	-	3.9	0.104
E-F	ball bearing	-	3.9	0.009
G-H	line from turboalternator to turbine-compressor	-	4.5	0.045
P-Q	ball bearing	-	4.5	0.061
R-S	scavenge line	60	4.8	0.052
S-T	line to cooler	110	9.3	0.006
T-U	line from cooler	110	9.3	0.066
U-V	scavenge return	110	9.3	0.134
V-A	separator	2	0.3	0.109

This alternate lubrication system provides greater margin in the uncertainties of two-phase flow, but only at a sacrifice in parasitic losses. If the basic system were found to be deficient, the alternate could be incorporated by changes in the turboalternator and external plumbing.

A third variation of the lubrication system was examined briefly. This alternate incorporates scavenge pumps similar to those used in SNAP-8. However, the preliminary examination indicated higher parasitic losses and this concept was not considered further.

B. Lubricant Evaluation and Selection

The lubrication system shown schematically in Figure 2 and described in Section IIIA above is a closed system with sufficient oil inventory to last the projected mission life of over 10,000 hours. The lubricant is used to cool and lubricate the bearings and seals in both the turbine-compressor and turboalternator. Hence, it is subjected to a range of temperatures from 100 to 400°F as it circulates through the system. In order to conserve the oil and argon inventories and to prevent contamination of the cycle argon, the argon that leaks past the seals into the bearing compartment must be separated from the oil and returned to the main cycle. Considering these system conditions and requirements, a list of desirable lubricant properties is as follows:

1) The lubricant must have favorable long-time lubricating characteristics for high-speed bearings and seals.

2) The lubricant must be thermally stable.

3) Any decomposition that takes place should not yield products harmful to either the lubricant or the powerplant.

4) The lubricant should have good heat transfer characteristics.

5) The lubricant must be chemically compatible with the various structural materials used throughout the lubrication system.

6) The vapor pressure and solubility of the oil-in-argon and argon-in-oil must be favorable. Heat transfer, lubricating, scavenging and separation characteristics could be adversely affected.

7) The viscosity characteristics must be compatible with the operating temperatures.

Three candidate lubricants were considered for this application, 1) five-ring polyphenyl ether (PWA-524), 2) four-ring polyphenyl ether (Monsanto MCS-333), and 3) super-refined mineral oil (MLO-7277). Factors considered in comparing the three lubricants are shown in Table 9.

Low temperature decomposition characteristics of the candidate oils were examined to determine if each lubricant is adequate for the mission life of over 10,000 hours. At 400°F, one percent of the mineral oil will decompose in 10,000 hours. The 4-ring polyphenyl ether has a decomposition rate which is over 5 orders of magnitude smaller. While no decomposition data is available for the 5-ring polyphenyl ether, it is expected to be similar to that of the 4-ring oil. Low- temperature decomposition of the 4-ring polyphenyl ether begins with the breaking of the carbon-oxygen bond and the formation of heavier and lighter ethers. At high temperatures, benzene, phenol, diphenyl ether and some volatiles would form. It is believed that the products of decomposition would not accumulate in sufficient quantity to affect the physical properties of the lubricant for the duration of the mission. The decomposition rate of the mineral oil and the 4-ring polyphenyl ether are presented in Figure 30.

The chemical compatibility of the candidate oils was compared and the results are summarized in Table 9. The mineral oil at 350°F is about as corrosive as the 4-ring polyphenyl ether at 500°F. The 5-ring polyphenyl ether attacks copper to some extent at 600°F. In general, the candidate oils exhibit reasonable chemical compatibility for the intended application.

The heat-transfer properties of the candidate oils were examined and it was found that the differences would not significantly affect the performance of the lubrication system. The density, specific heat, and thermal conductivity of the candidate oils are presented in Figures 31, 32, and 33.

The centrifugal separator upstream of the adsorber can efficiently remove oil droplets carried in by the argon, and droplets formed in the separator as the oil condenses. Therefore, low vapor pressure is a desirable property of the oil. The vapor pressure of the candidate oils is presented in Figure 34. The polyphenyl ethers exhibit lower vapor pressure than the mineral oil.

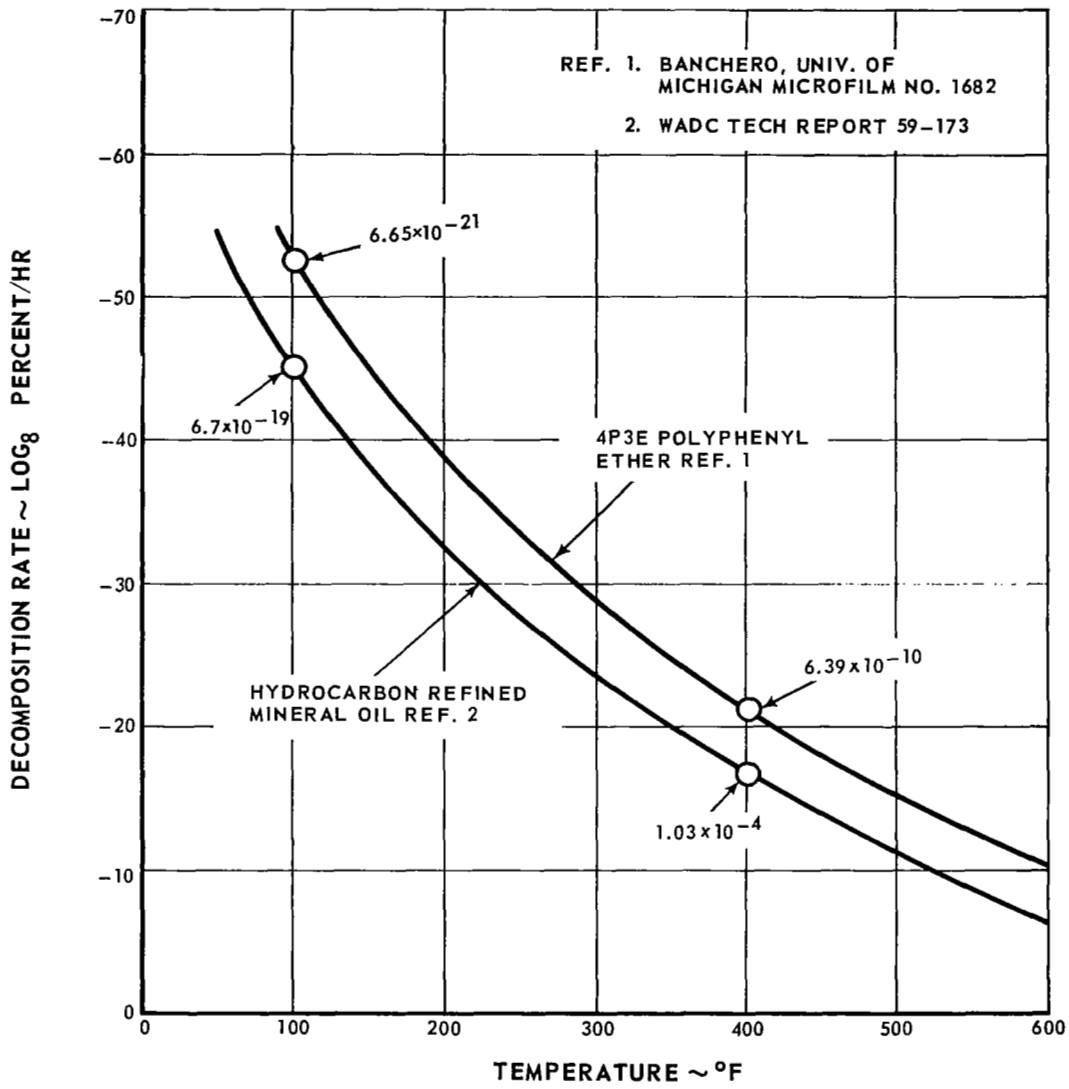

Figure 30 Thermal Decomposition Rate in Inert Environment vs Temperature

TABLE 9

Lubricant Comparison

Property	Lubricant			Remarks
	Super-Refined Mineral Oil	Four-Ring Polyphenyl Ether	Five-Ring Polyphenyl Ether	
	A	B	C	
density lb/ft3 at 350°F	49	66	68	
vapor pressure mm Hg at 350°F	0.38	0.11	0.03	
specific heat Btu/lb/°F at 350°F	0.59	0.47	0.57	
thermal conductivity Btu/ft/hr/°F at 350°F	0.0688	0.0686	0.0684	
viscosity Cs at 350°F	2.3	1.9	2.8	
ASTM pour point, °F	-30	10	40	
corrosiveness in air environment, method: FS791-5380 test duration: 48 hrs at temperature of:	347°F	500°F	600°F	tests of an inhibited 5-ring polyphenyl yielded following results at 600°F
wt. change, mg/cm^2				
magnesium	+0.07	-0.06	+0.25	+0.02
aluminum	+0.07	+0.01	+0.01	+0.01
steel	+0.08	+0.03	+0.05	+0.04
copper	+0.02	-0.01	-0.95	+0.29
silver	+0.01	-0.05	+0.32	-0.12
thermal decomposition rate in inert environment at 400°F; percent/hour	1.0×10^{-4}	6.4×10^{-10}	-	four and five-ring polyphenyl ethers are believed to have similar decomposition rates

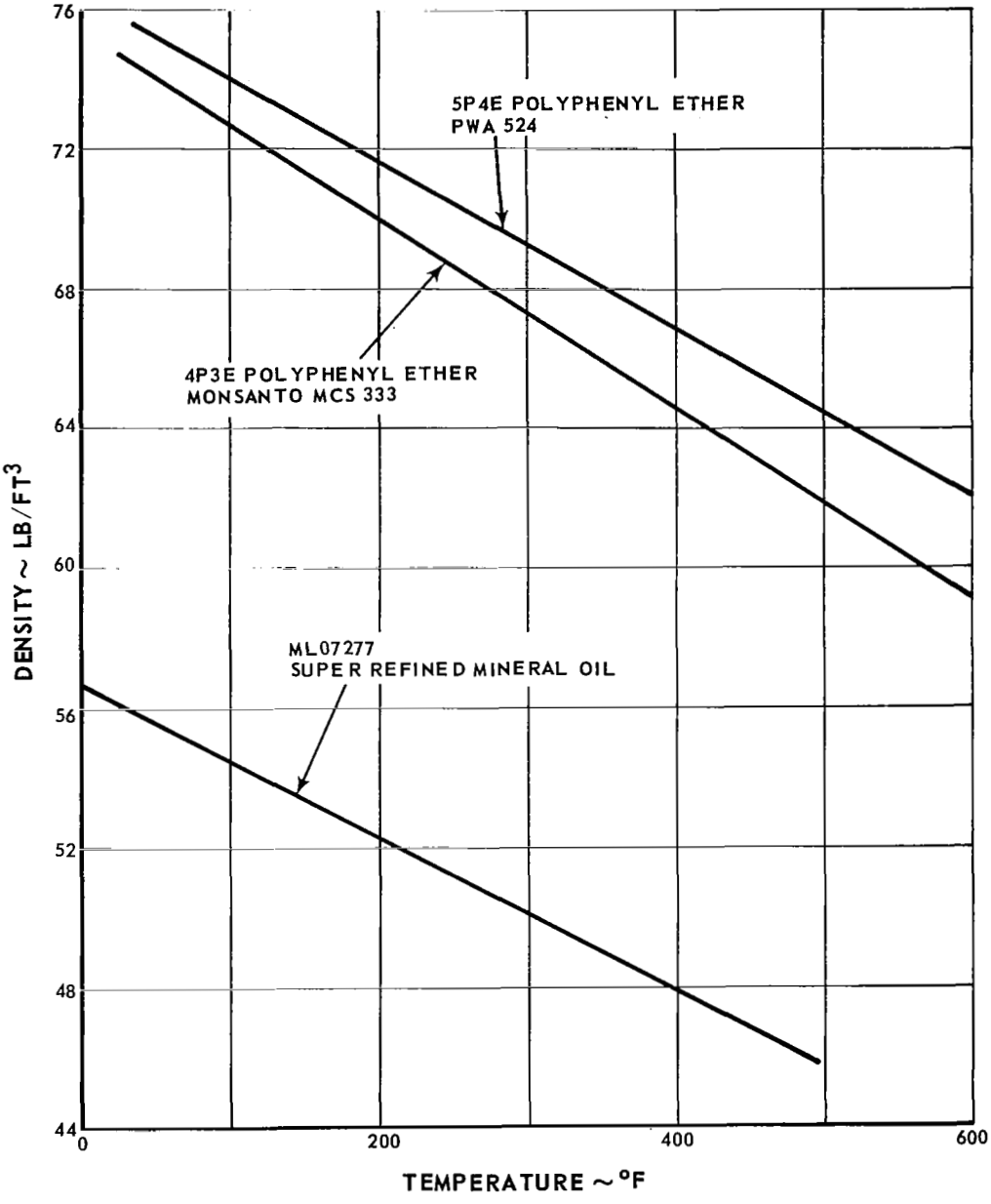

Figure 31 Density of Lubricant vs Temperature

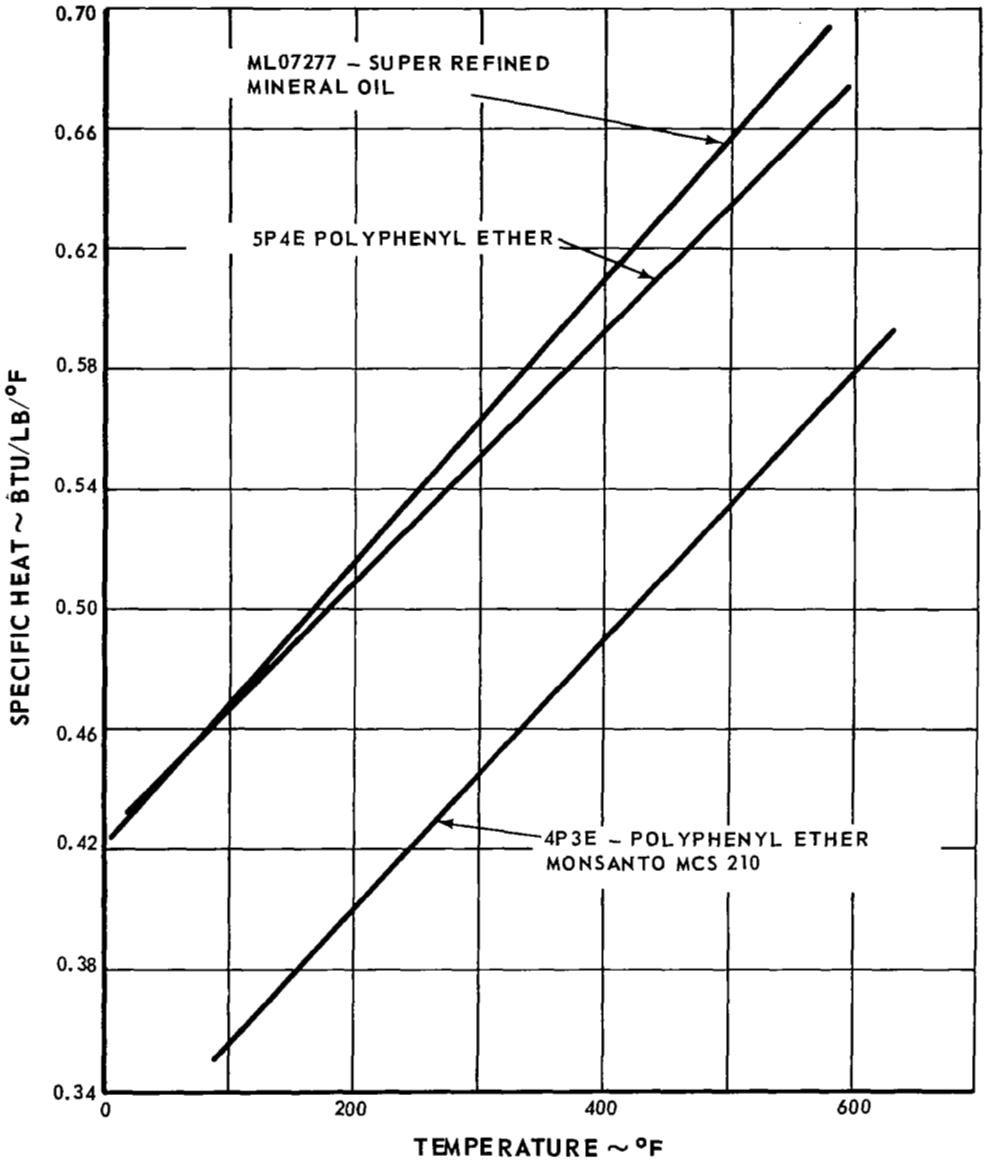

Figure 32 Specific Heat of Lubricants vs Temperature

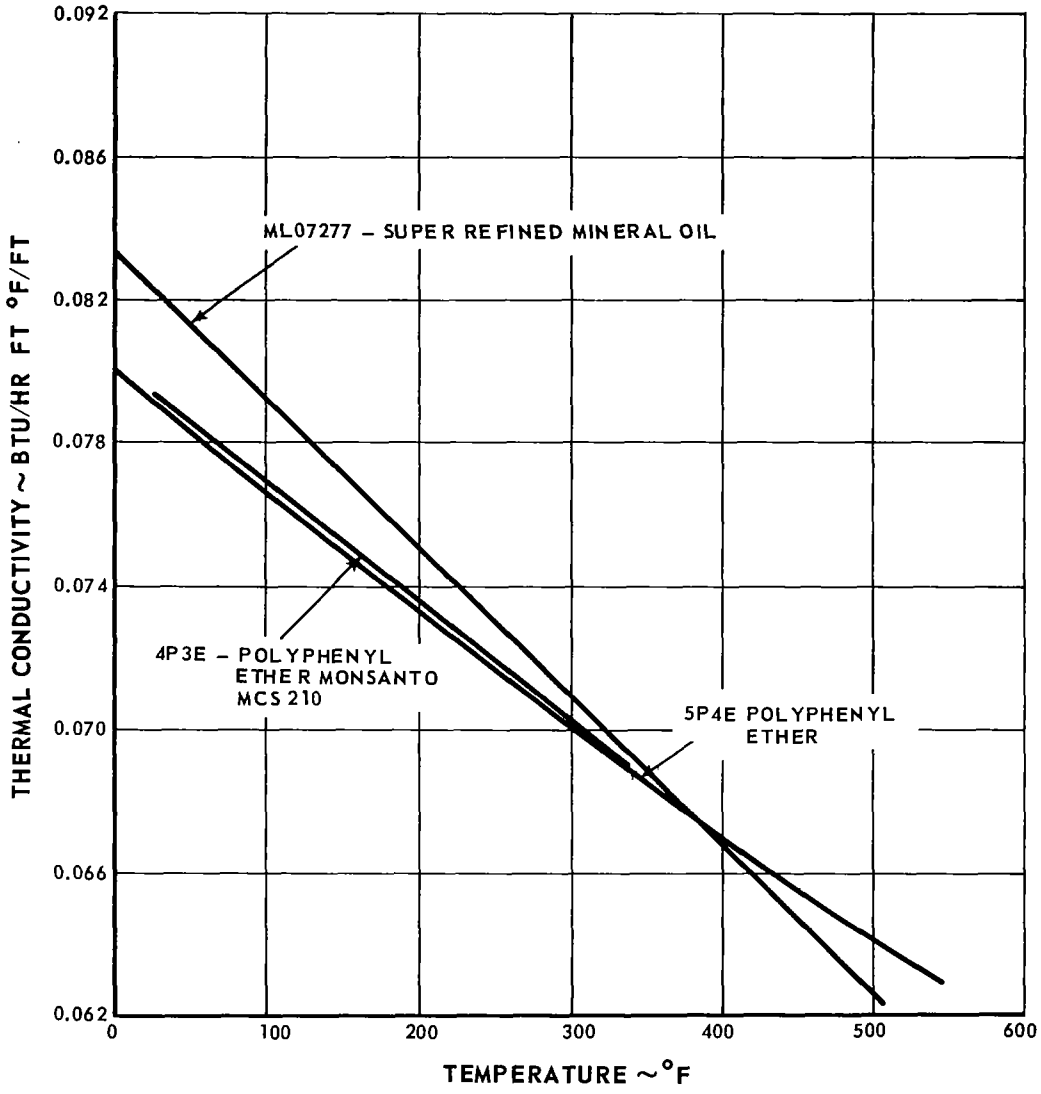

Figure 33 Thermal Conductivity of Lubricants vs Temperature

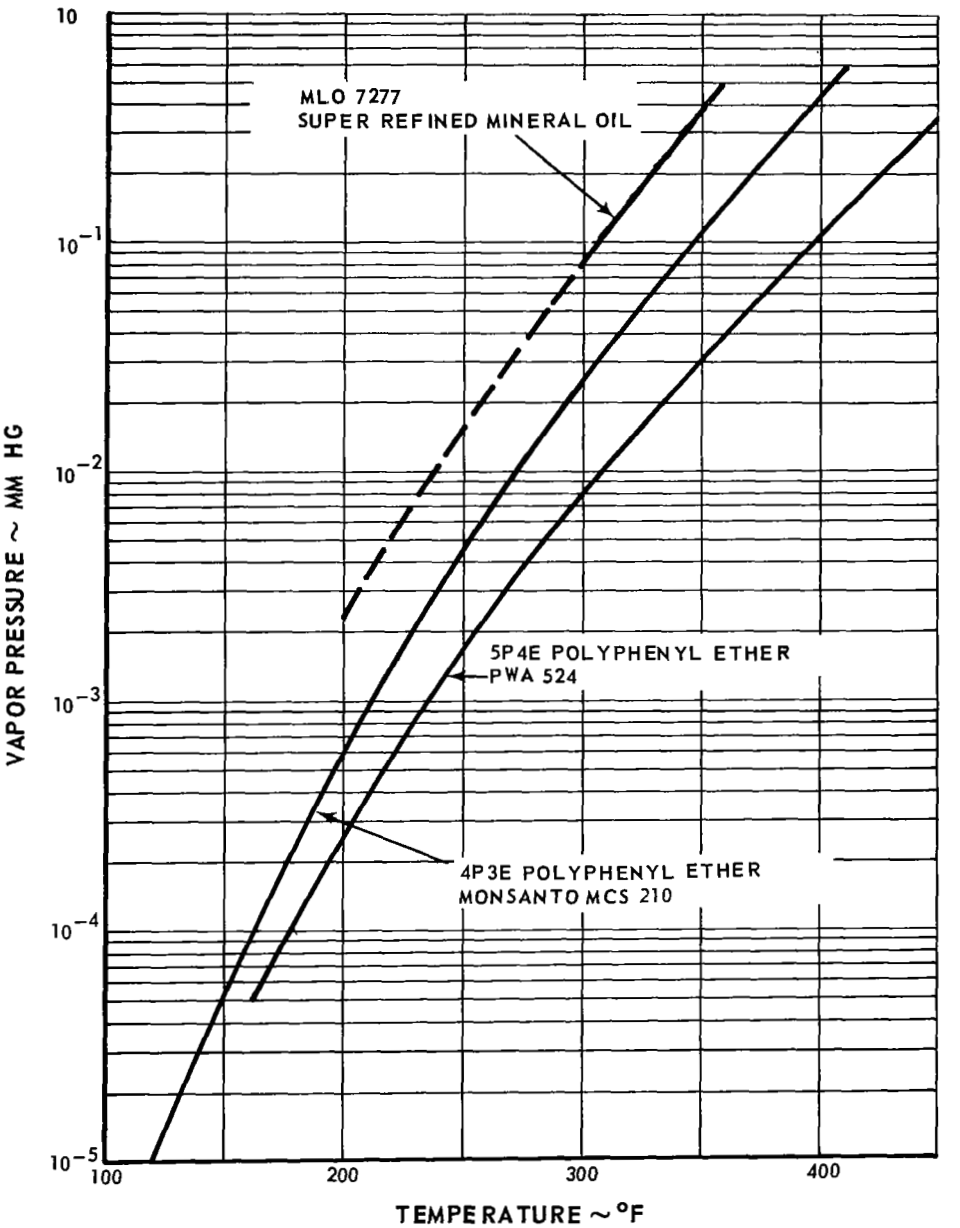

Figure 34 Vapor Pressure of Lubricants vs Temperature

The oil must serve as a lubricant and must have a reasonable viscosity. The low-pressure viscosity characteristics of the three oils is presented in Figure 35. Actually, the more important property is the viscosity of the oil under the high pressures encountered in the contact between the ball and race. Unfortunately, such data are not normally directly available and the results of in-

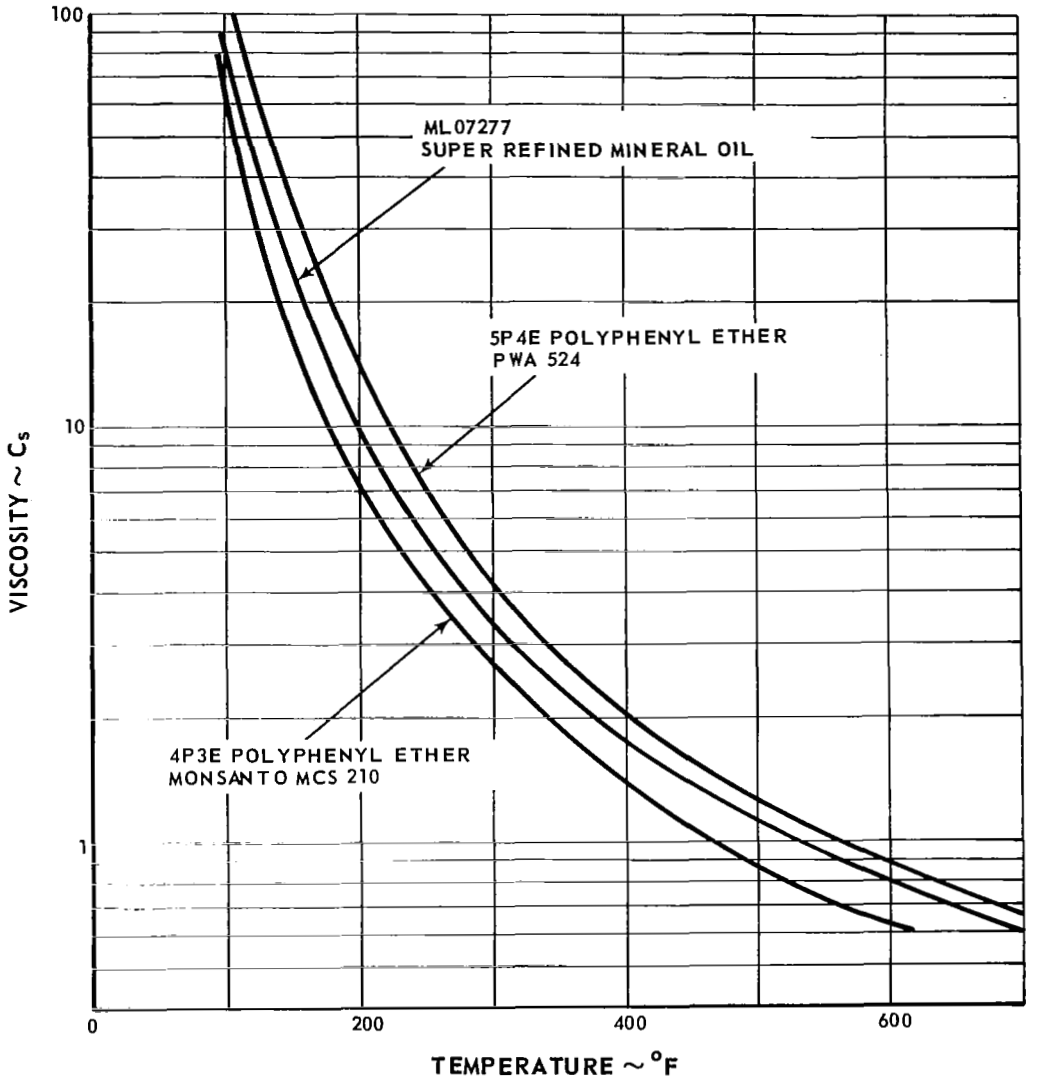

Figure 35 Viscosity of Lubricants vs Temperature

direct tests are usually required. Battelle Memorial Institute[18] has conducted rheology experiments on some oils using X-ray techniques to indicate film strength and lubrication properties. The results of tests with a highly-refined mineral oil and a 5-ring polyphenyl ether are presented in Figures 36 and 37. The polyphenyl ether provides larger oil film thickness and lower pressure than the mineral oil in these tests. NASA has conducted tests of the wear characteristics of MLO 7277 mineral oil with additives, and of a 4-ring polyphenyl ether without additives in a 5-ball tester. Pratt & Whitney Aircraft has tested a 5-ring polyphenyl ether with additives in high-speed ball bearings with excellent endurance results. A direct comparison of the lubricant properties of the polyphenyl ethers and mineral oil is not possible based on the data available. Unfortunately, no test of a direct comparison of the oils has been reported. Some tests have been conducted under similar circumstances, but in these cases one oil contained additives and the other did not. The only experimental data of the performance of the oils with the bearing material selected, vacuum melt M-50, are reported in Reference 20. This paper presents the results of endurance tests of 30 M-50 bearings lubricated with PWA-524, 5-ring polyphenyl ether oil. The oil-in temperature was 500°F and the bearings were run at speeds between 1.25

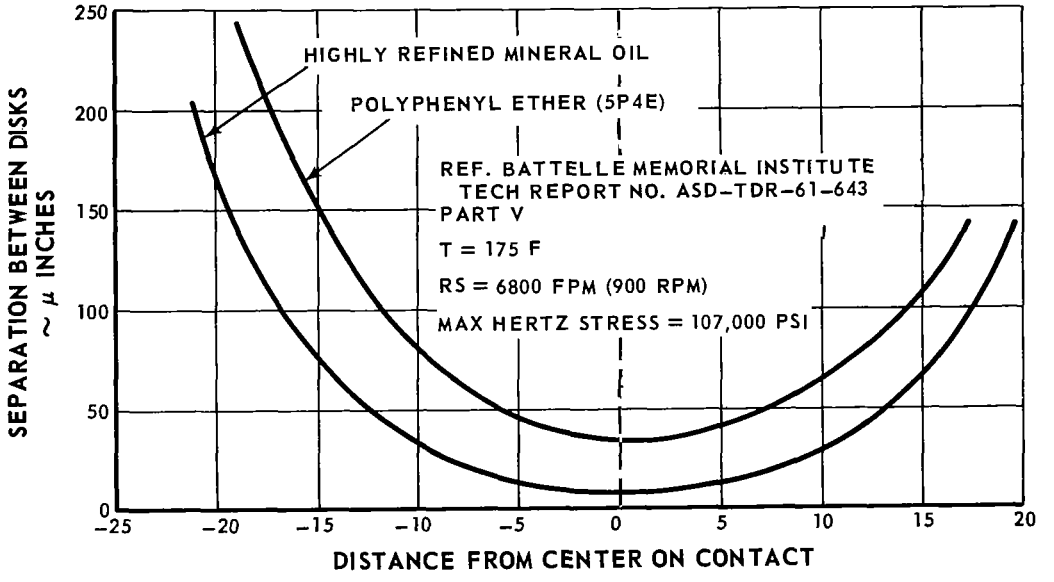

Figure 36 Circumferential Profile of Lubricated Rolling Discs

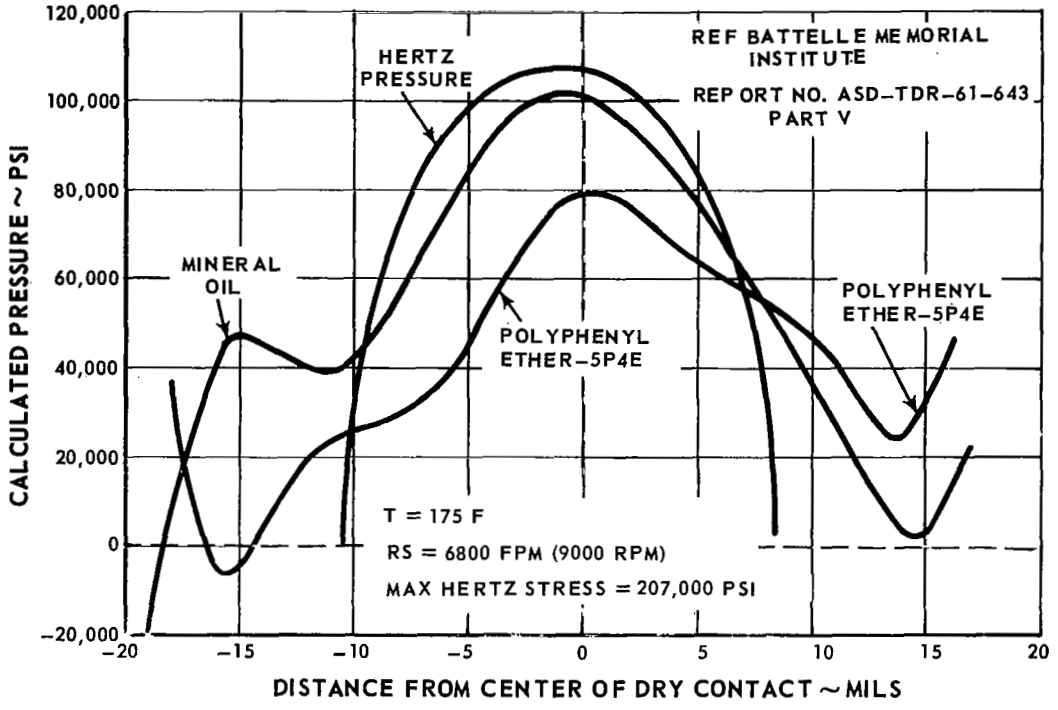

Figure 37 Pressures Calculated from Circumferential Profiles

and 1.5 million DN (diameter in millimeters × speed in rpm). Two different bearing sizes were tested. In the course of these tests none of the bearings failed, indicating a bearing life at least 14 times the AFBMA standard life. Unfortunately, comparable data with the other two candidate oils is not available.

Since the 5-ring polyphenyl ether (PWA-524A) oil produced excellent results in vacuum melt M-50 bearing endurance tests, and since it has low vapor pressure which minimizes the load on the adsorber, this oil was chosen for the Brayton-cycle application. Polyphenyl ethers are very promising materials for use as radiation-resistant high-temperature lubricants.

C. Lubricant Decomposition and System Contamination

Some small amount of oil will weep past the seals or migrate through the adsorber and enter the primary cycle. In order to establish the maximum quantity of oil contamination that can be allowed for a 10,000-hour mission, an investigation of the consequences of oil contamination was undertaken. This study involved three basic areas:

1) Identification of the products formed by pyrolysis (thermal decomposition) of the lubricant.

2) The distribution or location where the various products of the pyrolysis will accumulate in the system.

3) The consequences to powerplant performance from oil pyrolysis products in certain locations leading to the fouling of heat-transfer surfaces, blockage of flow passages, and introduction of gases into the argon.

The identification of the products produced by pyrolysis of the lubricant is restricted by the limited data available at the conditions encountered in the Brayton cycle, References 19 and 21-39. However, polyphenyl ethers can be expected to form tar containing carbon and polymer and to evolve a small quantity of gases. Solid products may be expected to build up in the hotter areas, such as at the heater where the highest temperature exists and therefore where rapid pyrolysis reactions will occur. Gaseous hydrogen will accumulate in the cycle fluid unless special precautions are introduced to prevent such an accumulation. There is a possibility that some low-volatility liquid products may condense in the cooler parts of the system.

Deposition of coke or tar in the heater will reduce system performance due to the increase in flow resistance. If the Brayton-cycle efficiency were reduced approximately 1.5 per cent which corresponds to an increase in $\Delta P/P$ of approximately 0.02 and if the material were deposited fairly uniformly, the system would be able to absorb slightly more than 5 pounds of oil in the course of the mission. The effect of such deposits on heat-transfer coefficients is relatively small because the thermal resistance of the gas film is fairly high.

The release of hydrogen gas as a result of oil pyrolysis appears to be the factor limiting the allowable Brayton-cycle oil contamination. The Brayton-cycle system was analyzed with various amounts of hydrogen gas added to a nominal inventory of 0.331 pound of argon. The thermodynamic properties of the mixtures of argon and hydrogen, presented in Figure 38, were used in the evaluation of cycle performance. As the gas properties vary, the performance of the various components of the powerplant also vary, and the variations in the performance

of the cooler, compressor, regenerator, heater and turbines were included. Compressor inlet temperature was assumed constant.

Two of the types of heat sources being considered for application with the Brayton-cycle machinery are solar energy and isotope decay. With the solar heat source in an earth orbit, the solar energy is concentrated on a heat receiver which contains heat storage material. Energy is stored by melting the storage material and is extracted as the material freezes. Since the melting temperature of the storage material is constant, this type of energy source is sometimes assumed to provide a constant turbine inlet temperature over a limited range. Therefore, the performance of the Brayton-cycle system with hydrogen addition and constant turbine inlet temperature was analyzed, and the results are presented in Figure 39.

As hydrogen gas is added to the cycle as a result of oil pyrolysis, the pressure level in the cycle is increased and the specific heat of the gas mixture is increased. Since, for this study the compressor inlet temperature is assumed constant and turbine inlet temperature is artificially held constant, the power output is increased as the hydrogen gas is added. The increase in power output is a result of the increased specific heat of the mixture and the increase in mass flow. However, the turbine-compressor speed also increases. It reaches 20 per cent overspeed with 0.0065 pound of hydrogen. The turbine-compressor was designed to be able to operate at 20 per cent overspeed for moderate periods. Since the maximum contamination occurs at the end of the life of the powerplant, the 20 per cent overspeed condition can be considered a limit. At this condition the power produced is increased by approximately 70 percent of the rated power, which exceeds the rating of the alternator (15 KVA at 0.8 power factor).

In order to prevent exceeding the alternator rating, the Brayton-cycle system performance was evaluated allowing the turbine inlet temperature to vary so as to maintain constant net power output with hydrogen addition. The results of this study are presented in Figure 40. The turbine inlet temperature must be reduced to maintain constant power output. As a result the cycle efficiency is reduced and the required input thermal energy is increased. The system becomes non-selfsustaining with more than about 0.014 pound of hydrogen contamination. The turbine-compressor speed is reduced with increasing hydrogen contamination in this case.

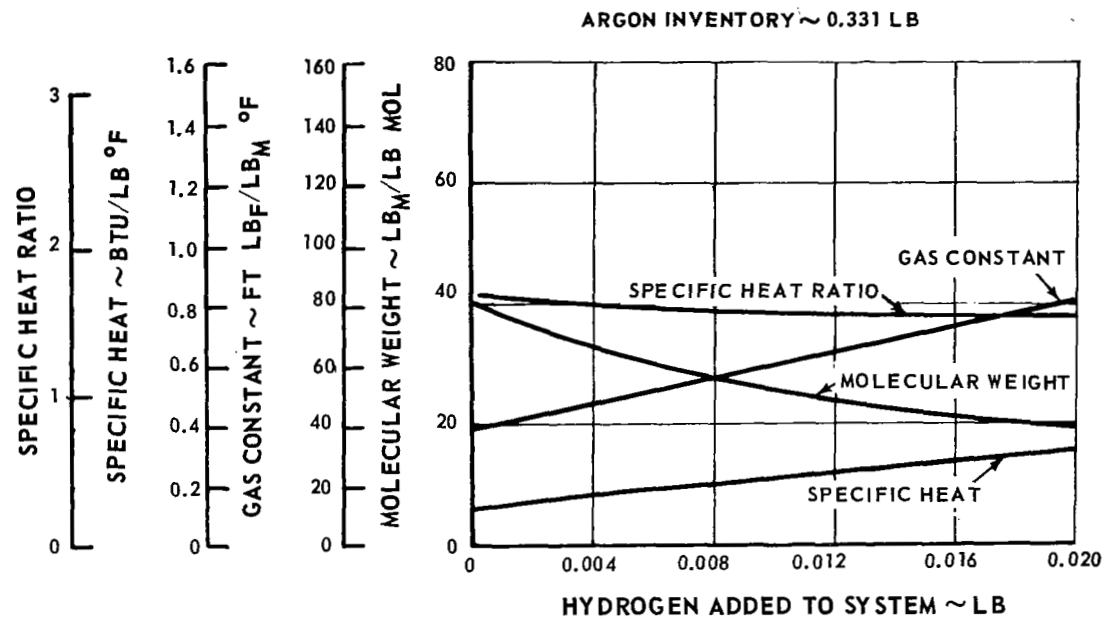

Figure 38 Effect of Hydrogen Addition on Properties of Working Fluid

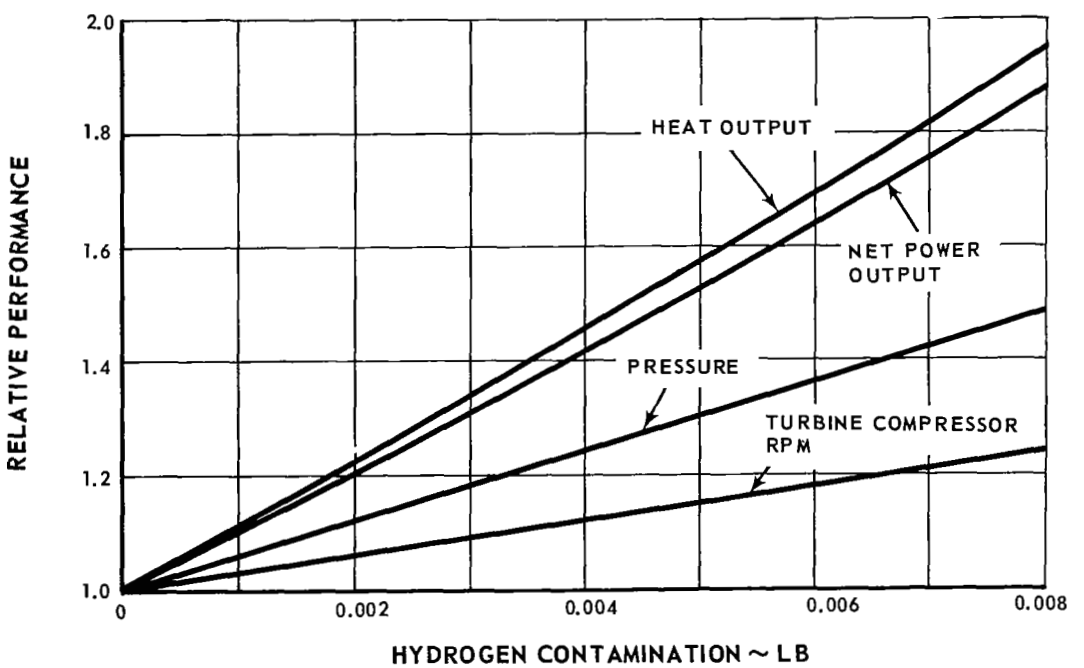

Figure 39 Effect of Hydrogen Addition on System Performance for Constant Turbine Inlet Temperature

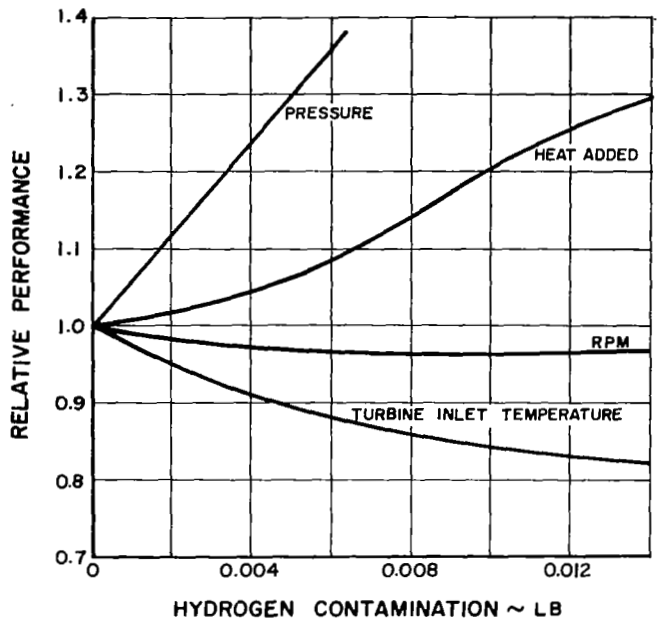

Figure 40 Effect of Hydrogen Addition on System Performance for Constant Net Power

One method of preventing the cycle power increase as hydrogen is admitted is to reduce the system pressure level with a pressure relief valve. If the net output power and the turbine inlet temperature were held constant, the compressor inlet pressure would vary as shown in Figure 41. The turbine-compressor rotor would run above design speed, reaching the limiting condition of 20 per cent overspeed with a contamination of 0.008 pound of hydrogen. At this condition the heat source would have to supply approximately 15 per cent more thermal energy than at normal operating conditions.

The isotope heat source is often considered to be a constant energy source. The performance of the power system with constant heat input is presented in Figure 42 for various levels of hydrogen contamination. In this case no pressure relief was assumed, resulting in increasing pressure level with the hydrogen addition. The turbine inlet temperature decreases as a result of the increasing specific heat and increasing mass flow of the working fluid. As a result of the reduction in turbine inlet temperature, the power output decreases and the system becomes non-selfsustaining with about 0.008 pound of hydrogen contam-

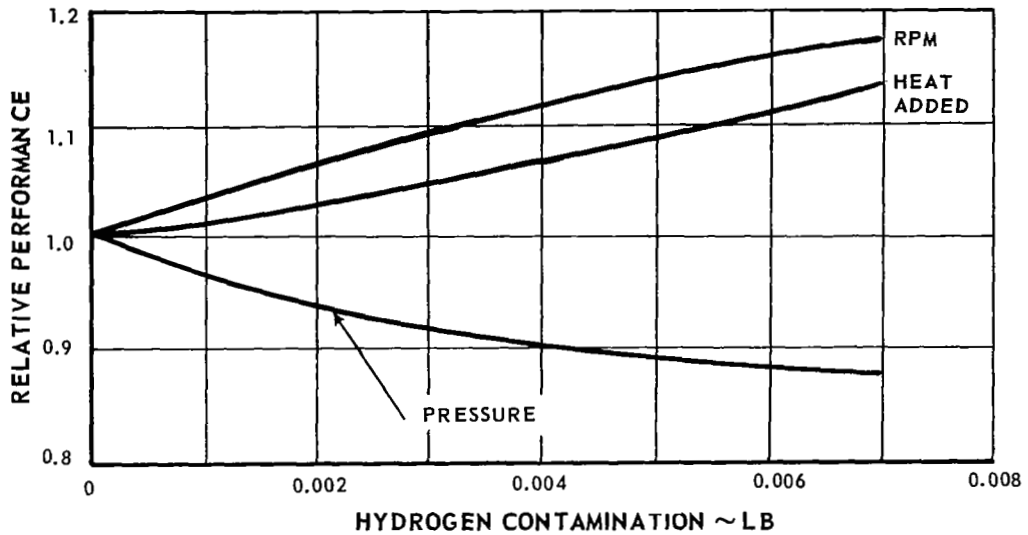

Figure 41 Effect of Hydrogen Addition on System Performance for Constant Net Power and Turbine Inlet Temperature

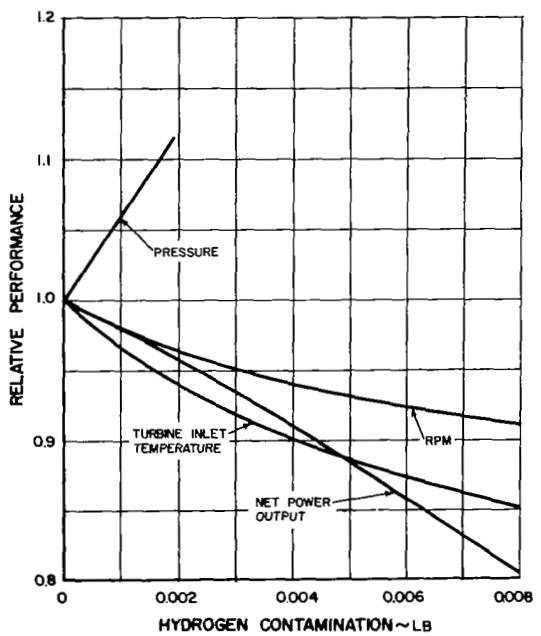

Figure 42 Effect of Hydrogen Addition on System Performance for Constant Heat Input

ination. If the pressure were not allowed to increase with hydrogen addition, but were held constant by a relief valve, and if the heat input were held constant, the system becomes non-selfsustaining with about 0.014 pound of hydrogen contamination. The results of this analysis are presented in Figure 43.

An isotope heat source will probably incorporate surplus material (fuel) to provide for control and the decay of the isotope. Therefore, some increase in heat input may be permissible. One case was examined where the pressure level was held constant by a pressure relief valve and the turbine inlet temperature varied to provide constant power output. The results are presented in Figure 44. In this case, the turbine-compressor speed exceeds 20 per cent overspeed with about 0.018 pound hydrogen contamination.

Since many of the cases studied involve an overspeed of the turbine-compressor, one case was examined in which the turbine-compressor speed and the net power output are held constant. Some pressure relief as well as control of the turbine inlet temperature are required. The results are presented in Figure 45. Because of the reduction in cycle efficiency due to the reduction in turbine inlet temperature, the heat source is required to supply more heat with hydro-

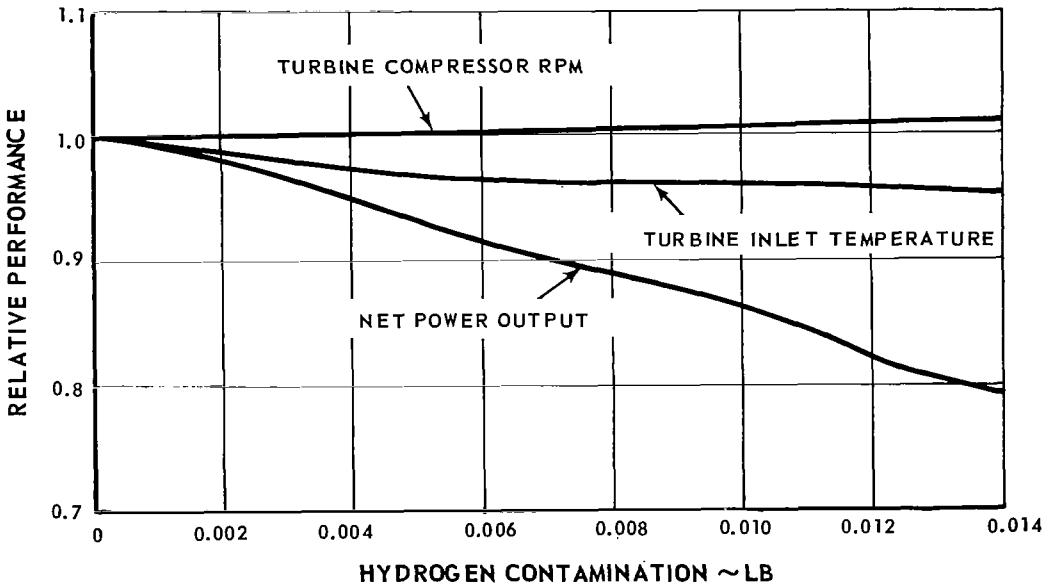

Figure 43 Effect of Hydrogen Addition on System Performance for Constant Heat Input and Pressure Level

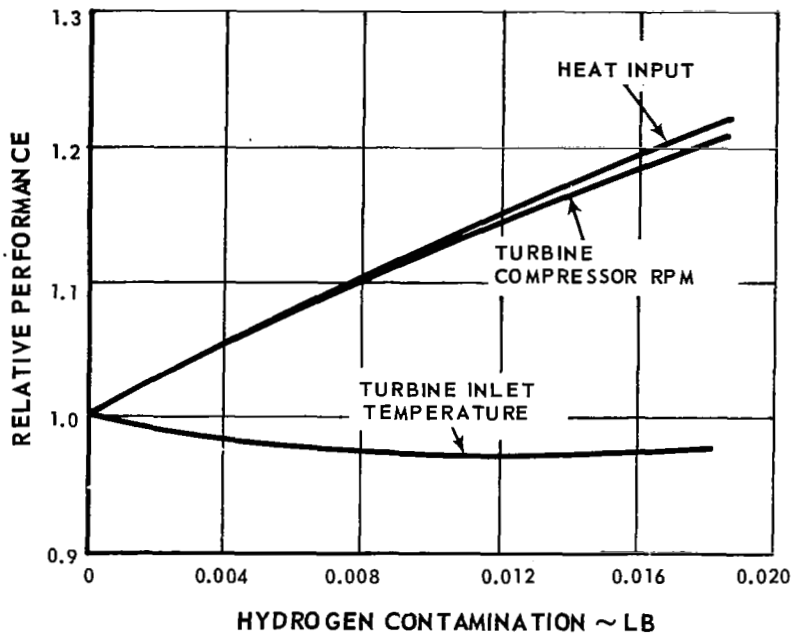

Figure 44 Effect of Hydrogen Addition on System Performance for Constant Net Power Output and Pressure Level

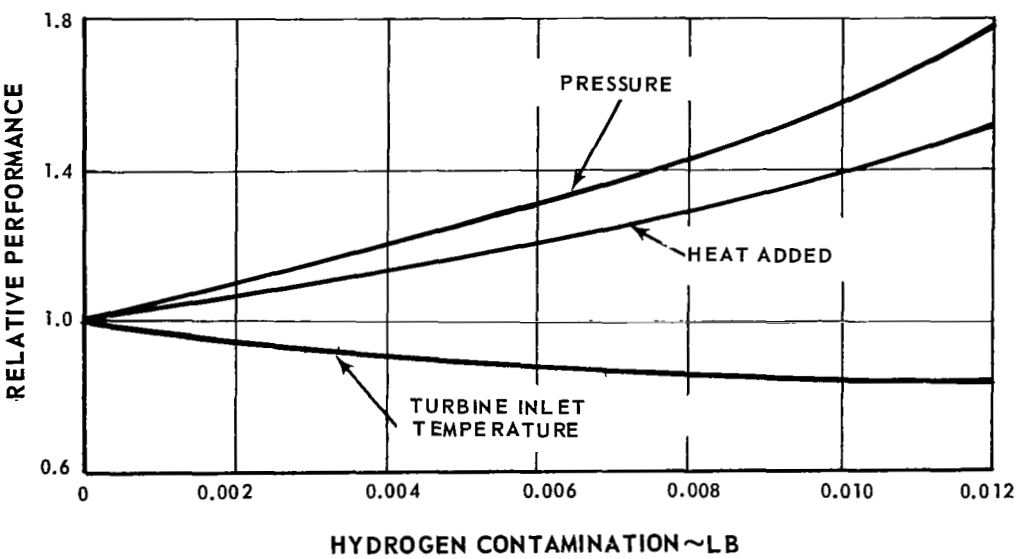

Figure 45 Effect of Hydrogen Addition on System Performance for Constant Net Power and Turbine-Compressor Speed

gen contamination. With 0.012 pound of hydrogen in the system the required heat input is increased 50 per cent.

The overall result of this study indicates that with some kind of control, either a pressure relief or heat source control (which controls turbine inlet temperature), contamination levels of 0.008 to 0.014 pound of hydrogen can be tolerated. Of course, this level of contamination is dependent on the inventory of argon assumed.

For this study a conservative (low) inventory of 0.331 pound of argon has been used. Inventories of 2 to 3 times this value may actually be involved in which the allowable contamination could be 2 to 3 times the values indicated. Since the selected polyphenyl ether oil contains 4.9 per cent of hydrogen, the allowable contamination of 0.008 to 0.014 pound of hydrogen represents 0.16 to 0.29 pound of oil (75 to 130 grams).

The hydrogen evolution will require some special consideration in the design of the Brayton-cycle powerplant. Perhaps the simplest approach is to provide a hydrogen window in the system to permit hydrogen to diffuse from the system while containing the cycle working fluid. For example, palladium can perform this function effectively. If such a window were employed, up to 5 pounds of oil can be accepted in the primary cycle fluid without seriously affecting the overall performance.

IV. TURBINE-COMPRESSOR DESIGN

The scope of the turbine-compressor design work was to adapt the turbine-compressor to use a rolling-element bearing system instead of the gas-bearing system developed under Contract NAS3-4179. The overall design objectives and considerations were: 1) to use a bearing, seal and lubrication system that would provide a high degree of reliability for a mission time of at least 10,000 hours, 2) to use a bearing, seal, and lubrication system having acceptable parasitic losses, 3) to evolve a mechanical design that would utilize existing aerodynamics, and 4) to minimize mechanical design changes.

The Brayton-cycle axial-flow turbine-compressor consisted of a six-stage compressor driven by a single-stage turbine at a design speed of 50,000 rpm, see Figure 46. Argon entered the compressor at 76°F through a duct which housed the front bearing compartment. The working fluid discharged radially into a scroll and then was piped to the heat source. The hot argon (1490°F) was returned to the single-stage axial turbine through an inlet scroll and then the gas flowed through an annular diffuser to the alternator drive turbine. The rear bearing compartment was located inside the exit diffuser downstream of the turbine. The rotor was of drum construction with the turbine blades and disk integral.

A. Mechanical Arrangement

The first consideration in the mechanical design of the turbine-compressor rolling-element bearing system was the location of the bearings. The gas bearings designed under Contract NAS3-4179 were located at the compressor inlet and between the compressor and the turbine. The compressor inlet was also a logical location for one of the rolling-element bearings. The shaft diameter required between the compressor and turbine to maintain shaft stiffness would require a large bearing operating at high speed with high parasitic loss. Also, seals would be required on both sides of the bearing with the bearing located between the compressor and turbine. Therefore, a straddle-mounted arrangement with bearings outboard of the compressor and turbine was selected.

The space available at the turbine discharge was limited. The exit duct was revised to provide more space and to provide a bearing mount arrangement with a long thermal path from the hot turbine discharge gas. The turbine rear bearing was mounted on a shaft extension to aid in the thermal isolation of the bearing compartment. A coupling was introduced in the compressor end of the shaft to permit fabrication and assembly of the unit.

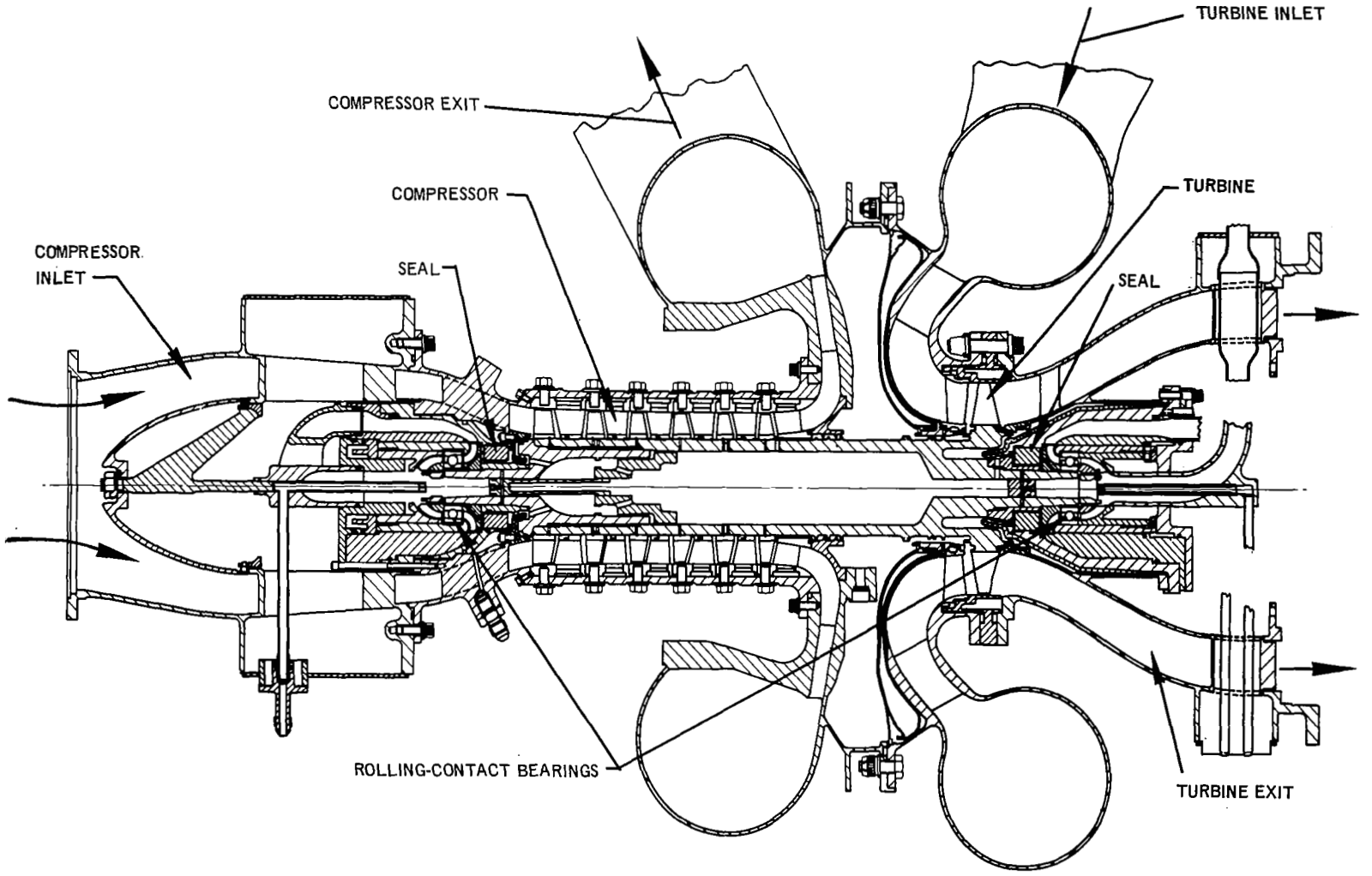

Figure 46 Brayton-Cycle Turbine-Compressor with Rolling-Contact Bearings

The front bearing was mounted on a separable extension of the shaft. The two bearing compartments were similar in design. Each contained a counterbore angular-contact ball bearing lubricated by a mixture of oil mist and argon, and cooled by oil supplied through the shaft and flowing through grooves in the inner race of the bearing. The cooling oil passed through the rotating sealplate to cool the face seal. The oil and the oil-argon mixture were pumped from the bearing area by impeller blades on the back surface of the sealplate. The bearings were supported by an oil film in a small annular gap in the bearing housings. This oil film provided squeeze film support and damping. This method of support also permitted axial motion of the front bearing housing which was spring-loaded. As a result, the bearings were preloaded in thrust to assure skid-free operation under all conditions.

B. Critical Speed Analysis

Analysis of the rotor system was particularly important to determine the resonant modes of shaft vibration (critical speeds).

The dynamic motion of the mechanical system consisting of a rotating assembly, its bearings, seals and bearing support structures was analyzed. The facets of the rotor dynamics considered were the rotor system resonant frequencies, the dynamic shaft displacements due to rotating unbalance, and the resultant bearing loads. In addition, aspects of seal performance and bearing installation and preload were considered relative to the rotor mechanical characteristics.

There were two essentially rigid-body critical speeds below the design operating speed of 50,000 rpm and a bent-shaft (free-free) critical speed above the design speed, Figure 47. In order to provide reasonable margin above the design speed, a bent-shaft critical speed above 70,000 rpm was selected as a design criterion. To meet this criterion the stiffness of the bearing and its support should be above 60,000 pounds/inch. Also an upper limit of 40,000 rpm was selected as the design criterion for the rigid-body critical speed which restricts the bearing and mount system spring rate to less than 160,000 pounds/inch.

Examination of the critical speed map shows that the operating speed of 50,000 rpm is near the second critical mode when the rotor is supported with an effective bearing springrate of approximately 250,000 pounds per inch, corresponding to the turbine-compressor ball bearings. The ball bearing springrate characteristics are shown in Figures 48 and 49 as a function of load and speed. The ball bearings require a minimum thrust load of 30 pounds to provide a small skid margin. To obtain the minimum dynamic response amplitude at the design speed, the spring and damping characteristics of the rotor support

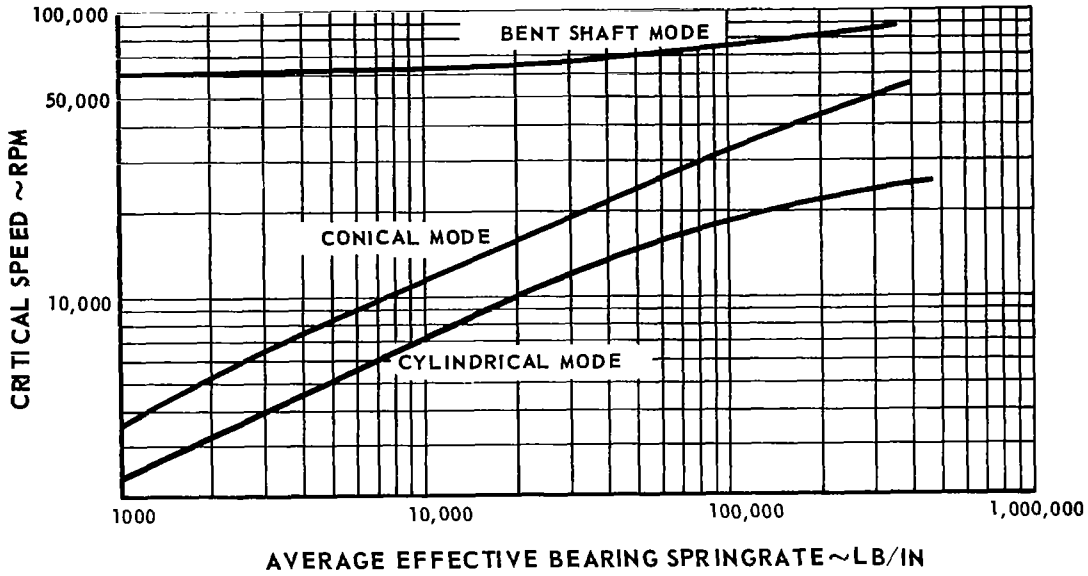

Figure 47 Critical Speed Map for Turbine-Compressor

system must be selected to provide critical speeds which are well removed from the operating speed. The problem then, of designing a rotor support is to select a method which will provide the required bearing-support springrate and damping as well as provide axial movement to accomplish bearing thrust loading.

Analysis of possible methods of providing the required rotor-support springrate, damping and bearing thrust load led to the selection of an oil squeeze film type of bearing support. The configuration of this support is shown in Figure 50. The outer race of the bearing is mounted in a nonrotating cylindrical member. The oil-support film is contained in the controlled clearance between the outside diameter of the cylinder and the bore of the compressor case. Radial forces from the rotor are transmitted through the ball bearings and support cylinder to the squeeze film. The oil film provides a nonlinear support as well as damping. Coil springs located at the end of the cylindrical member in which the bearing is mounted provide the necessary bearing preload. This feature also provides for axial movement of parts due to thermal expansion. The combination of the squeeze film and the spring loading into one assembly provides a relatively simple design.

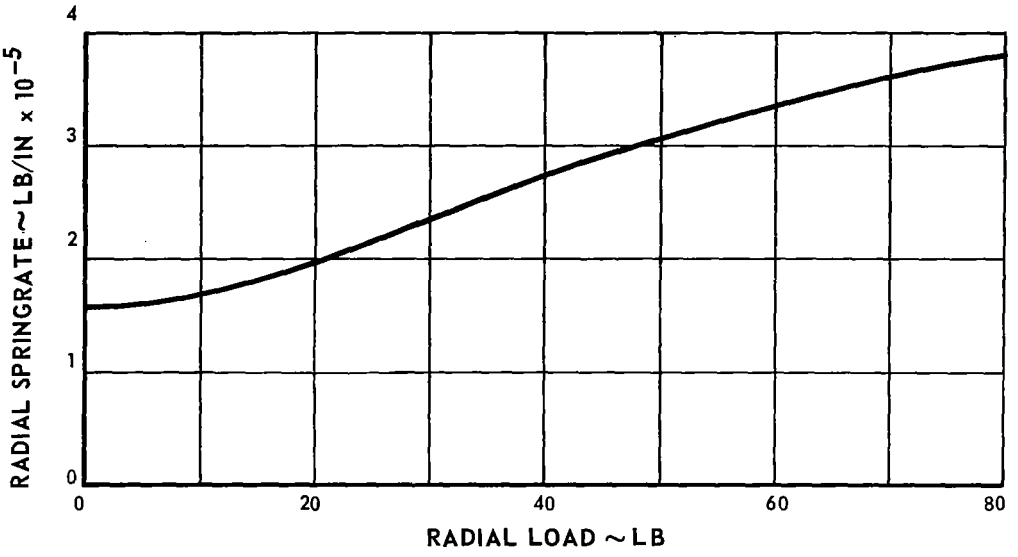

Figure 48 Turbine-Compressor Bearing Radial Springrate vs Radial Load at 50,000 rpm and Thrust Load of 30 lb

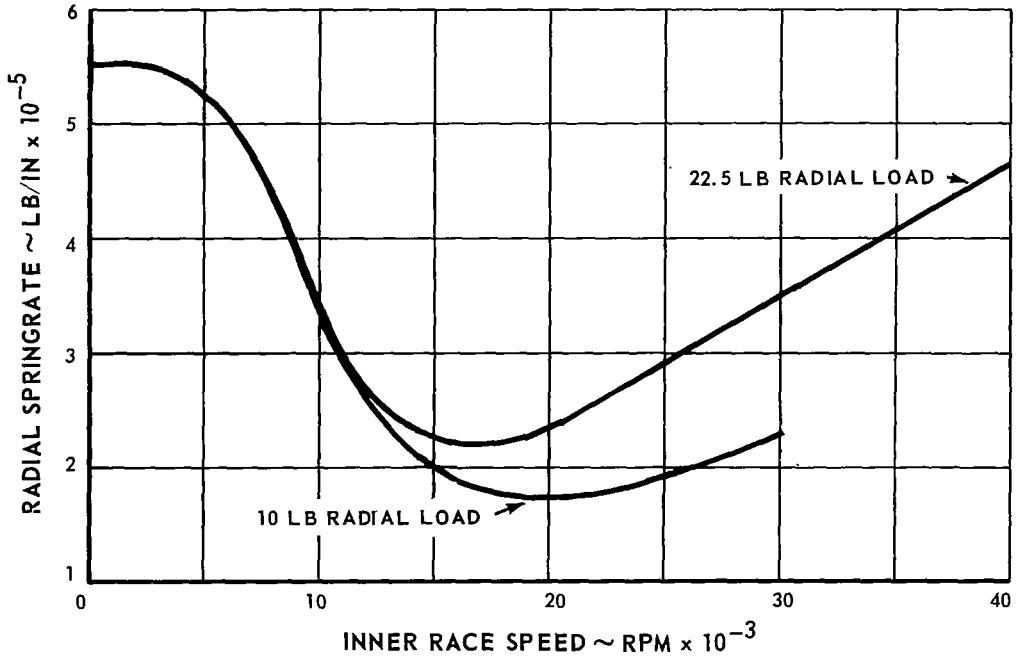

Figure 49 Turbine-Compressor Bearing Radial Springrate at Thrust Load of 30 lb vs Inner Race Speed

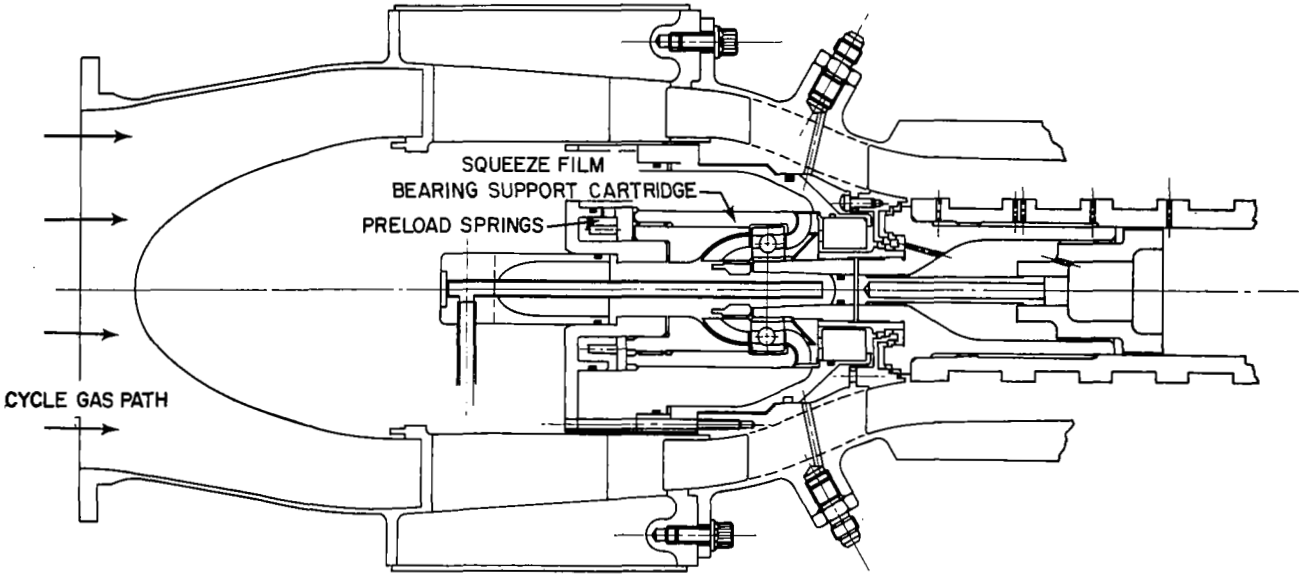

Figure 50 Turbine-Compressor Front Bearing Section

The dynamic rotor response characteristics at the turbine-compressor rear bearing, the most critical location, are shown in Figure 51. The total deflection is due to the deflection in the ball bearing and the oil squeeze film. The overall springrate of the rotor support consists of the springrate of the ball bearing and the oil squeeze film which operate in series. As shown on the curve, the total movement of the rotor at the rear support is less than 1 mil at 50,000 rpm with 0.002 ounce-inch unbalance which is the maximum amount of unbalance anticipated at the end of 10,000 hours of operation. The effectiveness of the oil squeeze film in reducing the overall rotor-support springrate to obtain critical speed margins is shown by Figure 52. This curve of the relationship of rotor speed to critical speed indicates that the oil film support provides a system having a safe margin between the operating speed of 50,000 rpm and the second and third critical modes.

As can be seen from the results of Figure 52, and by referring to the critical speed map of Figure 47, the effective rotor support springrate with the squeeze film is near 100,000 pounds per inch instead of near 250,000 pounds per inch, the rate with the bearings alone.

C. General Mechanical Design

The rear bearing was shifted axially along the shaft and the envelope increased in size radially to provide a cooler and larger bearing cavity, Figure 53. These changes necessitated a slight refairing of the turbine exhaust duct which should not influence the performance of the duct.

In order to reduce the heat flow from the ductwork surrounding the cavity, it was necessary to install a thermal barrier. As indicated in Section III above, more oil was circulated through this cavity than through the front cavity to aid in controlling the temperature of bearing and seal. The expected temperature pattern of this region is shown in Figure 54. Examination of this figure shows that the temperature of the bearing inner race was 371°F and that of the outer race 391°F. Also the temperature of the seal was estimated to be 430°F. Additional cooling and insulation could be added if necessary.

Installation of the squeeze film bearing support was similar to that at the front bearing location. The major difference was that the thrust load for this bearing was obtained from the springs located in the front bearing position. The inner race was attached to the shaft in compression with a nut. Thrust was taken through the inner race and through the balls to the outer race. The outer race was inserted in the squeeze film cylinder which was supported in the compressor case.

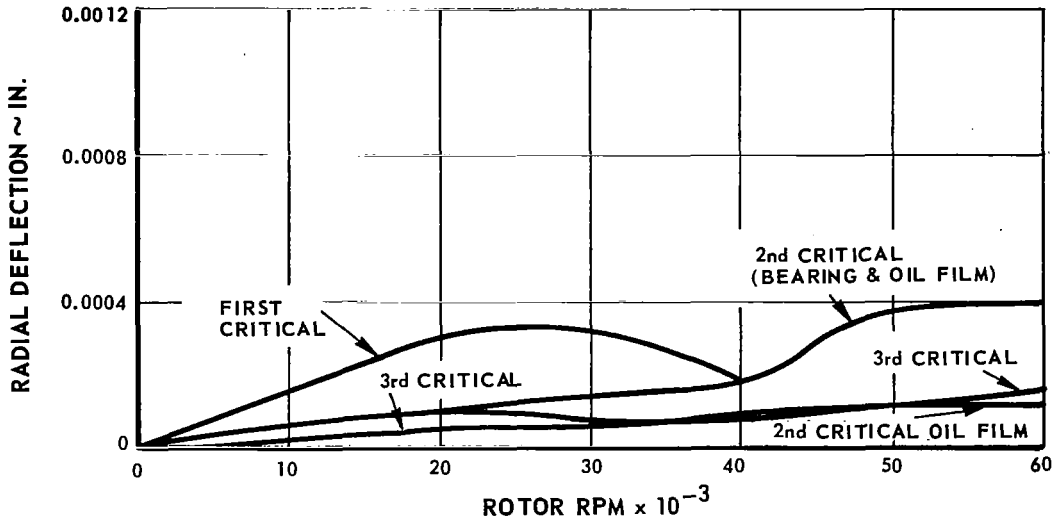

Figure 51 Dynamic Rotor Response at Turbine-Compressor Rear Bearing

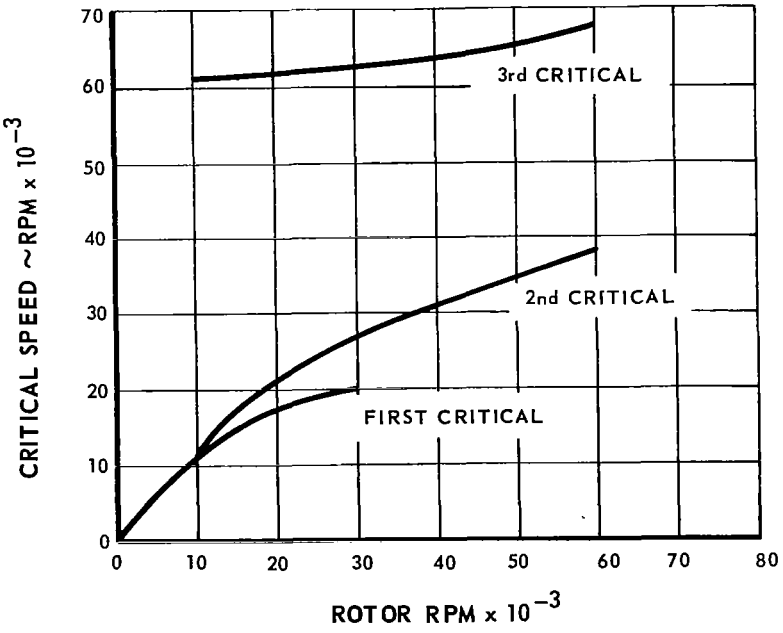

Figure 52 Relationship between Rotor Speed and Critical Speed for Turbine-Compressor with Squeeze Film Support

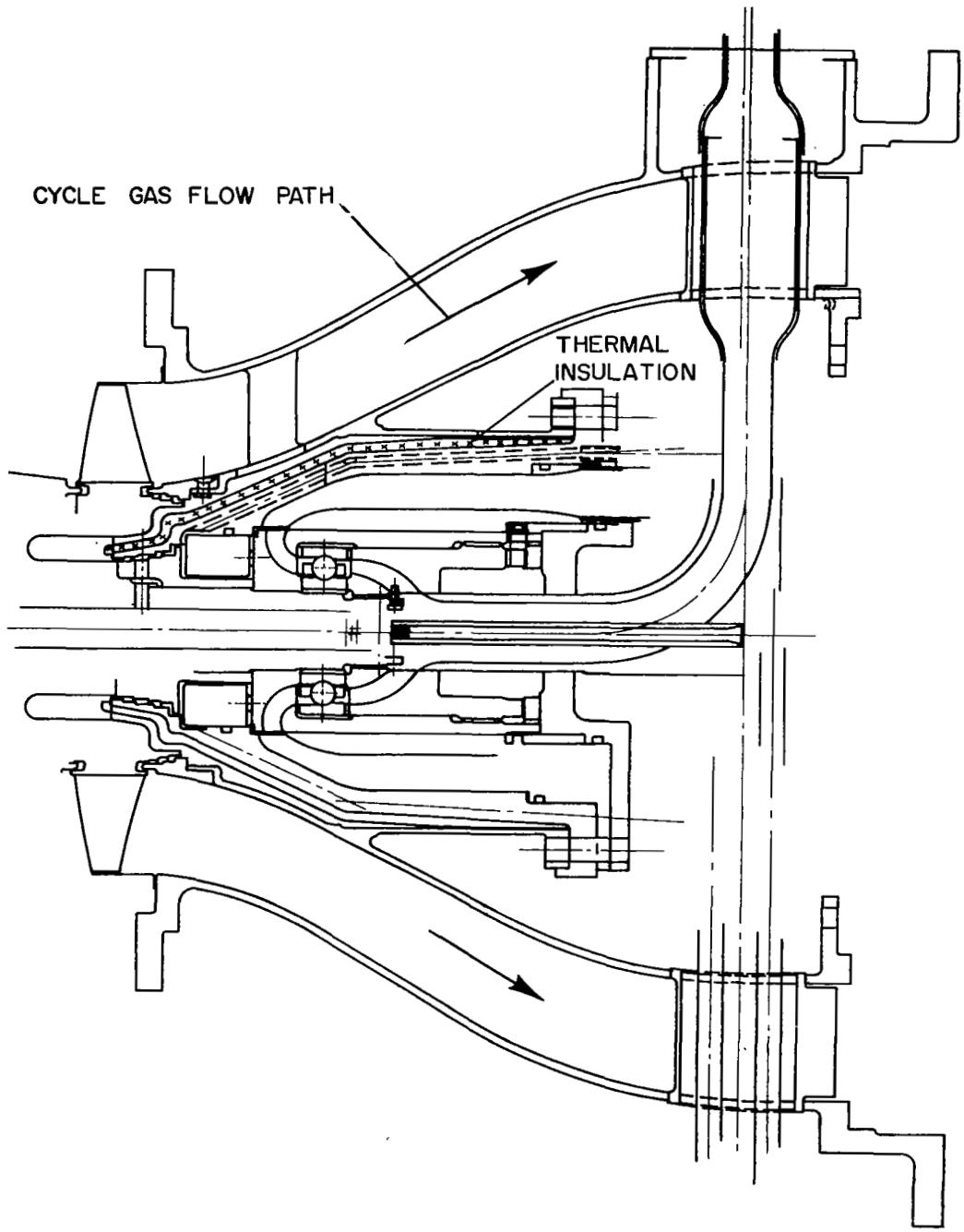

Figure 53 Turbine-Compressor Rear Bearing Section

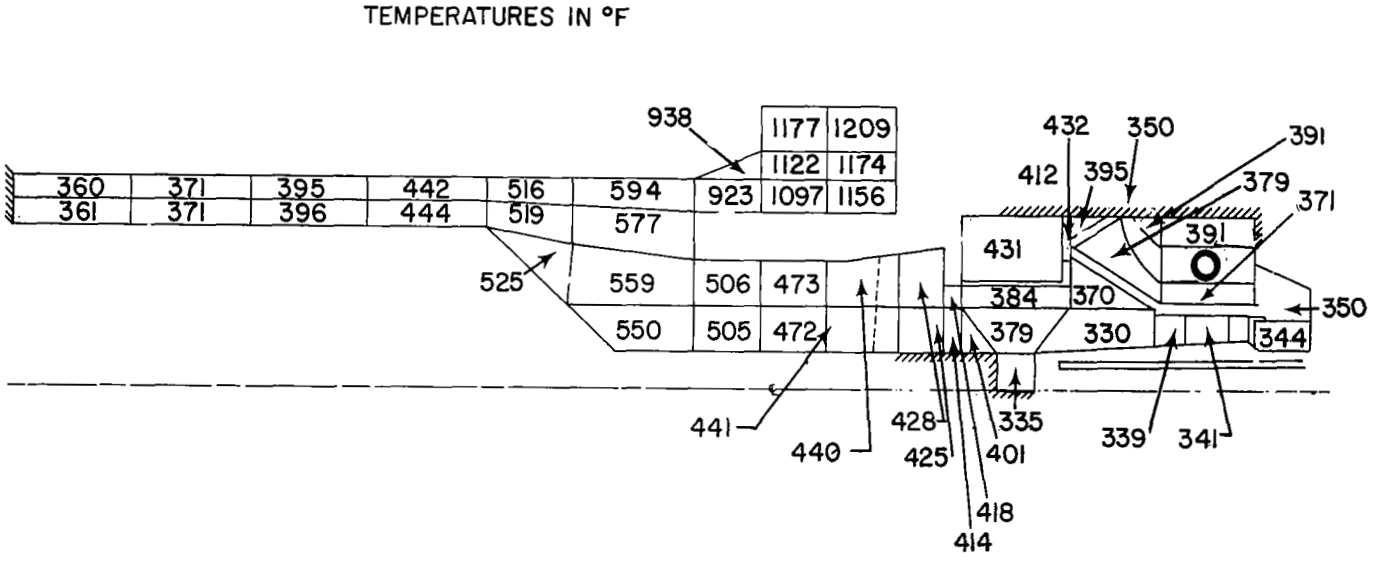

Figure 54 Typical Temperature Pattern in Turbine-Compressor Rear Bearing Region

Oil was introduced to the bearing via a small pressure tube located concentric with the rotor. As discussed in Section III above, the oil was pumped radially outward underneath the bearing race and then out through the sealplate. Gas was fed into the cavity in a tube surrounding the oil supply tube. This oil-laden gas was pumped through the bearing. The cooling oil flow and oil-laden gas joined in the sealplate impeller and were then discharged into the scavenge line.

Of necessity, there were some differences in mechanical arrangement between the rolling-contact bearing turbine-compressor and the gas-bearing version. The most significant was the method of fixing the axial location of the shaft. In the gas-bearing configuration, the thrust bearing was located at the compressor inlet, while in the rolling-contact bearing unit the axial position of the shaft was fixed by the ball bearing at the turbine discharge. Since preloaded ball bearings were employed, the spring-loaded bearing must be free to move axially to accommodate differences in thermal expansion and thermal transients. The limited space available restricted the location of the spring to the upstream side of the bearing in the front position, and the downstream side in the rear position. The turbine-compressor might be installed in the launch vehicle in the vertical position with the compressor end up. During launch, even though the rotor were stationary, the bearings must maintain the rotor position. Since accelerations of up to 4.6 g were anticipated, the bearings would have to support a thrust load of about 54 pounds. If the spring which preloaded the bearing were at the turbine discharge, and if the spring had a low spring rate, the thrust on the rotor would be supported on the counterbore side of the front bearing. Since only a very small shoulder existed on the counterbore side of the outer race to permit assembly of the bearing, this launch load might damage the bearing. Therefore, the bearing preload springs were applied to the front bearing and the rear bearing was fixed. With the shaft located axially at the turbine exit, the axial clearances in the compressor were examined. With a nominal axial clearance of 0.080 inch cold, the minimum axial clearance in the compressor was 0.030 inch due to thermal transients and tolerances.

The radial position of the shaft was fixed by different techniques in the rolling-contact bearing turbine-compressor compared with the gas-bearing design. In the gas-bearing machinery, proximity probes were included and the radial positions of the bearings were adjustable. Therefore, the bearings could be adjusted after assembly to center the shaft based on the probe data. No provisions for bearing radial position adjustments were included in the rolling-

contact bearing version. In this version, the bearing outer housing was supported by a thin oil film and rotor excursions of about 0.0004 inch were predicted from the dynamic analyses. The number of fits between mating parts was different in the two designs and allowance must be made for the tolerance buildup as a result. The radial clearances of the labyrinth seals and blade tips were examined for the rolling contact design and clearances 0.001 to 0.002 inch larger were required, depending on location, than were required in the gas-bearing turbine-compressor.

The materials selected for the rolling-contact bearing version of the turbine-compressor were identical with the gas-bearing version as far as possible. For example, the turbine and integral shaft was the same high-temperature nickel alloy in both cases. The use of the same materials in both designs was important for maintaining interchangeability and in order to restrict the areas requiring redesign. Where new selections were required in the bearing areas, the materials were selected for suitability for the function and compatibility and fit with adjoining parts. The calculated rotor weight in the oil-bearing design is slightly higher than in the corresponding gas-bearing design: 11.73 and 10.64 pounds, respectively.

In the gas-bearing version of the turbine-compressor, the significant stresses were analyzed. The rolling-contact bearing version of this unit employed many of the same parts subjected to the same conditions as in the gas-bearing configuration. Therefore, the stresses were identical and the design margins the same. A number of areas were modified to accommodate the rolling-contact bearing rotor-support system and a summary of significant stresses in these areas is presented in Table 10. The allowable stress presented in Table 10 is generally the yield strength of the material. However, in the compressor drum the allowable stresses were based on burst considerations, while creep was the criterion in the turbine.

TABLE 10

Turbine-Compressor Significant Stresses

Part	Material	Allowable Stress, psi	Calculated Stress, psi
tie bolt	AMS-5660	100,000	12,700
compressor drum, 1st stage	PWA-1007	119,300	32,500
compressor drum, 2nd stage	PWA-1007	118,600	29,250
compressor drum, 3rd stage	PWA-1007	117,300	26,250
compressor drum, 4th stage	PWA-1007	116,600	26,000
compressor drum, 5th stage	PWA-1007	115,900	26,000
compressor drum, 6th stage	PWA-1007	115,200	25,900
turbine disc, front	PWA-1007	115,000	98,000
turbine disc, rear	PWA-1007	110,000	88,000
bearing retainer nut	AMS-6304	130,000	3,700
bearing housing	AMS-6304	130,000	15,400
bearing thrust springs	AMS-5688	100,000	52,600
main shaft flange	AMS-5660	100,000	13,700
main shaft spline	AMS-5660	100,000	11,000
main shaft hub	AMS-5660	100,000	10,200

D. Bearing Analysis and Design

The objective in the design of bearings for the Brayton-cycle turbine-compressor was to provide a rotor support that would achieve a B_1 failure rate (1.0 percent) or lower for 10,000 hours with minimum power consumption and wear. The shaft diameter between the turbine and the compressor was approximately 50 mm which would result in a bearing DN (the linear speed of a bearing is usually defined as the product of the bore diameter, D, in millimeters and the shaft rotational speed, N, in rpm) of at least 2.5×10^6 at the design speed of 50,000 rpm, if a bearing were located between the turbine and compressor. To avoid this unreasonably high linear speed, a straddle-mounted concept was selected and the choice of bearing diameter became somewhat independent of shaft size. To preclude skidding which could occur in a lightly-loaded high-speed application such as this, the choice was made to incorporate two ball bearings to support the rotor, thrust-loaded against each other by springs,

rather than a ball bearing at one end and a roller bearing at the other. The turbine-compressor bearing arrangement is presented in Figure 46.

Having established the rotor-bearing arrangement configuration and envelope limitations, the selection of bearing size and geometry depended on three major factors: fatigue life, friction losses and skidding tendencies. In designing for long fatigue life, large bearings are normally selected. Fatigue life is usually improved with tight race curvatures and, in the case of pure thrust loading, high design contact angle. Unfortunately the skidding tendencies are increased by these factors as well. Also, large sizes, large contact angles and tight curvatures result in high levels of heat generation. Thus, the final bearing design is a compromise between long fatigue life on the one hand and low skidding characteristics and frictional power loss on the other.

Studies were conducted using digital computer techniques to evaluate the tradeoffs between bearing life, skidding margin and geometry. Power consumption, lubrication, installation, fabrication, and metallurgical factors were also considered. The life of bearings of various diameters was examined at the design speed of the turbine-compressor (50,000 rpm) with a combined radial and thrust load. A 20-pound radial load was selected as representative of the maximum radial force anticipated due to mechanical unbalance in the rotor at the end of 10,000 hours of operation. The minimum thrust load to assure operation without skidding was employed for each bearing size, and this value of thrust increases as the bearing size is increased. The results of these calculations are summarized in Figure 55, which presents bearing life as a function of size. In addition, the effects of misalignment of the shaft from 0 to 0.0005 radian on bearing life are included. While misalignments as large as 0.0005 radian are not anticipated, the bearing life would not be affected appreciably by such a misalignment. Bearing life increases as the bearing size is reduced, primarily because the linear speed of the bearing is reduced and the skid-free thrust load is reduced.

The predicted friction heat generated by bearings of various sizes with mist lubrication is presented in Figure 56. The lowest friction losses occur with the smallest bearing. Therefore, for a design with a thrust load to avoid skidding, the smallest bearings provide the longest life and lowest heat generation. The mechanical design of the bearing compartment indicates that difficulty would be encountered in providing the lubrication and cooling system for bearings of less than 20 mm bore. Therefore a 20 mm bore diameter bearing was selected.

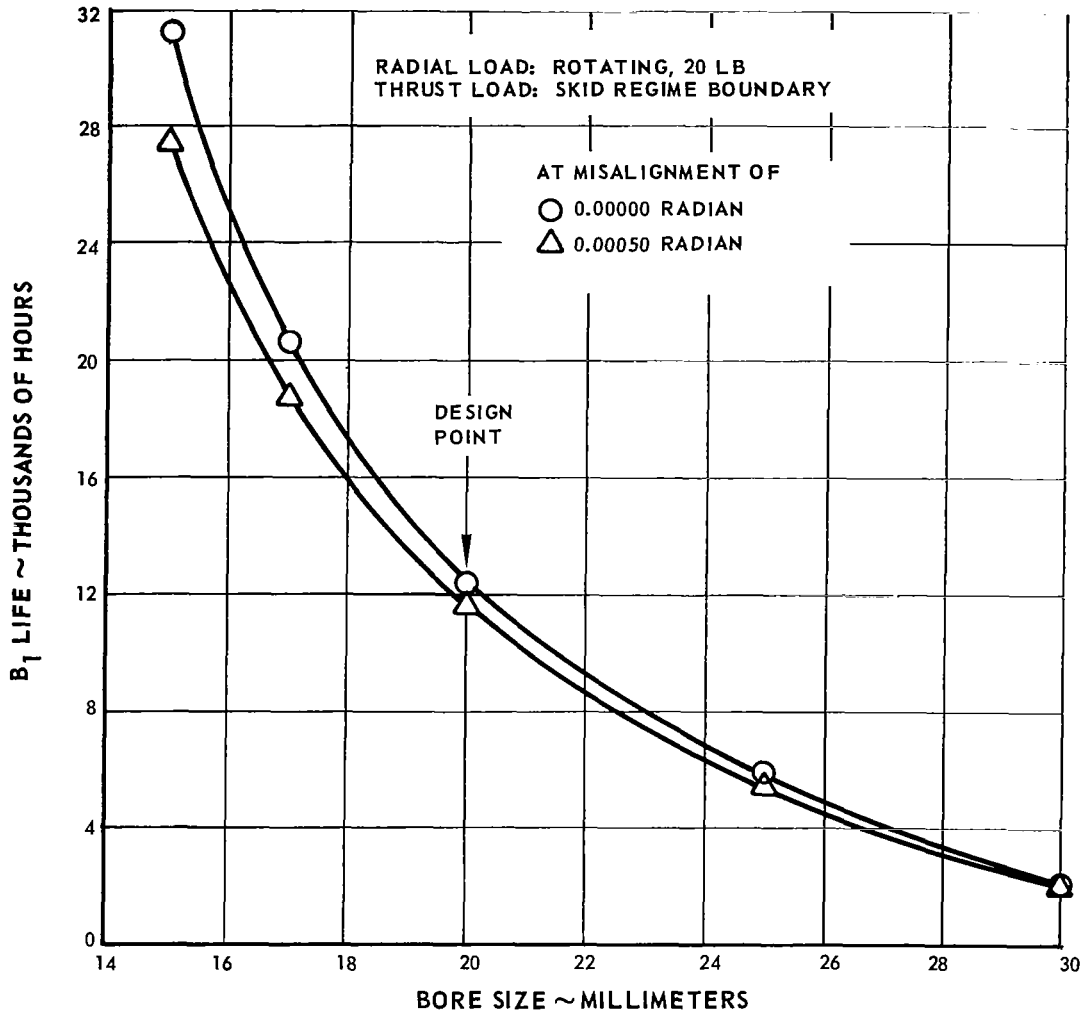

Figure 55 Bearing B_1 Life vs Bore Size

The results presented in Figure 55 include a ball diameter variation consistent with the standard extra-light series of bearings. The study included an examination of various ball diameters for 20 mm bore bearings and the results are presented in Figure 57. The life of the bearing improves as the ball diameter is reduced as a result of smaller centrifugal effects and the associated lower skid-free thrust loads. The 0.250-inch diameter ball was selected for this application to avoid excessive sensitivity to misalignment and internal clearance variations. Also, smaller balls would introduce difficulty in the mechanical design of the retainer.

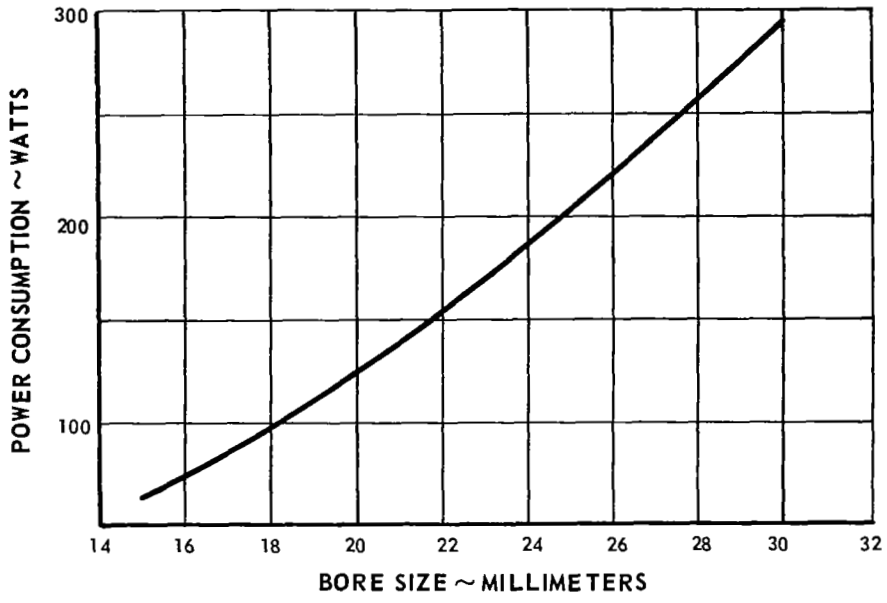

56 Power Consumption vs Bore Size

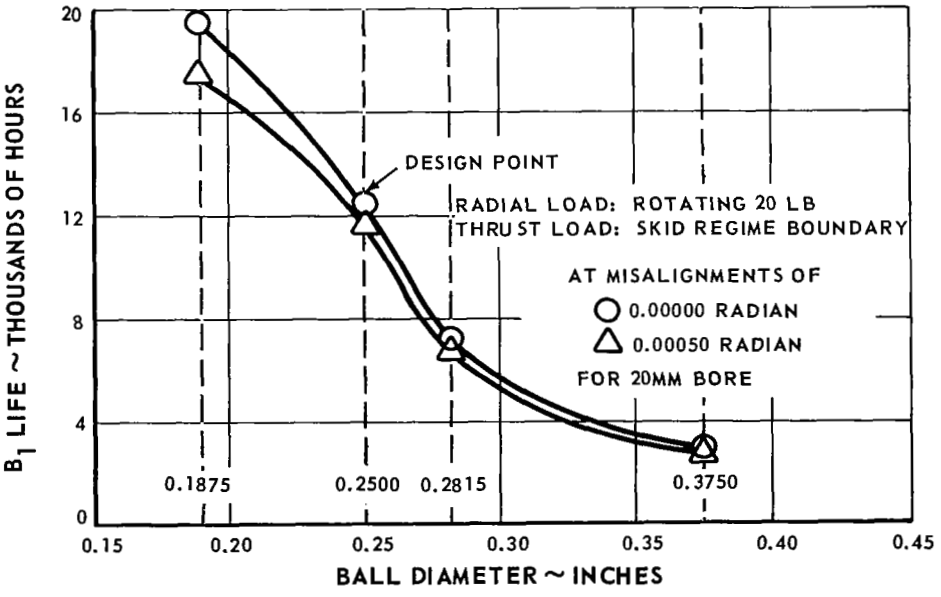

Figure 57 Bearing B_1 Life vs Ball Diameter

The effects of inner and outer race curvatures were examined and the results are presented in Figures 58 and 59. The optimum conformities were 51.75 and 51.83 percent for the inner and outer races, respectively (conformity is defined as the ratio of the radius of curvature of the race to the ball diameter). Fifty-two percent conformity is conventional for high-speed bearings and this value was selected for the turbine-compressor bearings. As indicated in Figures 58 and 59, the selected conformities do not appreciably compromise the bearing life.

The examination of the effects of mounted contact angle on bearing life is presented in Figure 60. The optimum contact angle was 16 degrees. The variation in contact angle with manufacturing tolerances and the effect of this variation on bearing life are also indicated in Figure 60.

With rolling-element bearings in the turbine-compressor, the aerodynamic thrust on the rotor is intended to be balanced. In order to account for possible variations in conditions, a range of aerodynamic thrust from -5 to +5 pounds is considered which produces a total variation of approximately 25 percent in bearing life.

All of the bearing life calculations were performed with a 20-pound radial load which is the maximum unbalance load anticipated at the end of 10,000 hours of operation. The bearing life characteristics with radial load are presented in Figure 61. With no radial load imposed, the bearing life is improved about 21 percent.

The bearing performance characteristics presented in Figures 55 through 61 were calculated at the design condition of 50,000 rpm in a gravity-free environment. These bearings will also be expected to operate with the turbine-compressor on the ground for development testing. If the shaft were horizontal in such a test, the net effect would be an increase in radial load of about 6 pounds on each bearing. An approximate indication of the associated reduction in life can be determined from Figure 61. With a 26-pound radial load, the life of the selected bearing is reduced to 11,000 hours. If the development testing were conducted in the vertical position with the compressor up, the thrust load on the rear bearing would increase by the weight of the rotor - approximately 12 pounds. The resulting B_1 life of the rear bearing is 9,500 hours, which should be satisfactory for development testing.

Since the bearing design objective was to provide maximum fatigue life consistent with low power consumption and the absence of skidding, the choice of bearing materials was carefully reviewed. Traditionally SAE 52100 steel has

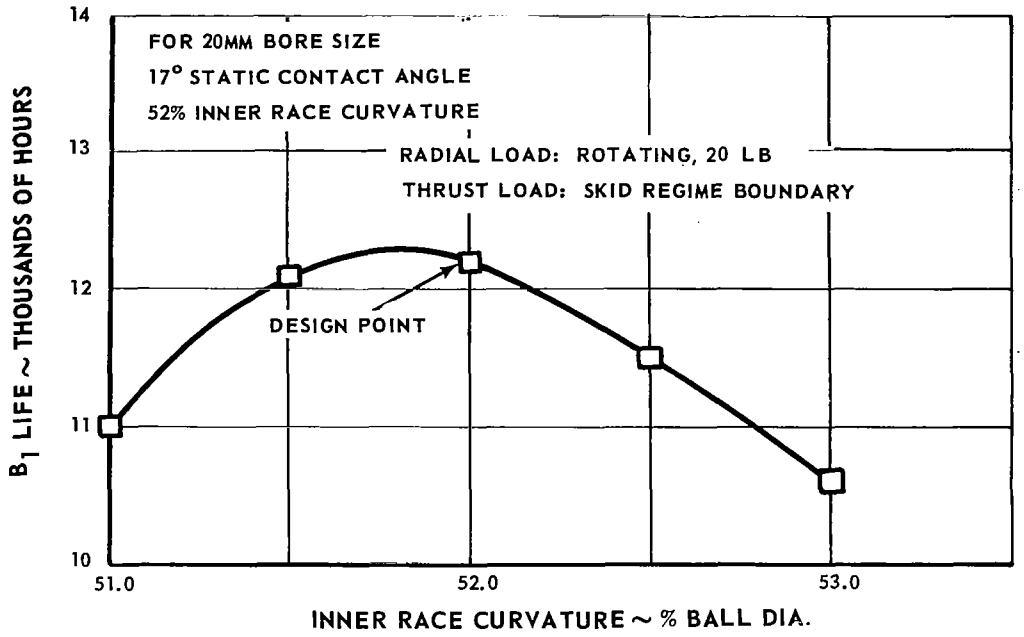

Figure 58 Bearing B_1 Life vs Inner Race Curvature

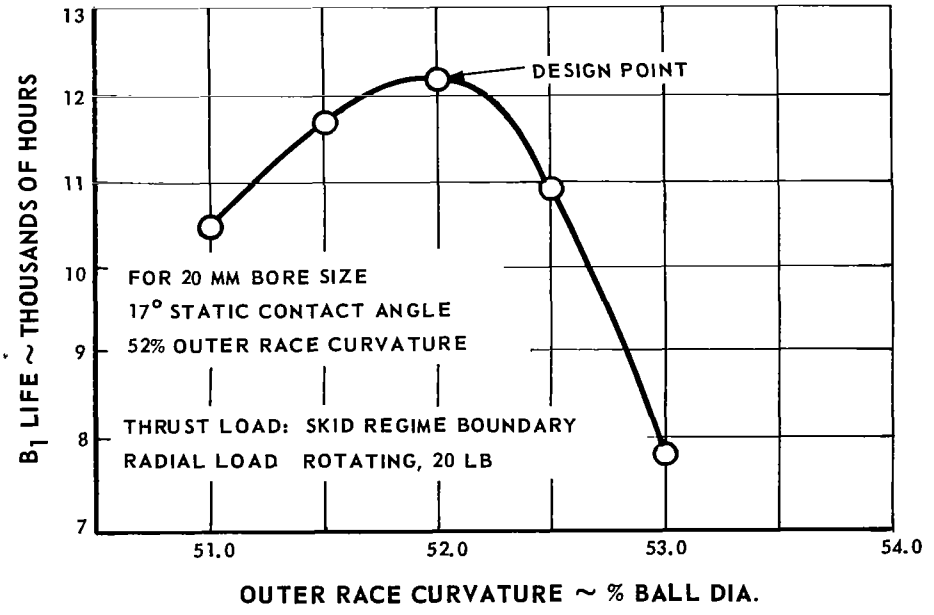

Figure 59 Bearing B_1 Life vs Outer Race Curvature

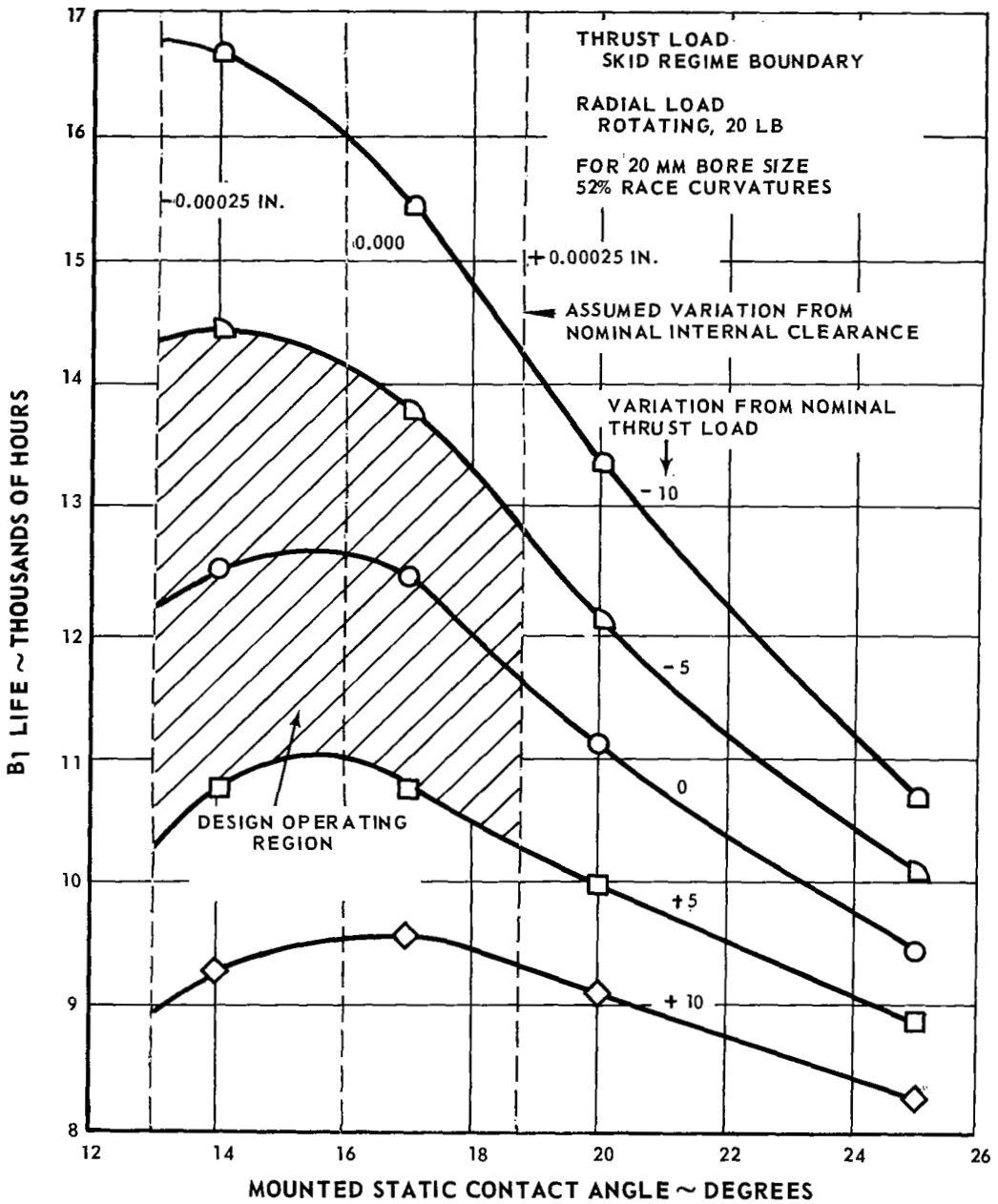

Figure 60 Bearing B_1 Life vs Mounted Static Contact Angle

been the standard bearing material. Developments such as vacuum melting of SAE 52100 have considerably improved bearing fatigue life. Current aircraft turbine engines require better properties than SAE 52100 offers and considerable experience has been accumulated with better bearing materials.

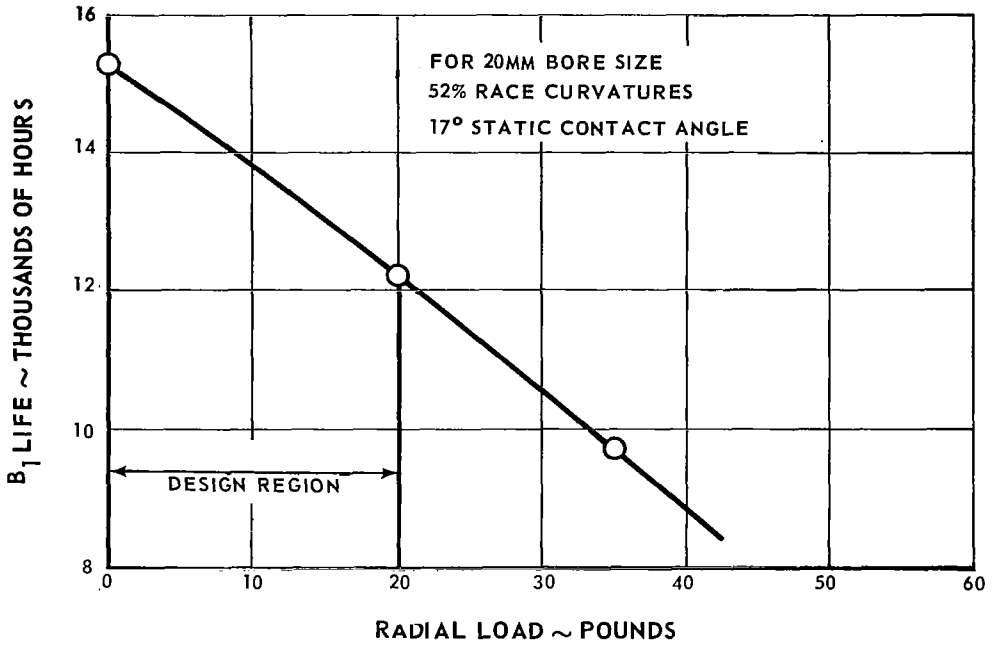

Figure 61 Bearing B_1 Life vs Radial Load

Consumable-electrode vacuum-melted M-50 tool steel has demonstrated superior fatigue life and is currently being specified for many of these high performance applications. Because of this favorable experience M-50 tool steel was specified for the turbine-compressor bearings.

The bearing life estimates included modifications to the usual AFBMA calculations based on experience in high speed application. These modifications accounted for the detrimental effect of centrifugal force on the balls and the advantageous effects of increased resistance to fatigue and narrower distribution of failure lives which is characteristic of the vacuum melted M-50 steel bearings. The estimated B_1 life at nominal design conditions was 12, 600 hours.

Experience has shown that for high-speed long-life applications such as the Brayton cycle, the ball retainer designs must be of one-piece fully-machined construction to achieve high strength and fine balance. An inner race riding retainer was selected because of the extensive experience with this configuration, the better bearing tolerance for short interruptions of oil flow, and the ability of the inner-race oil cooling to remove the heat generated in the retain-

er-race bearing area. Since a one-piece retainer was selected, the only bearing configurations that could be used were the counterbore type or the split inner-ring type. The risk in the split inner-ring configuration is that the ball-race contact ellipse may extend to the chamfer at the split on the inner race. If this were to occur, the stresses in the contact zone would be significantly increased and the bearing life would be reduced accordingly. The variation in mounted contact angle resulting from allowable internal tolerances is shown in Figure 60. While the calculations indicate that the ball would not ride on the chamfer at the split, some transient radial load might produce such a condition. Therefore, the counterbore configuration, which employs a solid inner ring, was selected.

In summary, the bearing selected and recommended for the turbine-compressor was a 20 mm-bore extra-light series ball bearing constructed of M-50 steel with a one-piece cage. The selected bearing design requirements are as follows:

Bearing Type	Angular contact ball bearing with counterbore outer race
Operating Conditions	Thrust load: 30 pounds Rotating unbalance radial load: 20 pounds maximum at 50,000 rpm
Oiling System	Mist lubrication Axial cooling slots on bore of inner ring
Heat Generation	125 watts/bearing
Bearing Size	20 mm bore diameter 44 mm outer diameter 12 mm wide
Internal Geometry	11 balls of 0.2500 inch diameter 1.288 inch pitch diameter (slightly larger than standard extra light dimensions) 16° nominal mounted contact angle at operating fits and clearances 52 percent inner and outer race conformity 10 percent shoulder height on the loaded half of outer race 20 percent inner-race shoulder height

E. Seal Design

The basic sealing concept for all bearing compartments consisted of two labyrinth seal assemblies adjacent to a face seal. High-pressure argon fed between the labyrinth seals provided a pressure differential across the face seal and provided a purge for oil that might leak past the seal. This pressure differential aided in containing the oil within the lubrication system. This feature also provided a buffer zone between the cycle gas and the bearing and seal cavities, to reduce cycle gas contamination. A system was provided to recover, clean up and re-use the bleed gas as well as the gas which leaked past the seals.

The primary consideration in designing face seals for this application was to weigh the performance characteristics of several possible designs against the complexity and degree of risk involved. Seal configurations considered minimized oil leakage, gas leakage and power consumption consistent with the Brayton-cycle power system durability and reliability for long-term operation.

Four seal designs were considered in detail for possible evaluation and use in the turbine-compressor. All four designs had the same overall envelope to permit interchangeability during evaluation and eventual use. A further requirement of these designs was to restrict oil leakage from the bearing compartment at shutdown. Each design became a positive-contact seal at shutdown. The designs can be categorized as 1) dry-face, 2) wet-face, 3) gas-lubricated, and 4) controlled-clearance.

1. Dry-Face Seal

The design selected for the basic evaluation of a dry-face contact seal is shown in Figure 62. The selection of design parameters for a rubbing-contact face-seal must begin with the choice of seal diameter and interface contact load and pressure. The seal diameter was made as small as possible to achieve the lowest power consumption and leakage with greatest durability. A mean seal face diameter of 1.53 inches was chosen to avoid undue restriction of the shaft outside diameter, resulting in a mean rubbing velocity of 335 ft/sec. To provide the most positive protection against oil leakage across the contact face, the choice was made to have the oil at the outer edge of the rotating interface so that any leakage had to oppose the centrifugal force of the rotating members.

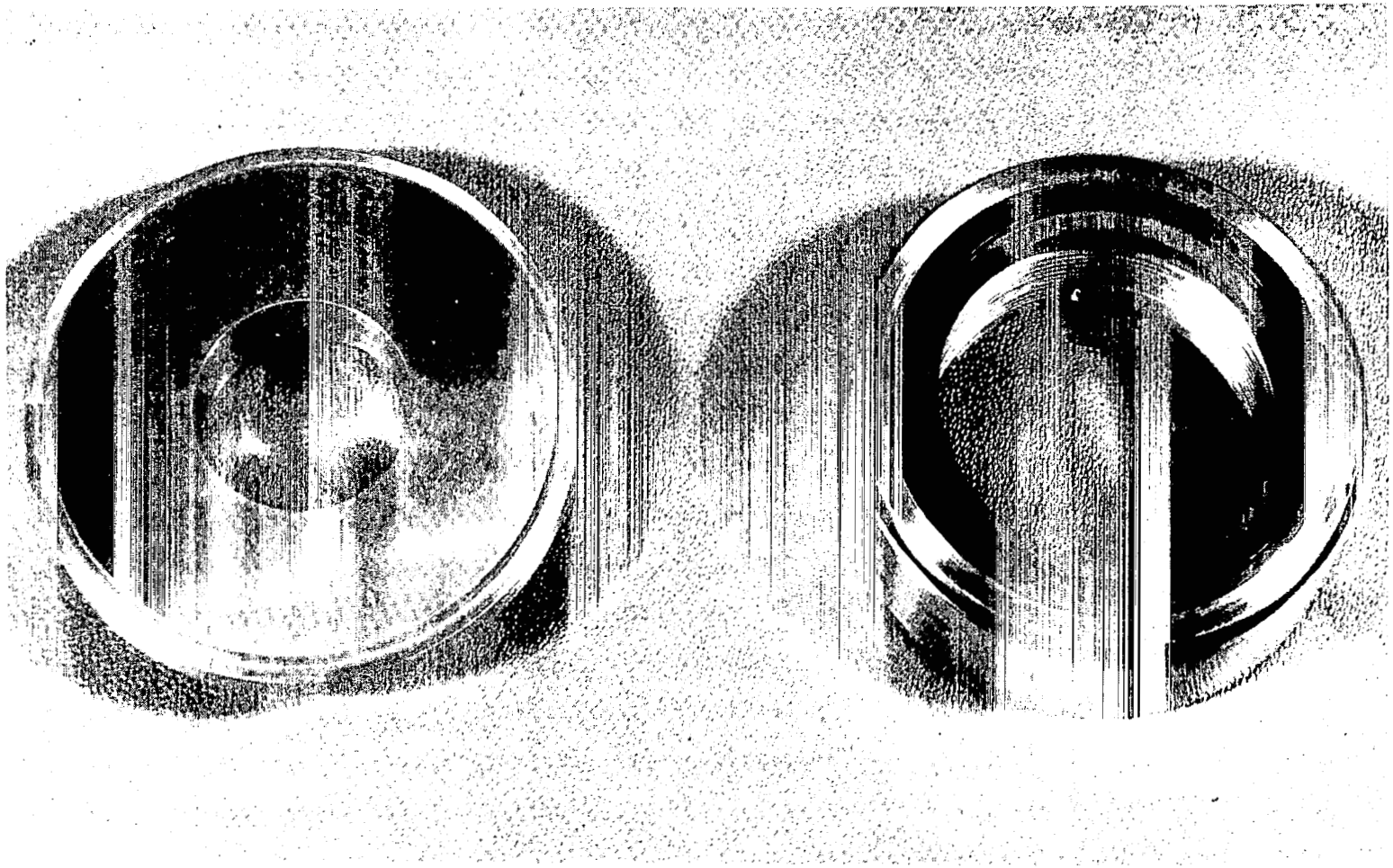

Figure 62 Dry-Face Seal and Sealplate M-44047

The choice of minimum seal contact load was a function of seal dynamics, minimum practical seal lip width, and minimum practical contact pressure for effective sealing. For the seal diameter selected and a seal face runout of 0.0005 inch FIR, the maximum acceleration of a point on the seal was 18 g. The weight of the seal assembly which must respond to the sealplate runout was a maximum of 0.065 lb. The minimum allowable load on the seal interface was the product of 18 g and 0.065 lb or 1.2 lb. The minimum practical seal lip width based upon experience is approximately 0.080 inch. The contact pressure on the seal face at 1.2 lb load was 3 psi which is a minimum value for general practice.

The choice of maximum seal contact load was largely a function of seal power consumption and durability. The value of 2.25 lb selected resulted in a maximum power consumption of 200 watts at a coefficient of friction of 0.2. Seal wear rates are extremely difficult to predict but an allowance of 0.030 inch was considered adequate based upon experience obtained on a wide variety of installations.

The difference between the 1.2 lb and 2.25 lb limits, when divided by the bellows springrate, represents the total seal travel allowance for wear and rotor-frame displacements.

The choice of bellows springrate, however, was largely dictated by space restrictions and the maximum pressure differential. The pressure and diametral restrictions dictated the use of a 0.003 inch bellows wall thickness. Eleven full convolutions were selected to provide a bellows stiffness of 21.2 lb/inch which provided a satisfactory springrate without placing serious demands on the space restrictions. A circumferential spring-loaded strip applied to the outside of the bellows convolutions provided damping and has demonstrated improved performance in other applications.

The choice of seal materials for this design was based upon experience. Current engine applications demonstrate excellent performance with sealplates of AMS-5613 hardened to a Rockwell C of 30-38, with a hard facing coating of chrome carbide bearing against CDJ-83 carbon. Both the sealplate and carbon ring flatness and surface finish are held to close tolerances.

The above physical dimensions and characteristics can be controlled to close tolerances in a dry-face contact design such as this and where the sealplates and bearings are adjacent to each other.

TABLE 11

Dry-Face Seal
Operating Conditions and Requirements

shaft speed, rpm	50,000
pressure differential at design point, psi	6 to 11
pressure differential, maximum range, psi	0 to 20
estimated power consumption, watts	200
maximum temperature, °F	400
seal fluids	argon and oil
seal sweep gas, argon, lb/hr	1.4
maximum leakage, argon, lb/hr	0.3

Specifications

Sealplate

material	AMS-5613
hardness	Rc 30-38
face treatment	chrome carbide
finish, multiple lay, microinches RMS	5
flatness, helium light bands	2
cooling holes, 12 equally spaced	0.050 dia.
maximum runout of face, inch FIR	0.0005

Carbon Ring

material	CDJ-83
flatness, helium light bands	2
finish, microinches RMS	4
mean rubbing velocity, ft/sec	335
allowance for wear, inch	0.035

Bellows

type	welded-nested
material	AM-350
number of convolutions	11
springrate, lb/in	21.2

damper, spring-loaded circumferential strip applied to bellows convolutions	
face loading, initial, lb	2.00 to 2.25
face loading, end of life, lb	1.36 to 1.6
minimum face load for satisfactory seal tracking, lb	1.2
fundamental resonant speed of undeflected bellows seal, rpm	3500
axial deflection of seal at operating conditions, inch	held within ±0.006

2. Wet-Face Seal

This type of seal incorporates oil passages through the rotating metallic sealplate which direct oil to the contact area between carbon and the metallic sealplate (Figures 63 and 64). The oil introduced forms a film between the mating surfaces. An anti-weepage annular groove prevents migration of the lubricant into the gas side of the seal.

Negligible wear is expected for the duration of the Brayton-cycle mission if the seal is properly matched to its operating conditions. Jet engine experience with similar seals sealing higher gas pressure dictates a face-loading spring force somewhat greater than that proposed for the dry-face seal.

Power consumption due to hydrodynamic drag on the portion of the seal wetted by the lubricant is inversely proportional to the film thickness. To set an upper limit on power consumption of 200 watts the lubricating film must be 0.0015 inch thick and the spring force determined experimentally to conform to this specification.

For the same conditions, the gas leakage rate was calculated to be 0.1 lb/hr.

Thermal maps were basically unchanged from those of the dry-face seal.

Bellows manufacturing, construction and method of damping would be essentially the same as for the dry-face seal. The carbon face width was increased to 0.200 inch to accommodate the anti-weepage groove and to insure adequate margin on the sealing surfaces.

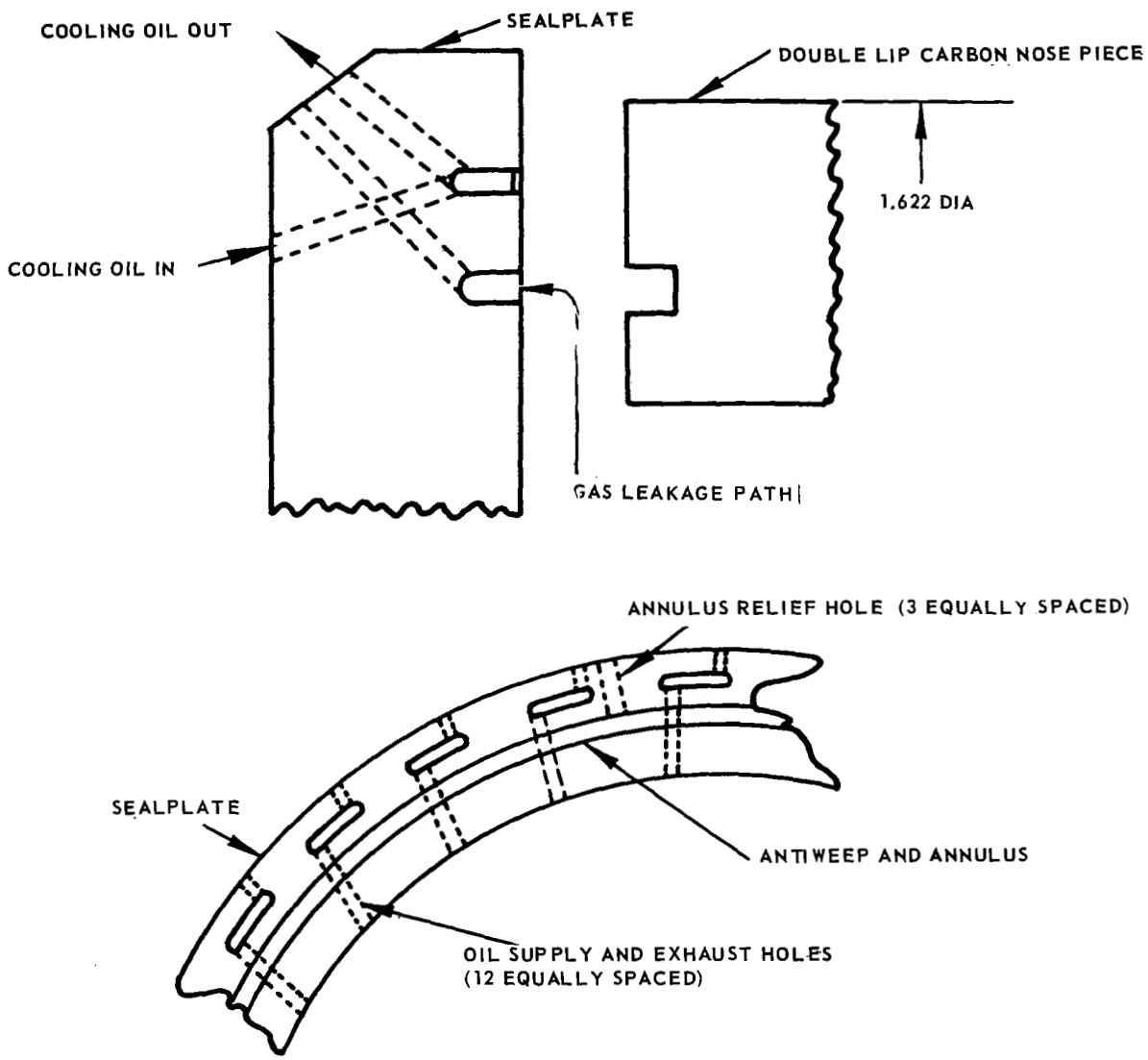

Figure 63 Wet-Face Seal Design

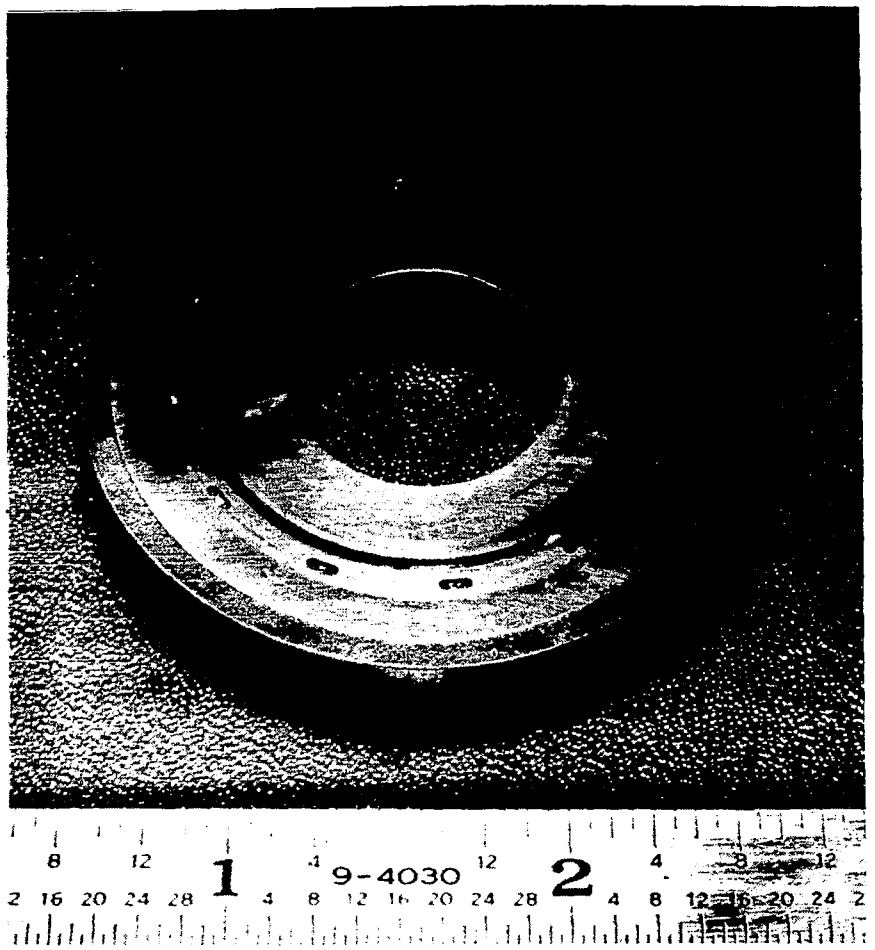

Figure 64 Wet-Face Sealplate M-49737

3. Gas-Lubricated Seal

Hydrodynamic lift with a relatively high film stiffness can be provided in the interface of a close contact seal by a series of spiral grooves machined or etched on one of the mating surfaces (Figure 65).

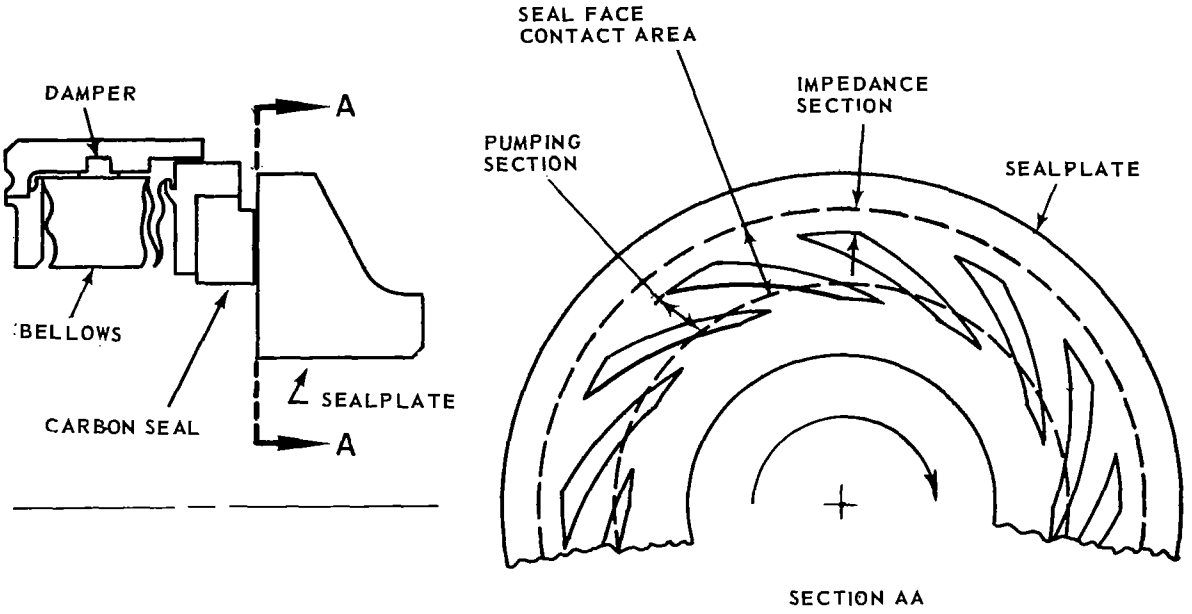

Figure 65 Spiral-Groove Seal

Because hydraulic resistance along the grooves is smaller than across the grooves, a relative sliding motion between the surfaces, in a direction inclined to the grooves, tends to induce flow along the grooves. This flow, because of the inclination of the grooves, has a component normal to the sliding direction. In this manner, the shallow inclined grooves function as a viscous pump. Capillary blockage of the induced flow causes the pressure in the gap to rise above ambient, thereby lifting the carbon away from the sealplate. Pressure gradient in the gap of this type of seal is primarily in the direction normal to that of sliding. Three major variations of annular spiral-groove seals are shown in Figure 66.

Figure 66 Three Types of Spiral Grooves

In the herringbone design two viscous pumps oppose each other. This latter type is not favored, because of its poorly defined performance and its added manufacturing complications.

The following design parameters were chosen for the gas-lubricated outward-pumping spiral-groove seal:

expected film thickness, inch*	0.0003
groove angle, deg.	72
groove depth, inch	0.00094
groove width-over-land ratio	0.65
impedance width, inch	0.061
number of grooves	12

*film thicknesses of 0.0003 to 0.0004 inch are needed to assure adequate margin between resonant frequency and operating frequency

The assumed performance characteristics are shown in Figures 67 and 68. Each individual film thickness represents a different spiral-groove configuration. Materials and general construction of this seal with its bellows secondary would be essentially the same as those of the dry-face seal.

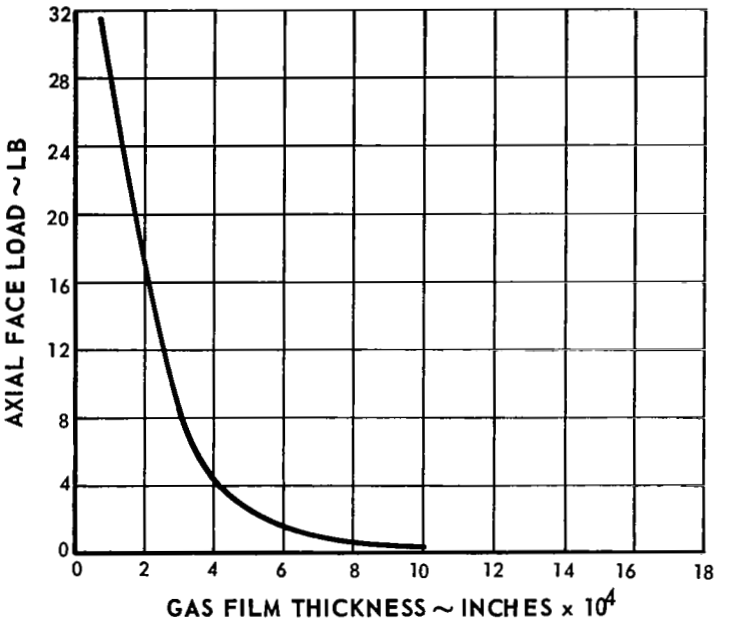

Figure 67 Turbine-Compressor Hydrodynamic Gas Film Seal. Spiral Groove Configuration. Load Carrying Characteristics

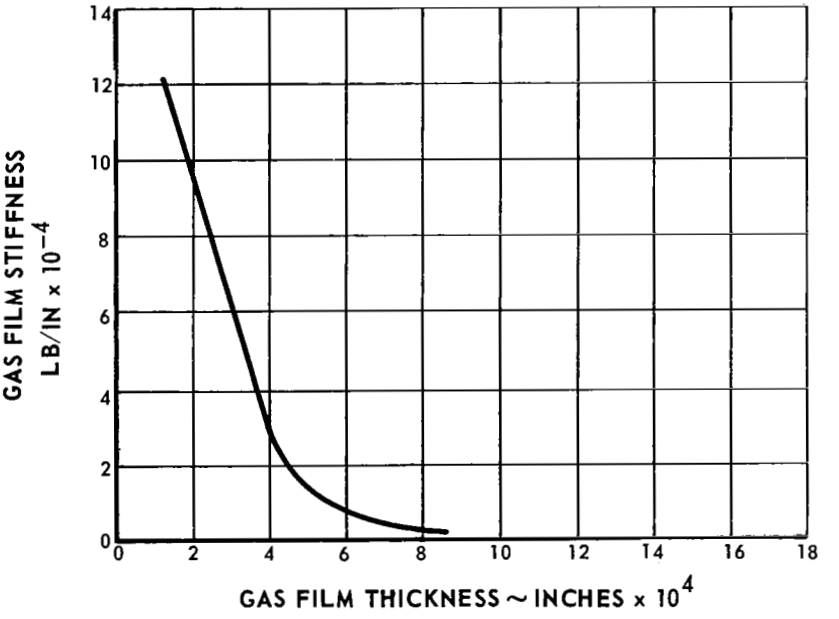

Figure 68 Turbine-Compressor Hydrodynamic Gas Film Seal. Spiral Groove Configuration. Gas Film Stiffness Characteristics

4. Controlled-Clearance Seal

The fourth design considered for the turbine-compressor was a controlled-clearance ring bellows seal (see Figure 69). The labyrinth is a floating carbon ring which has a close radial clearance with the rotating shaft. The carbon ring is free to move axially along the shaft and seat on the shaft-rotating sealplate on one side, and on a retractable bellows-supported sealplate on the other. Under static conditions this seal resembles a positive-contact face seal. That is, the bellows acts as a spring and clamps the carbon ring between two sealplates, one attached to the shaft and the other to the bellows. When operating under pressure and temperature, the nonrotating sealplate retracts, followed by the carbon ring, allowing a small clearance space between the shaft and the carbon ring to control the leakage. The expansion rate of the carbon ring is controlled by a metal shroud on the carbon outer diameter and thereby matched to the shaft expansion. There are two main advantages to this seal, 1) since the carbon does not continuously rub against a rotating part, the predicted heat generation is only about 15 watts, 2) the bellows is essentially static during normal operation and does not have to deflect to follow runout as in the case of a face seal. Therefore, the possibility of bellows fatigue is reduced. This design has a potential of low leakage (0.2 - 0.3 lb/hr), however, oil weepage characteristics are not well known.

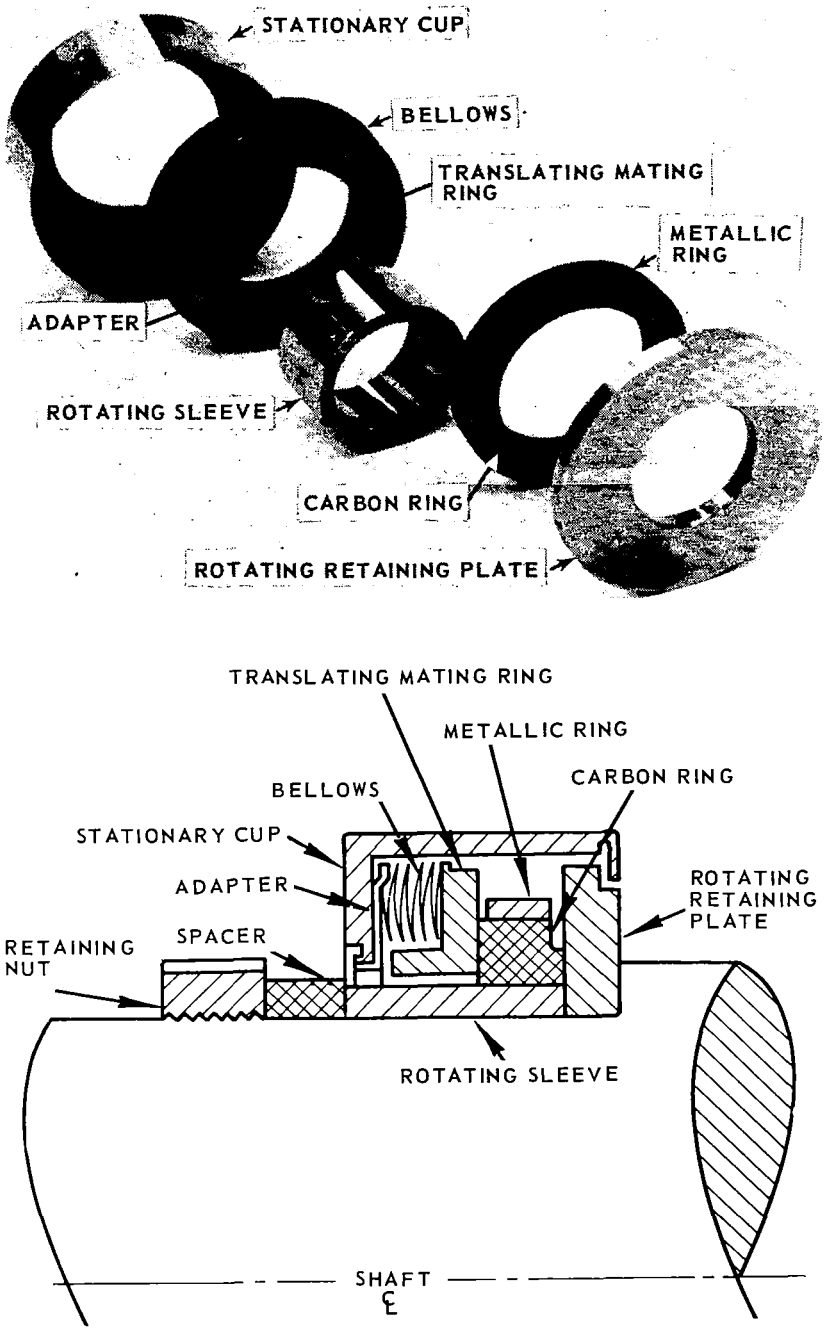

Figure 69 Controlled-Clearance Ring Seal

V. TURBOALTERNATOR DESIGN

A. General Arrangement

The design requirement for the turboalternator, like that of the turbine-compressor, was to design a rolling-element bearing system that could be used as an alternate to the gas-bearing design produced under Contract NAS3-6013. Similarly, the design objectives and considerations were 1) to use a bearing, seal, and lubrication system that would provide endurance capability for a mission time of at least 10,000 hours with a high degree of reliability, 2) to use a bearing, seal, and lubrication system having acceptable parasitic losses, and 3) to develop a mechanical design making use of the existing turboalternator aerodynamic and electrical design features developed under Contract NAS3-6013 with minimum alterations.

The turboalternator has three main sections, the alternator rotor, the drive turbine, and the oil-gas separator (Figure 70). The alternator is straddle-mounted between a ball bearing and a roller bearing. The turbine is overhung from one end of the alternator shaft and the gas-oil separator is overhung from the other end. The alternator consists of a four-pole brushless inductor which operates at 12,000 rpm to produce 400-cycle per second, 3-phase electric power. The alternator stator is cooled by liquid circulated in the stator housing. A two-stage axial-flow turbine drives the alternator. The turbine receives argon at approximately 1225°F from the discharge of the turbine-compressor turbine through an annular transition duct. After passing through the alternator drive turbine, the argon exhausts through the exit scroll and ducting. The ball bearing between the alternator and the gas-oil separator provides radial support and also absorbs the thrust load imposed on the rotor. In order to minimize windage losses, the alternator cavity is maintained at approximately 6 psia with argon fed from the discharge of the gas-oil separator. The alternator cavity is separated from the bearing cavities by labyrinth seals which permit some leakage of argon into the bearing cavities. The gas-oil separator is arranged so that no contact seal is required on that end of the machine. On the turbine end of the alternator shaft, a face seal similar in design to the face seals used in the turbine-compressor is provided. Argon bled from the compressor discharge pressurizes the face seal and also provides a small gas flow through a labyrinth seal past the turbine disc into the turbine gas path, which prevents hot gas from entering the area adjacent to the turbine disc.

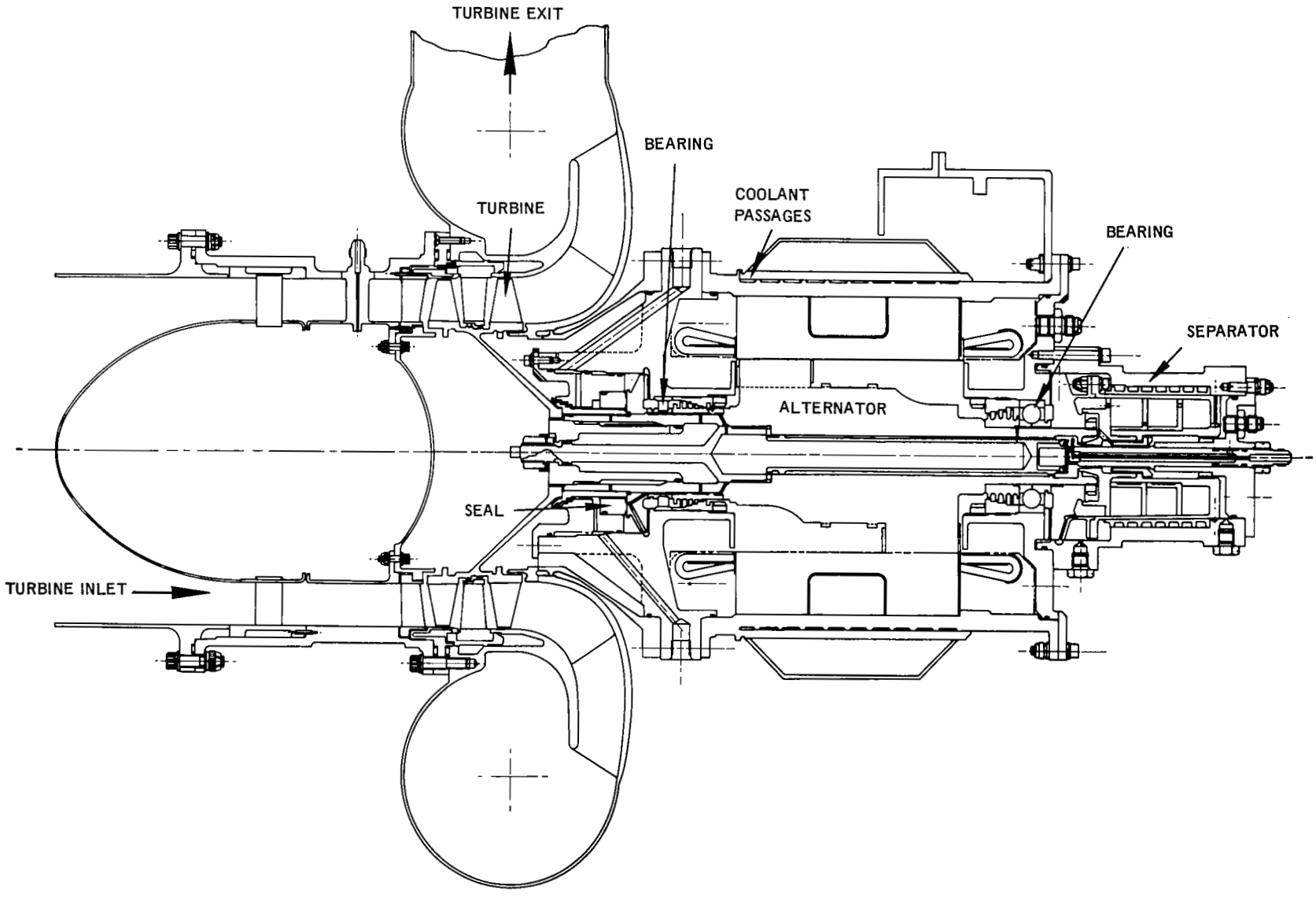

Figure 70 **Brayton-Cycle Turboalternator with Rolling-Contact Bearings**

B. Oil-Gas Separator

The oil-gas separator shown in Figure 71 consists of a cylindrical housing assembly attached to the end of the alternator shaft adjacent to the main-shaft ball bearing. This cylindrical housing contains a woven metallic matrix which provides a surface for the oil to coalesce on as the oil-gas mixture is centrifuged. An oil scoop is located at the center of the unit to pump oil from the annulus in the shaft. The small amount of oil not separated by centrifugal effects and the scoop is separated in the matrix and pumped along the tapered periphery of the matrix cylinder to the main slinger. The slinger adjacent to the ball bearing pumps this oil as well as the oil from the ball bearing out of the turboalternator. Figure 71 also shows that stationary cooling passages are incorporated around the circumference of the separator housing. The purpose of this cooling is to reduce the temperature of the oil-gas mixture as it passes through the separator. The cooling removes oil vapor from the gas.

C. Temperature Maps, Significant Stresses and Bearing Design

The thermal environments predicted for the bearing and seal regions at each end of the rotor are shown in Figures 72 and 73. Figure 72 shows the temperature pattern for the roller bearing and seal at the turbine end of the rotor. All temperatures are well within reasonable limits for the selected materials and anticipated operating conditions. The temperature pattern shown in Figure 73 for the separator end of the turboalternator also indicates that all temperatures are well within established limits. The anticipated cooling pattern for the oil-gas mixture as it passes through the separator is shown in this figure. The temperature of effluent gas from the separator is estimated to be reduced to approximately 100°F.

The turboalternator on rolling-element bearings employs many of the same components operating in the same environment to the same stress levels as in the gas-bearing configuration. However, a number of alterations to the gas-bearing design were required. In order to reduce the linear speed of the bearing and the seal and to reduce the associated heat generated, the roller bearing is smaller in diameter than the gas bearing. Therefore, in order to permit assembly, the turbine disc was modified in comparison to the gas-bearing configuration. Also, the gas-oil separator and oil pump on the free end of the alternator have no counterpart in the gas-bearing version. Many of the

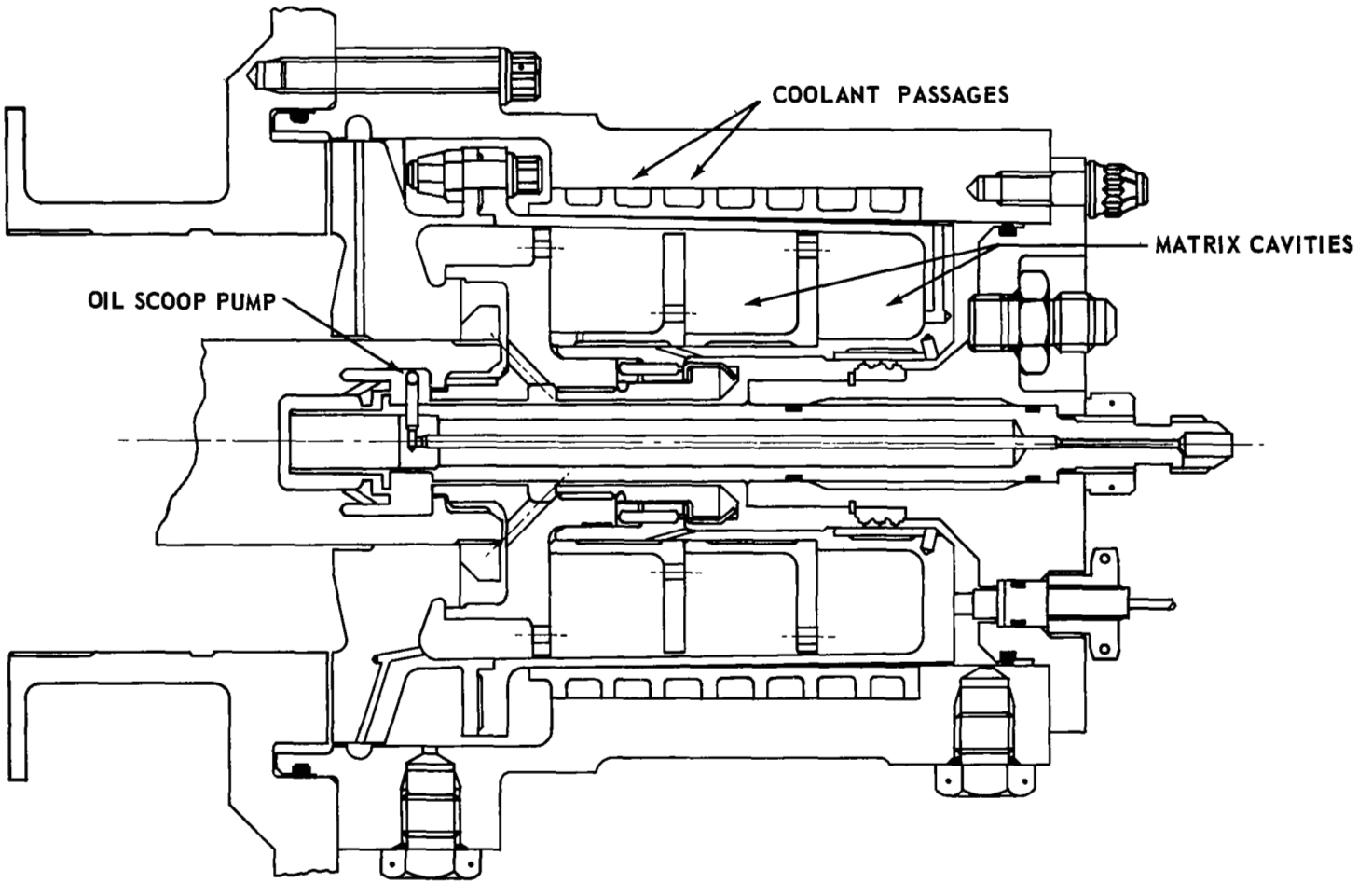

Figure 71 Turboalternator Oil-Gas Separator

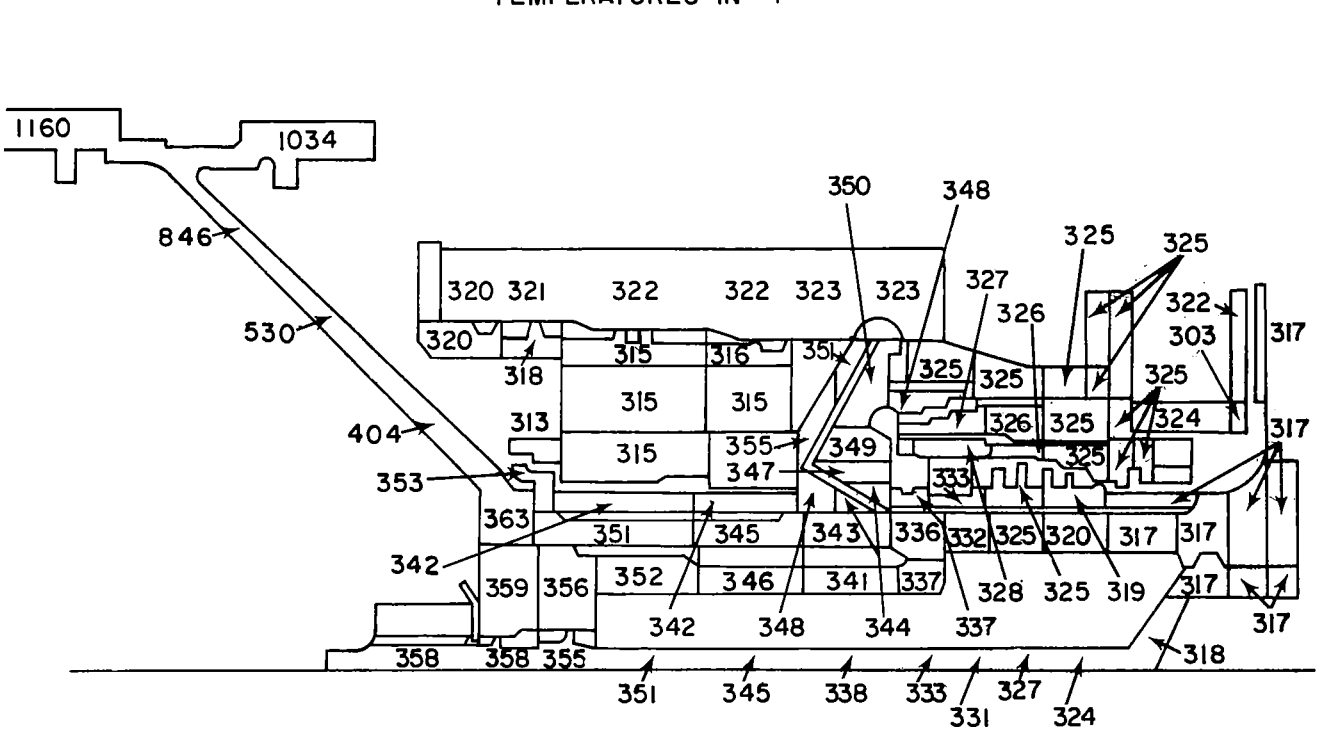

Figure 72 Thermal Map of Turboalternator No. 1 Bearing Region

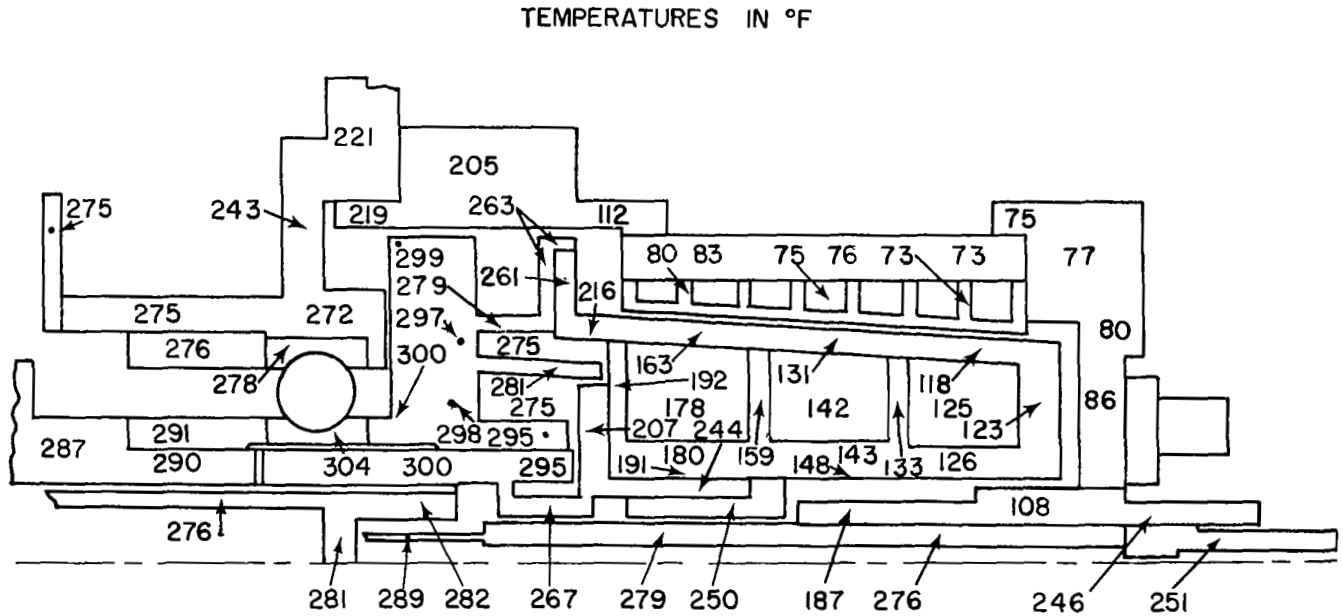

Figure 73 Thermal Map of Turboalternator No. 2 Bearing Region

stresses are the same as in the gas-bearing design. However, a number of stresses were changed and these are summarized in Table 12. The material selections are consistent with the gas-bearing alternator wherever possible and these are also shown in Table 12. As Table 12 indicates, ample design margins are provided for the turboalternator on rolling-element bearings, based on 0.2 percent yield criterion for each material.

TABLE 12

Turboalternator Significant Stresses

Part	Material	0.2% Yield, psi	Calculated Stress, psi
front bearing shroud	AMS 5667	100,000	32,500
front bearing support	AMS 5667	100,000	49,000
front tiebolt	PWA 1202	120,000	52,000
shaft at rear bearing	AMS 6415	90,000	59,950
rear shaft nut	AMS 5616	110,000	67,000
rear seal	AMS 5667	100,000	14,000
front retainer nut	AMS 5667	100,000	37,000
rear bearing support	AMS 5667	100,000	69,100
rear bearing inner race (axial compression)	M-50	323,000	30,750
separator housing	AMS 4928	110,000	21,400
separator bolt	AMS 4928	110,000	55,650
separator dividers	AMS 4928	110,000	18,900
separator dowel pins	AMS 5132	85,000	44,000
separator oil scoop	AMS 5570	25,000	1,730

In addition to the stress analyses, deflections were analyzed in critical areas. The most critical portion of the turboalternator design is the overhung separator on the free end of the shaft. The analysis of this area included a pessimistic assumption for unbalance due to maldistribution of oil in the separator. The resulting deflections were predicted to be small and ample clearances were provided.

A ball bearing located between the alternator and the separator provides radial support and locates the shaft axially. In order to incorporate a full ball complement in the bearing, to provide for a one-piece retainer and to simplify assembly, a split-inner-ring ball bearing was selected. The design characteristics of the selected ball bearing are summarized as follows:

Bearing Type	Angular-contact ball bearing with split inner ring
Oil System	Axial cooling slots on bore of inner ring
Bearing Size	40mm bore diameter 80mm outer diameter 18mm wide
Internal Geometry	11 balls of 0.500 inch diameter 2.40 inches pitch diameter 25-degree mounted contact angle 53 percent inner-race conformity, 52 percent outer-race conformity

As in the turbine-compressor ball bearings, consumable-electrode vacuum-melted M-50 tool steel was selected for the balls and rings.

The thrust load on the rotor due to electromagnetic forces is very small. However, the thrust load due to aerodynamic forces is approximately 70 pounds at the design conditions. The rotor weighs 44.7 pounds and, for ground operation with the turbine end up, the thrust load on the bearing will be 115 pounds. The radial load on the ball bearing due to magnetic forces should be less than 20 pounds, and the mechanical unbalance radial force should be less than 2 pounds. In the unlikely event that the oil in the separator were to well up on one side, a radial load of up to 35 pounds might be applied to the ball bearing. Therefore, the maximum radial load which can be envisioned in space operation is about 55 pounds, but the anticipated radial load is less than 20 pounds. Operation in the horizontal position on the ground will increase the radial force at this location due to the weight of the rotor by 22 pounds.

The ball bearing provides a predicted B-1 life well in excess of 10,000 hours over the range of load conditions anticipated. The predicted bearing life as a function of radial load, at the design thrust load of 70 pounds, is presented in Figure 74. The use of a split inner ring implies that the possibility exists for a bearing to wipe the unloaded half of the inner race. This bearing can accept radial loads up to 140 pounds without encountering this condition. Since the maximum radial load is 77 pounds based on pessimistic assumptions, ample design margin is provided to prevent wiping.

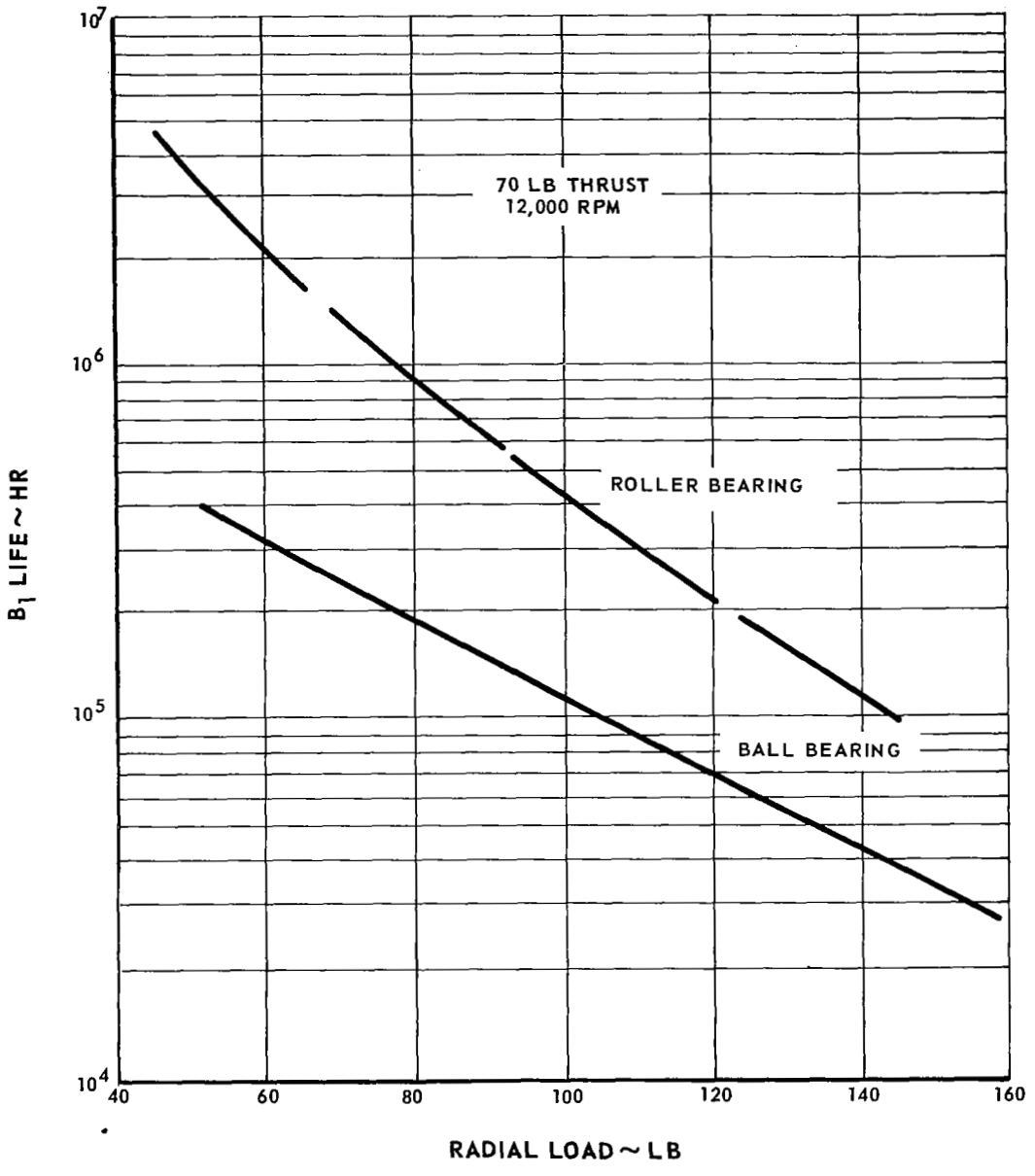

Figure 74 B_1 Life vs Radial Load for Turboalternator Bearings

The roller bearing is subject to smaller radial loads than the ball bearing, since the influence of a maldistribution of oil in the separator is very small at this location. The predicted life of the roller bearing is very large over extensive range loads, as indicated in Figure 74. The selected design characteristics of the roller bearing are:

Bearing Type	Cylindrical roller bearing
Oiling System	Axial cooling slots on bore of inner ring
Bearing Size	55mm bore diameter 80mm outer diameter 13mm wide
Internal Geometry	24 rollers of 6mm diameter and 7mm length 2.70 inches pitch diameter

Consumable-electrode vacuum melted M-50 tool steel was selected for the rollers and rings.

D. Critical Speeds

Evaluation of the rotor critical speeds was determined as a function of bearing stiffness. The stiffness of the roller bearing was estimated to be 1,400,000 lb/inch, while the stiffness of the ball bearing was predicted to be 240,000 lb/inch. The critical speeds of the rotor configuration are presented in Figure 75. The first critical speed is a rigid-body conical mode which occurs at over twice the design speed in the range of interest. The second critical speed is a rigid-body translatory mode and the third is the bent-shaft or free-free mode. Two sets of curves are shown in this figure which represent two possible alternatives in the design of the separator. Since the density of the metallic gauze in the separator was to be based on experimental results, a pessimistic (heavy) separator was represented in Figure 75, as well as a separator consistent with the anticipated configuration. The turboalternator has a rigid-body critical speed at 19,000 rpm and bent-shaft critical speeds at 33,800 and 40,800 rpm, if the pessimistic separator weight is used. If the normal separator weight is employed, the third critical speed is raised to 45,200 rpm. There are no critical speeds in the range of the operating speed or in the range of the equivalent electrical speed for this machine.

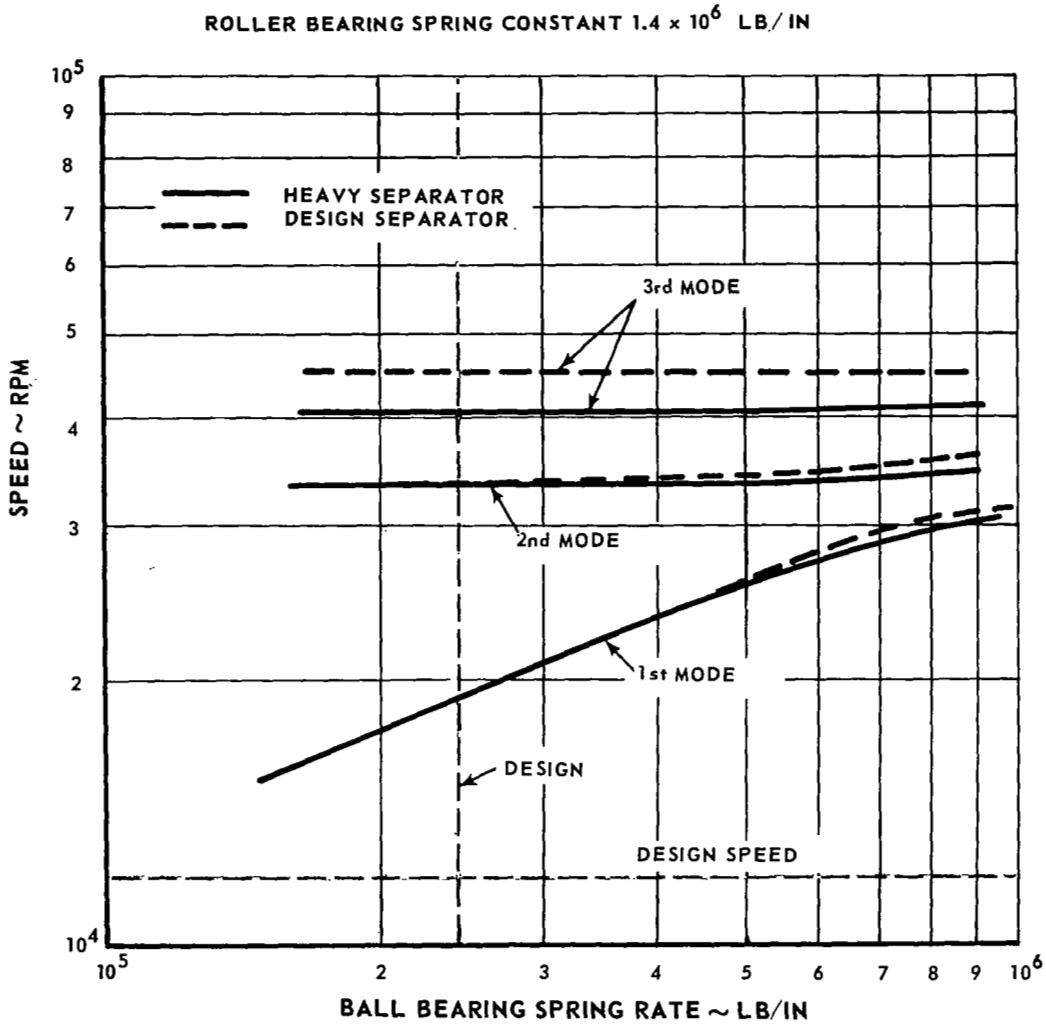

Figure 75 Turboalternator Critical Speeds

VI. TEST RIG DESIGN AND FABRICATION

A. Turbine-Compressor Bearing Compartment Rigs

Performance investigation of selected elements of the oil-lubricated rolling-element bearing system was required as a part of the overall program. Turbine-compressor components were selected for experimental evaluation because at the higher speed and in the more confined space, they were considered to be more critical than similar elements in the turboalternator. In order to conduct the experimental investigations, test rigs were required. Since the turbine-compressor bearings, seals and scavenge pumps were similar in size and located adjacent to each other, one basic type of test rig was selected to test each element separately or in combination with a minimum number of changes. Two versions of the turbine-compressor bearing compartment test rig were designed: a seal-test rig and a bearing-scavenge rig. The bearing-scavenge rig could also incorporate a seal for certain tests. The arrangement for seal-test evaluation is shown in Figure 76 and that for bearing and scavenge test in Figure 77. In both configurations the drive turbine and interconnecting housings were common, only the test section was different.

In the seal-test configuration the major considerations were 1) to provide an environment for the seal that duplicated the turbine-compressor environment, and 2) to provide a method of evaluating seal performance, leakage in particular, with a high degree of accuracy. The rig was made up of three assemblies, an air drive turbine, a test adapter, and the test region. The drive turbine was designed to operate on shop air to provide approximately 5 horsepower at speeds up to 60,000 rpm. The function of the test adapter was merely to provide a structural support between the drive turbine and the test region and to provide a means of controlling pressures in the test region to simulate those in the turbine-compressor. The purpose of the test region was, as the name implies, to house the test seal. Oil to cool the sealplate was introduced in the drive end of the shaft. Figures 78 to 83 are photographs of the actual test hardware.

The purpose of the rig configuration shown in Figure 77 was to evaluate the performance of the turbine-compressor bearing, the scavenge pump, and the combination of bearing, seal, and scavenge pump. This design was a duplicate of the arrangement at one end of the turbine-compressor. Oil and oil-argon mist were introduced at the free end of the shaft and passed through the bearing

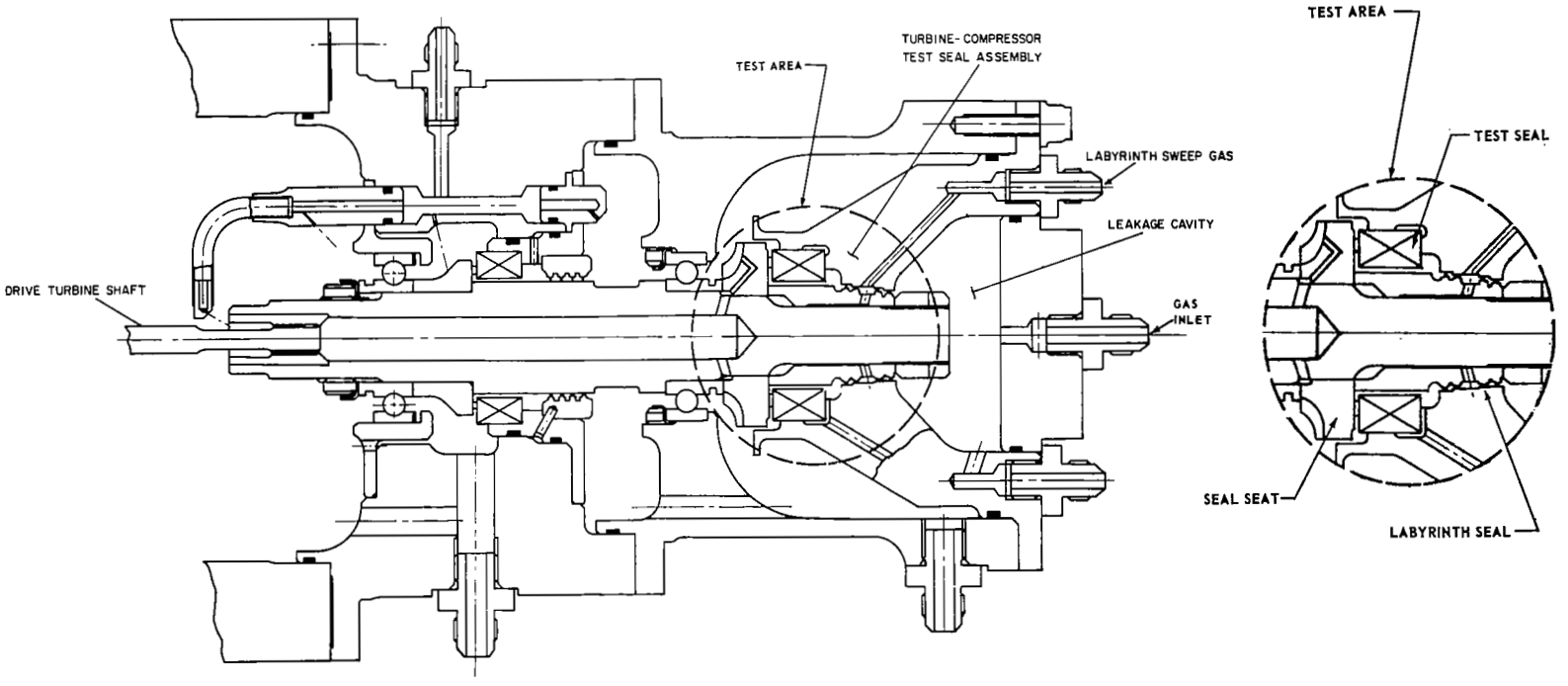

Figure 76 Turbine-Compressor Seal Test rig. Design Speed 50, 000 rpm

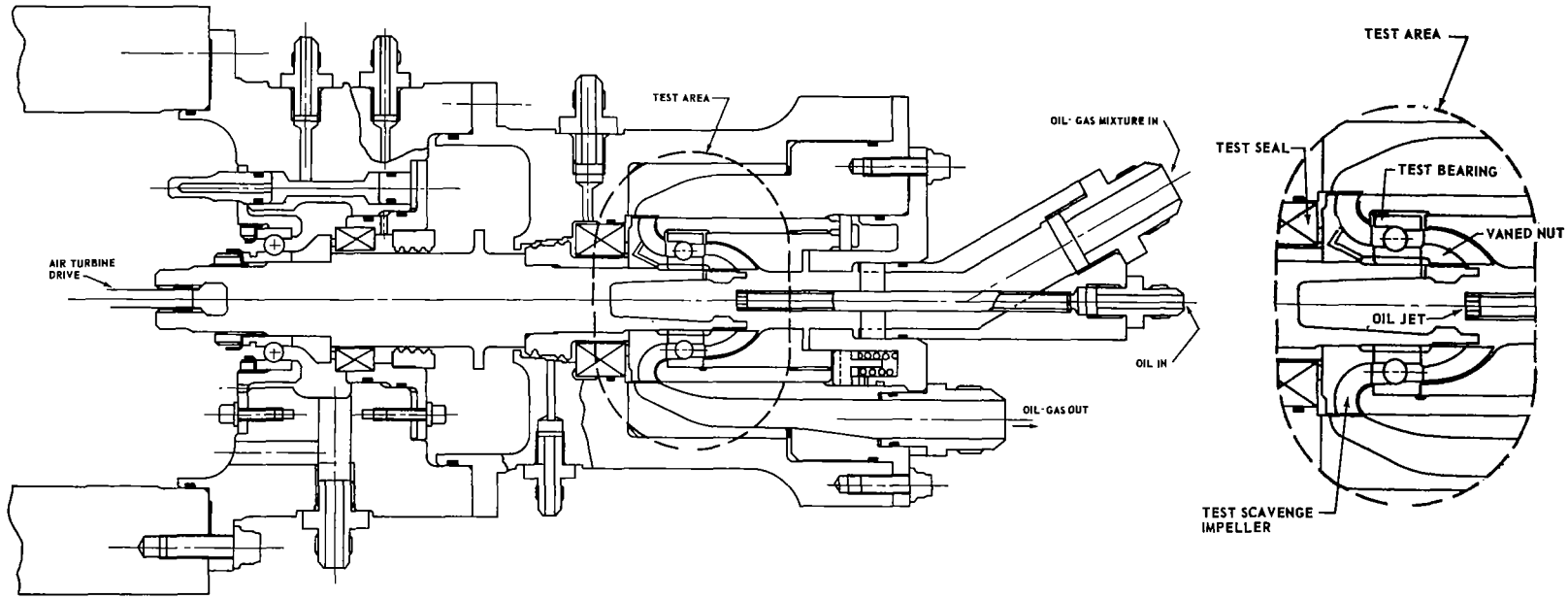

Figure 77 Turbine-Compressor Bearing Compartment Rig.
Design Speed 50, 000 rpm

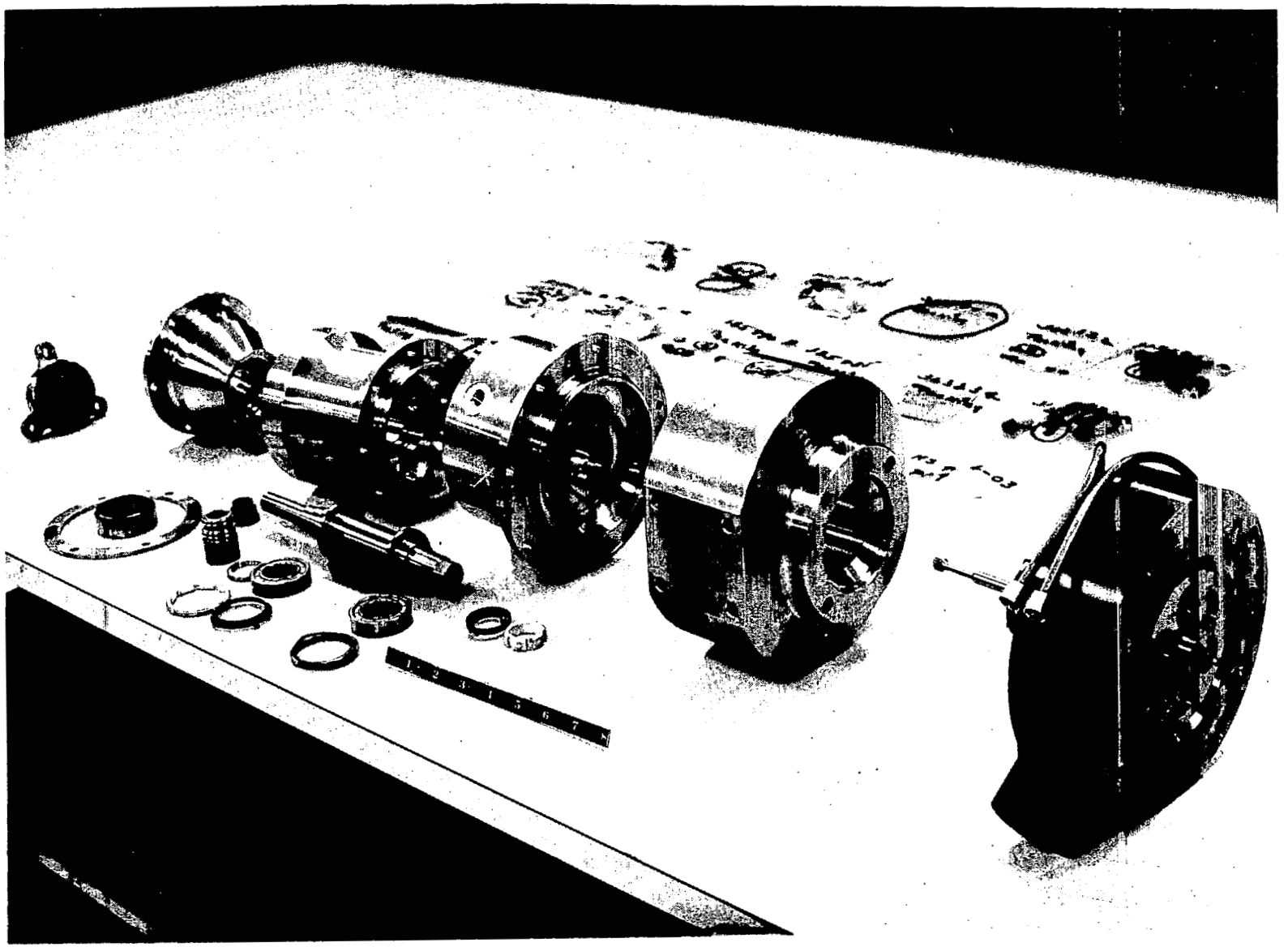

Figure 78 Seal Test Rig Parts X-22339

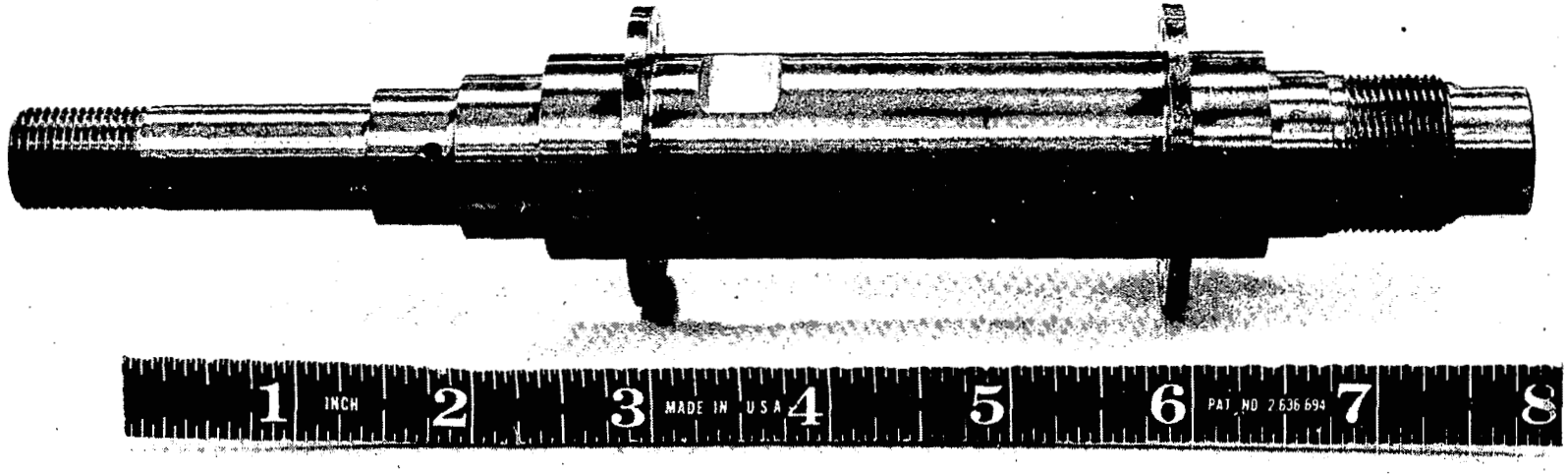

Figure 79 Shaft - Seal Test Rig X-22340

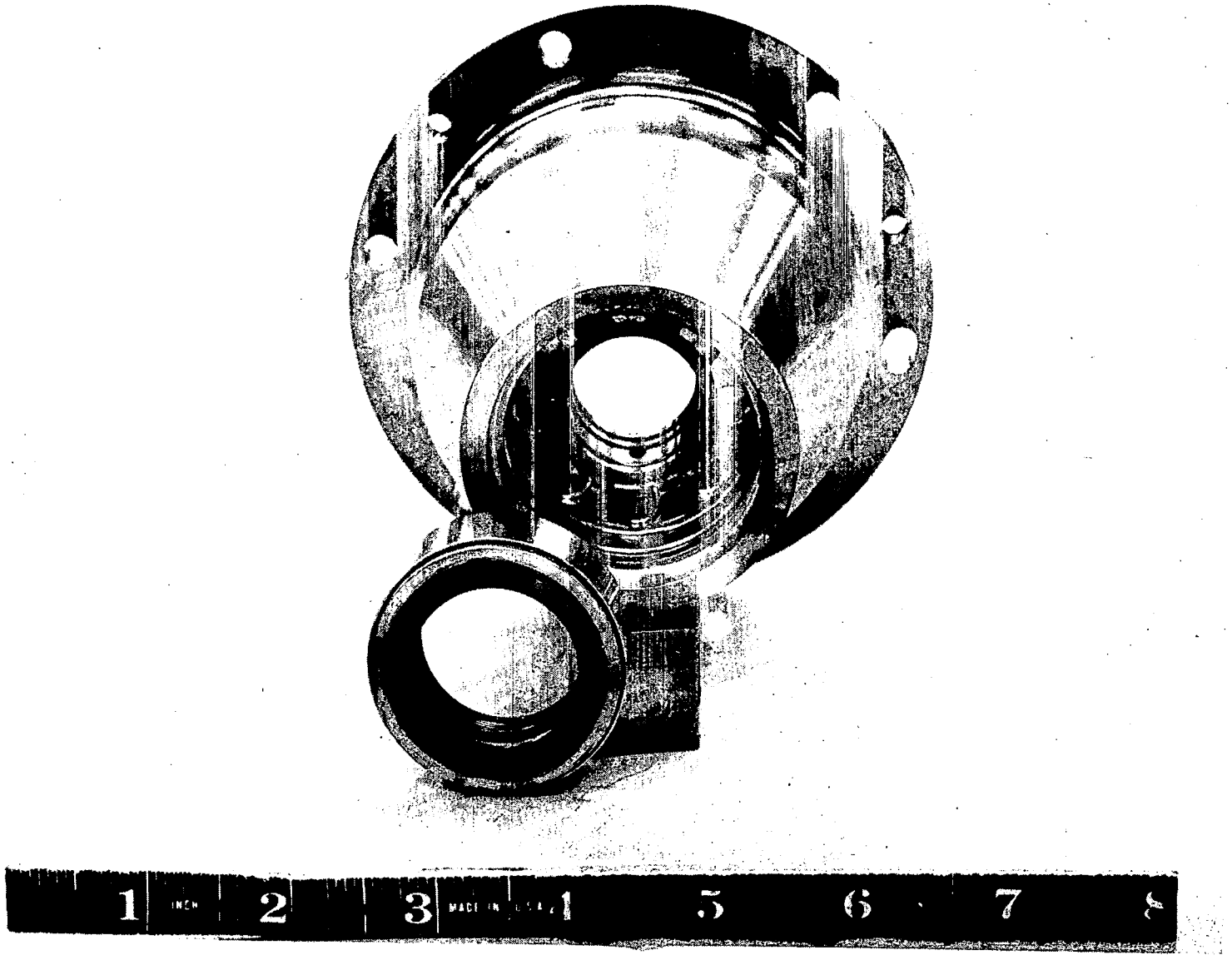

Figure 80 Seal and Seal Housing - Seal Test Rig X-22338

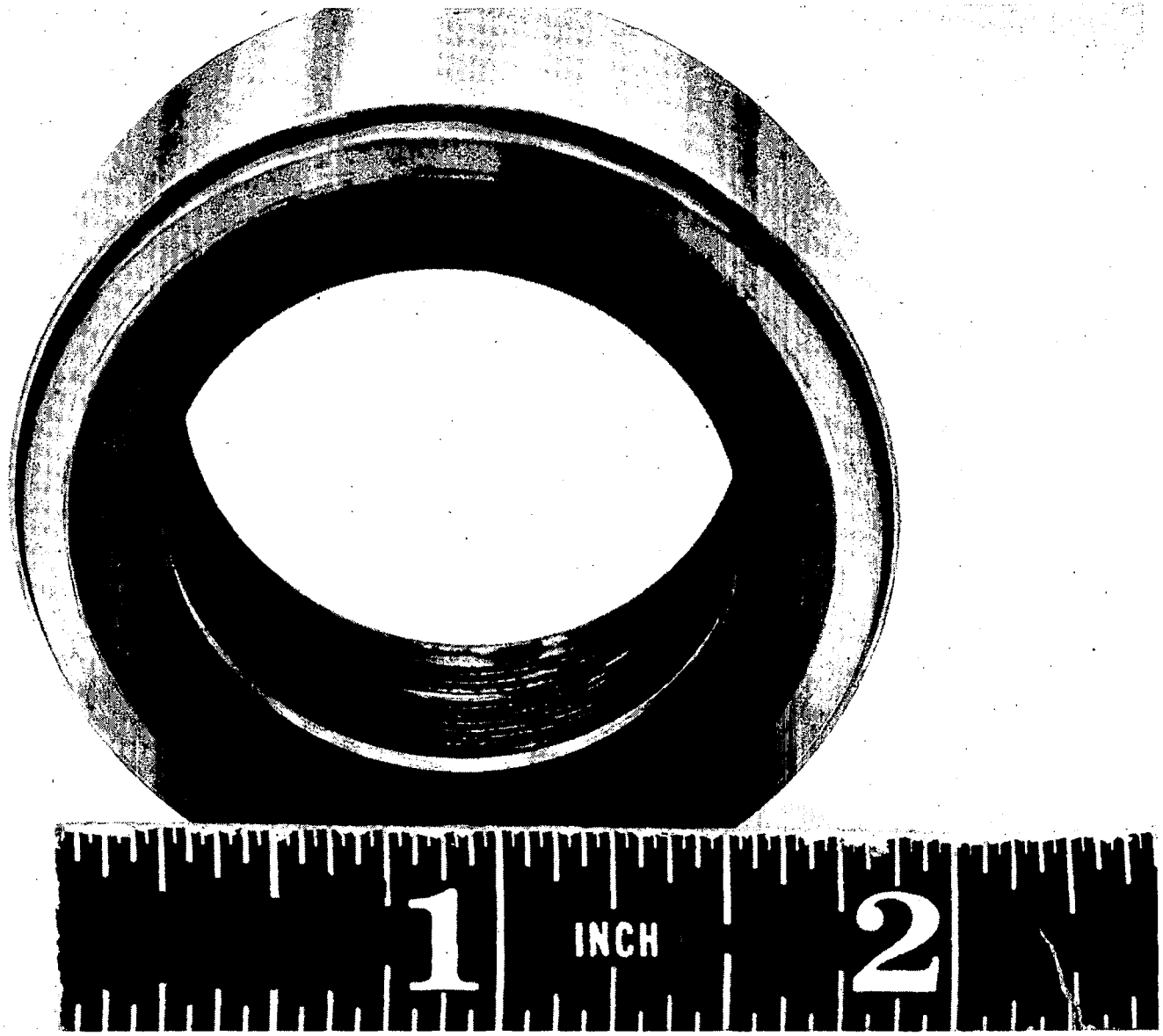

Figure 81 Face Seal - Seal Test Rig X-22341

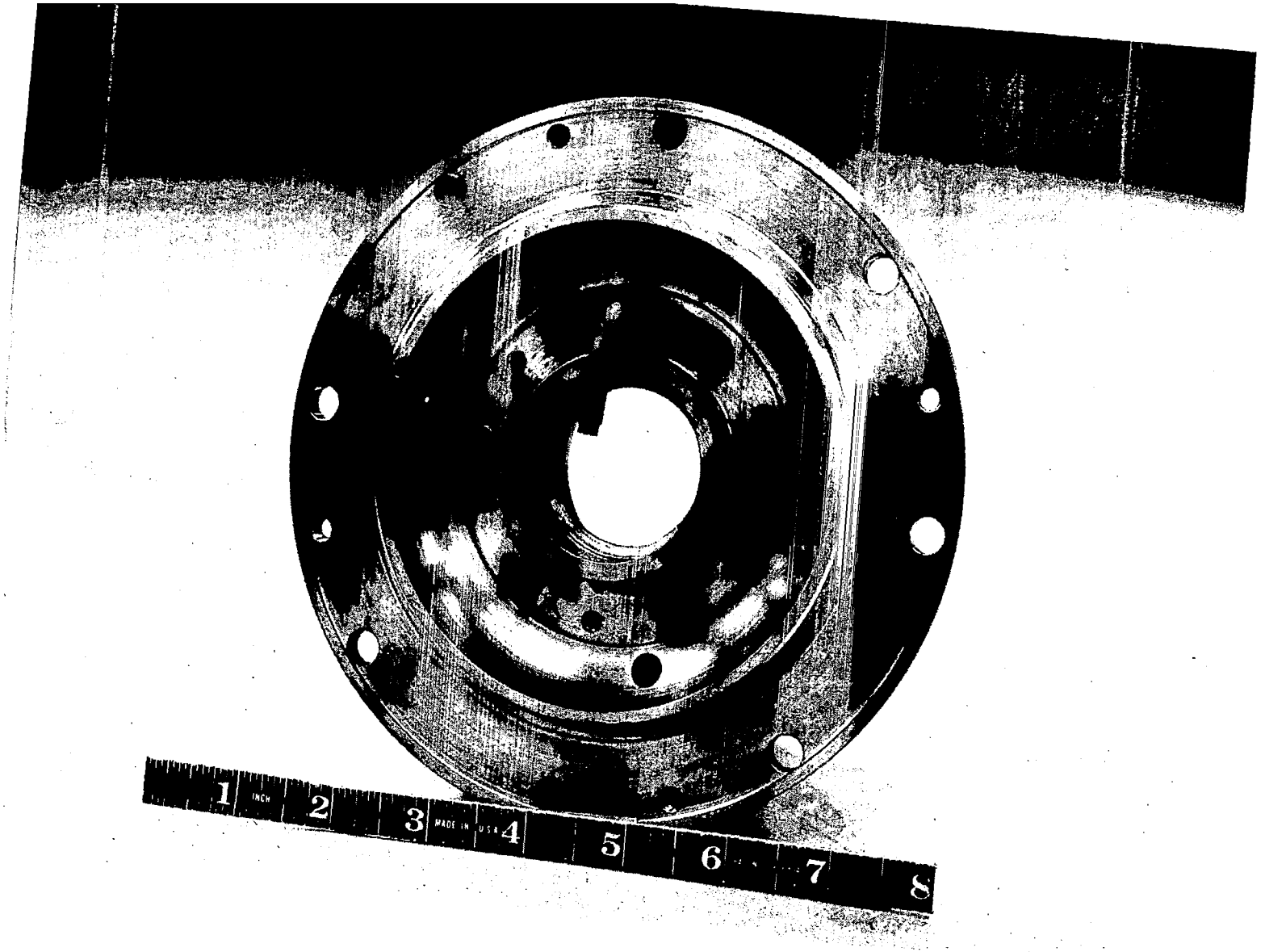

Figure 82 Intermediate Housing - Seal Test Rig X-22343

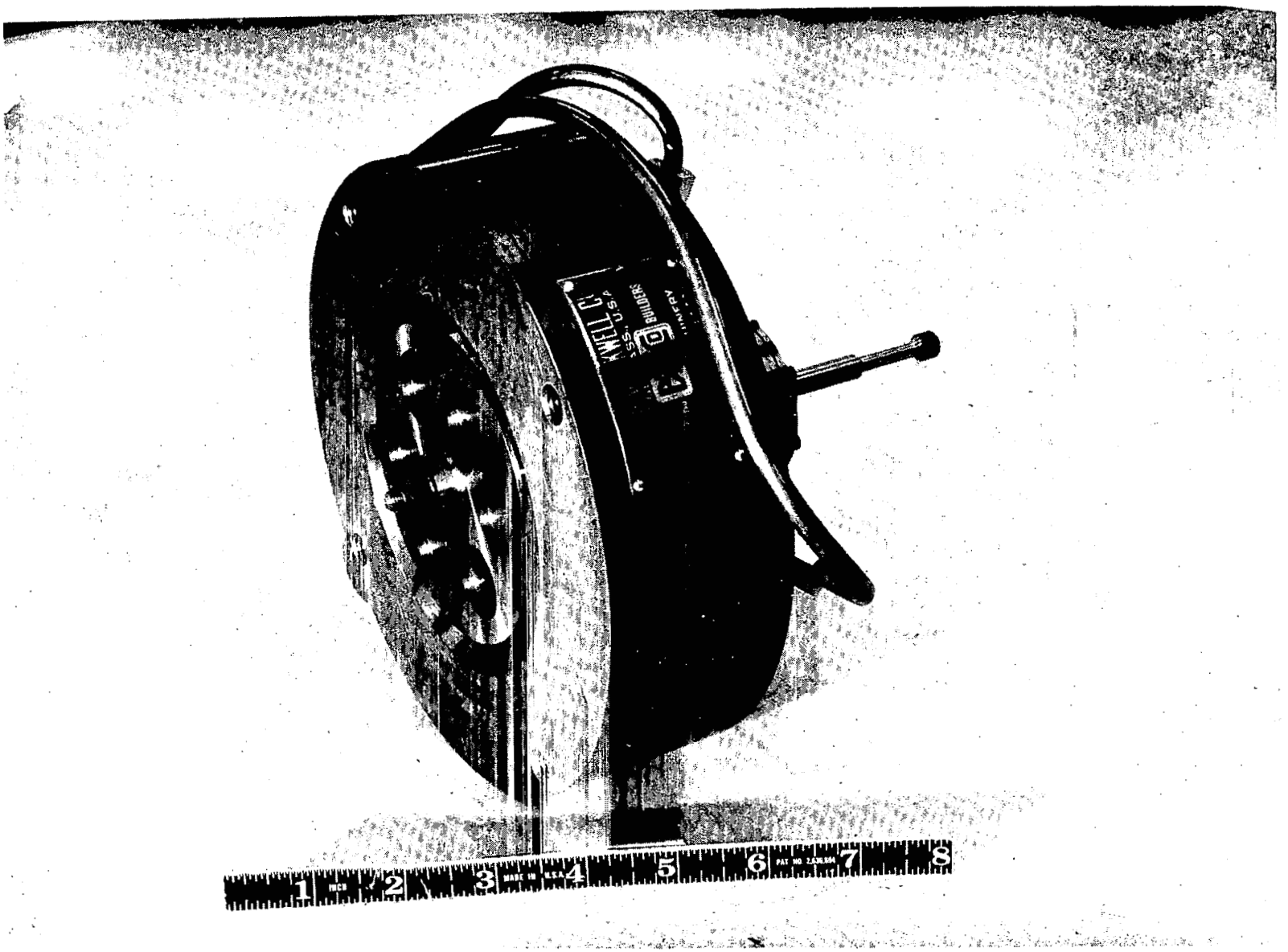

Figure 83 Drive Turbine - Seal Test Rig X-22344

and scavenge pump in the same way as in the actual turbine-compressor assembly. The seal could be included in this arrangement if desired. The design of this rig utilized the same drive turbine and test adapter as the seal rig. The drive shaft design was similar to that of the seal rig. In the bearing test configuration, bearing cooling and lubrication could be investigated at various speed levels from 0 to 60,000 rpm, with most of the testing at 50,000 rpm. Bearing loads, shaft speed, oil flow, oil temperature rise and bearing temperatures were determined. Power consumption was estimated from the test data. Visual and dimensional nondestructive inspection of test parts was made to determine the adequacy of the basic bearing design.

Since scavenging oil from bearing compartments with a minimum amount of power consumption was of major concern, several scavenge tests were made to investigate the problems of scavenging the oil-argon mixture from the turbine-compressor bearing cavities. Two types of scavenge pumps were designed, a centrifugal impeller type, and an annular jet pump type discussed in Section III. In both cases a mixture of gas and oil was pumped. Tests were run at various shaft speeds including 12,000 and 50,000 rpm with the shaft in both horizontal and vertical attitudes. Oil and argon flow into and out of the bearing compartment were monitored and varied at each speed. Photographic observation was made of the exit mixture flow.

The test region of the bearing compartment rig was versatile and would accept the complete turbine-compressor rotor support system, including the squeeze-film support and the axial springs. Parts for the bearing compartment rig are shown in their relationship to one another in Figure 84.

B. Separator Rig

The oil-gas separator, in addition to the turbine-compressor bearing, seal, and scavenge components, was selected for experimental investigation. The separator test rig was designed to evaluate pump performance, separator performance, and combined pump-separator performance. The general design configuration for the separator test rig shown on Figure 85 is similar to that of the bearing, seal, and scavenge test rigs. The rig was driven by an air turbine unit identical to the one for the bearing-compartment rigs. The test components were overhung from

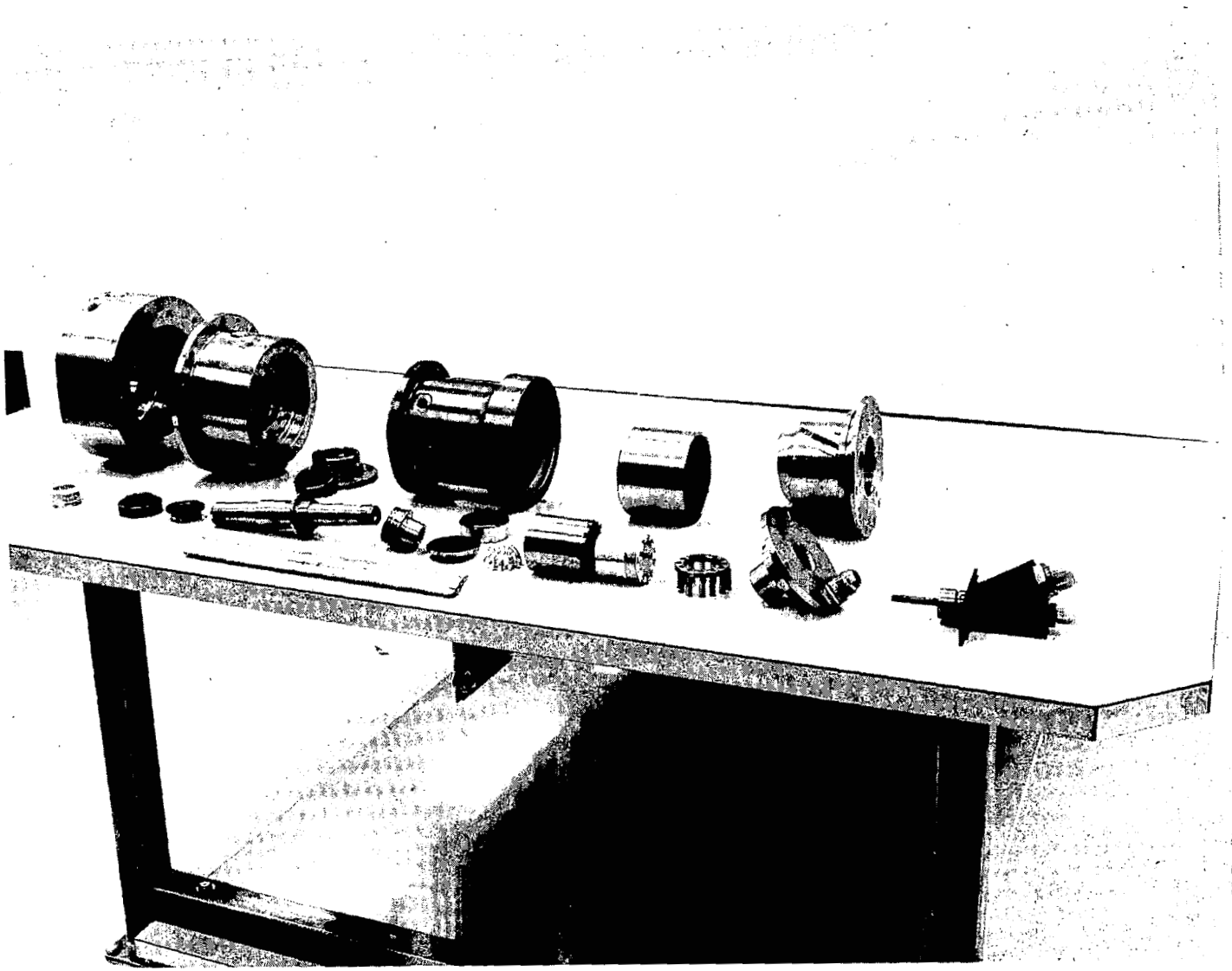

84 Turbine-Compressor Bearing Compartment Rig X-22440

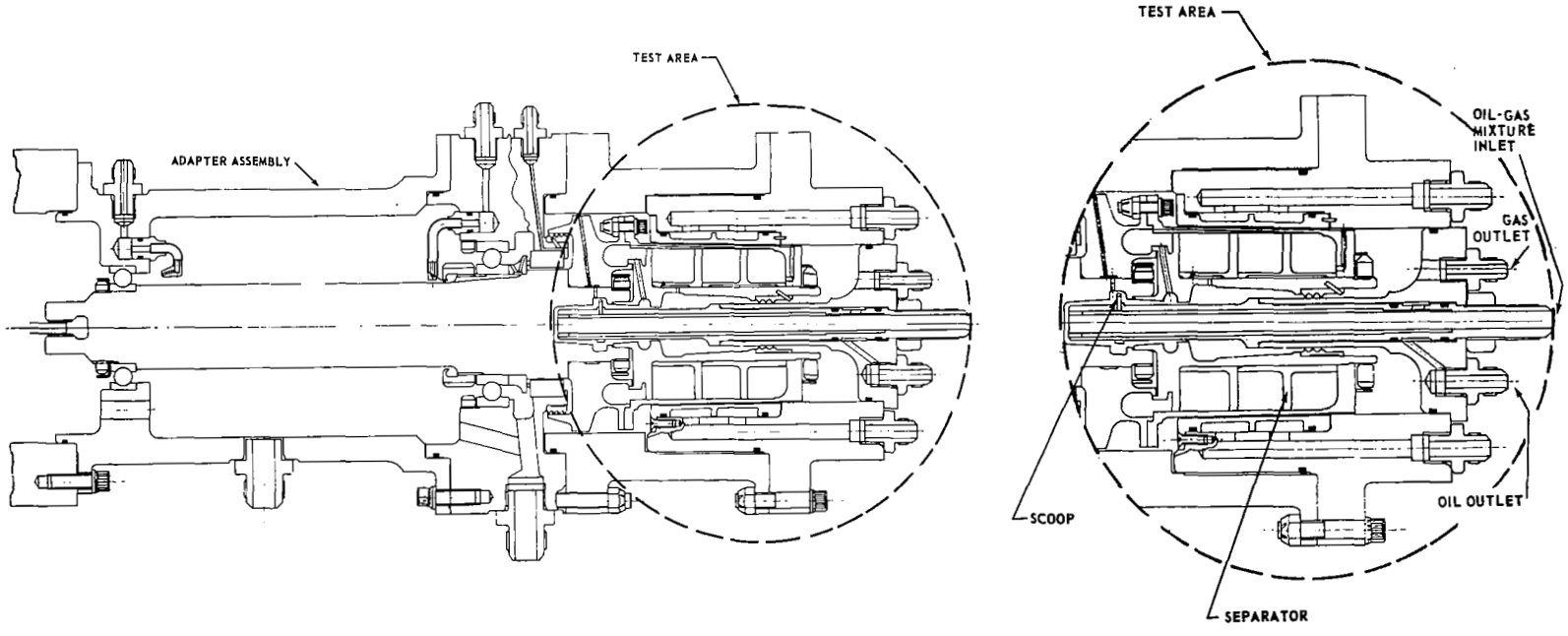

Figure 85 Turboalternator Separator Rig

an intermediate housing as in the other rigs. The configuration presented in Figure 85 combines a scoop pump and a separator section. First-stage separation was accomplished at the scoop pump where the bearing compartment scavenge gas-oil mixture was introduced, filling the shaft reservoir with oil and bypassing the gas, oil vapor, and overflow oil to the separator. Oil was pumped from the shaft reservoir to the accumulator by the scoop pump. The argon and some of the oil flowed into the separator where the oil and gas were separated by centrifugal forces. The separated oil was pumped along the sloping outer wall and discharged forward towards the bearing compartment, while the argon was discharged from the rear of the separator and was piped out of the compartment. The test rig design provided the versatility necessary to evaluate pump and separator designs individually as well as simultaneously. Evaluation of pump concepts was accomplished by removing the separator section and installing the pump test section shown in Figure 86. This test section permitted various gas-oil mixtures to be introduced into the shaft reservoir to evaluate scoop pump flow and pressure performance. First-stage separation efficiency at the scoop pump was evaluated by measuring the oil-to-gas ratio of the pump discharge.

Separator designs were evaluated by replacing the shaft oil reservoir feed assembly in the configuration shown in Figure 85 with a shorter oil-gas mixture feed line which discharged to the separator inlet only. Separator concepts were tested by varying the inlet oil-gas mixture and measuring the oil content of the gas discharged from the separator. Transparent sections were incorporated in the oil-gas mixture inlet line and gas discharge line to permit photographic records of the flow patterns to be made.

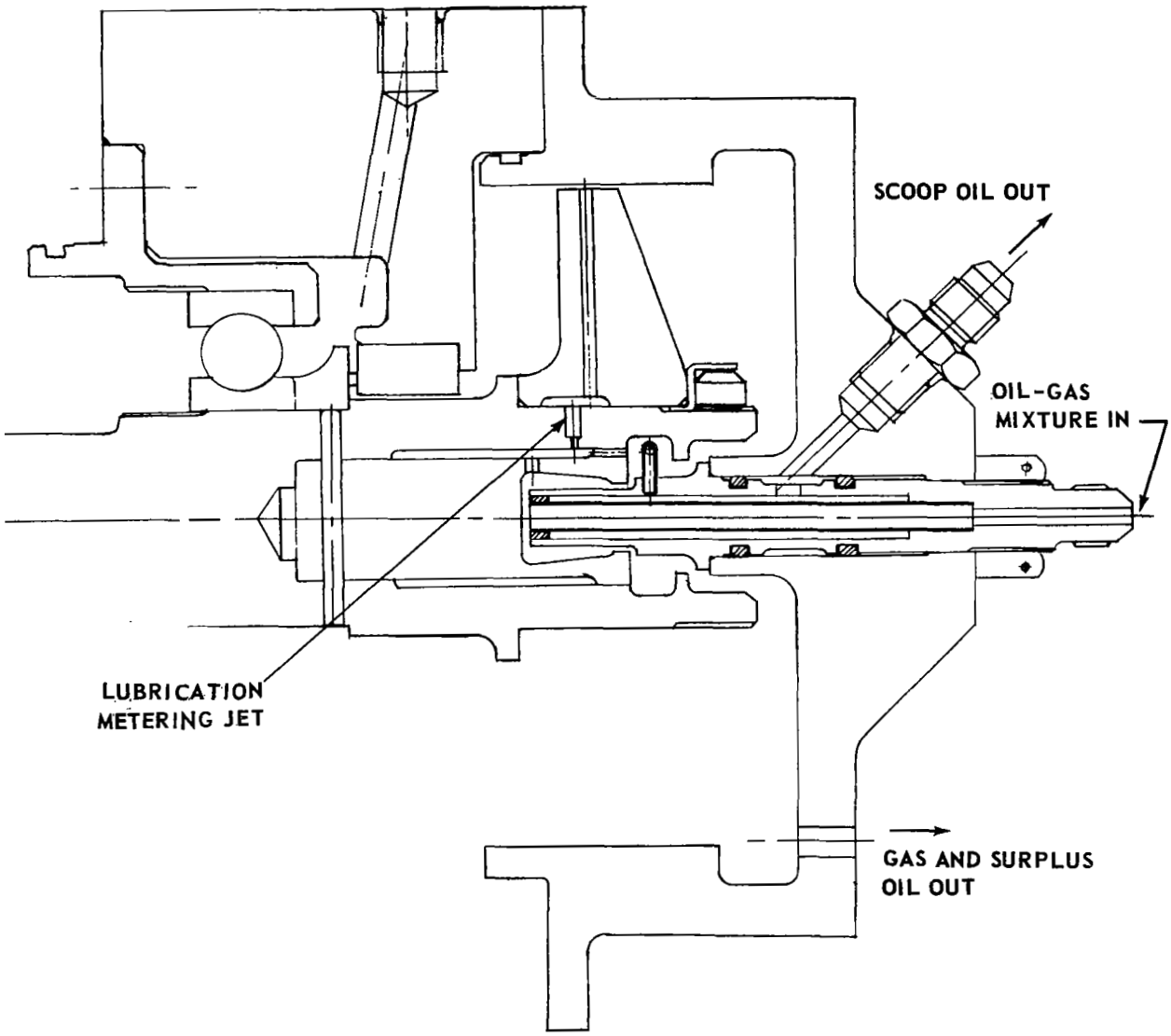

Figure 86 Separator Rig for evaluation of Scoop Pump

VII. COMPONENT TESTS

The component test program was formulated to investigate the performance of certain critical areas of the design. These critical areas were defined during the analytical and design phases of the program. The first area selected for test was the turbine-compressor bearing compartment. This compartment includes three test items, the bearing, the seal and the scavenge impeller. The second area selected for test was the oil-gas separator from the turboalternator. The third area, also from the turboalternator, was the oil pump. The fourth area selected for test evaluation was the gas cleanup adsorber. Performance curves, photographs and test results for each component are presented in the following sections. Endurance test results are also presented.

A. Turbine - Compressor Bearing Tests

Bearing tests were run to determine the performance of lubrication and cooling provisions as applied to the basic turbine-compressor bearing. The detail design of the turbine-compressor bearing was presented in Section IV. The rig in which the tests were conducted was described in Section VI (see Figure 77). The test parameters were selected to investigate lubrication and cooling, consistent with minimum power consumption. In the bearing design (see Figures 87 and 88), two paths for gas and oil flow through the bearing were provided. One path was under the inner ring via the grooves machined axially along the ring inside diameter. The other path was directly through the balls. Two lubrication and cooling provisions were evaluated. In the first, called "dry mist", very small quantities of oil were passed through the balls with varying quantities of oil passed through the inner-race cooling grooves. In the second provision, called "flood lubrication", much larger quantities of oil were passed through the balls with the same range of flow introduced under the inner race.

The turbine-compressor bearing lubrication and cooling test results are presented in two series of curves. The first series, Figures 89 through 94, covers the results using dry-mist lubrication, and the second series, Figures 95 through 97, flood lubrication.

When testing with dry-mist lubrication, argon at 300°F containing a small quantity of oil mist was introduced into the test bearing port marked "oil-gas mixture in" on Figure 77. This mixture, consisting of 0.004 to 0.014 pound per hour of oil and 6.66 to 8.86 pounds per hour of argon was passed through the bearing for lubrication. A much larger quantity of oil, for

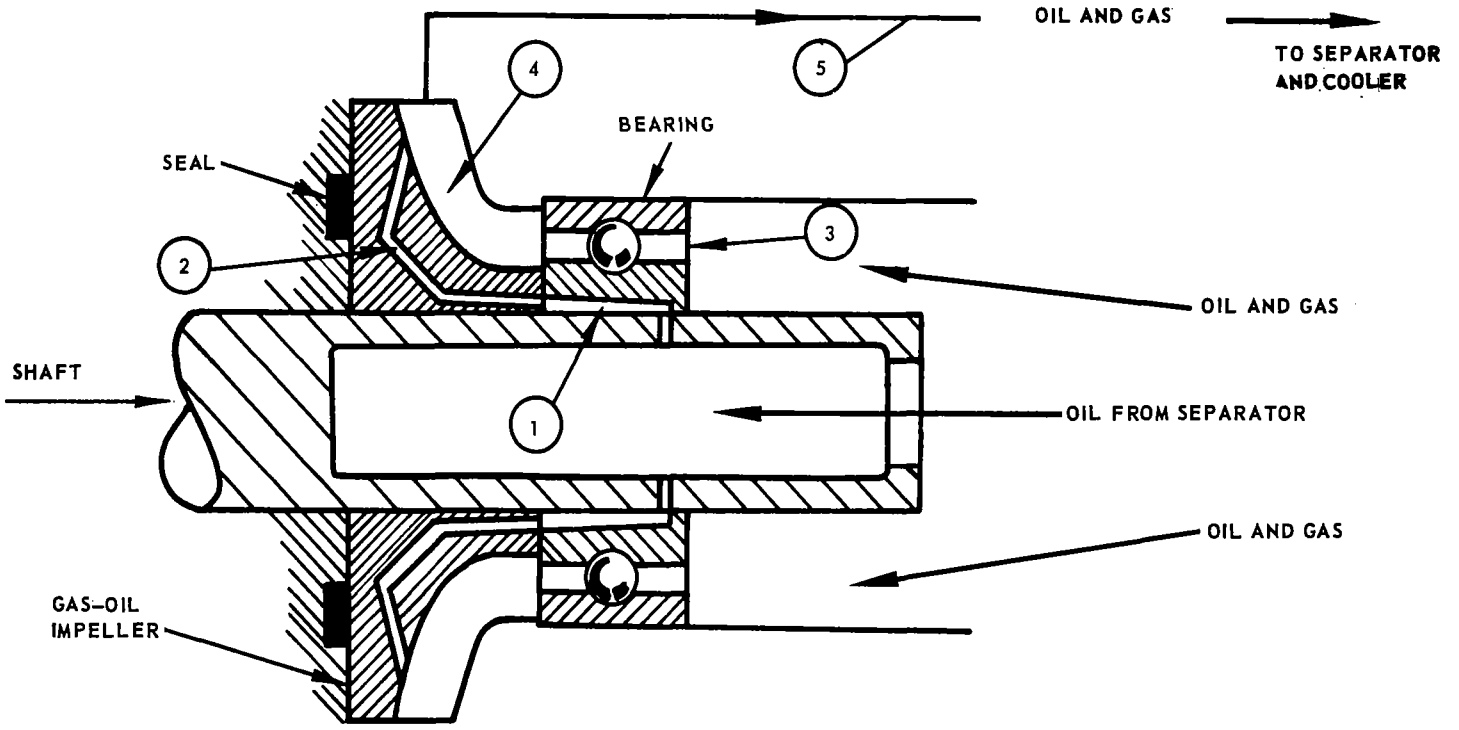

1. UNDER RACE BEARING COOLING – FORCED OIL FLOW FROM ROTATIONAL CENTRIFUGAL EFFECTS
2. SEALPLATE COOLING WITH FORCED OIL FLOW FROM 1
3. LUBRICATION THROUGH BEARING WITH GAS–OIL MIXTURE
4. BEARING–SEAL CAVITY SCAVENGING WITH CENTRIFUGAL IMPELLER
5. OIL TRANSPORT THROUGH SYSTEM WITH GAS. GAS PRESSURE REQUIRED FOR CIRCULATION GENERATED IN CENTRIFUGAL IMPELLER

Figure 87 Lubrication System Concept

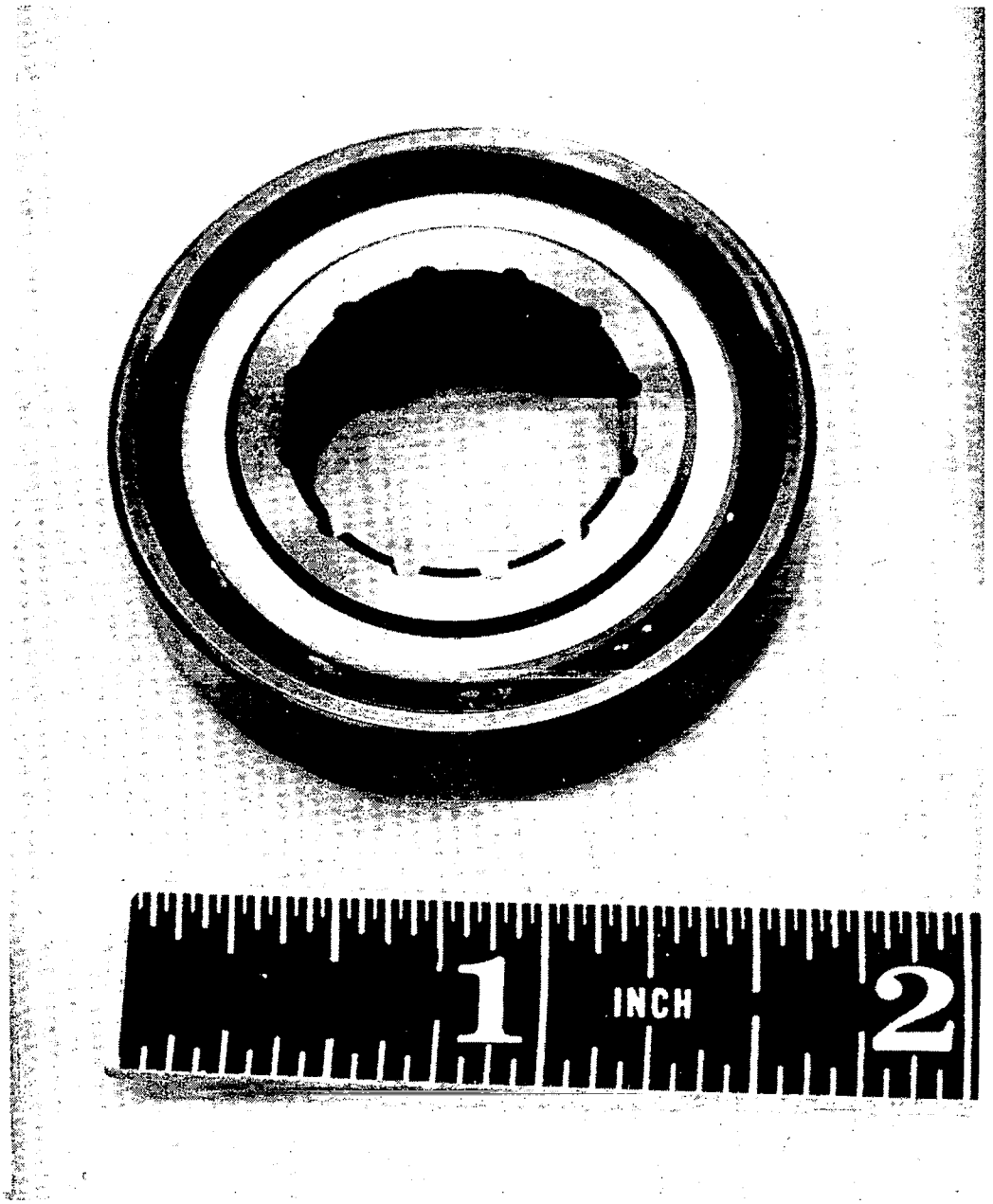

Figure 88 Turbine-Compressor Bearing X-22824

cooling, 54 to 150 pounds per hour, was introduced at the fitting marked "oil in" on Figure 77, and passed under the bearing inner race by the way of the grooves cut in the inner race. All of the oil and argon was discharged at the sealplate. Figure 89 presents the bearing outer-race temperature as a function of under-race oil flow for speeds of 12,000, 30,000 50,000 and 60,000 rpm with three mist ratios. The 60,000 rpm curve was held to 400°F because of facility limitations. Figure 90 presents the total heat added to the oil as a function of oil flow, mist flow and shaft speed. This quantity of heat includes oil and argon pumping energy as well as the heat generation associated with the bearing. Figure 91 is a curve of total rig power consumption determined by air turbine enthalpy. This curve is useful in determining the effect of a selected variable at a given speed since only the test bearing was influenced by the variable being examined. The data of Figures 92, 93 and 94 were taken in order to obtain experimental information from which the influence of viscosity due to temperature change could be assessed, as it pertains to heat generation, pumping power, etc.

When testing with flood lubrication, several orders of magnitude more oil was introduced at the port marked "oil-gas mixture in" with considerably less argon than used with dry mist lubrication. Figures 95, 96 and 97 which present the flood lubrication results, are the counterparts of Figures 89, 90 and 91. This manner of presentation allows direct comparison. By making this comparison, it is evident that significant differences exist between the two. However, either method is acceptable from the standpoint of the variables examined. Examination of the 50,000 rpm data in Figure 97 raises some doubt as to the validity of the turbine power data at low under-race oil flows. Since other parameters are within expected limits, it is concluded that the turbine power data is in error at the 0.9 and 1.7 lb per minute under-race oil flows. Figure 98 is intended to show the differences that are encountered between two extremes of lubrication. Tests for longer periods would have to be run to determine the endurance characteristics of the bearing using either lubrication provision.

Strain gages were used to measure ball-pass frequency. The results of this measurement compared to calculated frequency are presented in Figure 99. Within the accuracy of measurement no skidding is evident.

The test apparatus mounted in the test stand is shown in Figure 100. A photograph of the actual bearing tested with strain gages and thermocouples installed is shown in Figure 101. The pilot system endurance test of 2500 hours was completed using another bearing with no detectable wear. The results of this inspection are given on page 264 along with other pilot system test results.

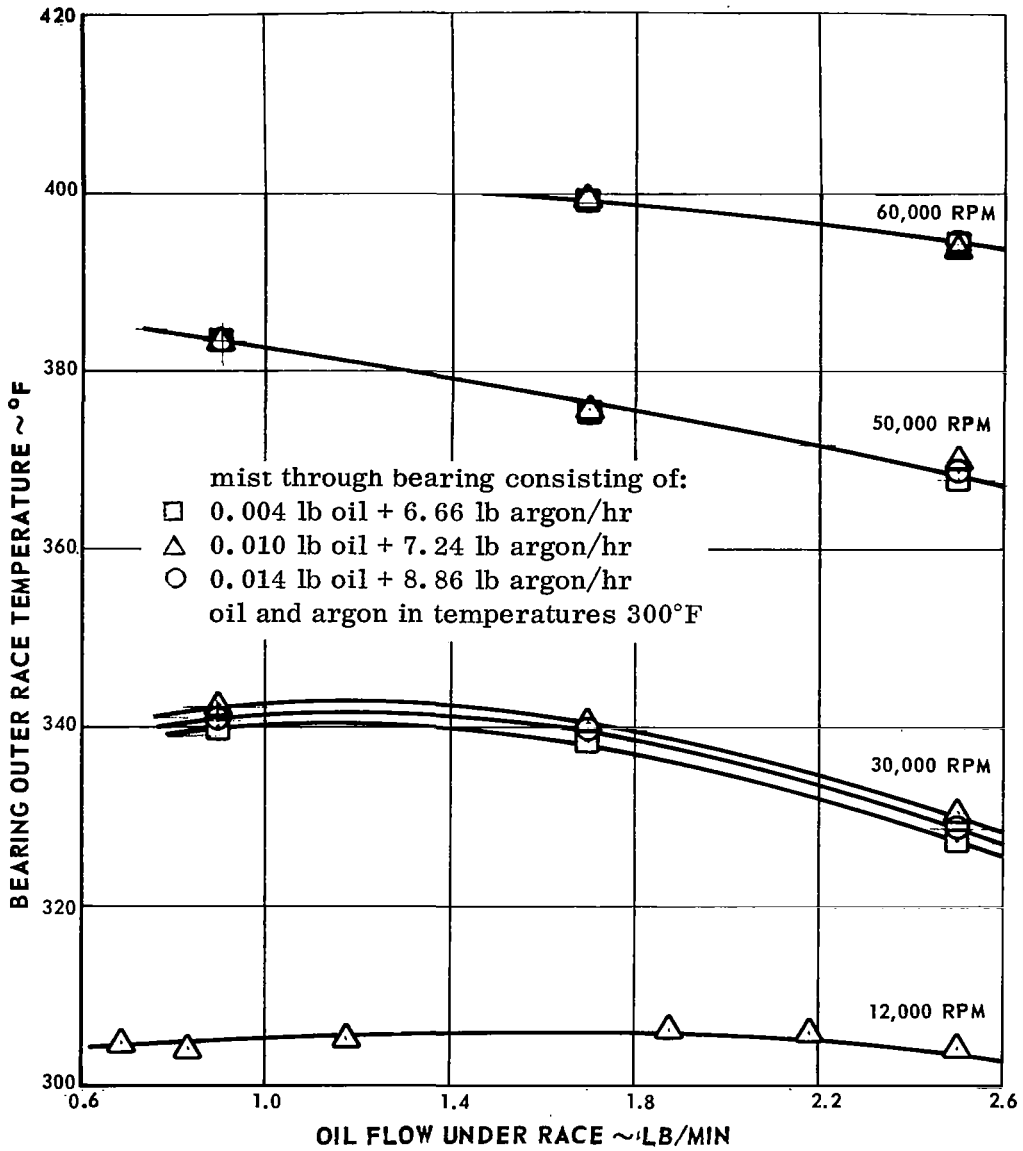

Figure 89 Bearing Temperature with Dry-Mist Lubrication

mist through bearing consisting of:
□ 0.004 lb oil + 6.66 lb argon/hr
△ 0.010 lb oil + 7.24 lb argon/hr
○ 0.014 lb oil + 8.86 lb argon/hr
oil and argon in temperatures 300°F

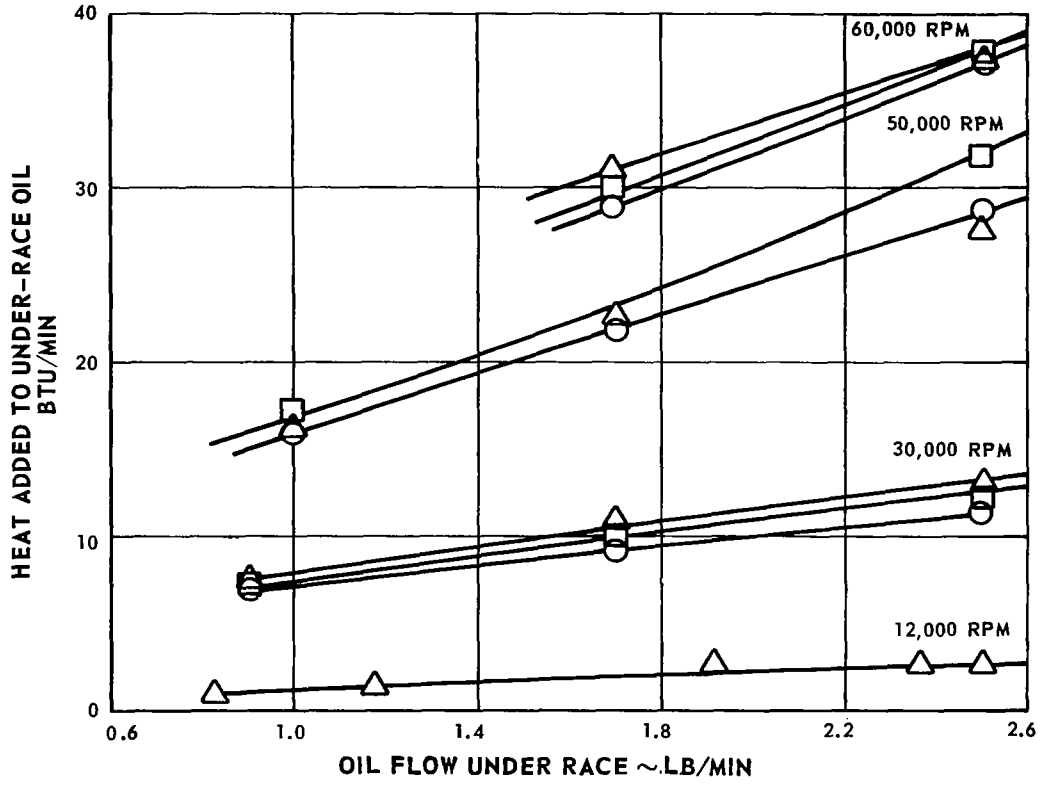

Figure 90 Heat Added to Under-Race Oil with Dry-Mist Lubrication

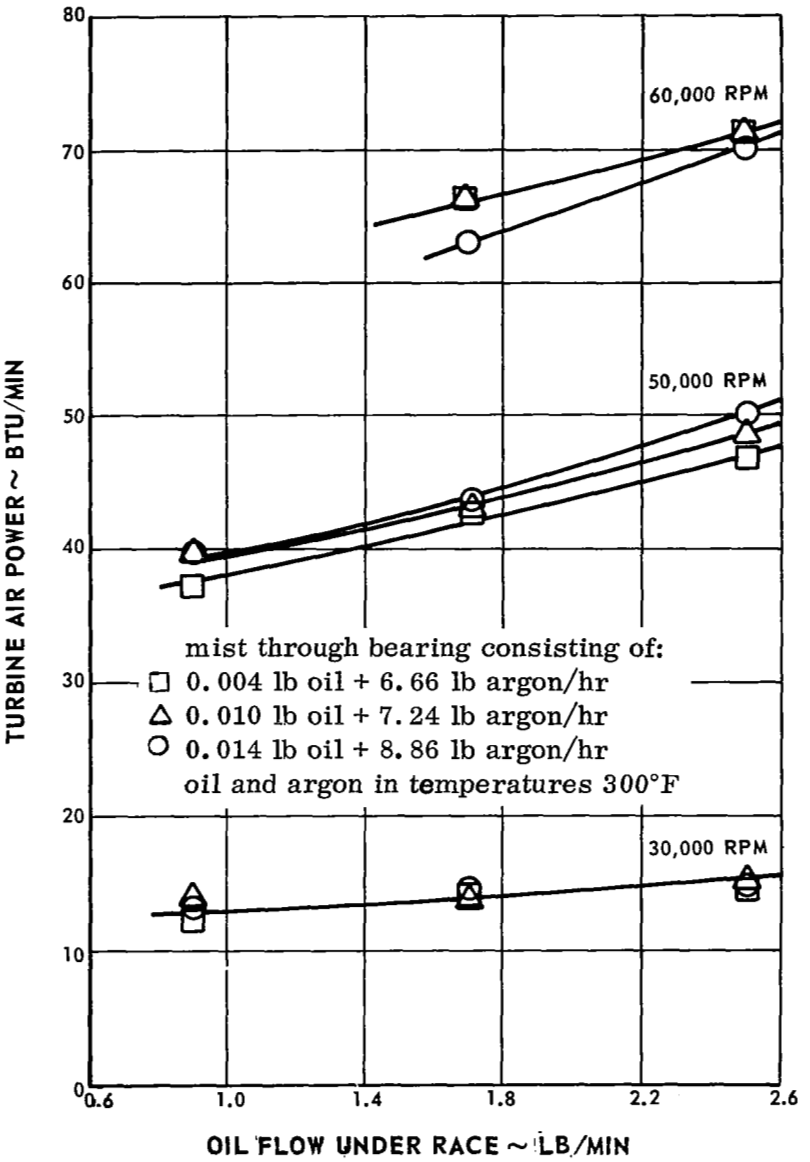

Figure 91 Total Rig Power Consumption with Dry-Mist Lubrication

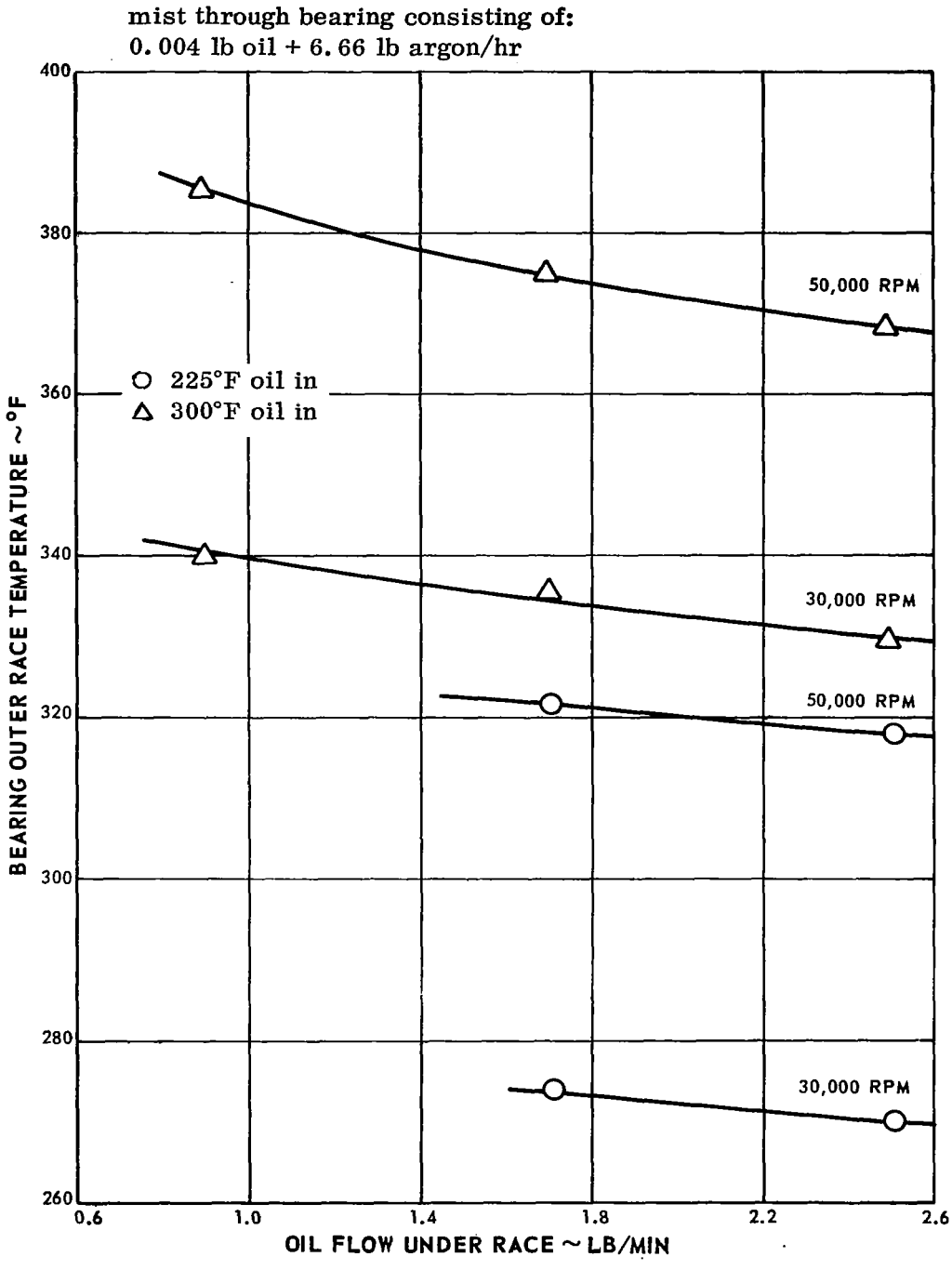

Figure 92 Effect of Oil-In Temperature on Bearing Temperature with Dry-Mist Lubrication

mist through bearing consisting of:
0.004 lb oil + 6.66 lb argon/hr

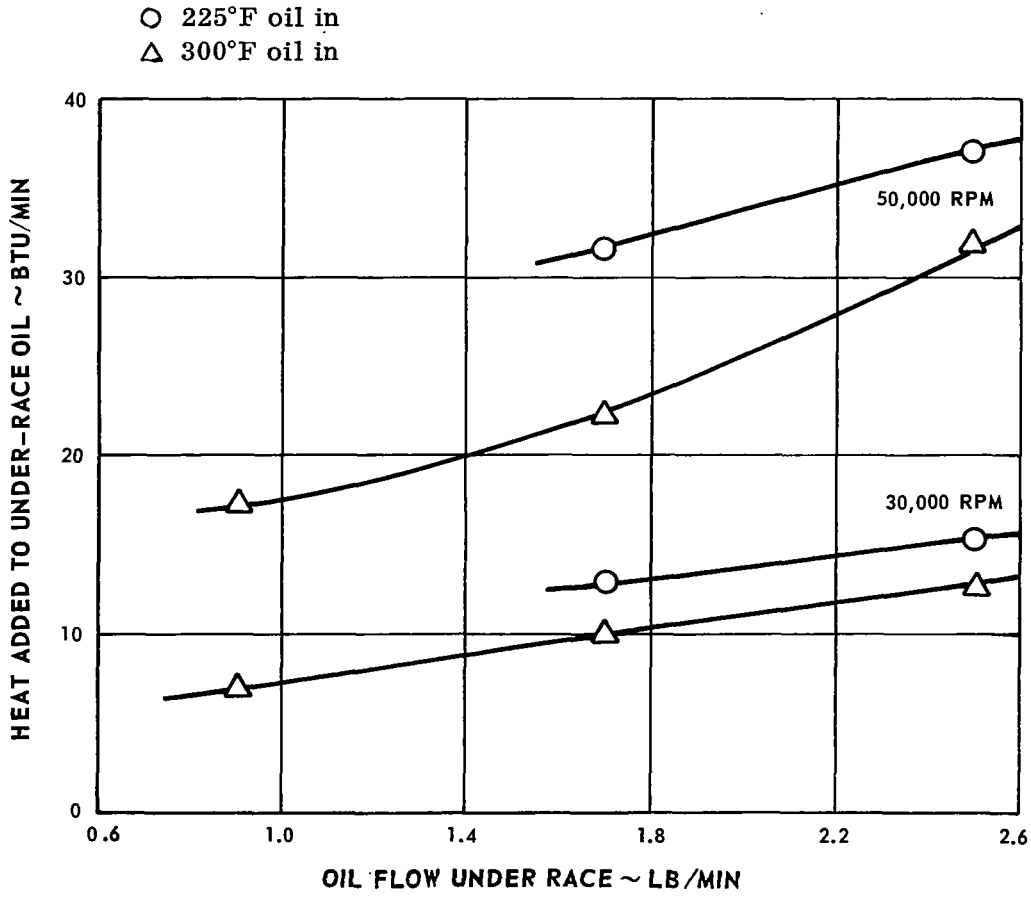

Figure 93 Effect of Oil-In Temperature on Heat Added to Under-Race Oil with Dry-Mist Lubrication

mist through bearing consisting of:
0.004 lb oil + 6.66 lb argon/hr

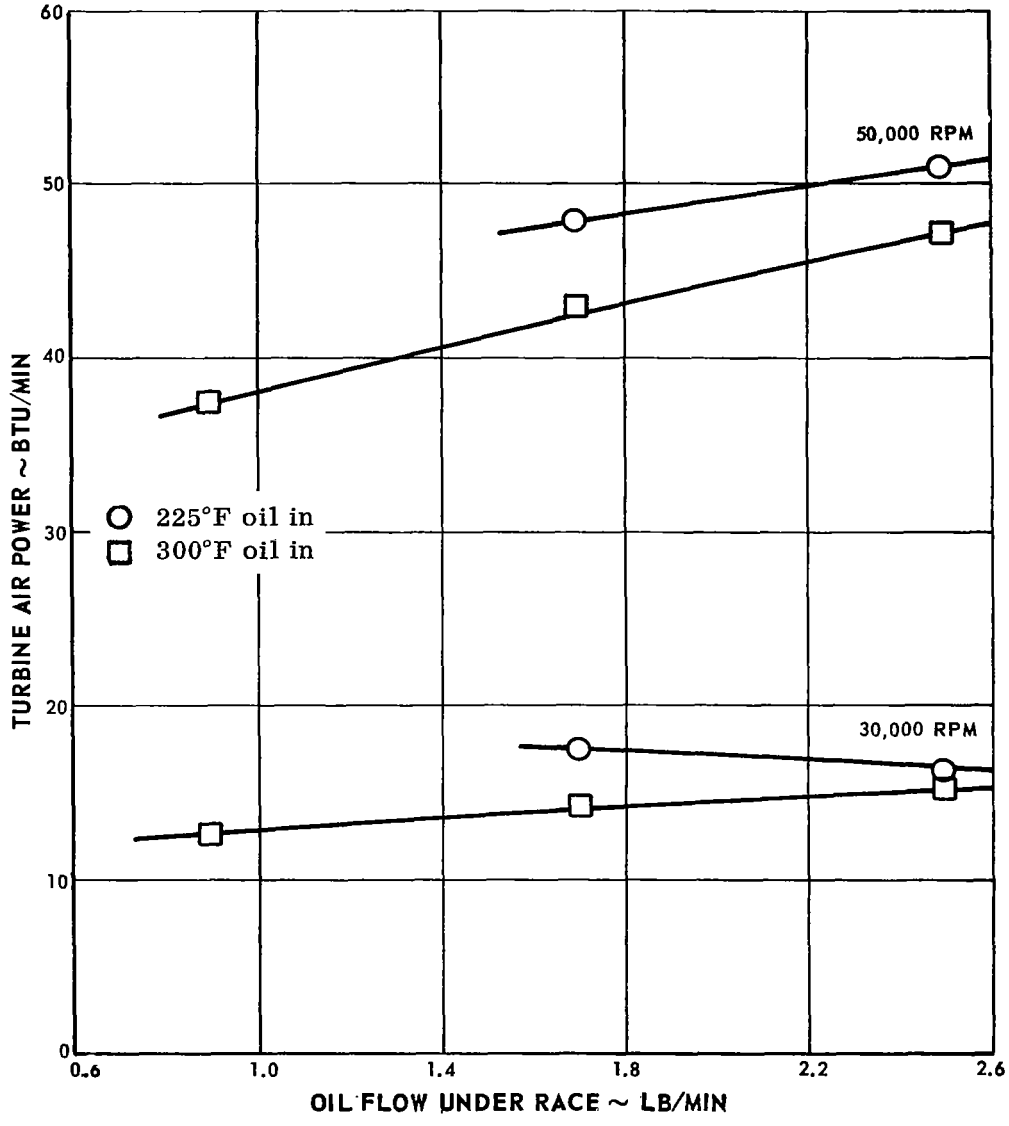

Figure 94 Effect of Oil-In Temperature on Total Rig Power Consumption with Dry-Mist Lubrication

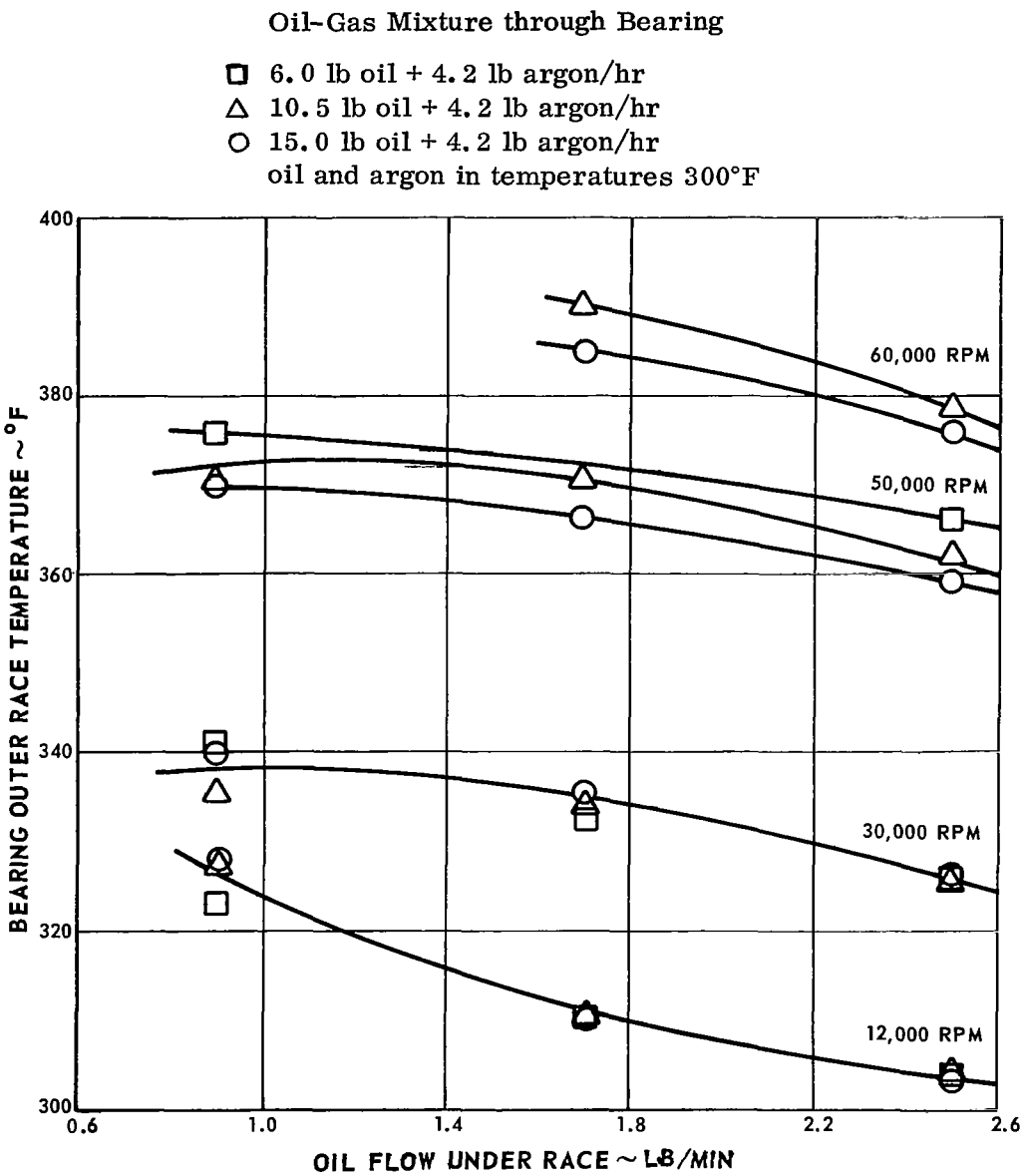

Figure 95 Bearing Temperature with Flood Oil Lubrication

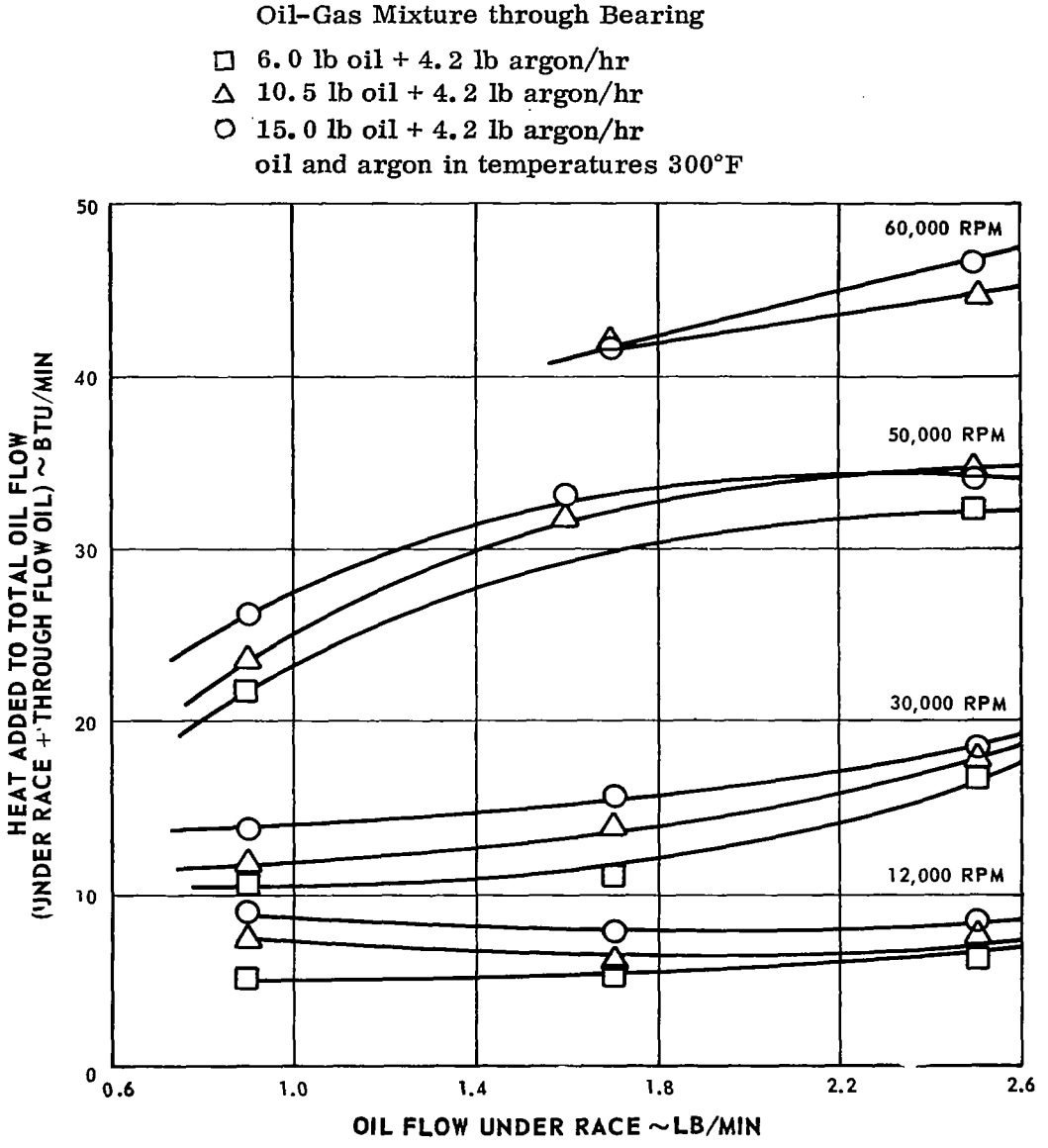

Figure 96 Heat Added to Total Oil Flow of Bearing with Flood Oil Lubrication

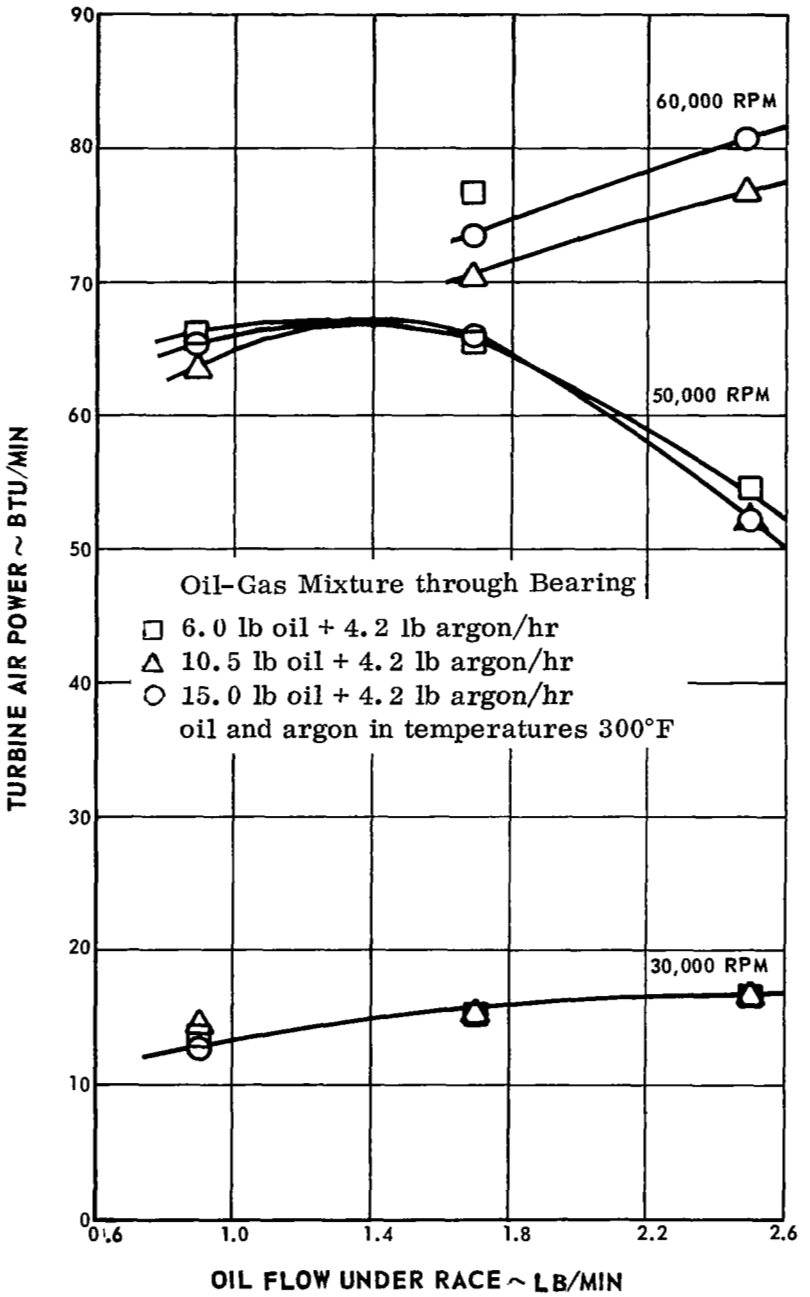

Figure 97 Total Rig Power Consumption with Flood Oil Lubrication

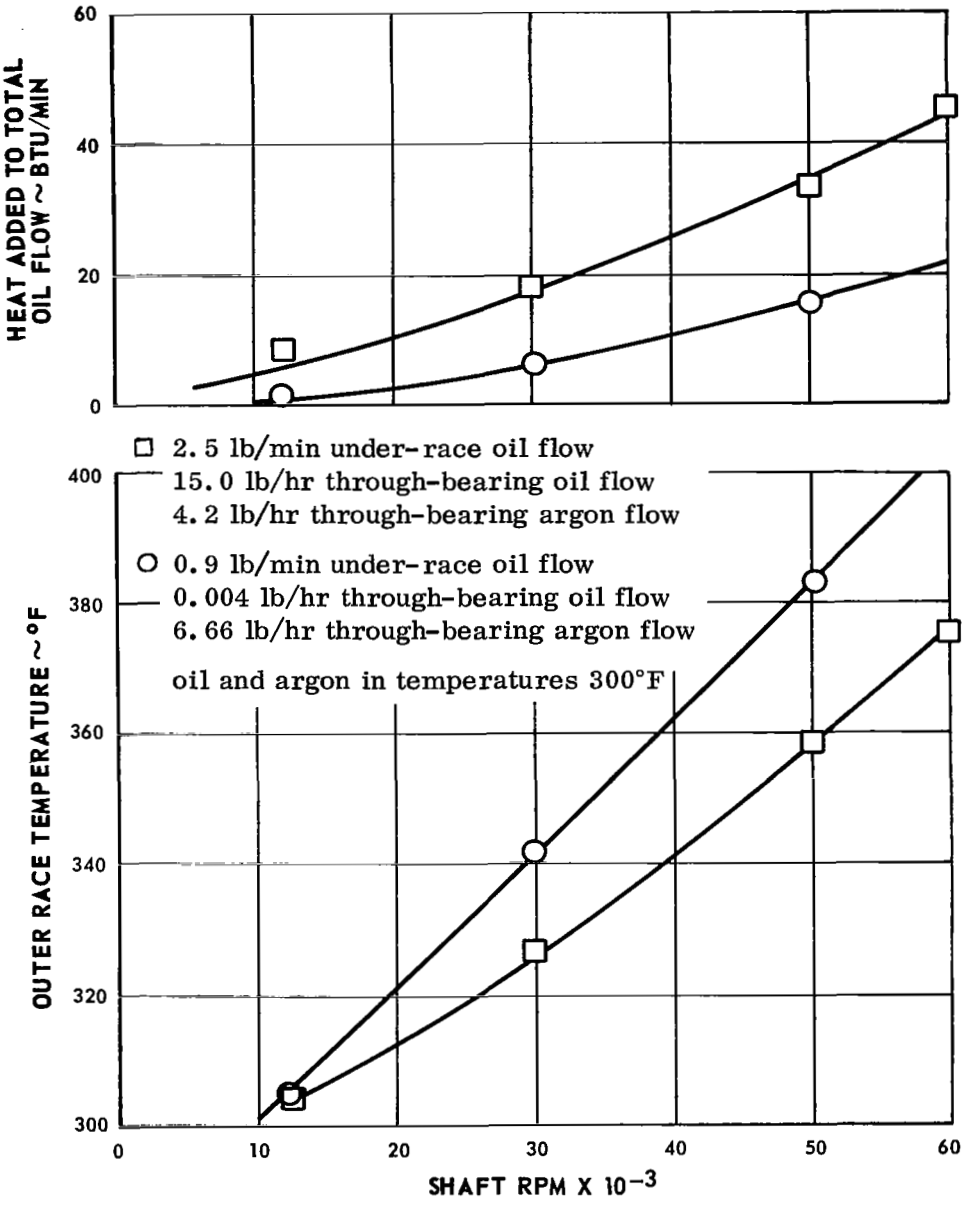

Figure 98 Bearing Performance with Maximum and Minimum Oil Flows

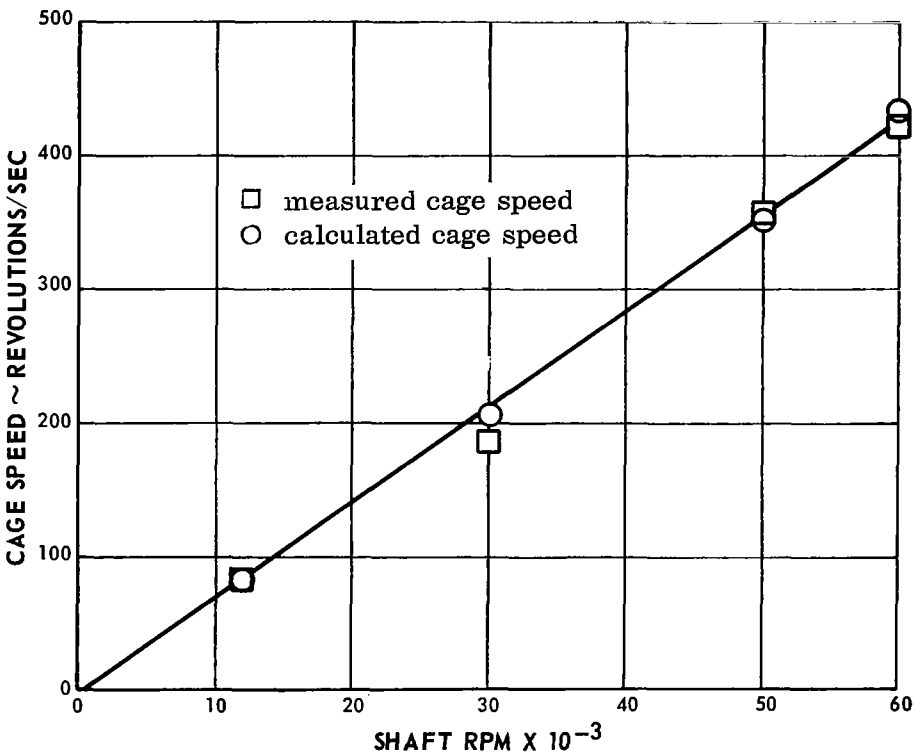

Figure 99 Bearing Cage Speeds

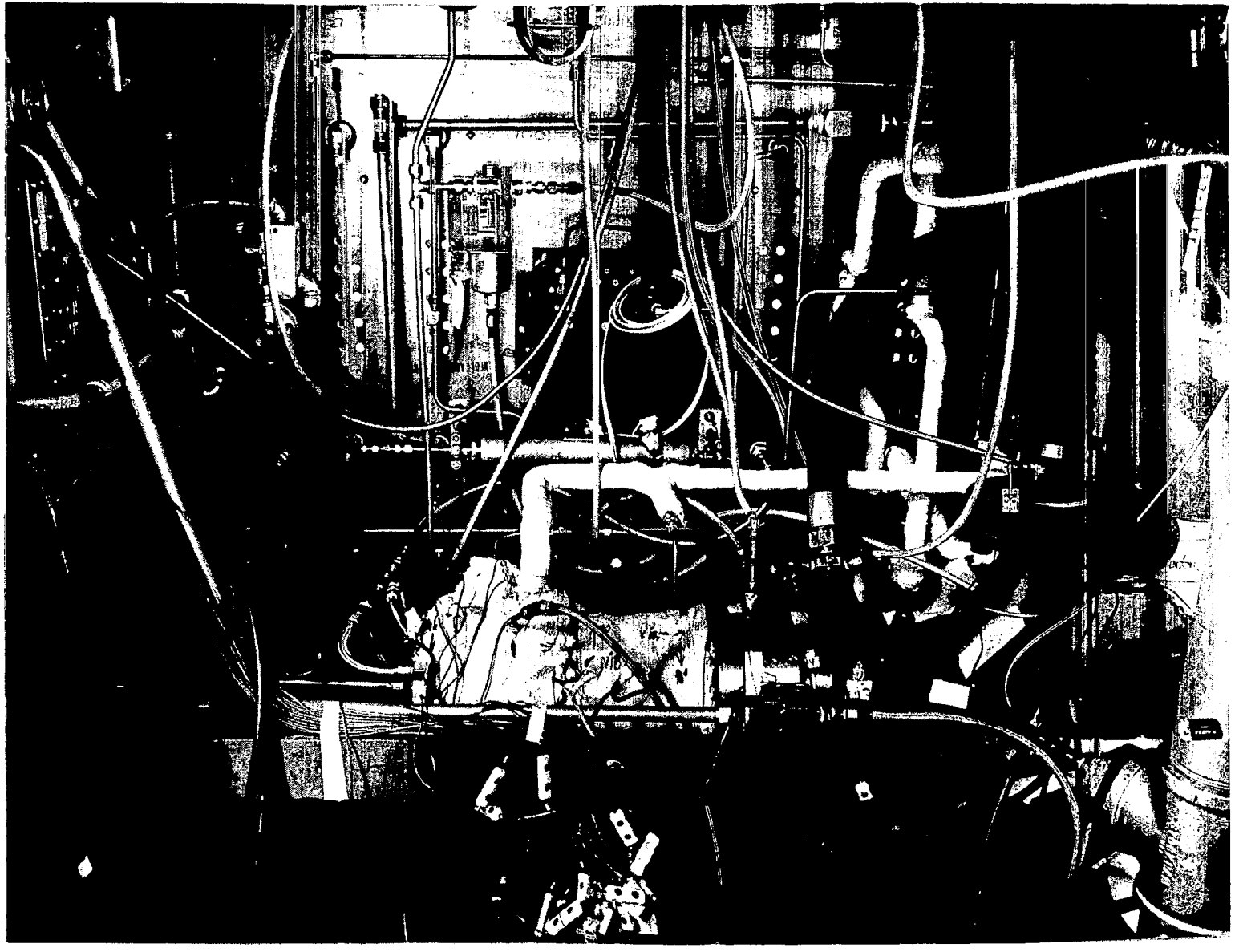

Figure 100 Turbine-Compressor Bearing Compartment Test Rig X-23299

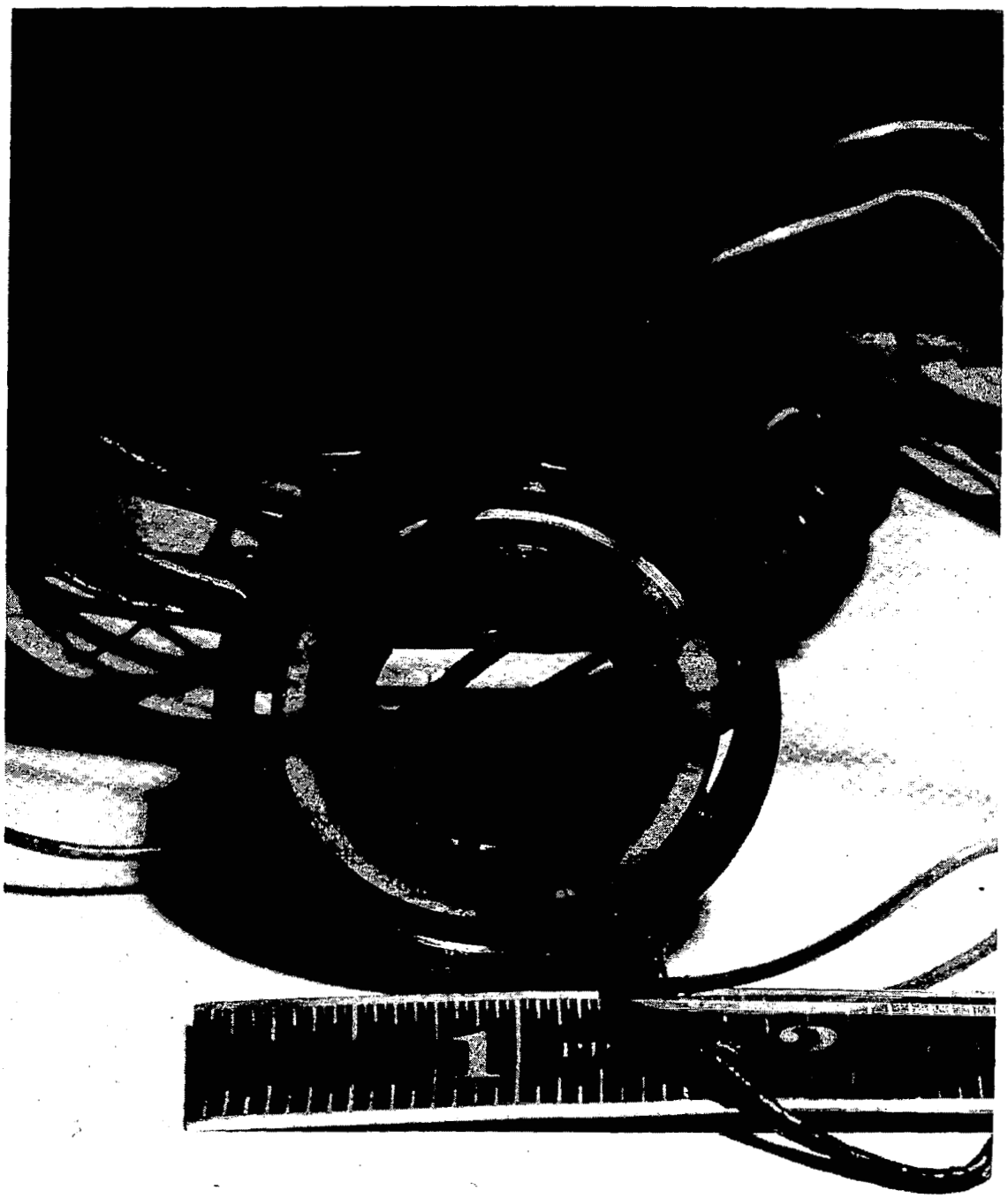

Figure 101 Turbine-Compressor Bearing with Strain Gages and Thermocouples

B. Turbine - Compressor Seal Tests

Seal tests were conducted to determine the performance of three turbine-compressor seal designs discussed in Section IV. The rig in which the tests were run was described in Section VI (see Figure 76). Gas and oil leakage rates were determined for each design. The power consumption was estimated from test data. The gas leakage was determined by measuring the rate of pressure change with time in a known volume of gas connected to the seal cavity. In all tests the oil leakage was very low, in fact, so low that only minor wetting on the surface could be detected. The amount of oil leakage was determined by washing the parts subjected to leakage in solvent, then chromatographically determining the amount of oil in the solution. Upon completion of the performance calibrations, the dry-face seal design was selected for endurance testing at 50,000 rpm. Two seals were tested for 2500 hours. The results of the seal test program are presented below for each design. Figure 102 shows a photograph of the seal rig installation and Figure 76 shows the design of the rig.

1. Wet-Face Seal Tests

Figures 103 through 106 present the performance of the wet-face design shown in Figure 63. Figures 103 and 104 show the leakage characteristics of the seal as a function of pressure drop and speed for both argon and helium. The leakage rate is approximately one order of magnitude less than the design estimate. The power consumption of the seal is shown in Figures 105 and 106. By either method shown the seal consumes more power than the 300 watts calculated for the design. The seal configuration and post-test condition are shown in Figures 64, 107, 108 and 109. As indicated by these illustrations, the seal was in excellent condition and practically no wear was detected

2. Controlled - Clearance Seal Tests

The performance characteristics and post-test condition of the controlled-clearance seal (Figure 69) are presented in Figures 110 through 113. Argon and helium leakage characteristics are shown in Figures 110 and 111. Figure 112 presents the power consumption determined from test data. As in the wet-face seal case, the leakage was less and the power consumption greater than predicted. The tests were limited to 30,000 rpm due to what appears to be inadequate clearance at the more severe operating conditions above 30,000 rpm. Figure 113 shows the condition of the seal after test. Some damage is evident as a result of the inadequate clearance. This design deficiency could probably be corrected by incorporating either cooling, clearance increase or material change, or a combination of these features.

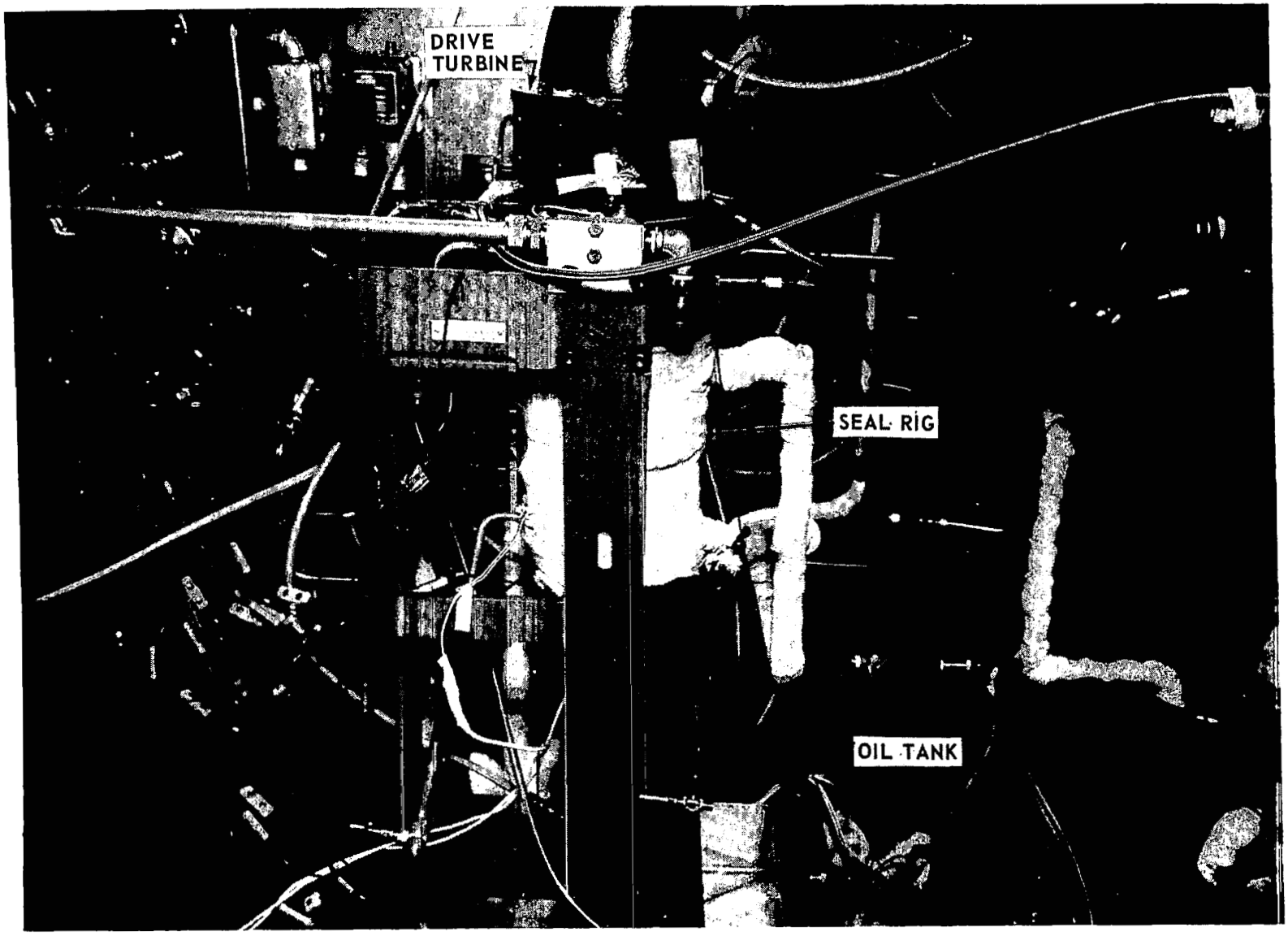

Figure 102 Turbine-Compressor Seal Rig Installation X-23779

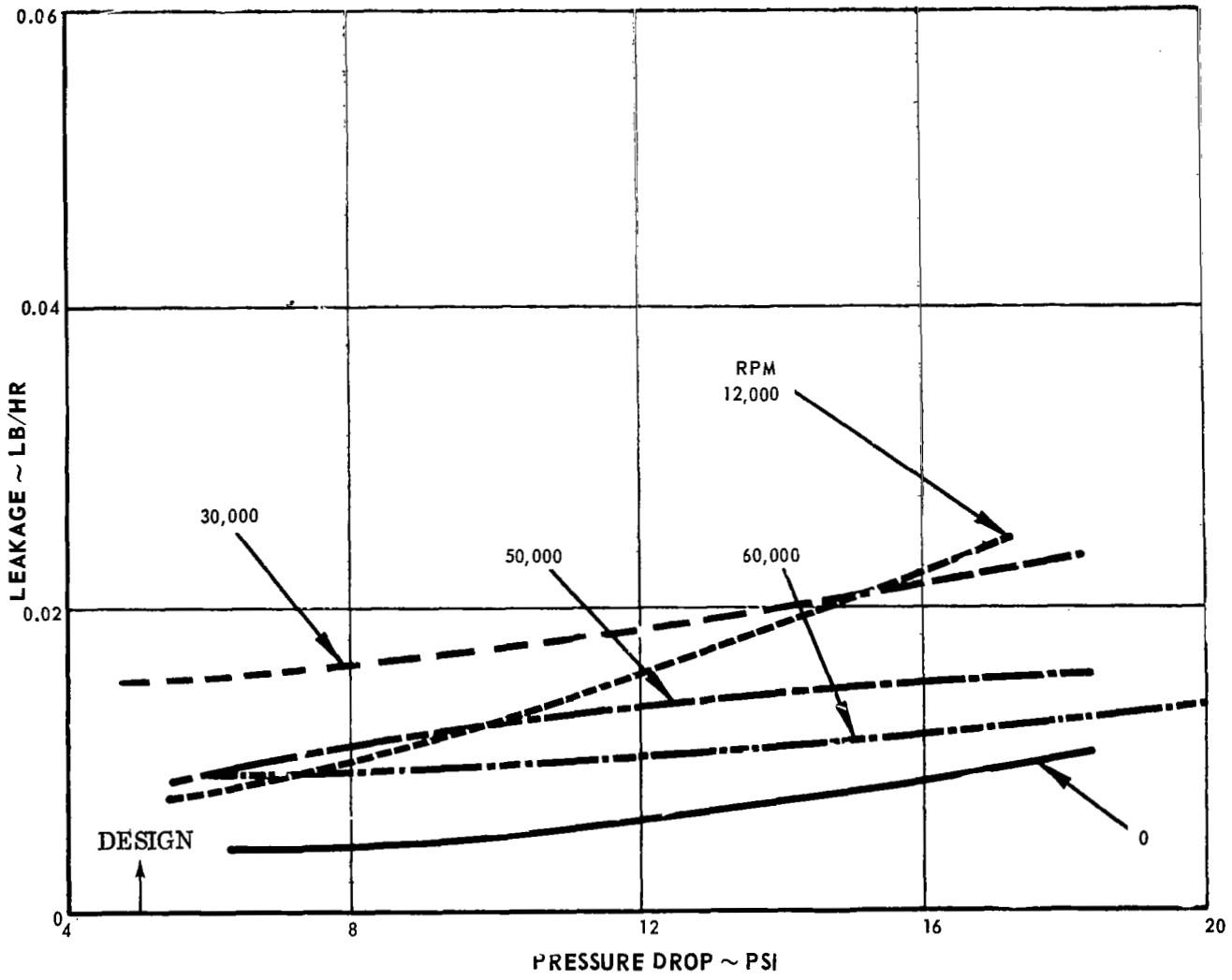

Figure 103 Wet-Face Seal Leakage with Argon

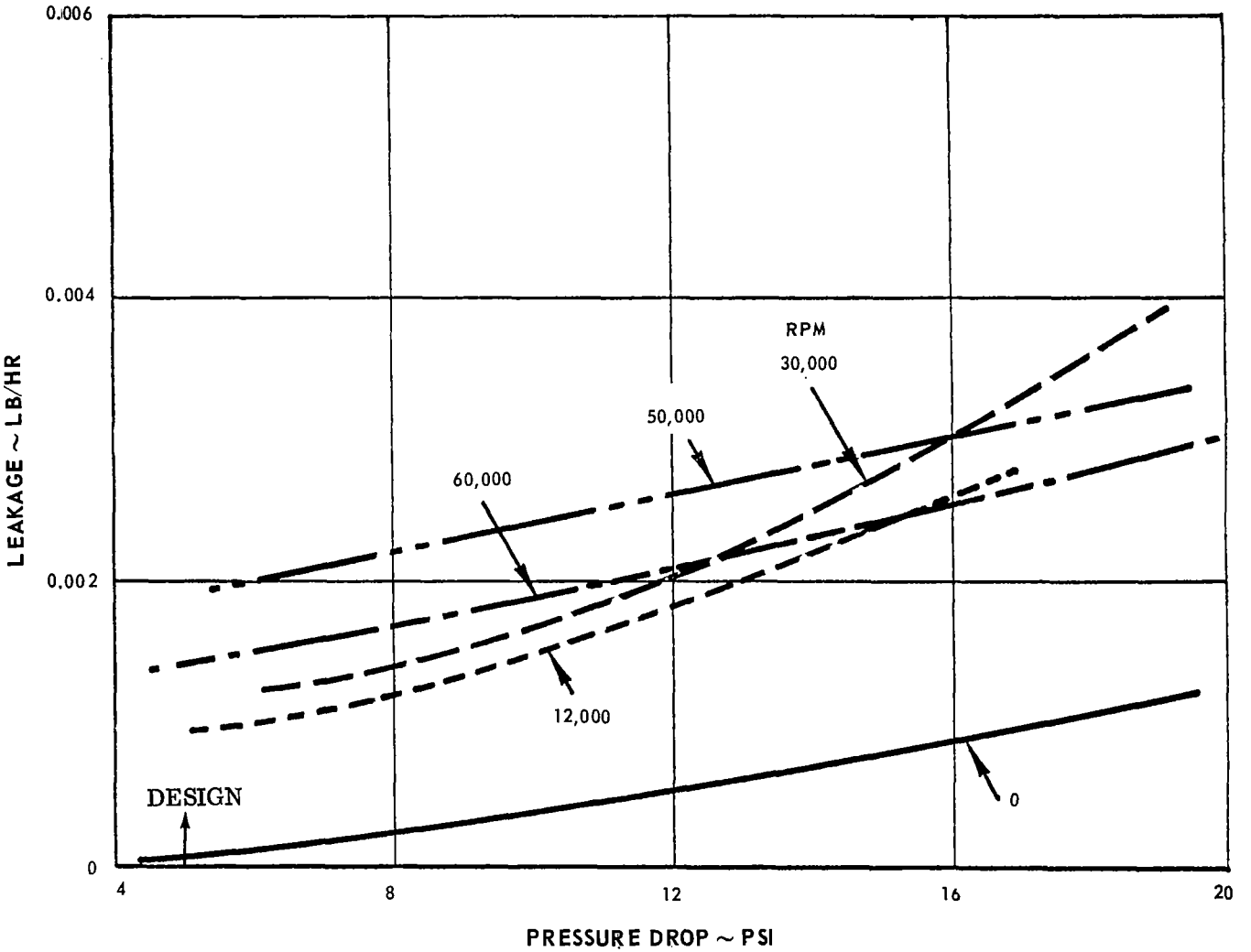

Figure 104 Wet-Face Seal Leakage with Helium

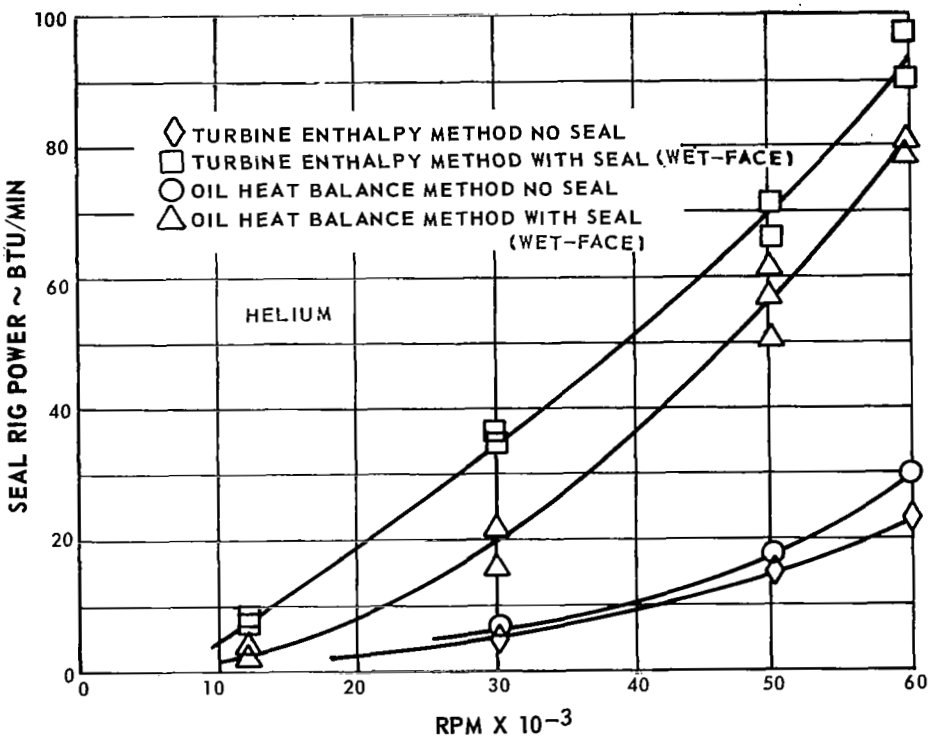

Figure 105 Seal Rig Power

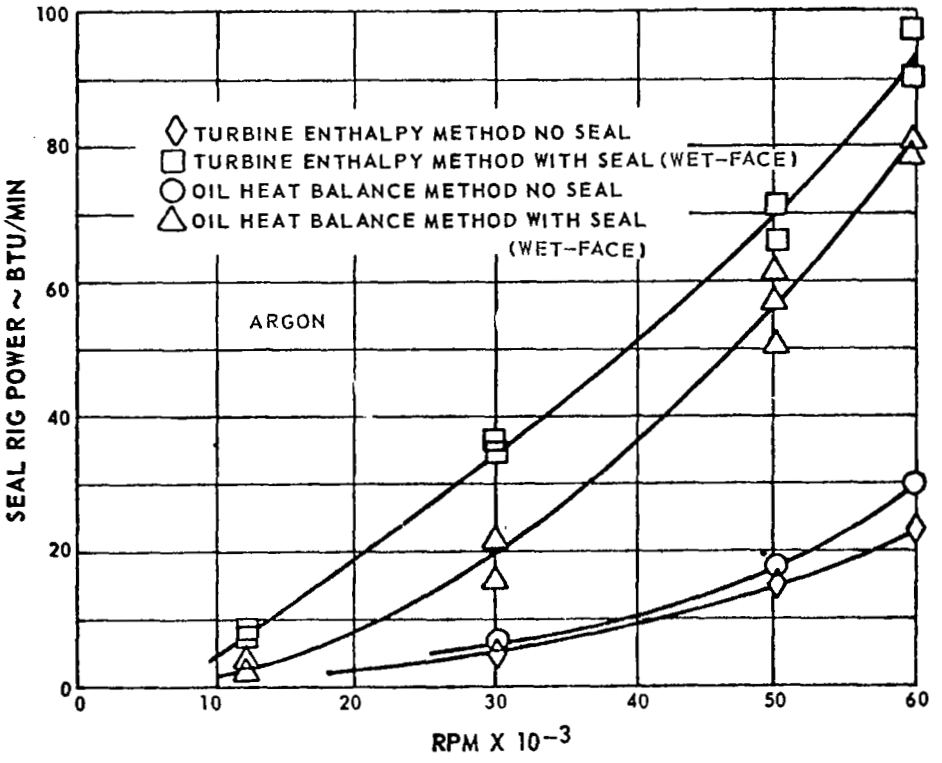

Figure 106 Seal Rig Power

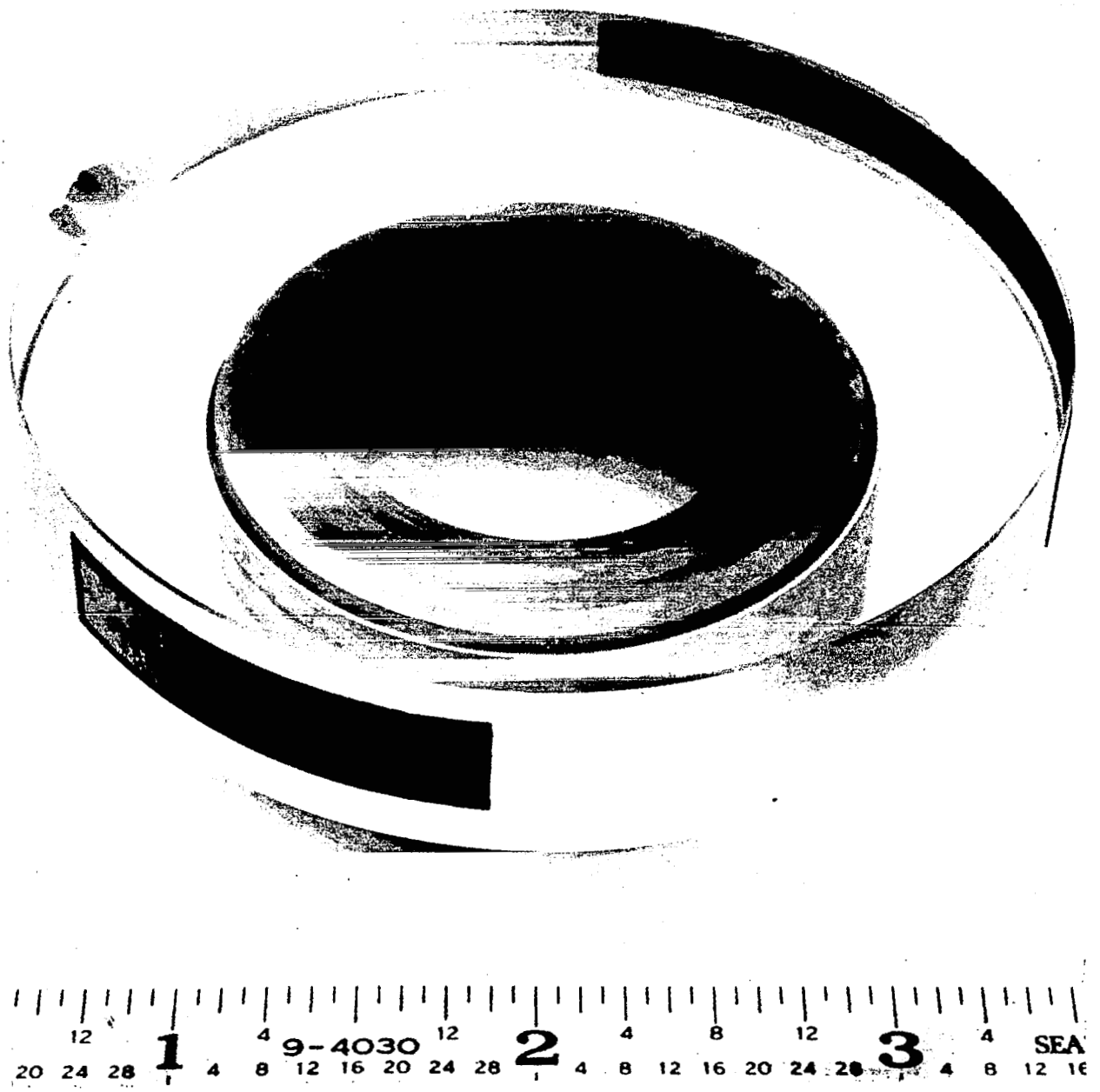

Figure 107 Optical Flat on Wet Face Seal after Test

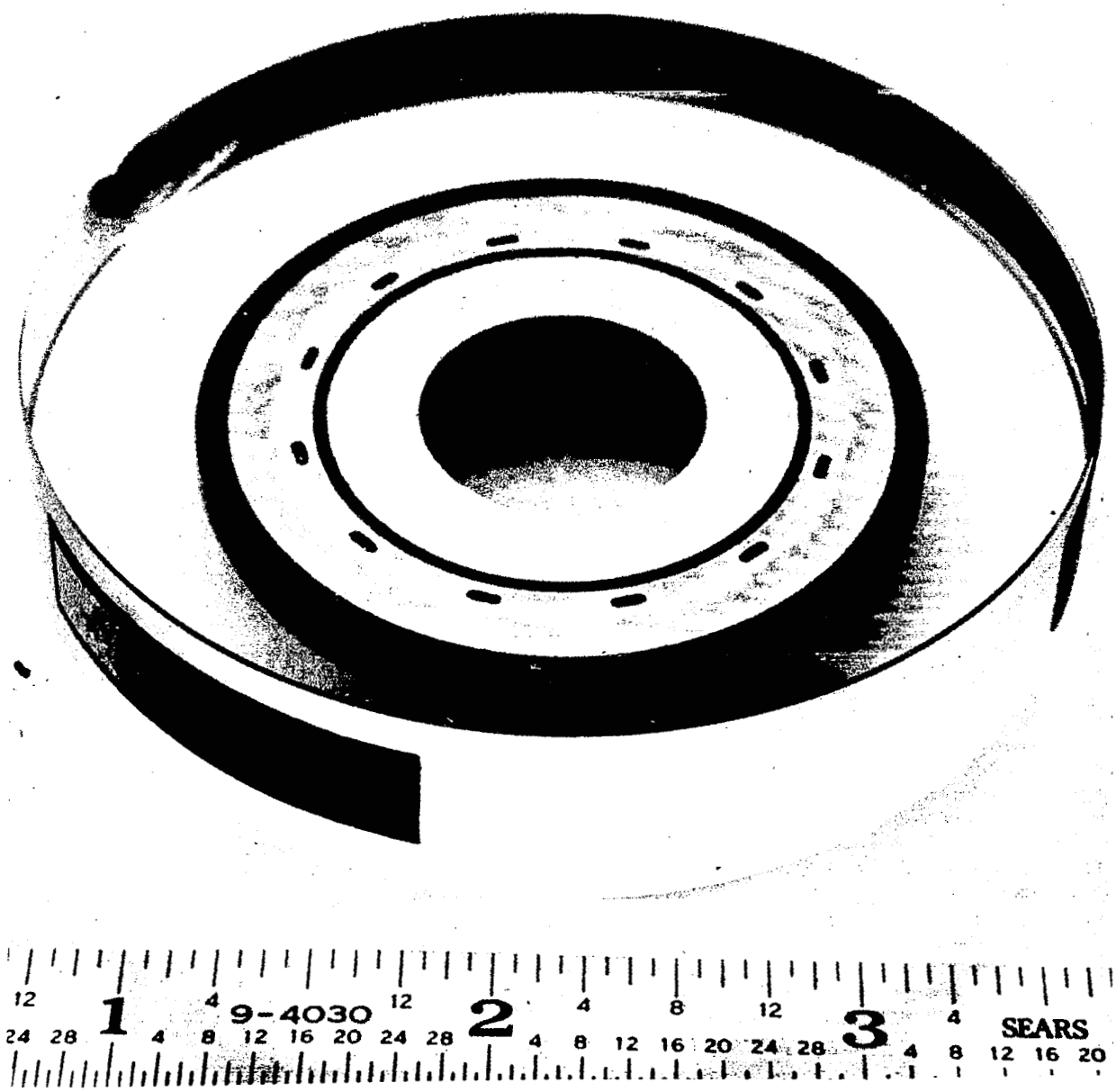

Figure 108 Optical Flat on Wet-Face Sealplate after Test

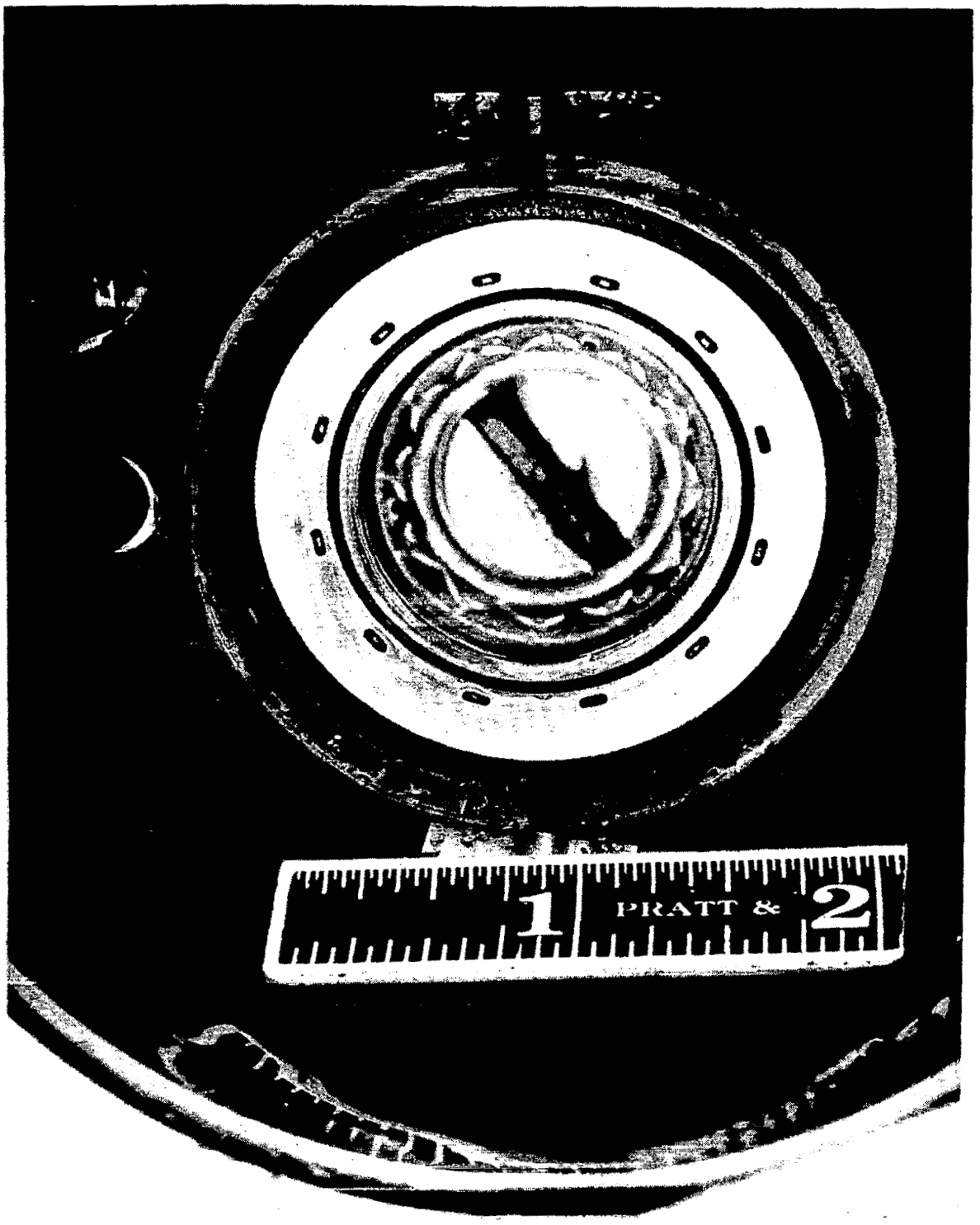

Figure 109 Wet Face Seal Cavity after Test. X-24195

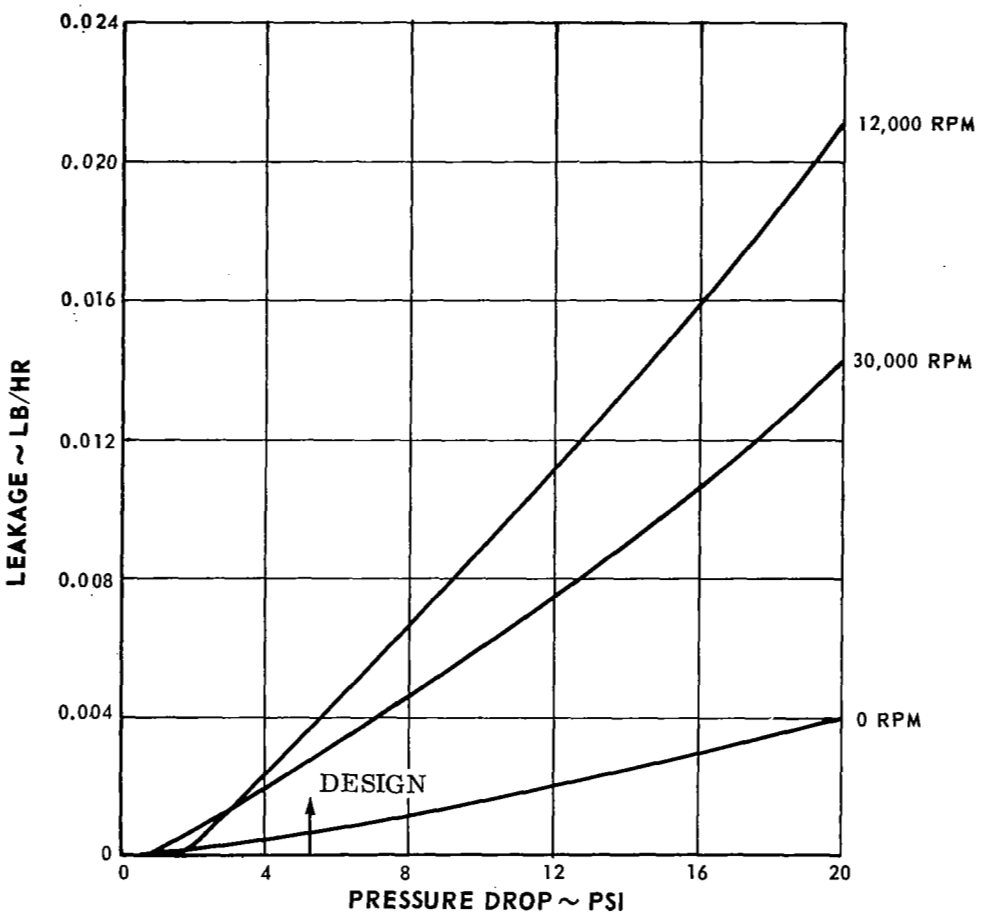

Figure 110 Argon Leakage with Controlled-Clearance Seal

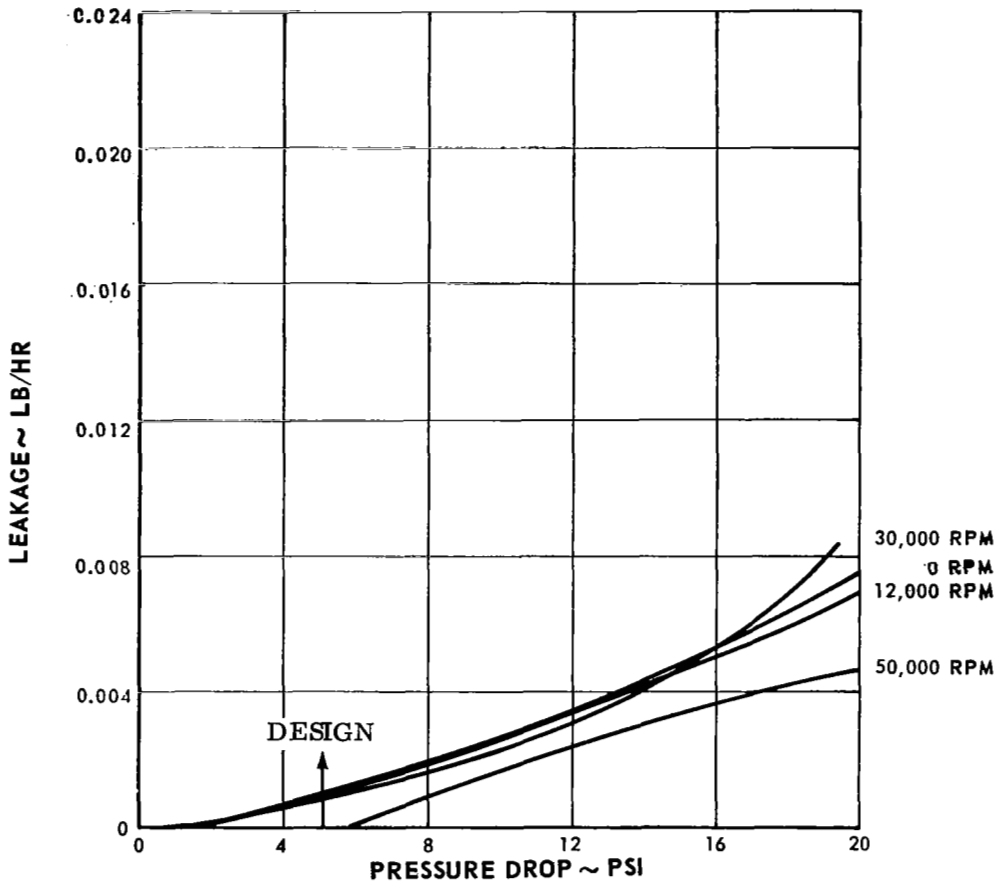

Figure 111 Helium Leakage with Controlled-Clearance Seal

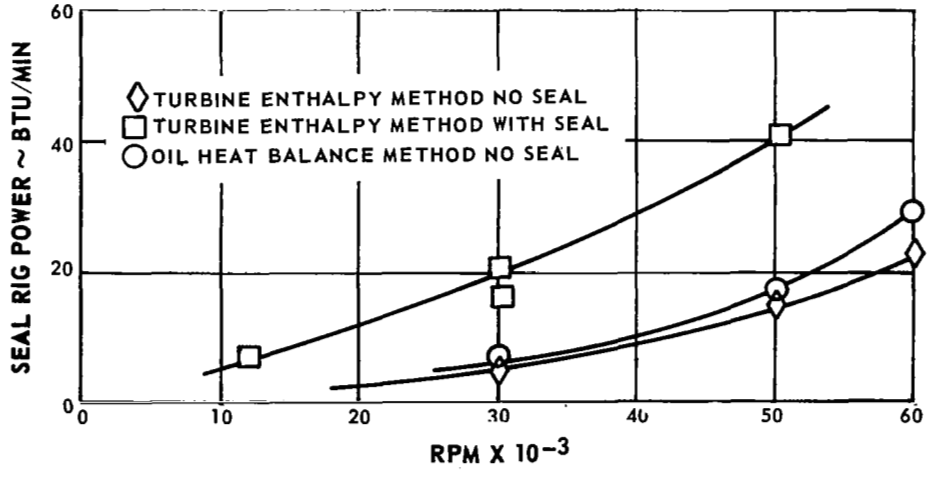

Figure 112 Seal Rig Power for Controlled-Clearance Seal

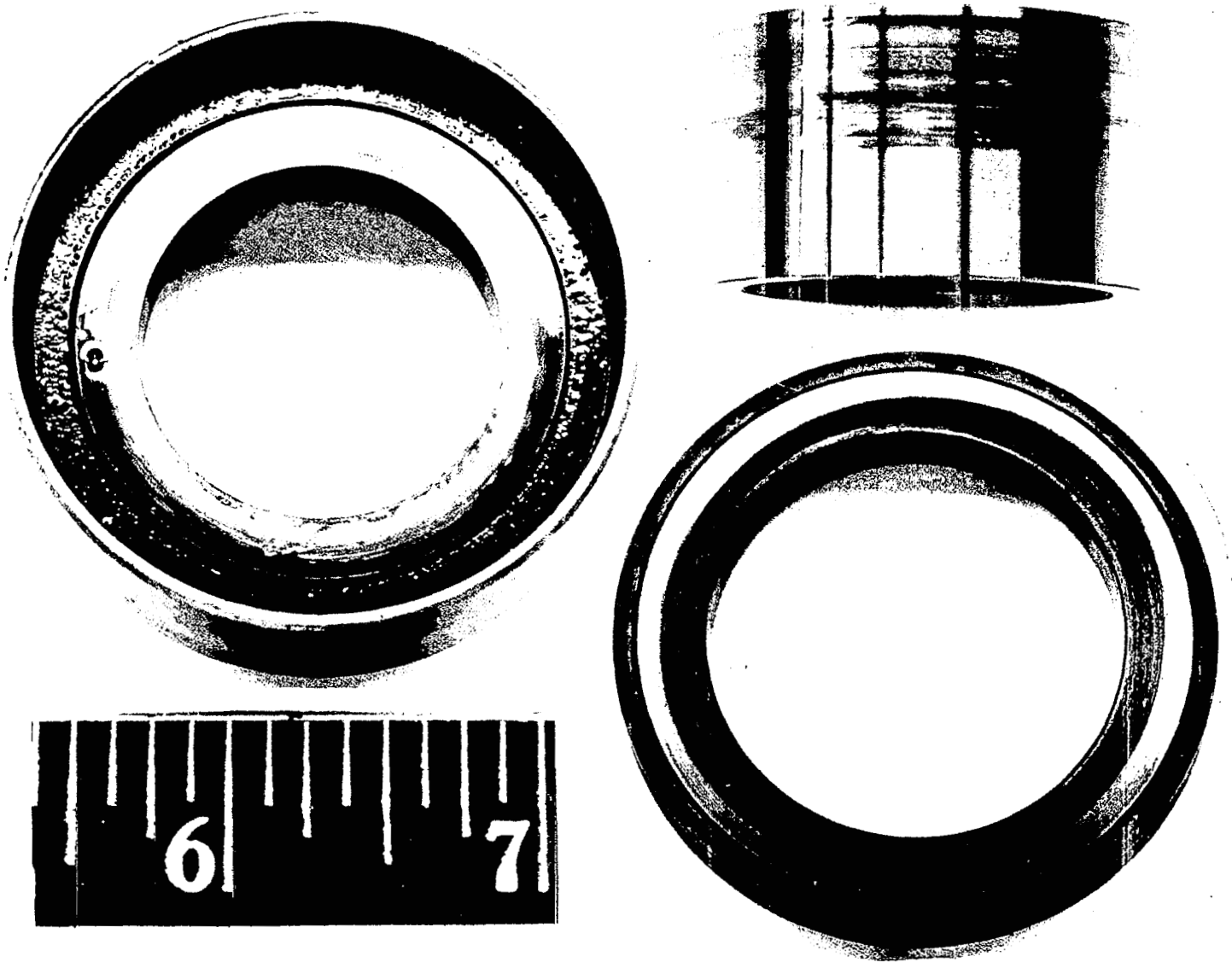

Figure 113 Bellows and Shell, Rotating Sleeve, and Carbon Ring of Controlled-Clearance Seal after Test X-24698, X-24696, X-24697

3. Dry - Face Seal Tests

The performance characteristics of the dry-face seal are shown in Figures 114 through 124. Argon and helium leakage rates are shown in Figures 114 and 115, and the power consumption in Figures 116 and 117. As in the case of the other two designs, the gas leakage was less and the power consumption more than predicted.

Based upon the calibration test results, the dry-face seal was selected for a 2500-hour test at design conditions of 50,000 rpm and 5 psi pressure differential. This test was completed with no deterioration in either performance or seal condition, as evidenced by Figures 118 through 121. The carbon wear during the test was as follows: 0 to 10 hours 0.0004 inch, 10 to 100 hours an additional 0.00015, for a total wear of 0.00055 inch.

Significant design and performance parameters are tabulated in Table 13. The oil and gas leakage rates as well as the carbon wear are presented as linear extrapolations from 2500-hour data. The carbon wear characteristics as a function of running time are shown in Figure 122. Wear measurements were made at 10, 100 and 2500 test hours. This curve also includes the wear characteristics of the seal used in the 2500-hour pilot system test.

TABLE 13

Turbine-Compressor Dry-Face Seal
2500-Hour Test

RPM,	50,000
rubbing speed, ft/sec	335
carbon	CDJ-83
sealplate surface	chrome carbide
carbon wear allowance, inch	0.030
gas leakage, lb/10,000 hr	2
oil leakage to sweep gas, gm/10,000 hr	11
carbon wear, inch/10,000 hr	0.0087
sweep gas flowrate, lb/hr	0.7
sweep gas oil vapor carrying capacity, gm/10,000 hr	635

Seal gas leakage was continuously monitored during the test. This gas leakage with time is shown in Figure 123. The meter used for the measurement could be read to a minimum flow rate of 0.0002 pound per hour. Examination of the curve shows that most of the data points are between 0 and 0.0002. Some points

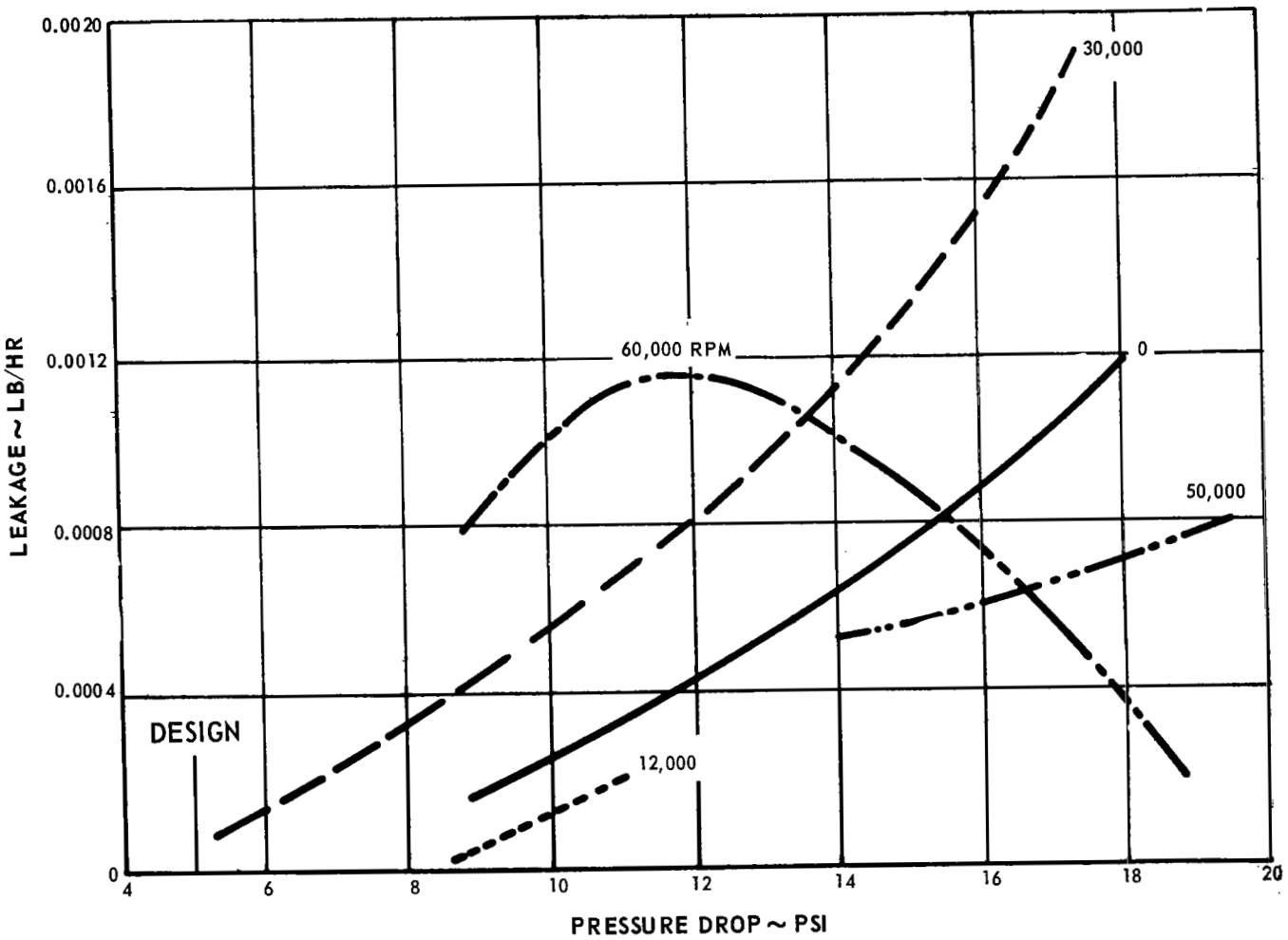

Figure 114 Dry-Face Seal Argon Leakage

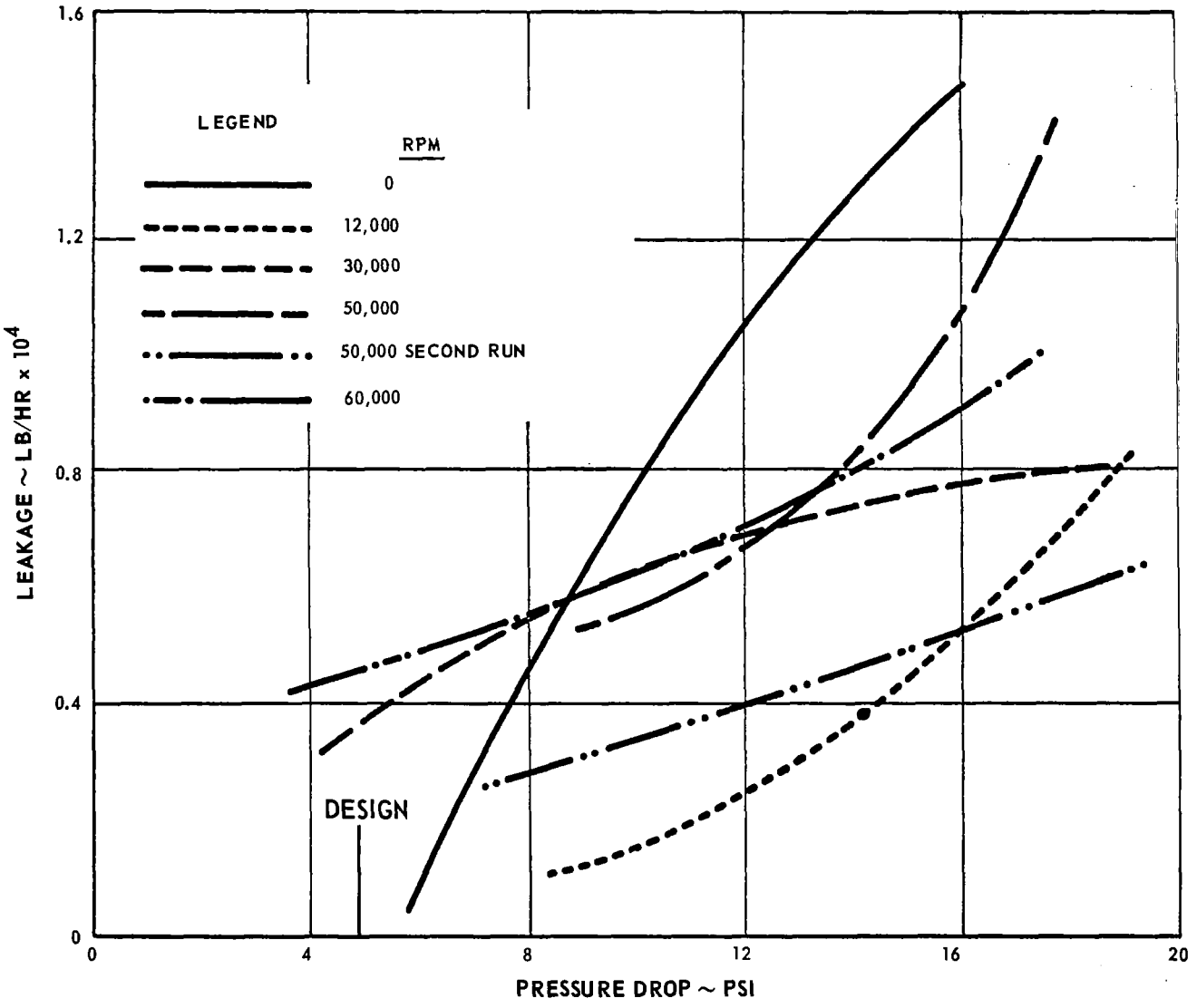

Figure 115 Dry-Face Seal Helium Leakage

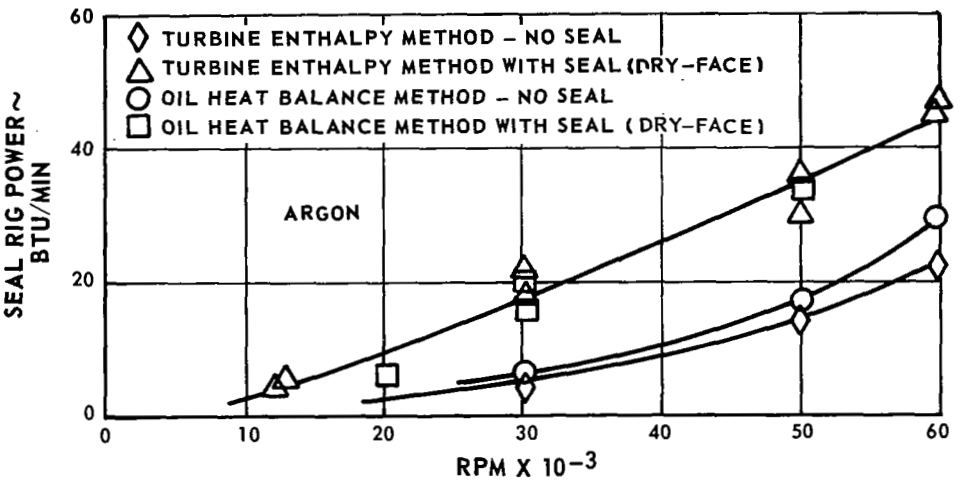

Figure 116 Seal Rig Power

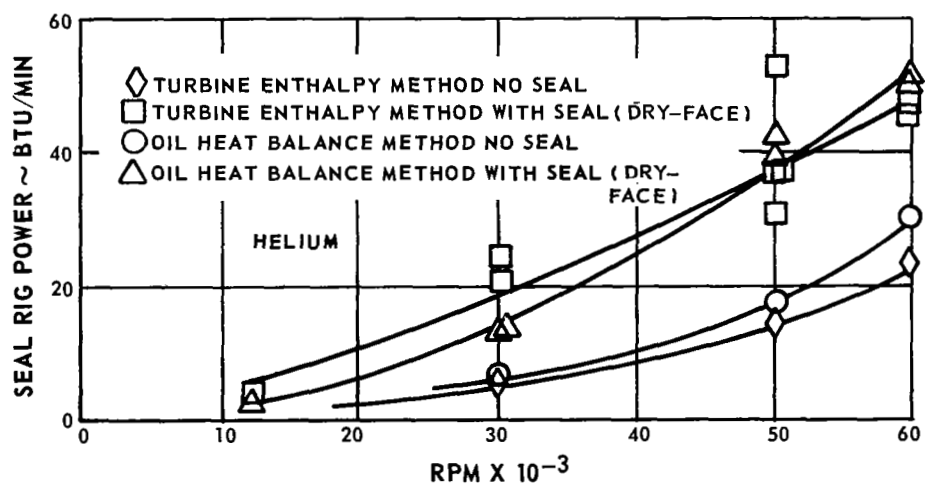

Figure 117 Seal Rig Power

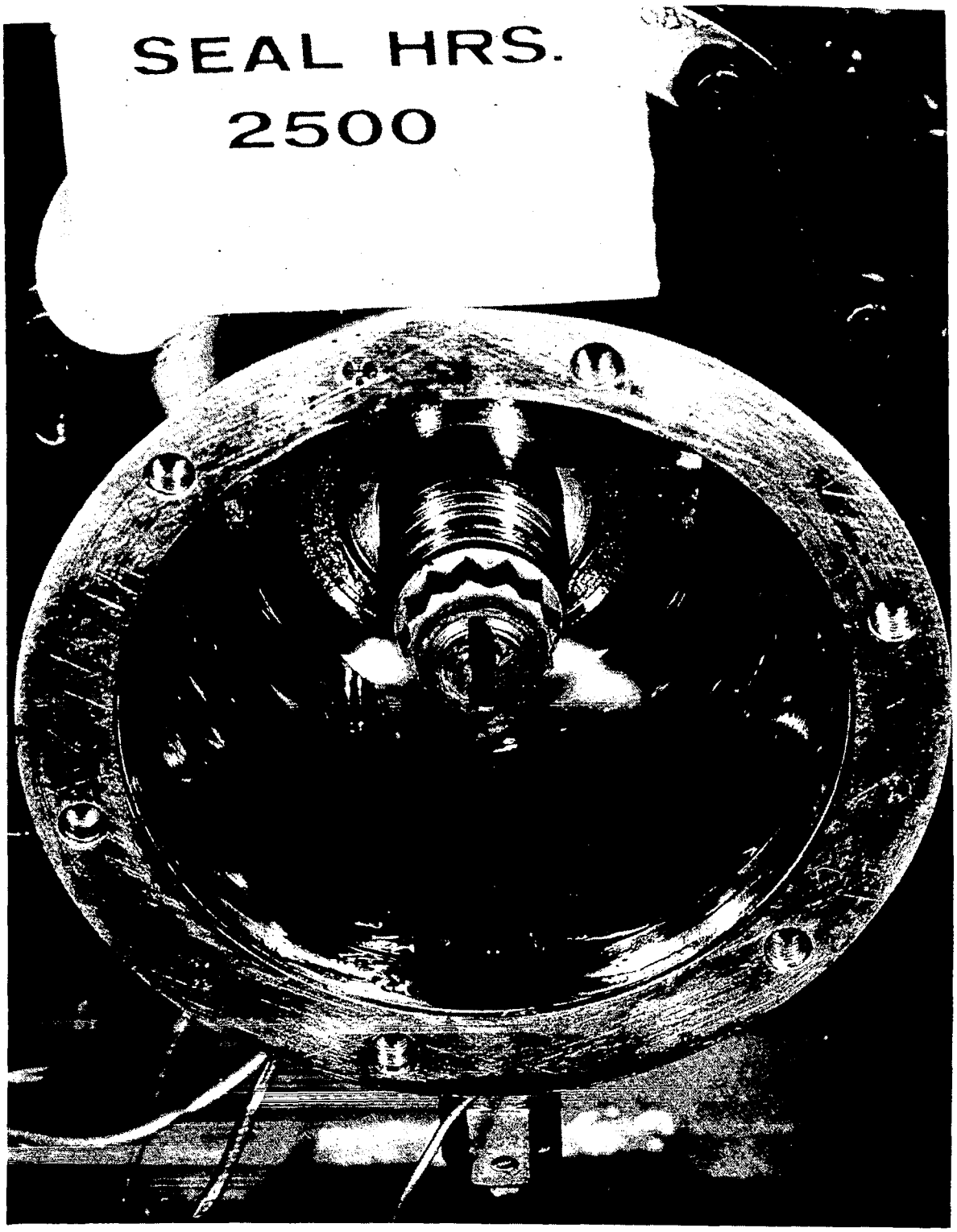

Figure 118 Dry-Face Sealplate after 2500-Hour Test before Removal and Cleaning

Figure 119 Dry-Face Seal and Holder after 2500-Hour Test at 50, 000 rpm

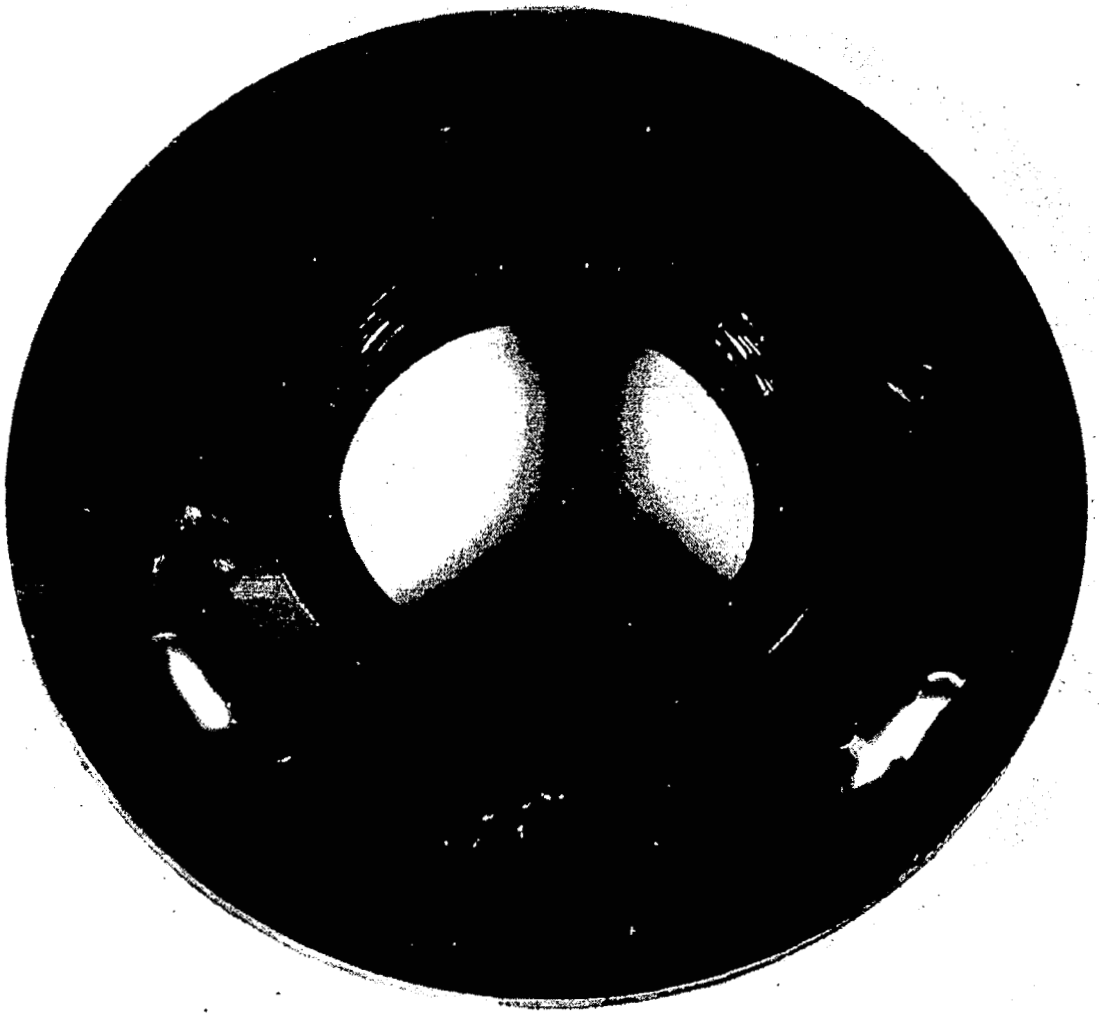

Figure 120 Dry-Face Sealplate after 2500-Hour Test at 50, 000 rpm CN-11527

Figure 121 Dry-Face Seal and Sealplate after 2500-Hour Test at 50, 000 rpm CN-11526

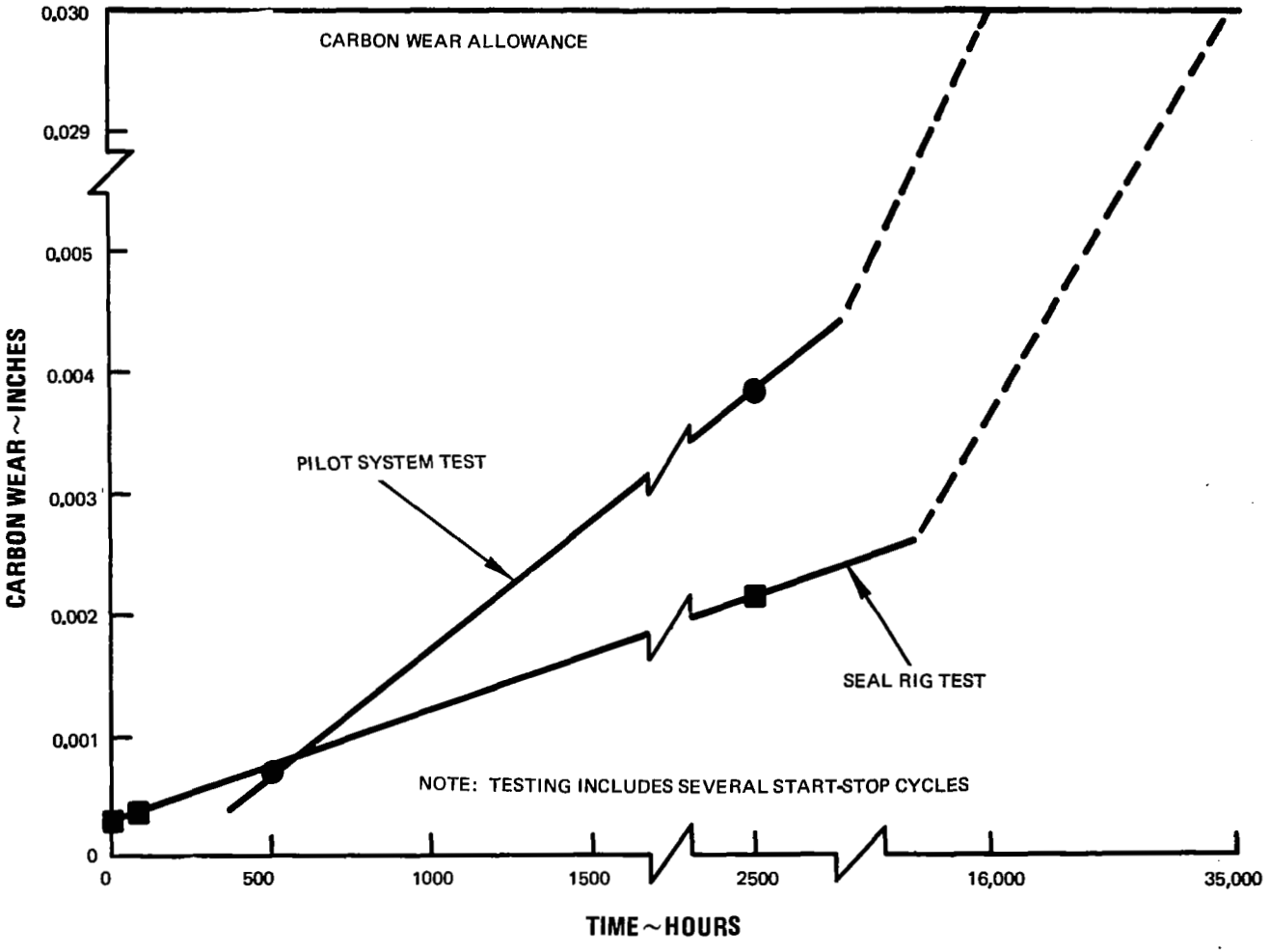

Figure 122 Turbine-Compressor Dry-Face Seal Wear M-49226

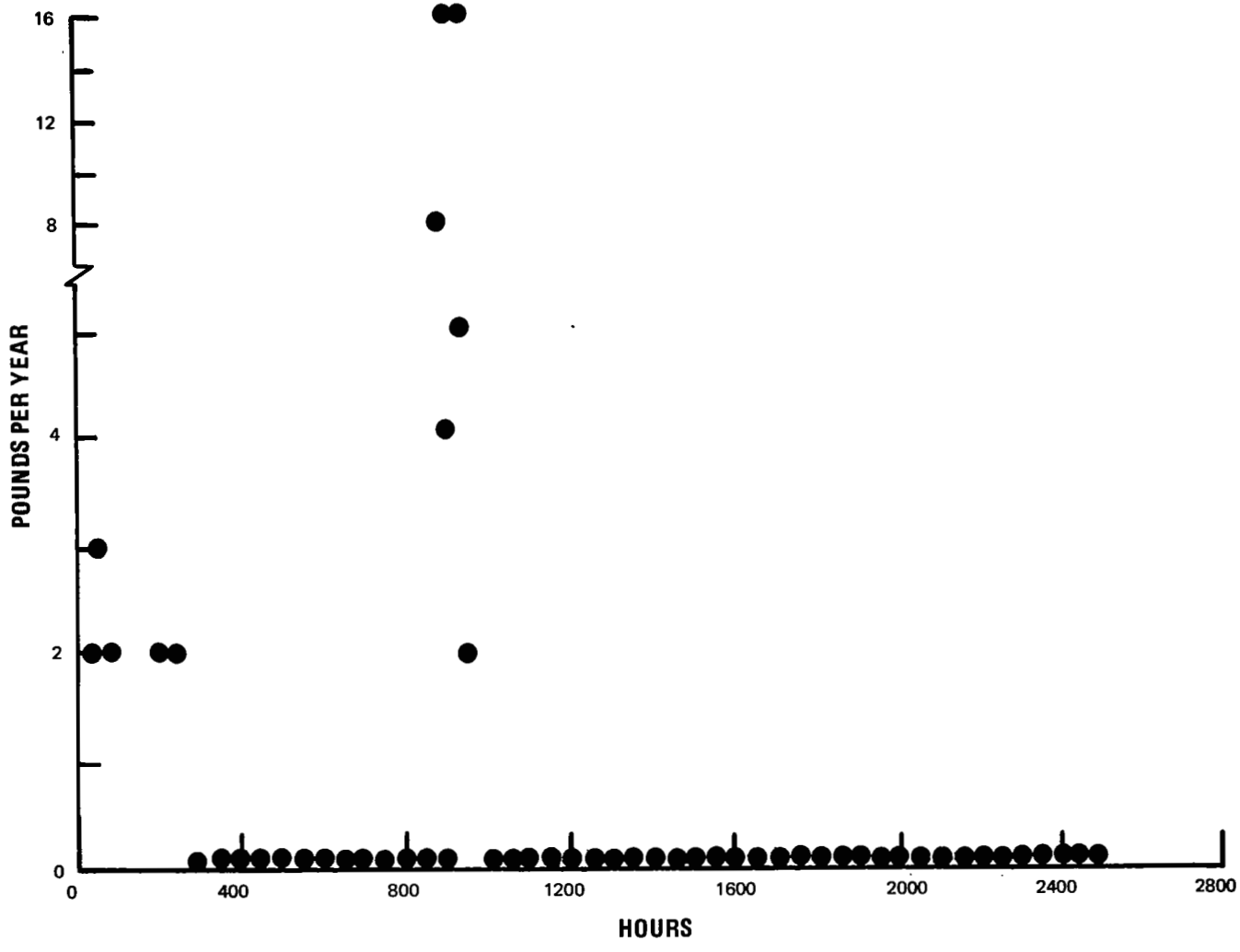

Figure 123 Seal Gas Leakage M-49779

are near 0.0002 pound per hour and a few are greater than 0.0002. One can conclude from this curve that the leakage rate is not constant, and, more important, that the seal recovered from the perturbations which caused the leakage rate to change. The cause may have been small particles of dirt or wear debris in the contact zone.

Power consumption data from Figures 116 and 117 was combined and replotted as an average curve in Figure 124.

The solubility of oil in argon as a function of temperature is shown in Figure 125. Data from this curve was used to establish the oil-vapor carrying capacity of the sweep gas shown in Table 13.

C. Scavenge Tests

Two types of tests were made on the scavenge rig, Figure 77. The first was to determine the head-flow characteristics of the scavenge impellers and the second to confirm and demonstrate the two-phase flow phenomena upon which the lubrication system design was based.

The head-flow characteristics of the vaned centrifugal impeller operating in conjuction with the turbine-compressor bearing and vaned retaining nut, Figure 126, are shown in Figures 127 and 128. Comparison of Figures 127 and 128 indicates that orientation did not strongly influence performance.

The data in Figure 129 were obtained to investigate the effect of higher inlet pressure on performance with the same mass flow rates that were used in the 6 psia inlet pressure tests. This data established the upper limit on the head rise that could be used in the pilot endurance system test to follow. The test was run with 0.9 pound per minute of oil under the bearing race and 0.1 pound per minute of oil through the bearing being considered for the pilot endurance test. From Figures 127, 128 and 129 it can be seen that at 50,000 rpm a head rise of approximately 8 inches of water is available for two-phase scavenging with 6 psia scavenge impeller inlet pressure, and about 32 inches of water with 14.2 psia inlet pressure.

The results of typical two-phase flow demonstrations are pictorially summarized in Figures 130 and 131. In Figure 130 a section of Pyrex glass is shown installed in the vertical discharge line from the vaned centrifugal impeller. In this demonstration 60 pounds per hour of oil and 6 pounds per hour of argon were pumped through the vaned impeller and then vertically upward 24 inches in a two-phase regime. The photograph clearly shows stable annular flow. The Griffith and Wallace flow criterion used in the system design indicates annular flow for this operating condition. Figure 131 shows stable horizontal annular-slug flow. The Baker flow criterion for horizontal flow indicates annular-slug flow for this particular condition.

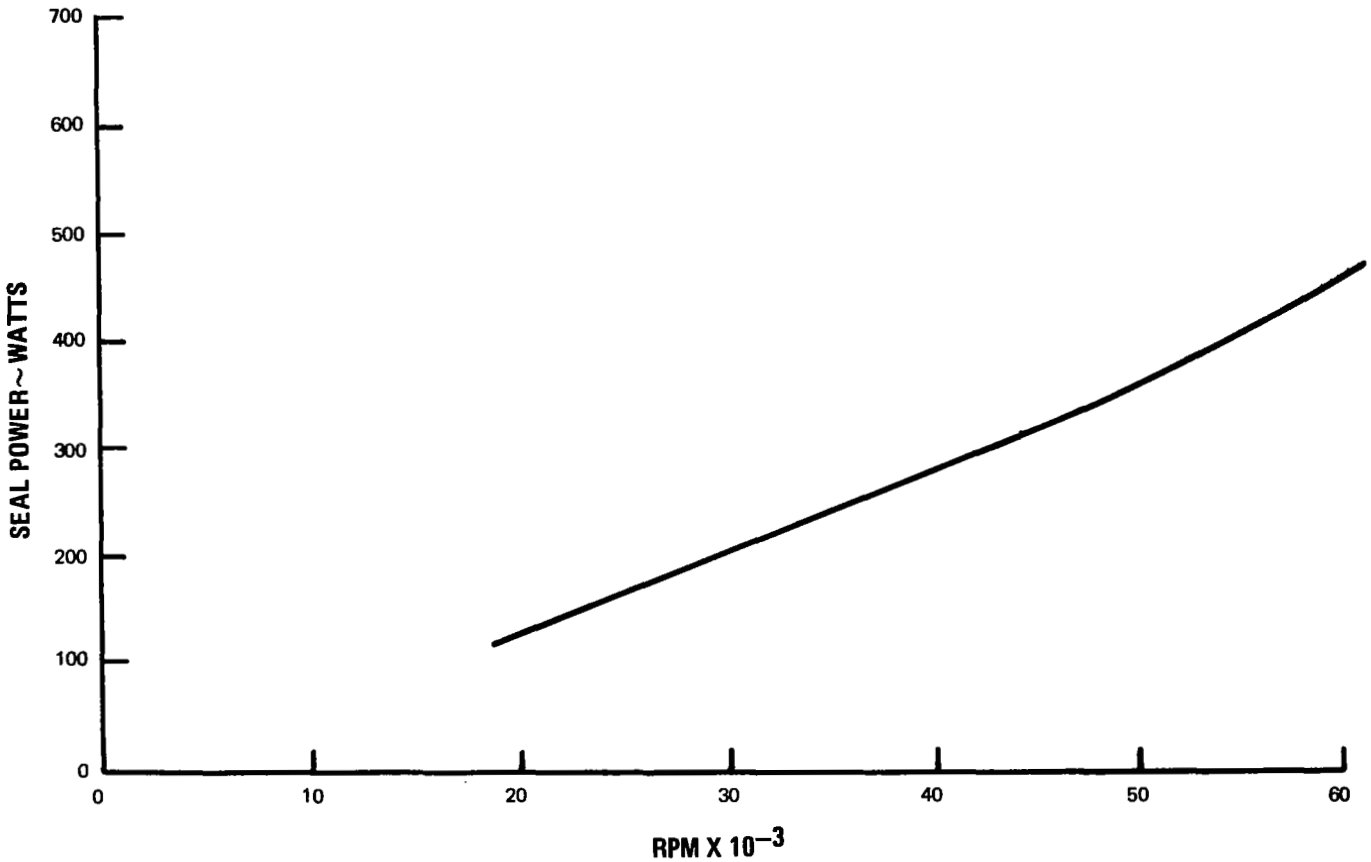

Figure 124 Turbine-Compressor Dry-Face Seal Power M-44073

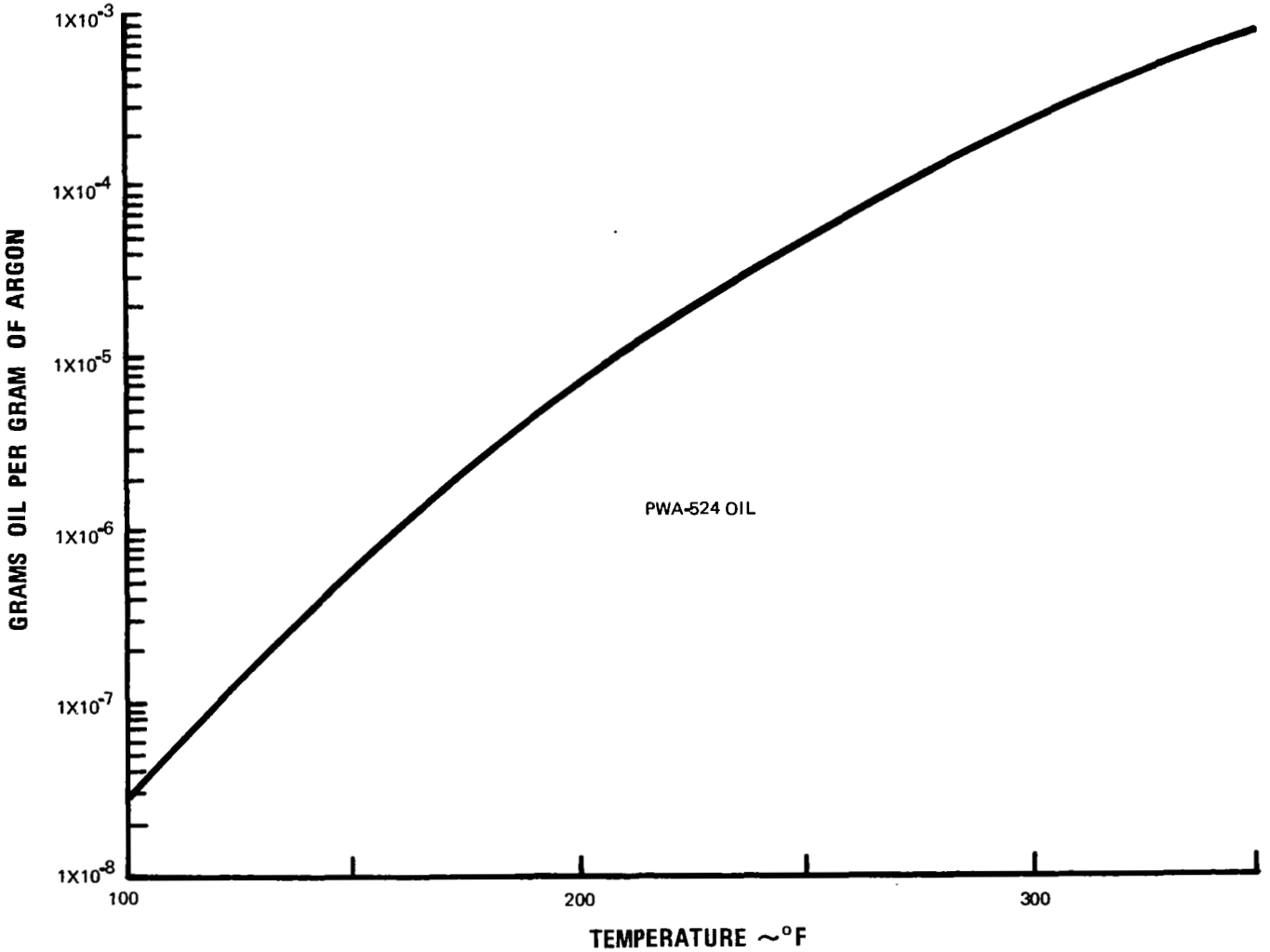

Figure 125 Solubility of Oil in Argon M-49780

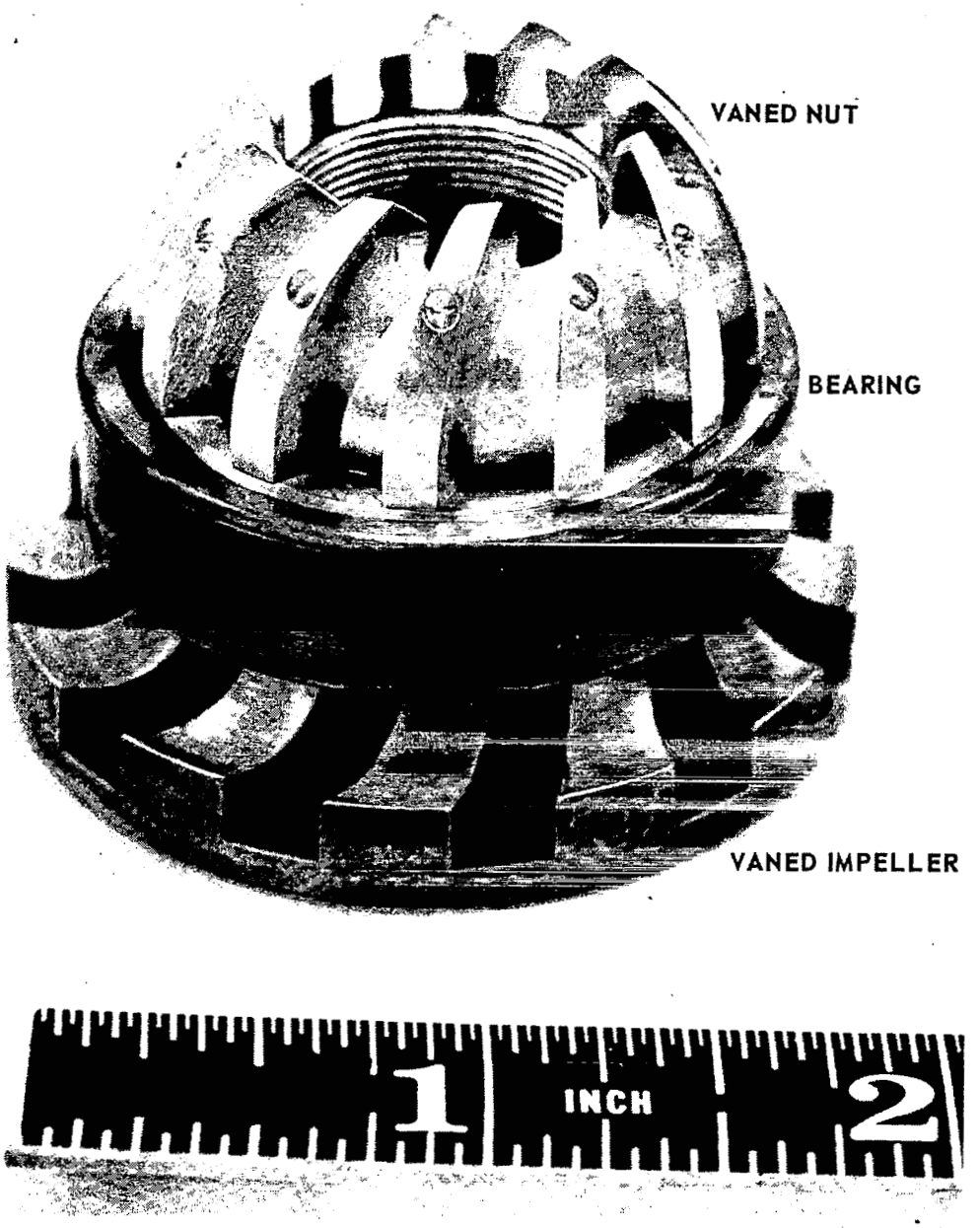

Figure 126 Vaned Impeller, Bearing, and Vaned Nut of Turbine-Compressor

○ 0.9 lb oil under race + 0.1 lb oil through bearing/min.
△ 1.7 lb oil under race + 0.175 lb oil through bearing/min.
□ 2.5 lb oil under race + 0.25 lb oil through bearing/min.
oil and argon in temperature 300°F

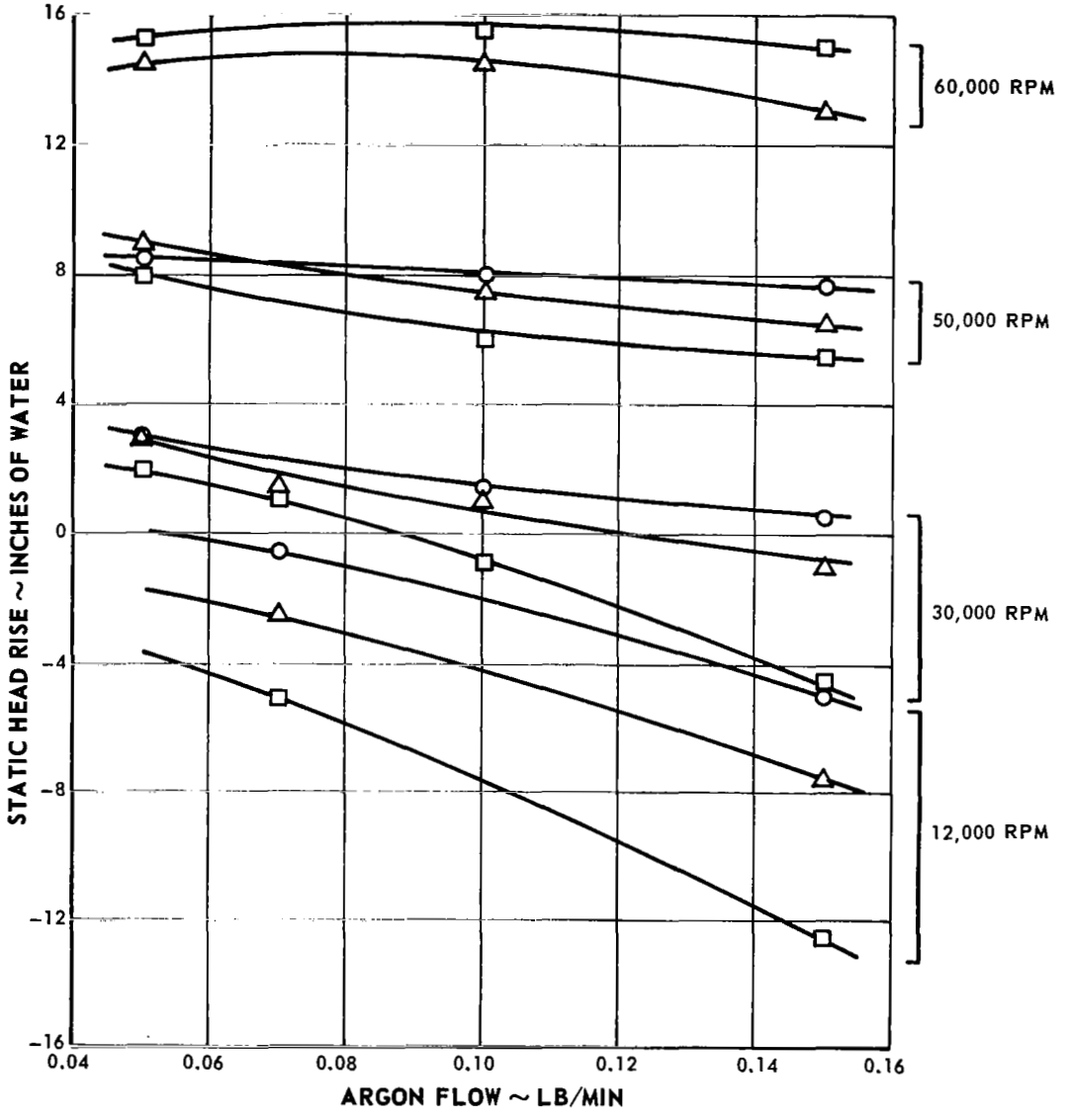

Figure 127 Performance of Centrifugal Scavenge Impeller Operating in Horizontal Position. Inlet Pressure 6 psia

○ 0.9 lb oil under race + 0.1 lb oil through bearing/min.
△ 1.7 lb oil under race + 0.175 lb oil through bearing/min.
□ 2.5 lb oil under race + 0.25 lb oil through bearing/min.
oil and argon in temperature 300°F

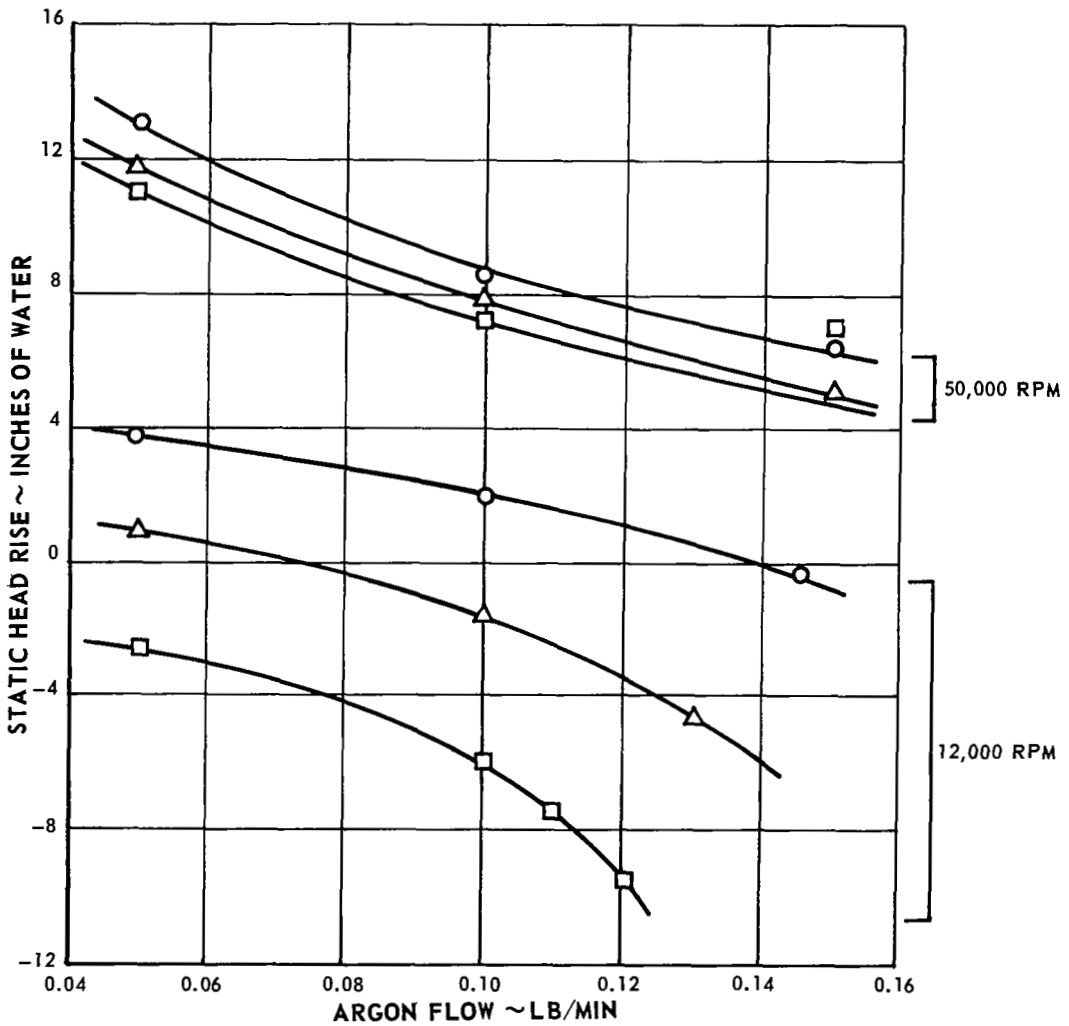

Figure 128 Performance of Centrifugal Scavenge Impeller Operating in Vertical Position with Horizontal Discharge. Inlet Pressure 6 psia

△ 0.9 lb oil under race + 0.1 lb oil through bearing/min.
○ 2.5 lb oil under race + 0.25 lb oil through bearing/min.
oil and argon in temperature 300°F

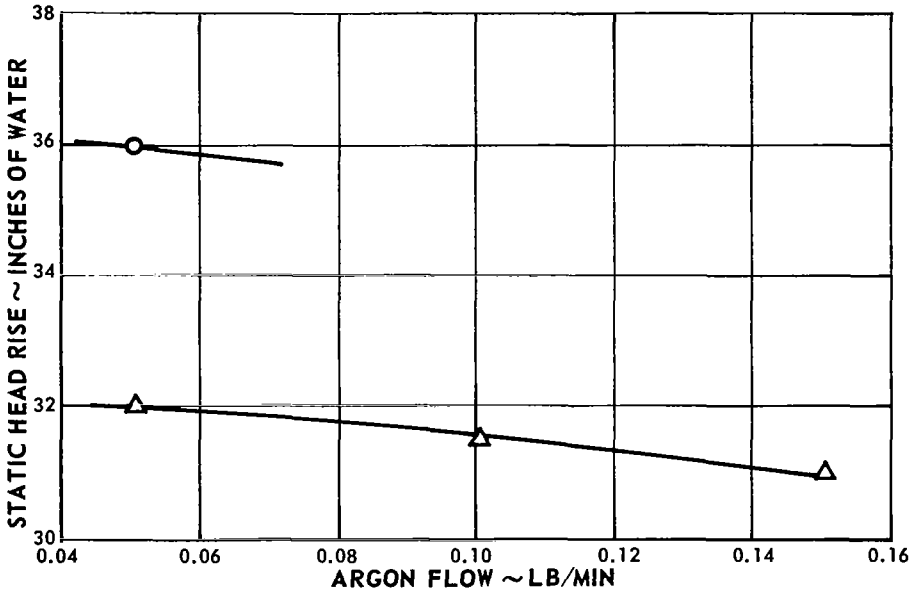

Figure 129 Performance of Centrifugal Scavenge Impeller Operating at 50,000 rpm in Vertical Position with Horizontal Discharge. Inlet Pressure 14.2 psia

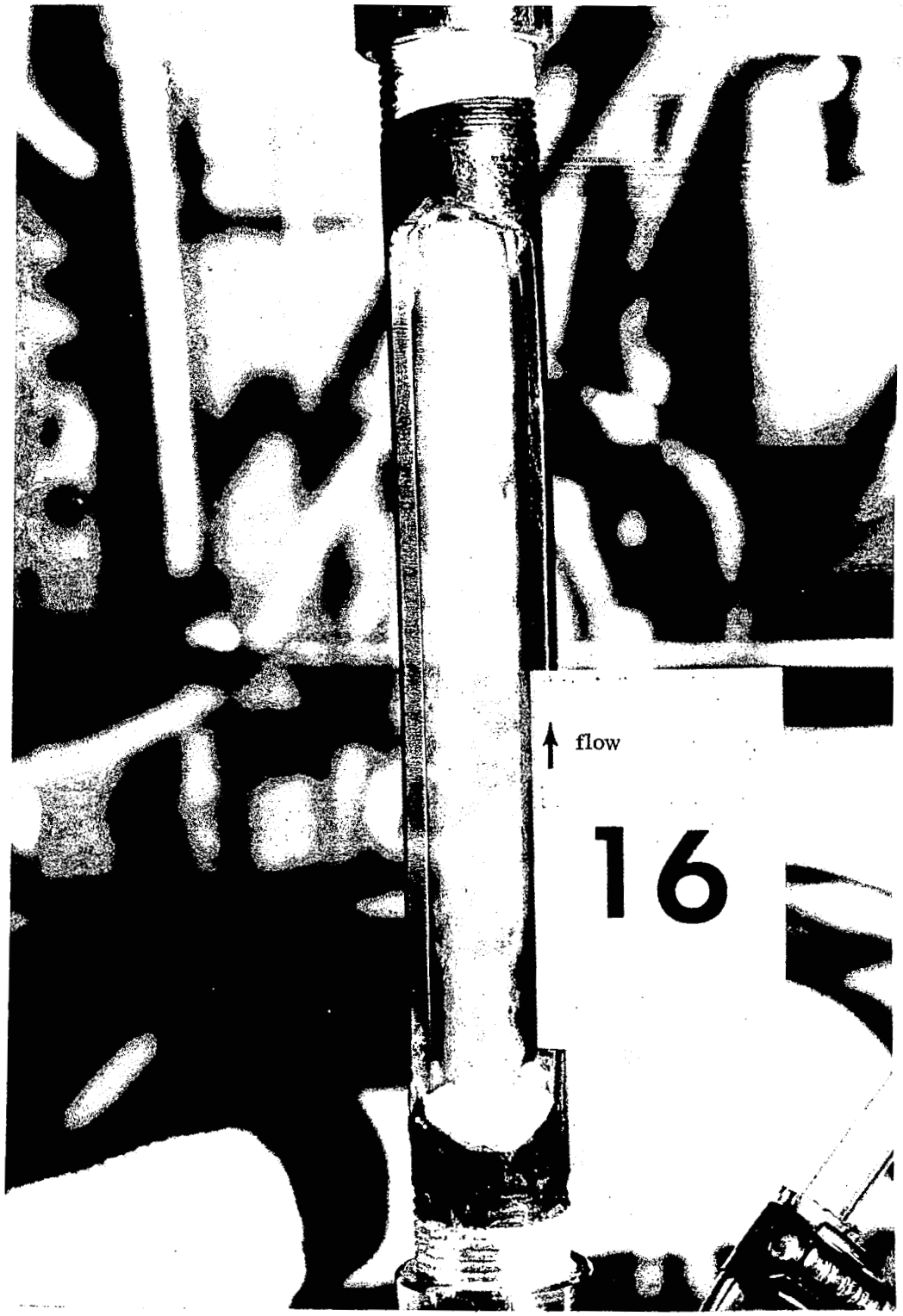

Figure 130 Vertical Two-Phase Flow X-24576

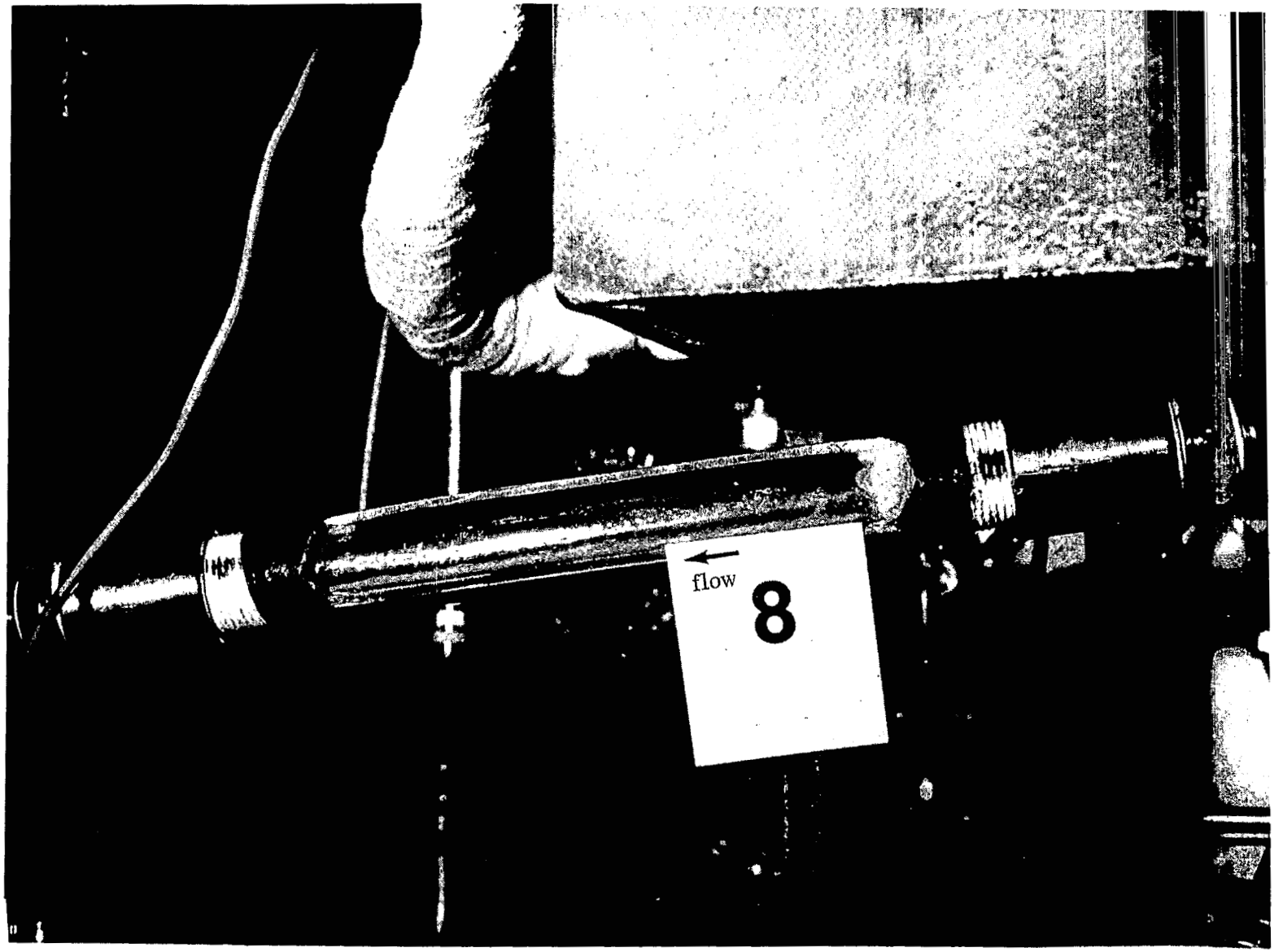

Figure 131 Horizontal Two-Phase Flow X-24566

The scavenge tests demonstrated the feasibility of the basic two-phase scavenging concept. Oil circulation was accomplished with an acceptable gas flow rate and head. Early concern over oil foaming due to violent mixing with the gas did not prove to be a problem. In fact, circulation, separation and lubrication functions were performed without any evidence of performance degradation. The tests were run over a wide range of gas and oil flows to establish off-design performance and the sensitivity to gas and oil flow variations.

Tests using krypton and helium-xenon mixture were conducted in the pilot system to establish the performance of the turbine-compressor bearing compartment (bearing, seal, scavenge impellers) and separator with the Brayton rotating unit (BRU) gases and system pressure levels. These tests were performed at 50,000 rpm and with pressure levels corresponding to the BRU system pressure level at power outputs of 2.25, 6.00 and 10.5 KW. Data were also obtained at a system pressure level of 11 psia, the pressure level selected for the argon pilot system test, see Section IX.

Figure 132 presents the scavenge impeller head rise as a function of system pressure level for the three gases and four pressure levels. Similarly, in Figure 133 bearing compartment power determinations are given using calorimetric techniques as applied to oil flow and temperature rise. Finally the bearing outer race temperature is shown in Figure 134. One can conclude from these tests that the scavenge impeller output increased as expected with density changes and that inconsequential changes in bearing temperature were measured.

Scavenge tests were performed on the annular jet pump concept in both the horizontal and vertical orientations. Figure 135 is a photograph of the jet sealplate and mating collector-discharge. Figure 136 is a view of the jet impeller showing the oil discharge holes which supply oil to the periphery of the impeller. The test parameters were varied over the same range as they were in testing the centrifugal pump-scavenge configuration. Two jet-to-throat discharge locations were evaluated. In addition, the density ratio between the gas and oil was varied, first by changing the inlet pressure of the gas, and secondly changing the inlet temperatures of the oil. The viscosity of the oil changed appreciably with the temperature change.

Figure 137 shows the performance at 12,000, 30,000 and 50,000 rpm with the unit mounted in the horizontal position. The performance was somewhat below expectations. In an attempt to improve the head rise the jet discharge was shifted axially with the hope that a more favorable energy interchange would

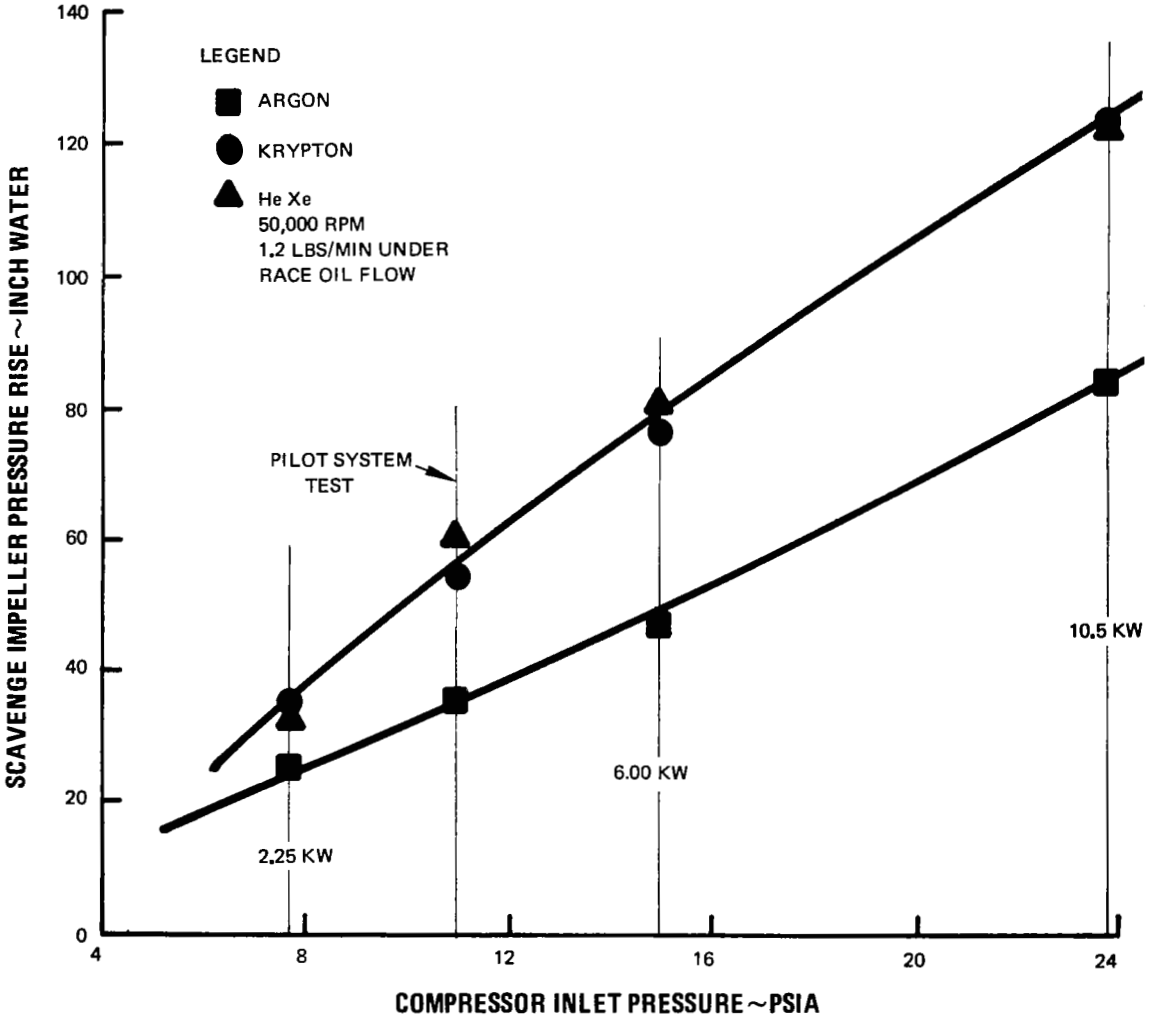

Figure 132 Performance of Scavenge Impeller M-49452

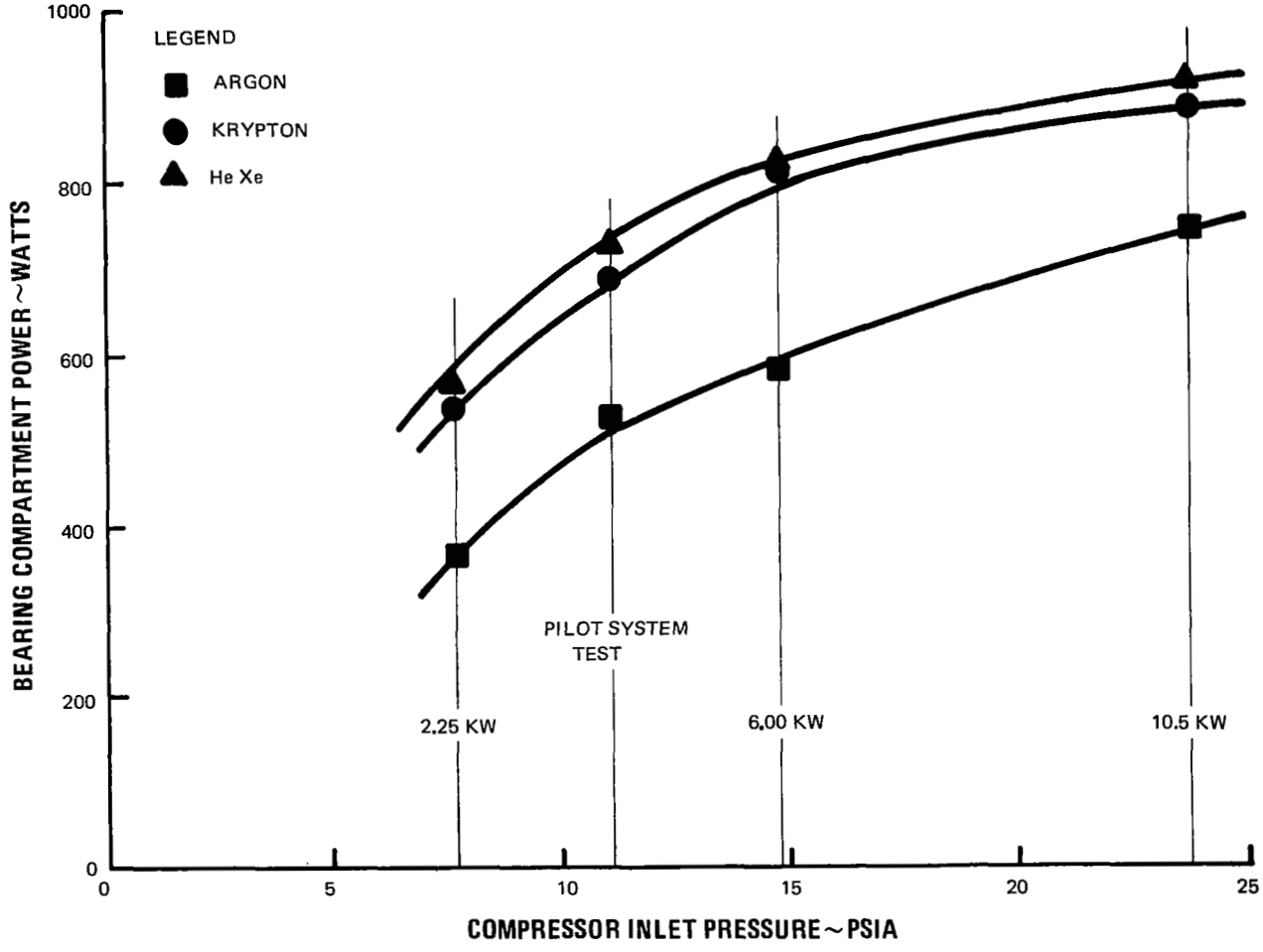

Figure 133 Turbine-Compressor Bearing Compartment Power at 50,000 rpm M-49729

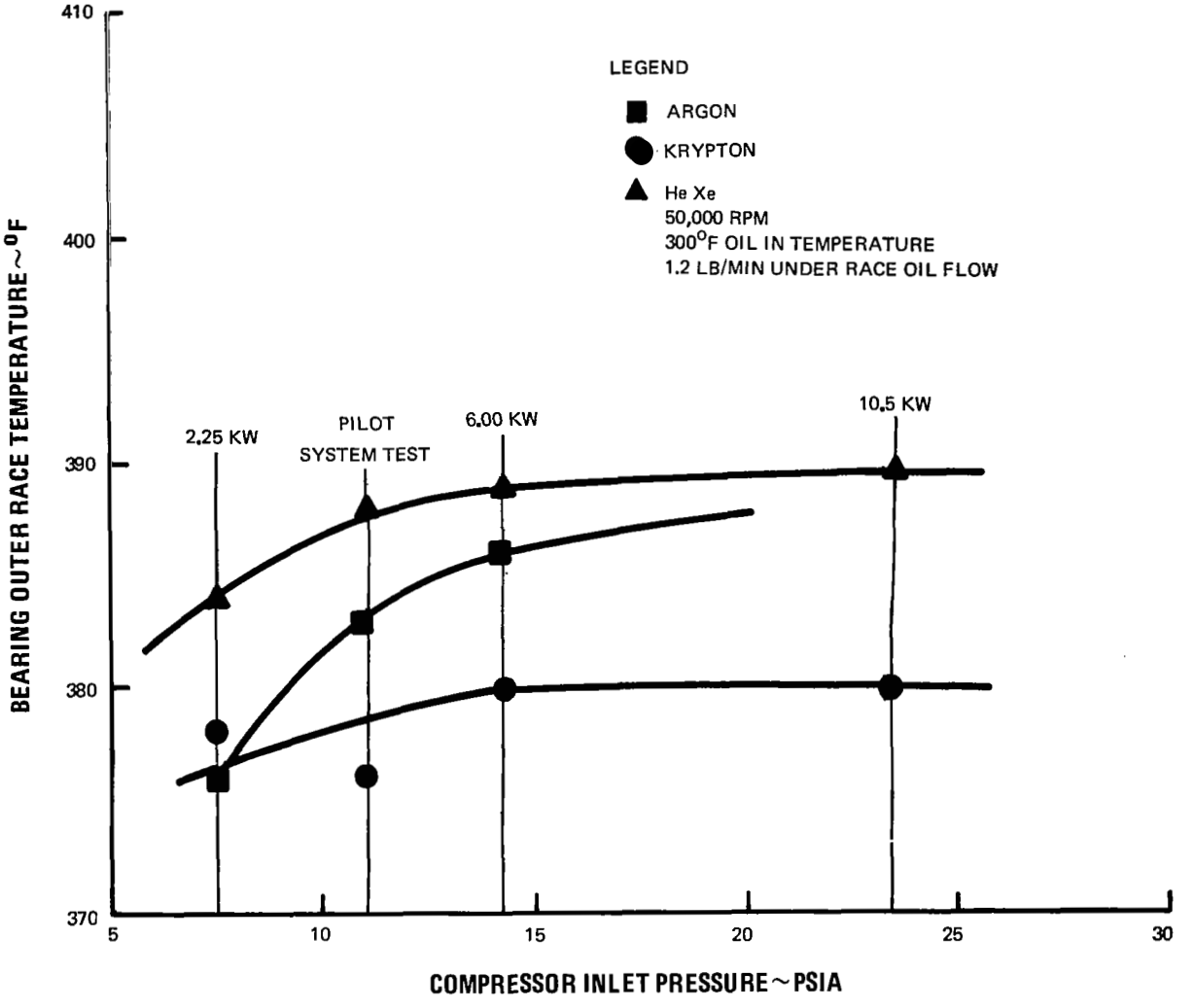

Figure 134 Turbine-Compressor Bearing Temperature M-49451

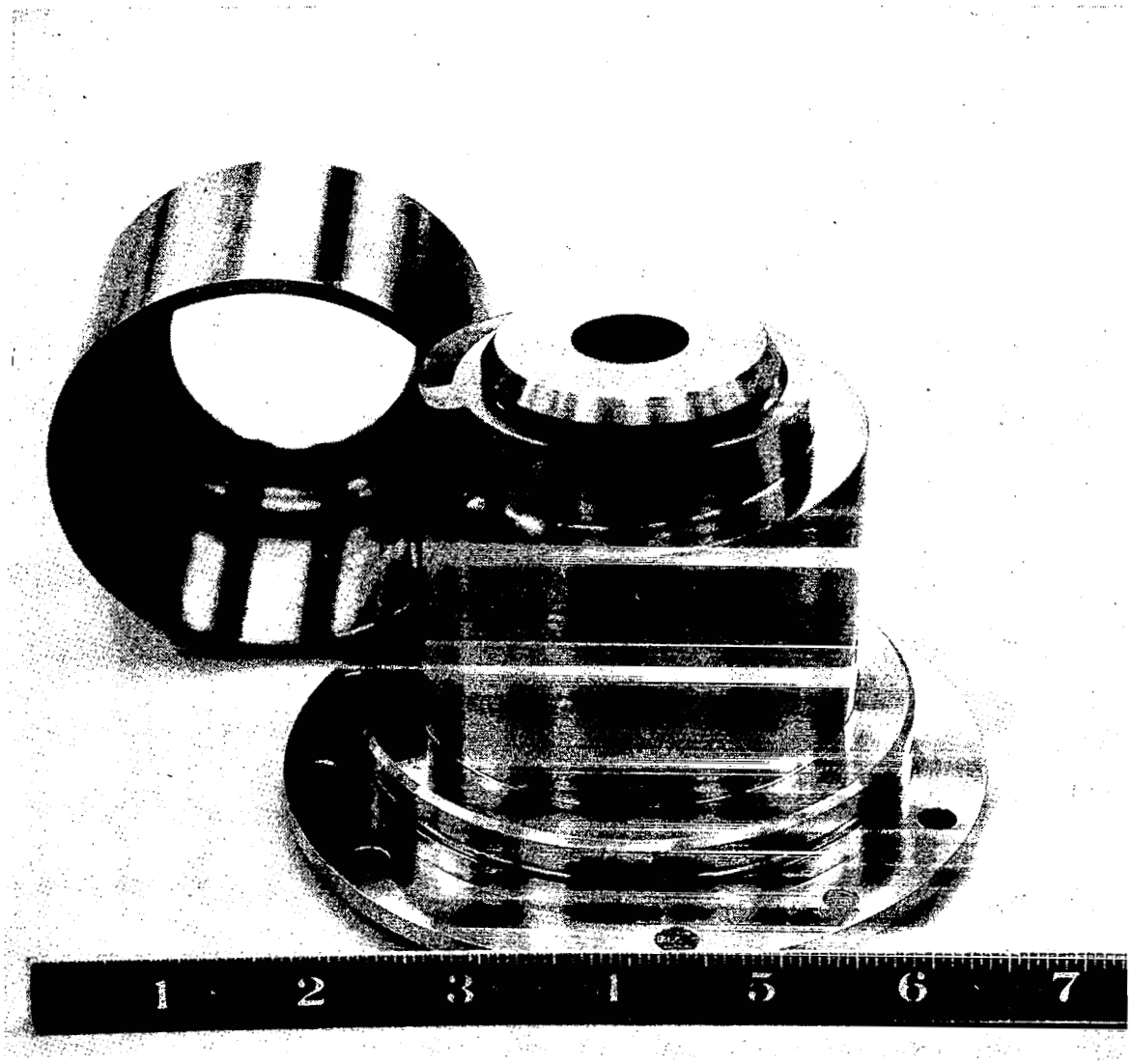

Figure 135 Annular Jet Scavenge Impeller and Collector-Discharge X-22829

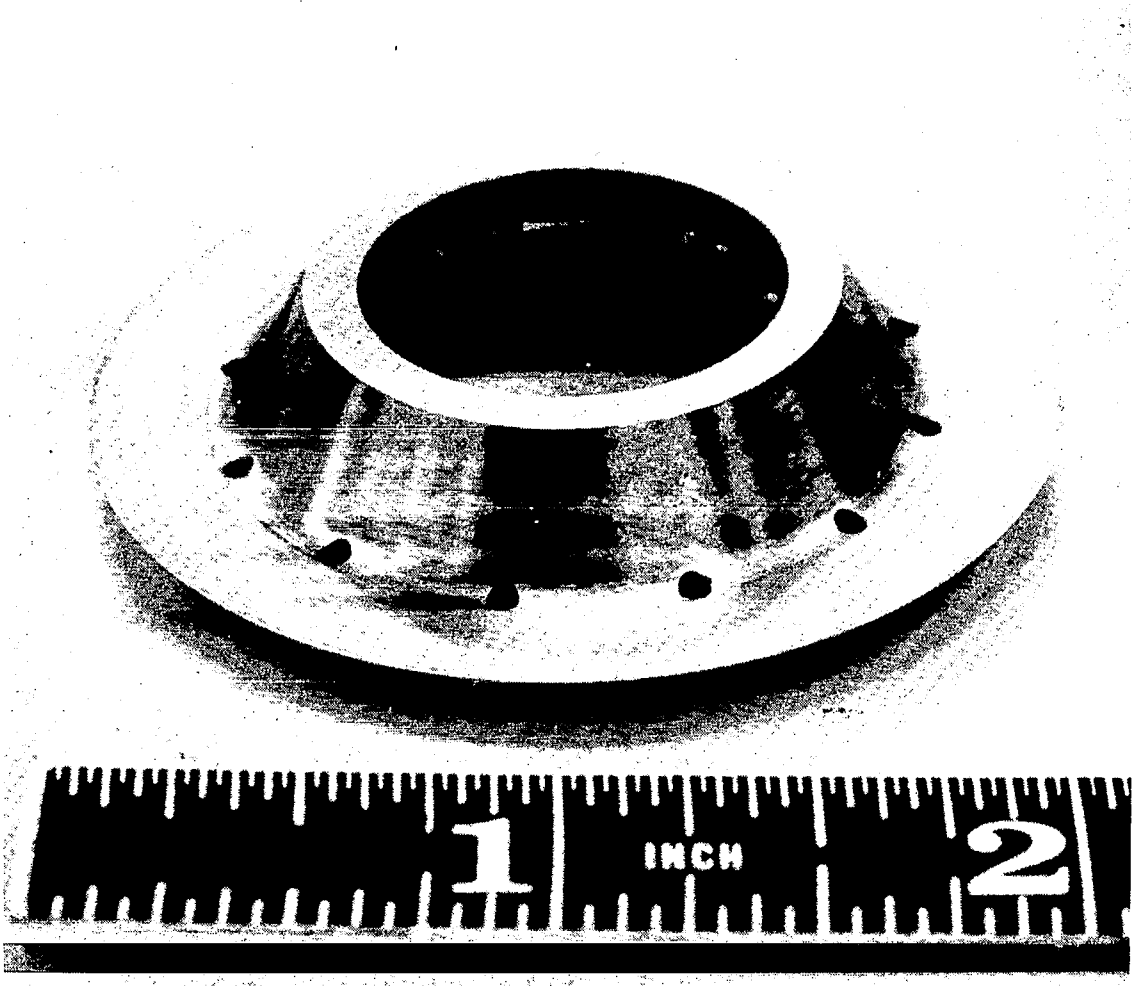

Figure 136 Annular Jet Scavenge Impeller X-22826

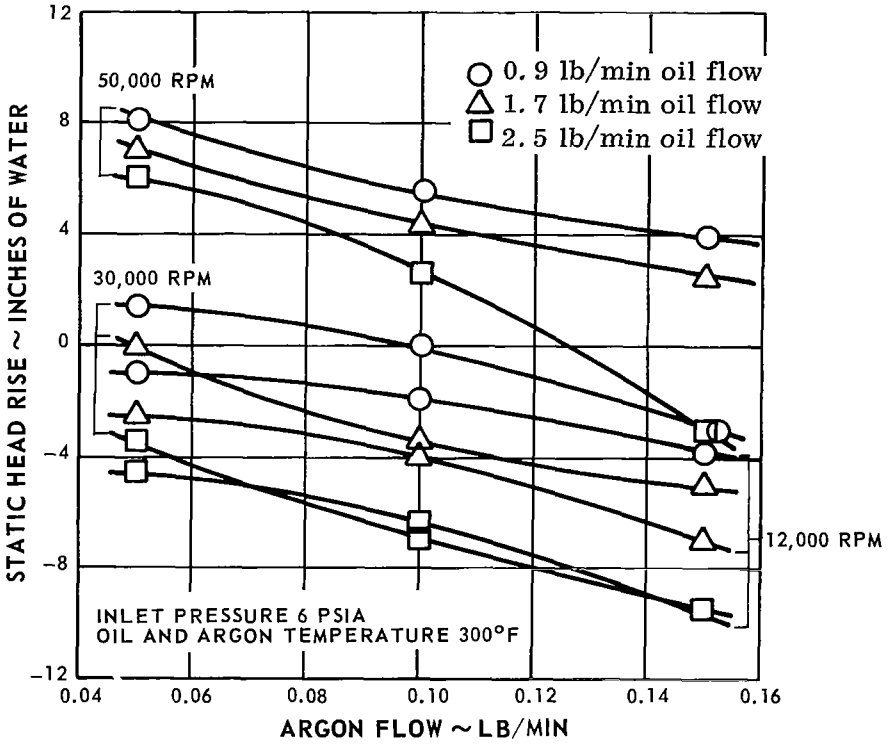

Figure 137 Performance of Annular Jet Scavenge Pump in Horizontal Orientation

result. The performance with this adjustment is shown in Figure 138. Essentially no performance change was obtained. The effects of gas pressure change and colder oil temperature are also shown on this curve. The performance in the vertical position is shown in Figure 139.

D. Separator Pump Tests

The lubrication system described in Section III incorporates an oil scoop pump in the separator to provide a source of pressurized oil for use in several parts of the lubrication system and to control the circulating oil inventory. The scoop, which is stationary, is immersed in a rotating pool of oil from which it develops oil head and flow. Since the gas and oil have different densities, the first stage of separation is also accomplished at this location. The pump tests were run to determine the performance of the scoop as a function of shaft speed, oil-in flow rate, gas flow rate and scoop pump back pressure. Figure 86 shows the design of the separator rig. Figures 140 and 141 are photographs of the test hardware. The curves on Figures 142, 143, and 144 present the head out-flow characteristics of the pump at 12,000, 9600 and 14,000 rpm and at several oil-in flow rates. The difference between oil-in flow and oil-out flow is accounted for by 1) bypass flow around the pump through a lubrication jet, and 2) oil splash from the pool.

A redesign of the scoop was made in order to improve both the head and flow characteristics of the pump. The redesigned scoop is shown in Figure 145. As shown in the photograph, a larger fabricated scoop was used in place of the small formed tube scoop. The configuration of the new scoop was arranged to provide interchangeability of parts without modification of the shaft pool. Tests were run on the larger scoop using the same procedures as for the original design. Figures 146, 147, and 148 show the redesigned unit performance. These are head-flow curves with the flow presented as a ratio of outflow to inflow.

E. Separator Tests

The lubrication system described in Section III depends upon oil-gas separation in order to function properly. Two degrees of separation are required. The first degree of separation must be complete enough to provide separate sources of gas and oil for lubrication and circulation. The second degree of separation must be essentially 100 percent complete to insure that only small quantities of oil will be transported to the adsorber with the leakage gas. Figure 85 displays the test apparatus which was designed specifically for use in evaluating the oil pumping and separation problems. Figure 149 shows a view of the test control panel. Figure 150 shows the separator rig assembly as installed for test.

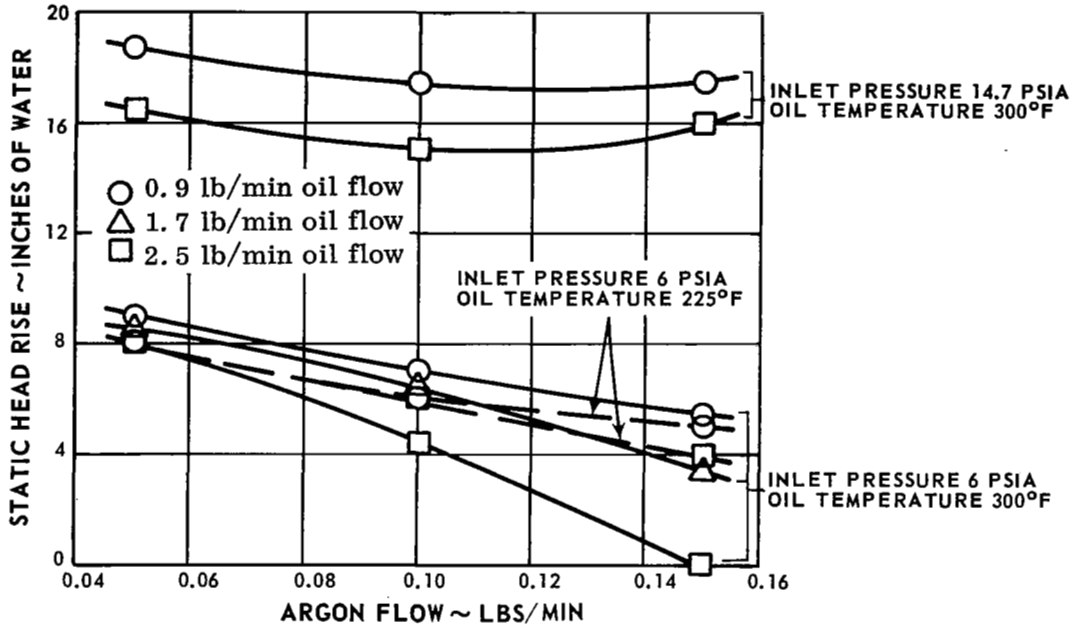

Figure 138 Performance of Annular Jet Scavenge Pump in Horizontal Orientation at 50, 000 rpm. Adjusted Location of Jet in Throat

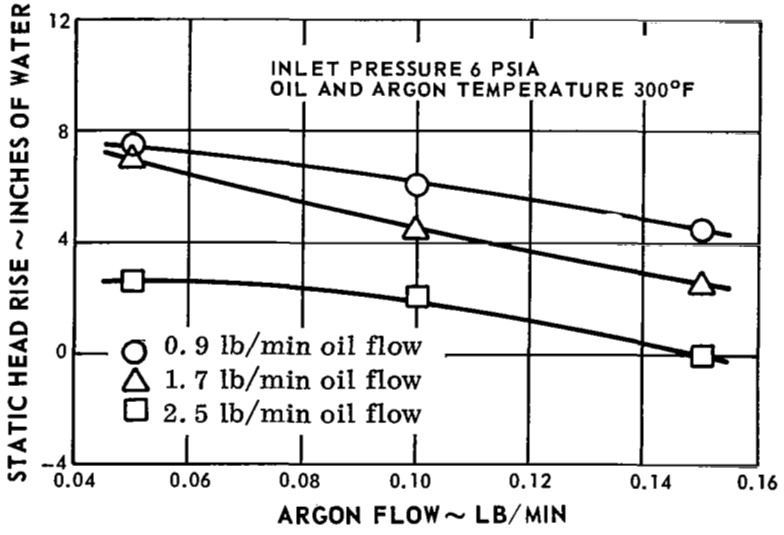

Figure 139 Performance of Annular Jet Scavenge Pump in Vertical Orientation at 50, 000 rpm. Adjusted Location of Jet in Throat

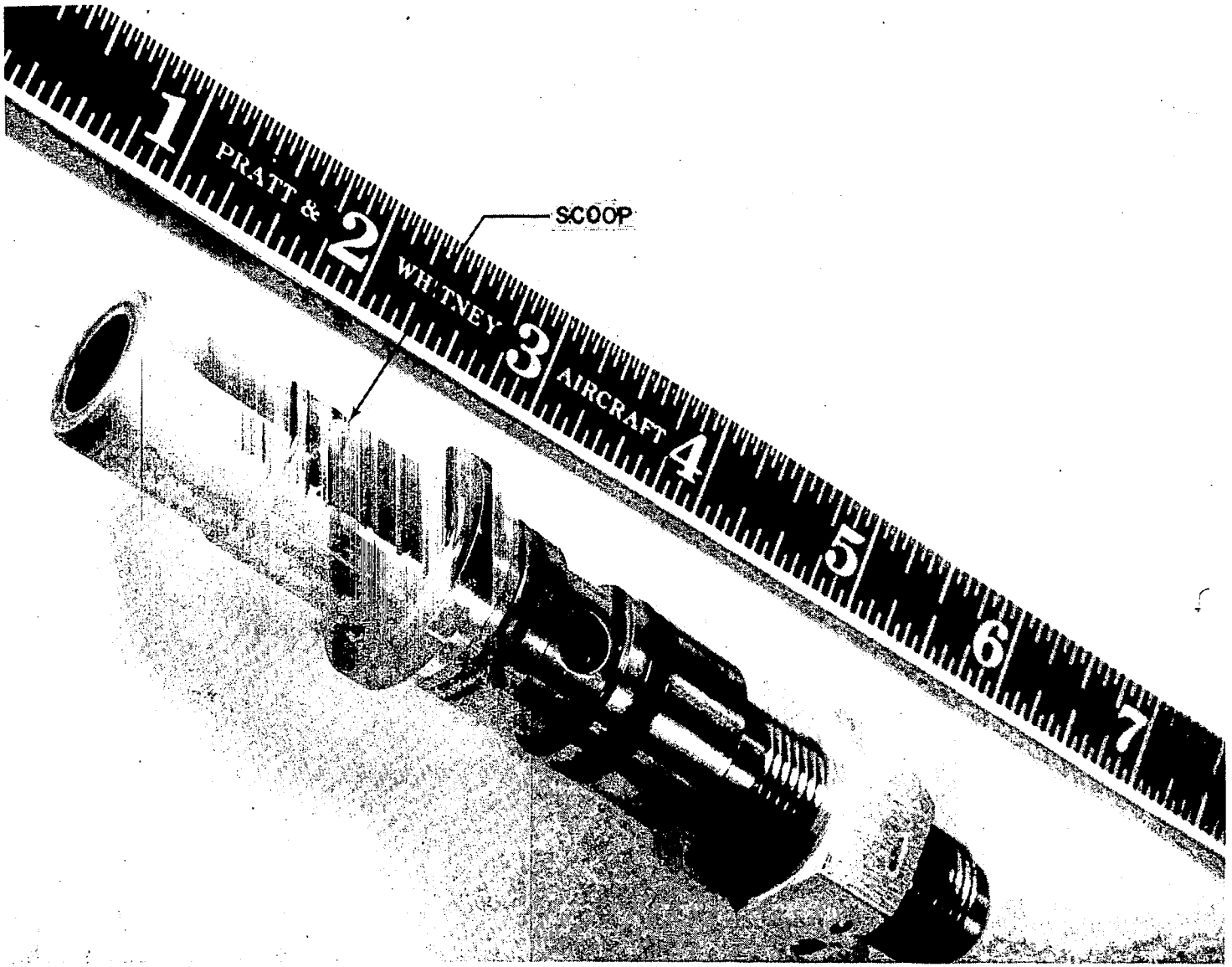

Figure 140 Scoop Pump X-23709

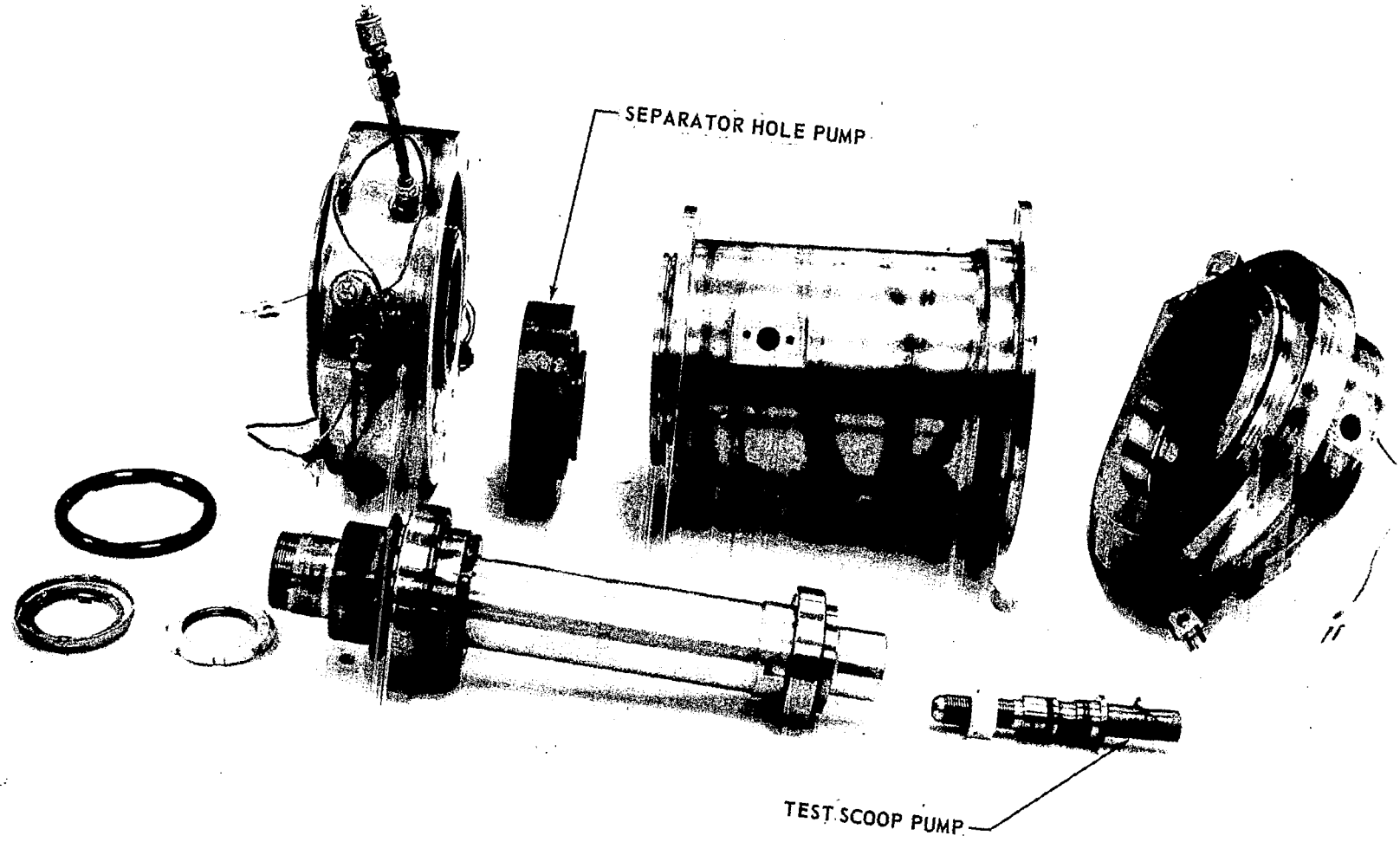

Figure 141 **Pump Test Rig** X-23715

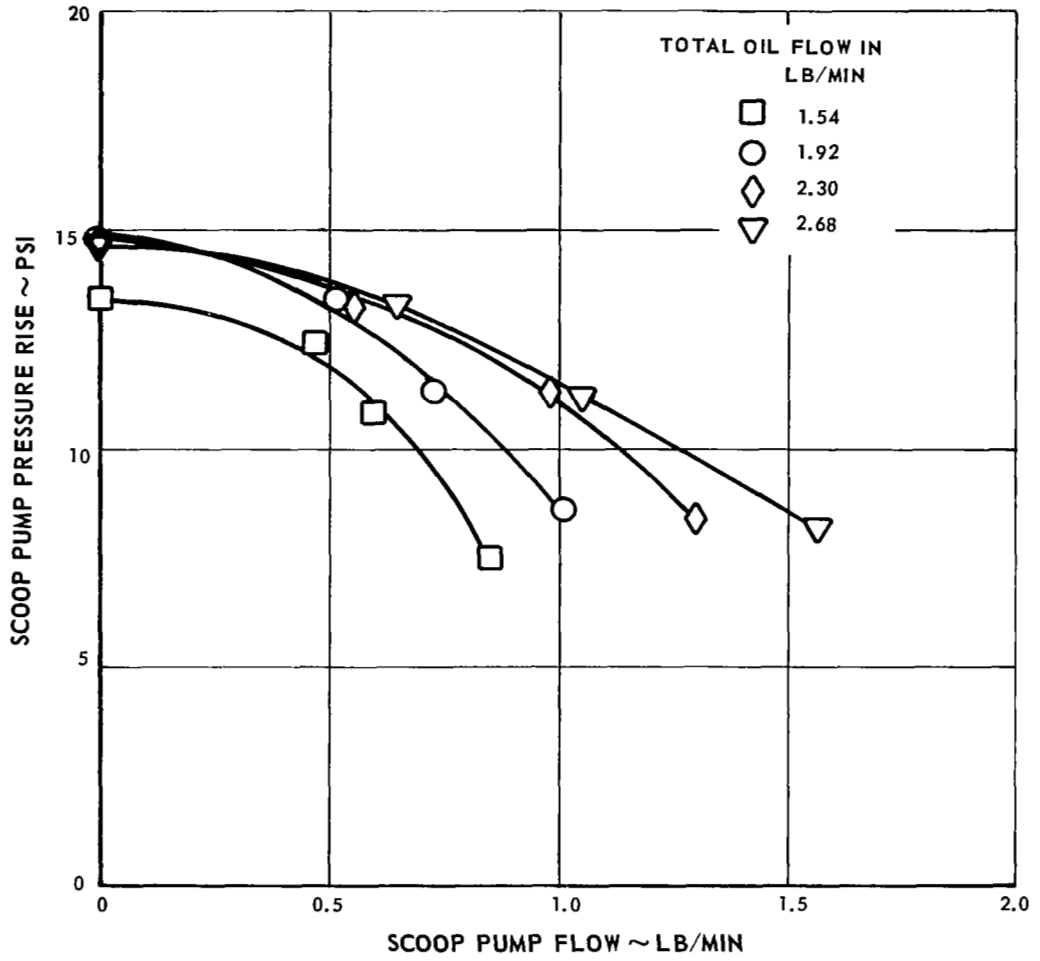

Figure 142 Scoop Pump Performance at 12,000 rpm (Original Design)

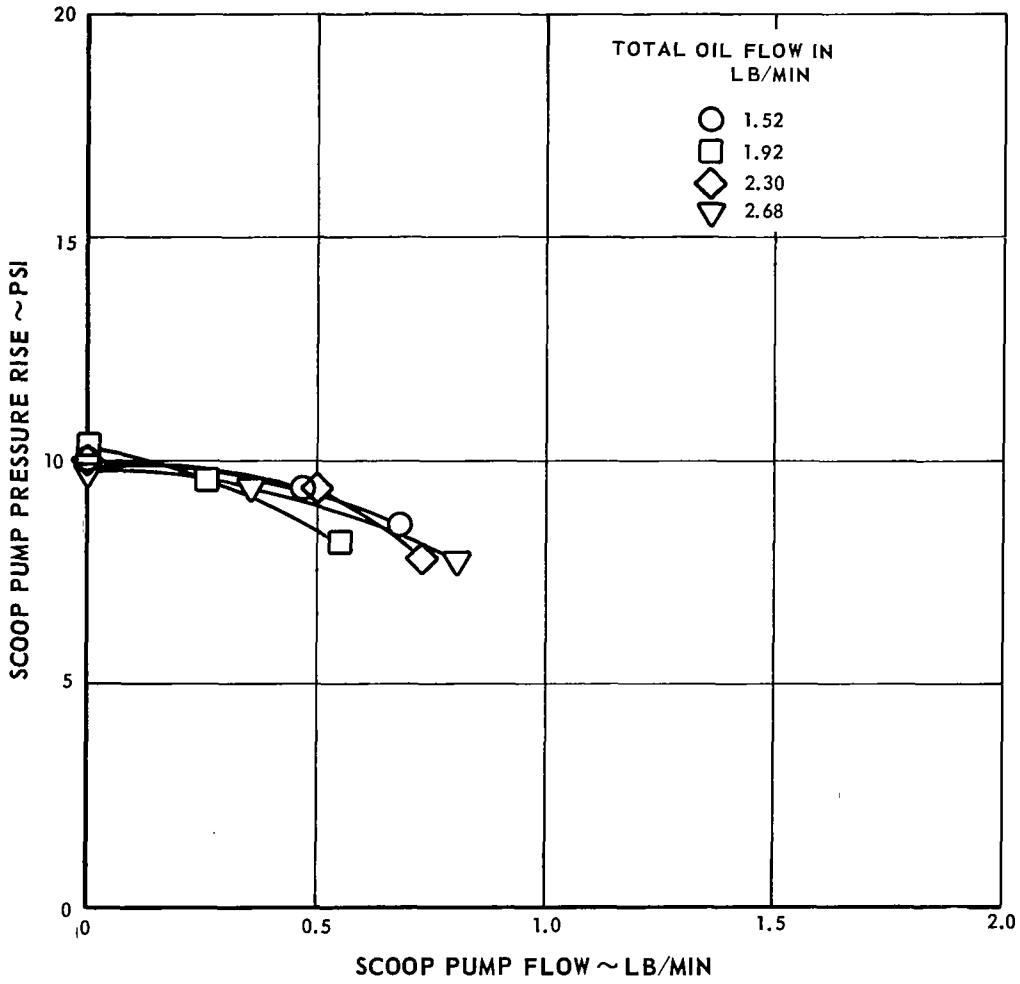

Figure 143 Scoop Pump Performance at 9,600 rpm (Original Design)

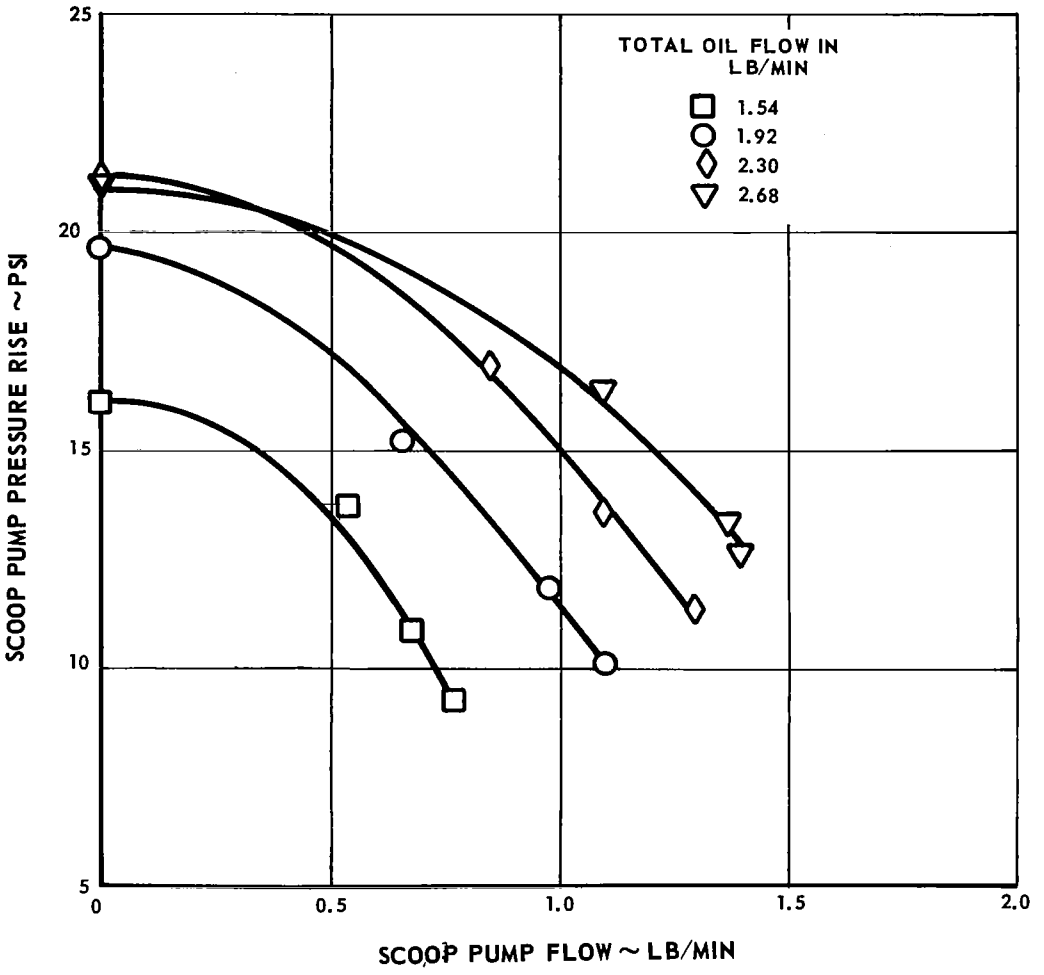

Figure 144 Scoop Pump Performance at 14,400 rpm (Original Design)

Figure 145 Increased-Capacity Scoop Pump X-24609

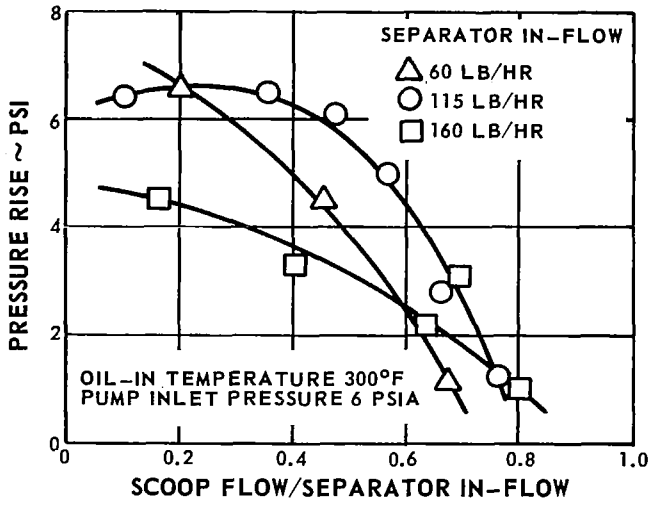

Figure 146 Performance of Separator Scoop Pump with Increased Capacity Scoop at 9, 600 rpm

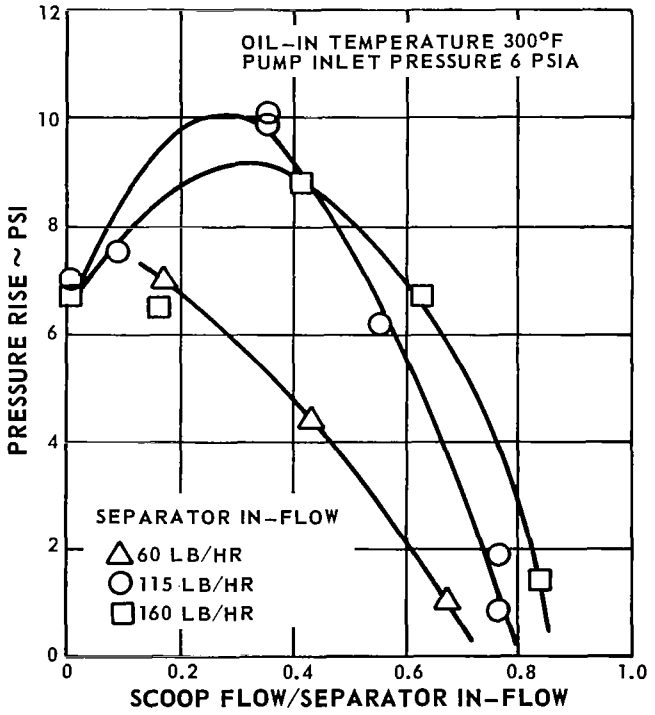

Figure 147 Performance of Separator Scoop Pump with Increased Capacity Scoop at 12, 000 rpm

Two sets of matrix hardware were evaluated for oil-gas separation performance, one set with 10 percent density mesh and the other with 23 percent density. Figure 151 shows the major parts of the rotating assembly including one set of mesh. In each case the separation capability was determined as a function of rotational speed, gas flow and oil flow.

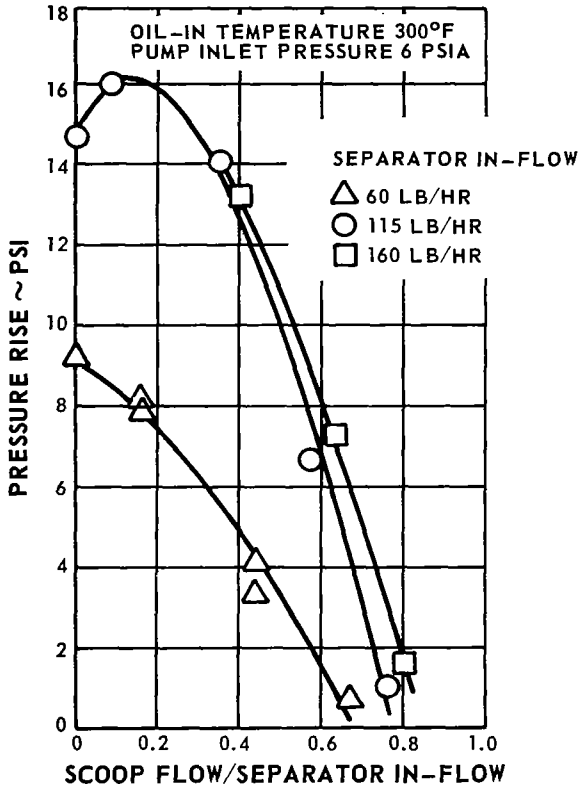

Figure 148 Performance of Separator Scoop Pump with Increased Capacity Scoop at 14,400 rpm

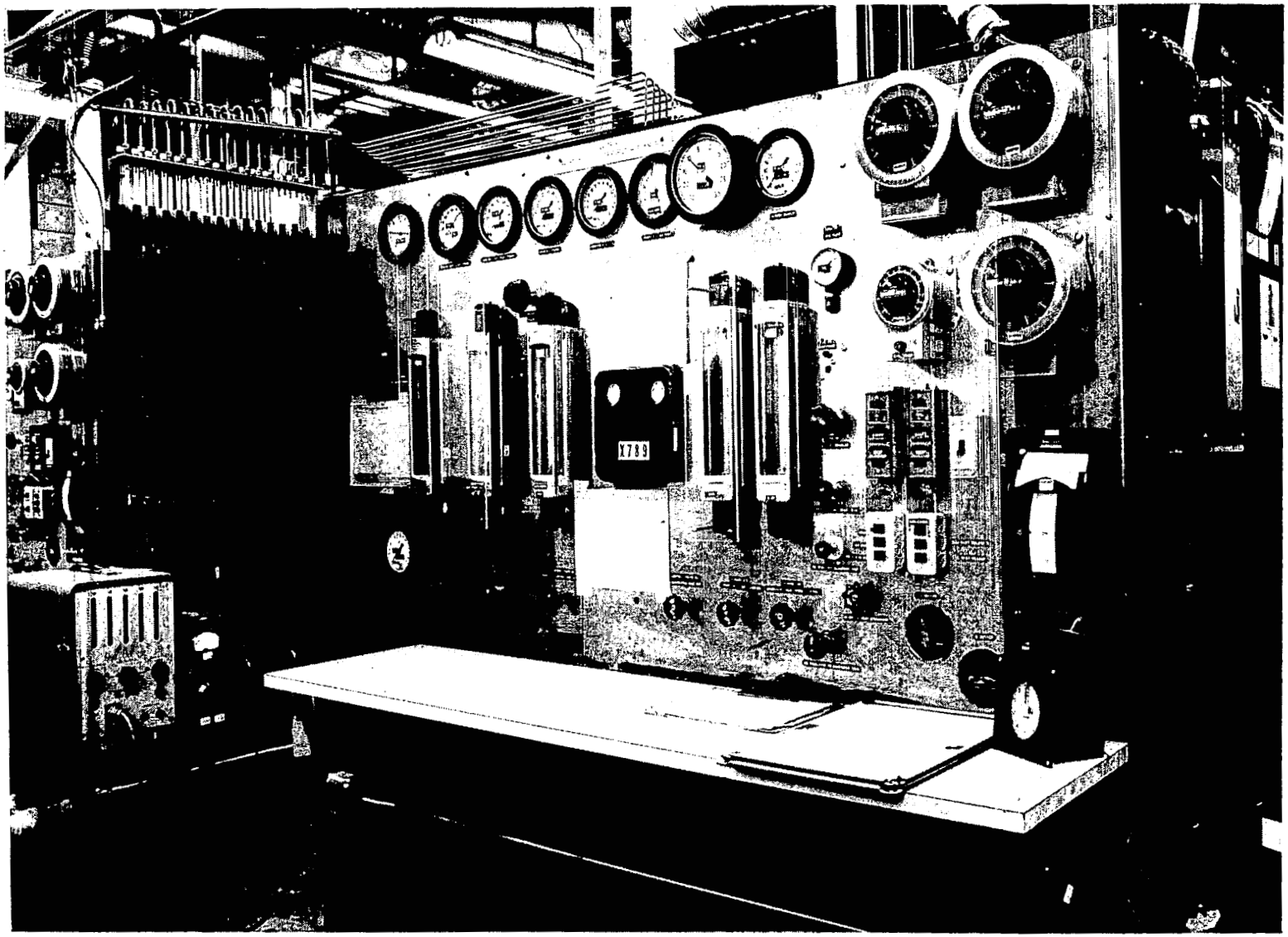

Figure 149 Separator Test Bench X-23297

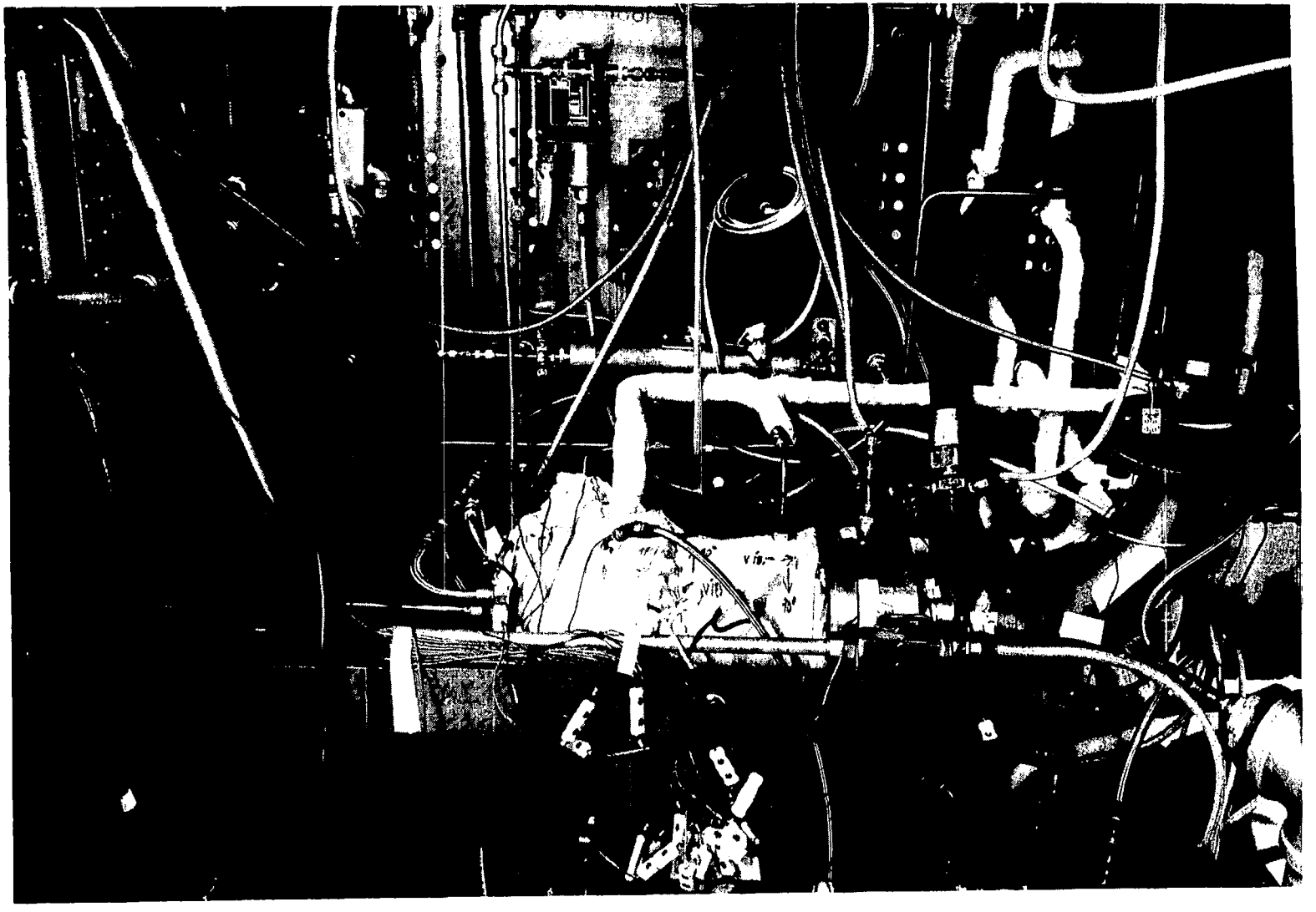

Figure 150 Separator Rig Installed in Test Bench X-23299

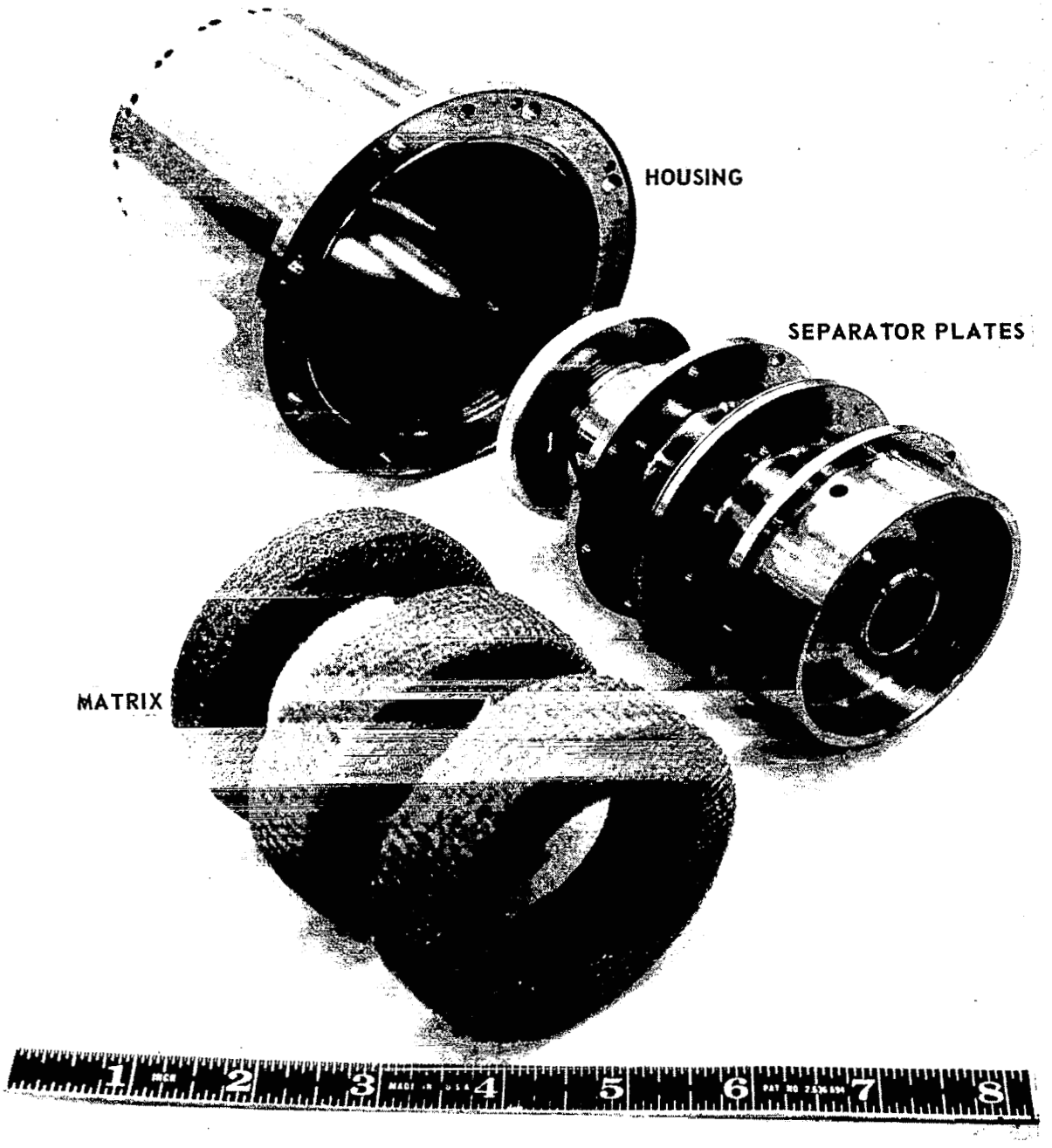

Figure 151 Separator Rotating Parts X-22837

A tabular summary of the 10 percent and 23 percent density mesh separator tests is shown below. The results are on a 10,000-hour basis and it is apparent that the 10 percent density mesh performed the best.

	Inflow, lb/hr		Oil in Gas Effluent to Adsorber lb/10,000 hr*	
RPM	Oil	Gas	10% Density	23% Density
12,000	15.2	8.55	0.26	2.76
12,000	12.0	10.26	1.56	1.09
12,000	18.0	4.2	0.02	2.75
14,400	15.1	8.55	0.76	1.62
9,600	15.1	8.55	0.03	0.12

* One pound per hour of gas flow to adsorber

All tests were conducted for six hours at steady state, with an argon outflow to adsorber of 1.2 pounds per hour. The adsorber gas from the separator was passed through a Pyrex glass wool adsorber to remove the remaining oil which allowed determination of the separator performance. Figure 152 is a photograph showing the entering gas-oil mixture flowing downward in the vertical glass tube. The clean gas is flowing out from right to left in the horizontal glass tube. No evidence of oil can be detected in the gas-out sight tube.

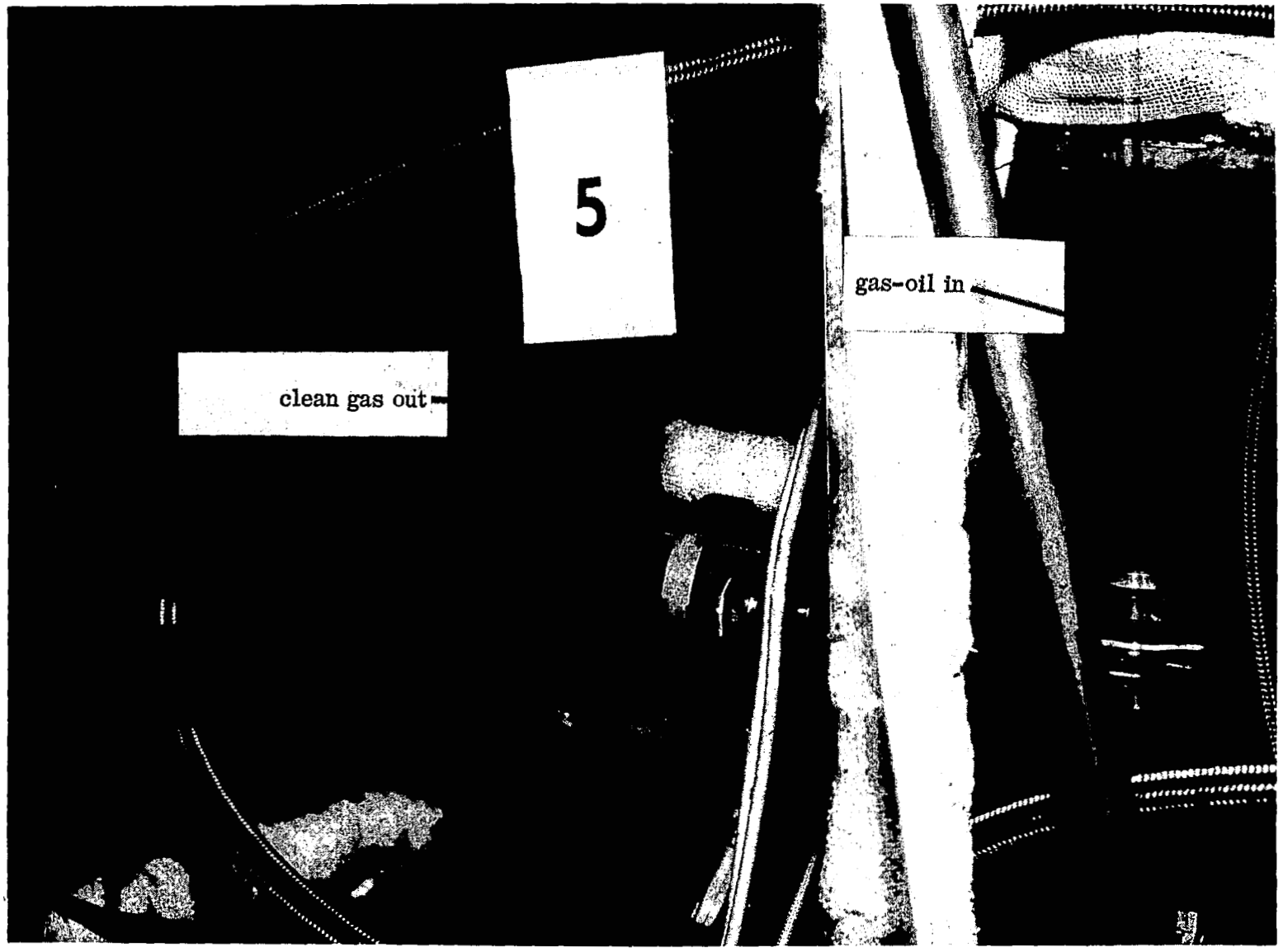

Figure 152 Separator Test X-24783

VIII. ADSORBER PROGRAM

A. Phase 1 - Screening and Preliminary Tests

The lubricant for the rolling-element bearings must be contained within the lubrication system. The design concept to accomplish this containment used a combination of face and labyrinth seals. The labyrinth seals are fed a controlled flow of gas from the compressor. A small portion of the bleed gas passes through the face seals into the bearing compartments and the remainder sweeps past the face seals to entrain any lubricant that migrates out of the bearing compartments through the face seals. This bleed argon must be purified before being returned to the main cycle. Oil is also removed from the gas which leaks through the face seals in a centrifugal separator. Purification of the argon from the separator and labyrinth seals is accomplished by passing it through an adsorber before returning it to the main cycle at the compressor inlet.

A survey of available technical information on adsorption of large-molecule organic compounds resulted in the selection of molecular-sieve materials for removal of lubricant from argon (References 17 and 40). The molecular-sieve materials are alkali-metal aluminosilicates that have been conditioned by removal of the water of hydration. Unlike most other hydrated materials, the physical structure of the molecular-sieve crystal does not break down or reform when the water of hydration is removed. This characteristic results in a conditioned or activated structure which contains a network of interconnected cavities and passages constituting approximately one-half of the total volume of the crystal. Three types of molecular sieve are commercially available. These are Linde Types 4A, 5A and 13X. All three have a cubic structure. Types 4A and 5A have a cubic cell edge dimension of 12.32 angstroms while the type 13X has a cubic cell edge dimension of 24.95 angstroms. The structural configuration of the 4A, 5A and 13X sieve materials is such that molecules having critical dimensions of up to 4, 5 and 13 angstroms, respectively, can be admitted into the structural cavities and adsorbed. The 4A and 5A materials have a void volume of 0.28 cubic centimeter per gram and the 13X material has a void volume of 0.35 cc/gm. The molecular-sieve materials are available in 1/8 inch and 1/16 inch diameter pellets and in powder form. An inert material which represents 20 percent of the total pellet weight is used to bond the pellets.

An adsorber test rig was designed and constructed to evaluate sieve materials. A schematic diagram of this test apparatus is shown in Figure 153. A photograph of the Perkin-Elmer Model 800 gas chromatograph is shown in Figure 154. The configuration of the test rig is shown in Figure 155. The test rig consisted of a vaporizer, a swirl separator, and an adsorber column. Argon was bubbled through heated oil in the vaporizer to produce a mixture containing argon, oil vapor, and entrained oil. The gas-oil mixture leaving the separator was cooled to 100°F, corresponding to system adsorber inlet design temperature. This cooling caused precipitation of finely-divided oil particles in the gas stream which remained suspended in the stream. The gas stream passed through a swirl separator before entering the adsorber test section to remove the large entrained oil droplets. This separator simulated the function of the centrifugal separator attached to the turboalternator. After leaving the separator, the gas stream which contained oil vapor and aerosol passed into the adsorber column. The tubing connecting the vaporizer to the adsorber column as well as the adsorber column was wrapped with electrical resistance tape to provide the heat necessary for temperature control of these components.

Testing was initiated using highly-refined four-ring polyphenyl ether and Linde 4A molecular sieve to investigate the operating characteristics of the test rig and to develop instrumentation techniques. The gas pressure and flow rate entering the vaporizer were varied over a range from 1 to 5 psig and 1 to 4 liters per minute respectively, at a constant vaporizer oil temperature of 350°F. The vaporizer oil temperature was varied from 290 to 350°F at constant inlet gas pressure and flow, to determine the effect of these variables on the concentration of oil in the gas entering the adsorber. The concentration of oil in the gas stream was found to be approximately 100 ppm by weight, and no significant change in concentration was detected over the range of variables investigated. Apparently, the concentration of oil in the gas stream was dependent upon an equilibrium condition which was established as the gas and oil vapor leaving the vaporizer were cooled to adsorber inlet temperature. This characteristic permitted operation of the test rig at a constant oil flow rate into the adsorber, with an adequate tolerance on pressure and temperature control at the vaporizer. It also permitted the flow rate of oil into the adsorber to be varied in proportion to the gas flow rate.

Adsorption evaluation tests of Linde 4A and 13X molecular sieve materials were performed using the adsorber test rig. The sieve materials were in powder form having a particle size corresponding to 60 to 80 mesh, or 1/16 inch pellets. In each test the adsorber column was loaded with approximately 36 grams of the molecular-sieve material. The test rig was operated with four-ring polyphenyl ether heated to 350°F in the vaporizer, with an argon flow rate of 1 liter per minute.

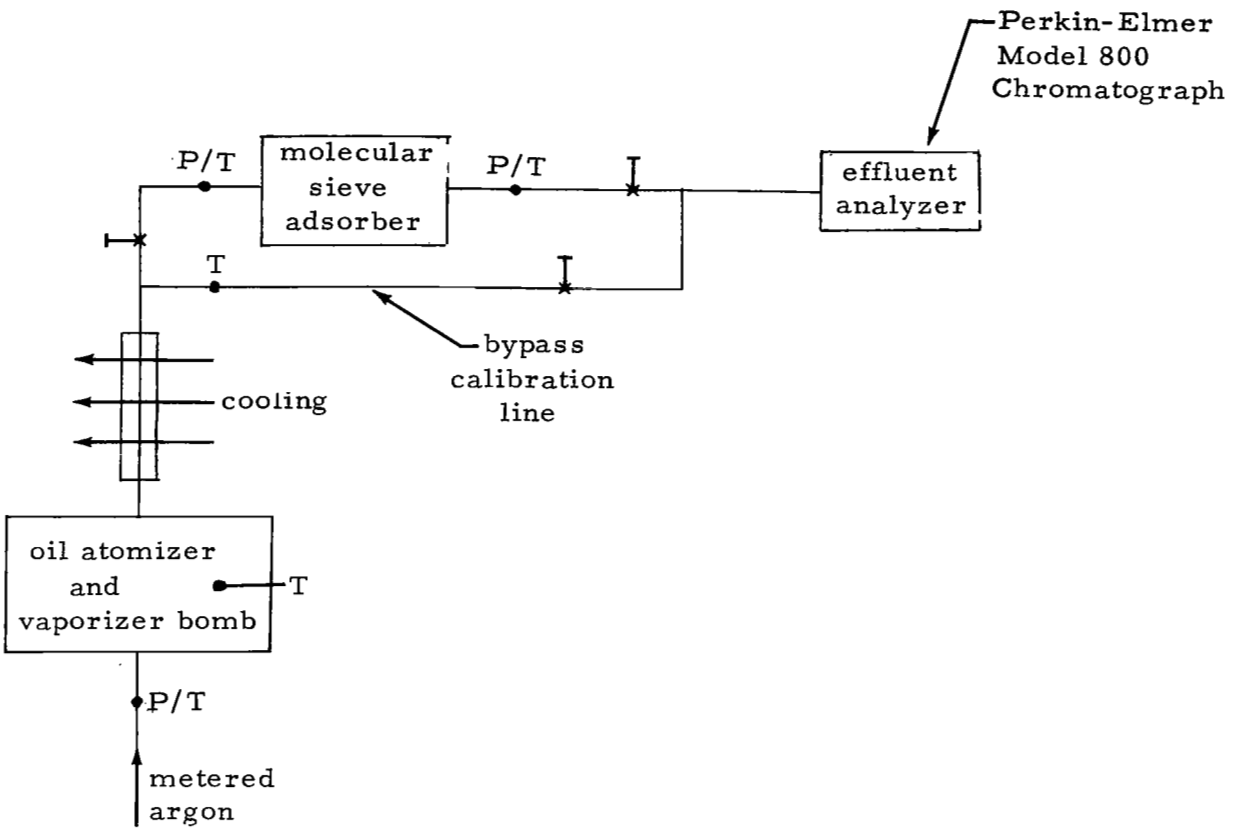

Figure 153 **Schematic Diagram of Adsorber Evaluation Apparatus**

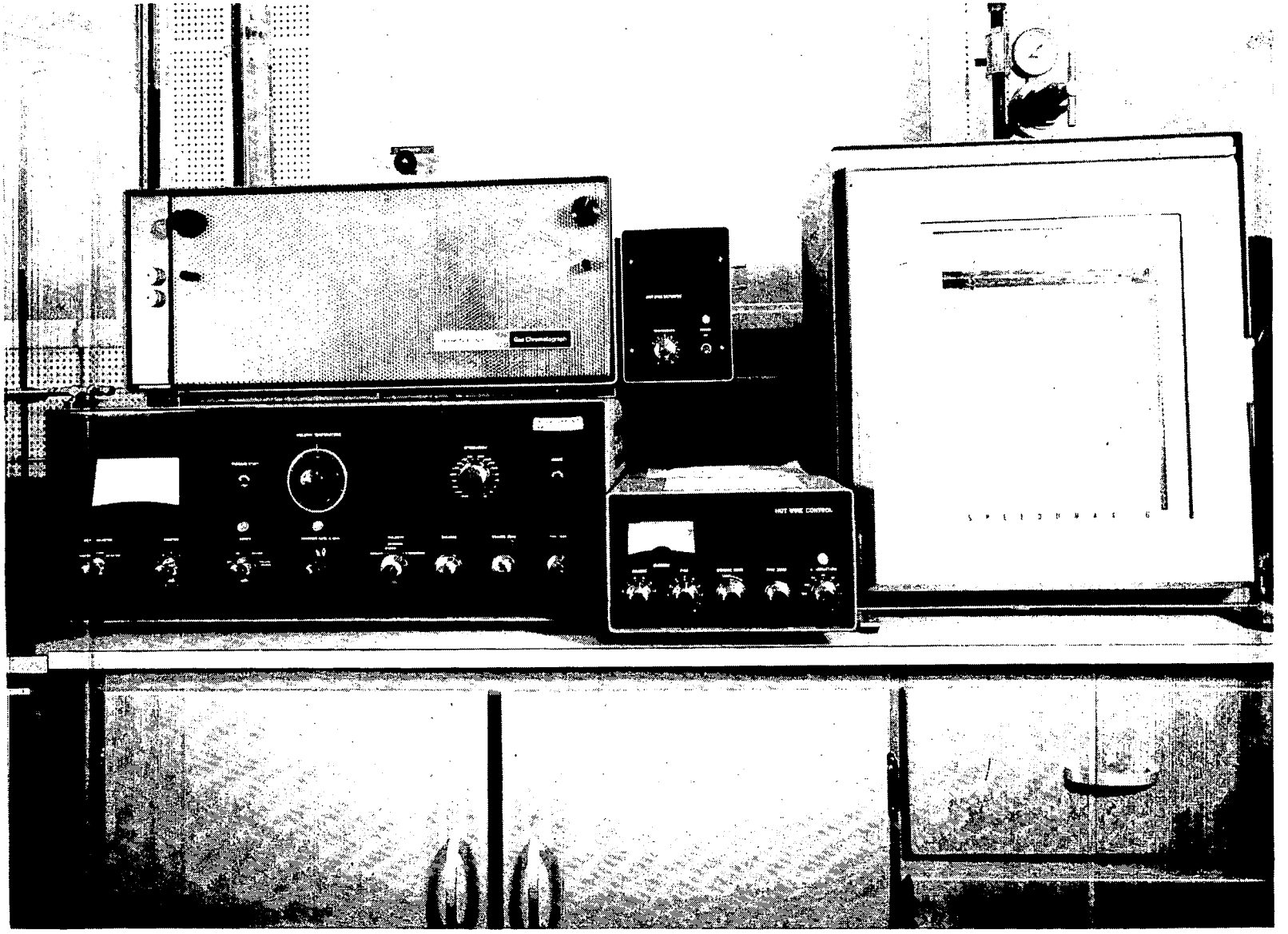

Figure 154 Perkin-Elmor Model 800 Chromatograph H-53856

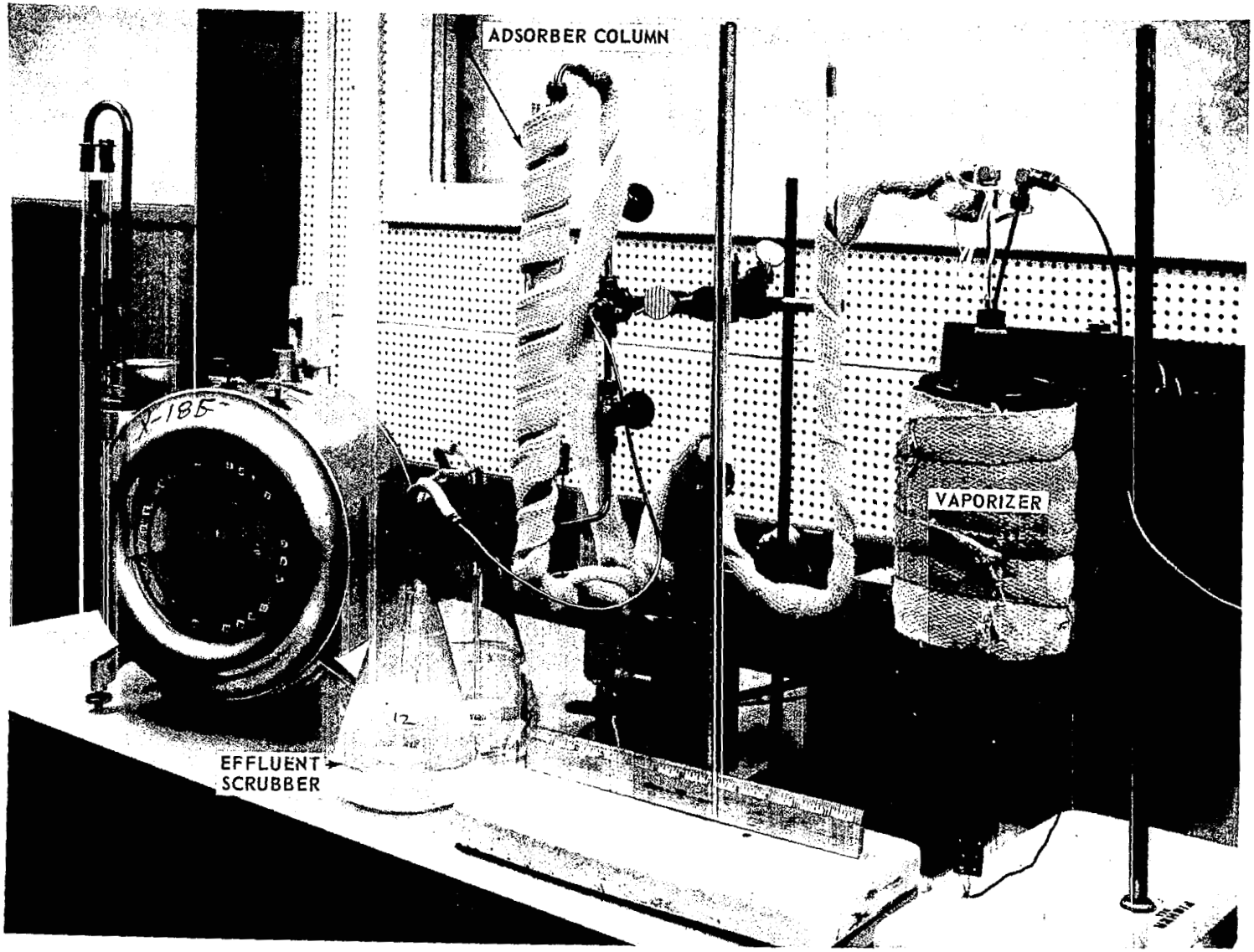

Figure 155 Test Apparatus for Adsorbate Evaluation H-55931

The duration of each test was 100 hours. Less than 0.008 gram oil was detected in the argon downstream of the adsorber column during the tests. At the end of the test period the contents of the adsorber column were divided into sections and the oil content of each section was extracted and measured. The results of the adsorber column oil content analysis for the first two tests were as follows:

100-Hour Test of Linde Type 4A Molecular-Sieve Powder

Portion of Column	Grams of Oil Adsorbed	Gm Oil/Gm Adsorber
first 1/4 (inlet)	0.746	0.083
second 1/4	0.521	0.058
third 1/4	0.025	0.0028
remainder	0.003	0.0003

100-Hour Test of Linde Type 13X Molecular-Sieve Powder Conditioned at 300°F for 15 Hours

Portion of Column	Grams of Oil Adsorbed	Gm Oil/Gm Adsorber
first 1/16	0.885	0.420
second 1/16	0.039	0.019
second 1/8	0.022	0.0053
third 1/8	0.0012	0.0003

A post-test closeup view of the inlet section of an adsorber column is shown in Figure 156. In this test the adsorbate was molecular sieve having a particle size corresponding to 60 to 80 mesh. A band of oil-saturated adsorbate is evident at the column inlet.

The test results of the second test indicated that approximately 5 grams of 13X molecular-sieve powder per gram of oil would remove essentially all of the polyphenyl ether entering the column. However, column pressure drop is inversely proportional to particle size and the pressure drop for the powder adsorber was excessive. Therefore, to meet pressure drop requirements, the use of a pellet material was more attractive.

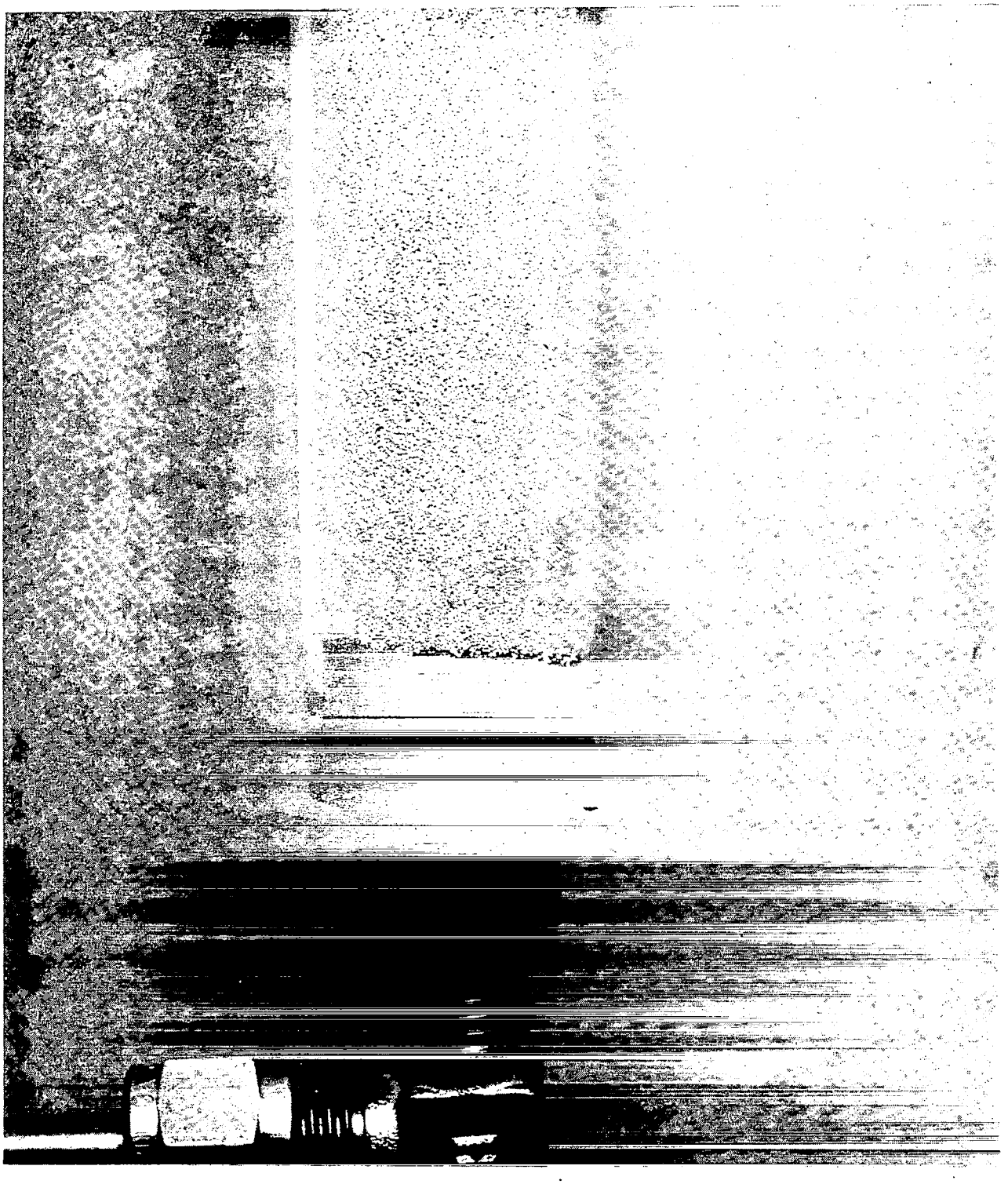

Figure 156 Inlet Section of Adsorber Column Filled with Adsorbate H-54926

A third 100-hour evaluation test was conducted using approximately 40 grams of 1/16 inch diameter Linde 13X molecular-sieve pellets in the adsorber column. The 13X pellets were conditioned at 300°C for 15 hours before the start of the test. The test rig vaporizer was charged with 5-ring polyphenyl ether oil and was operated at 350°F. The adsorber bed column was maintained at 100°F during the test which was operated for a period of 100 hours at an argon flow rate of approximately 1 liter per minute. The results of the analysis of the oil distribution for the adsorber material in this test were as follows:

Portion of Column	Grams of Oil Adsorbed	Gm Oil/Gm Adsorber
first 1/8	0.238	0.047
second 1/8	0.029	0.0058
third 1/8	0.008	0.0016
fourth 1/8	less than 0.0004	less than 0.00008
cumulative fifth through eighth	less than 0.0004	less than 0.00008

A test was conducted to determine the saturation capability of the 1/16-inch diameter 13X molecular-sieve pellets for adsorption of five-ring polyphenyl ether oil. A weighed quantity of the 13X pellets were soaked in PWA-524 oil and subsequently desiccated at 200°F over wire screen and filter paper for 50 hours. The weight of oil adsorbed per gram of 13X molecular sieve pellet material in this test was determined to be 0.3305 gm.

The pressure drop across the adsorber bed determines the argon pressure in the bearing compartments, which determines the pressure difference across the face seals. In order to minimize oil weepage through the face seals, a high pressure difference should be maintained which requires a low pressure drop across the adsorber. Therefore, tests were conducted to determine the pressure drop with various adsorber configurations. Adsorber columns were fabricated with static taps located 10 inches apart near the inlet and discharge of the column. Three adsorber columns were constructed with inside diameters of 0.41, 0.87 and 1.34 inch. A photograph of one adsorber column setup for pressure drop tests is shown in Figure 157. The pressure-drop results using this apparatus with an argon flow rate of 1 liter per minute were:

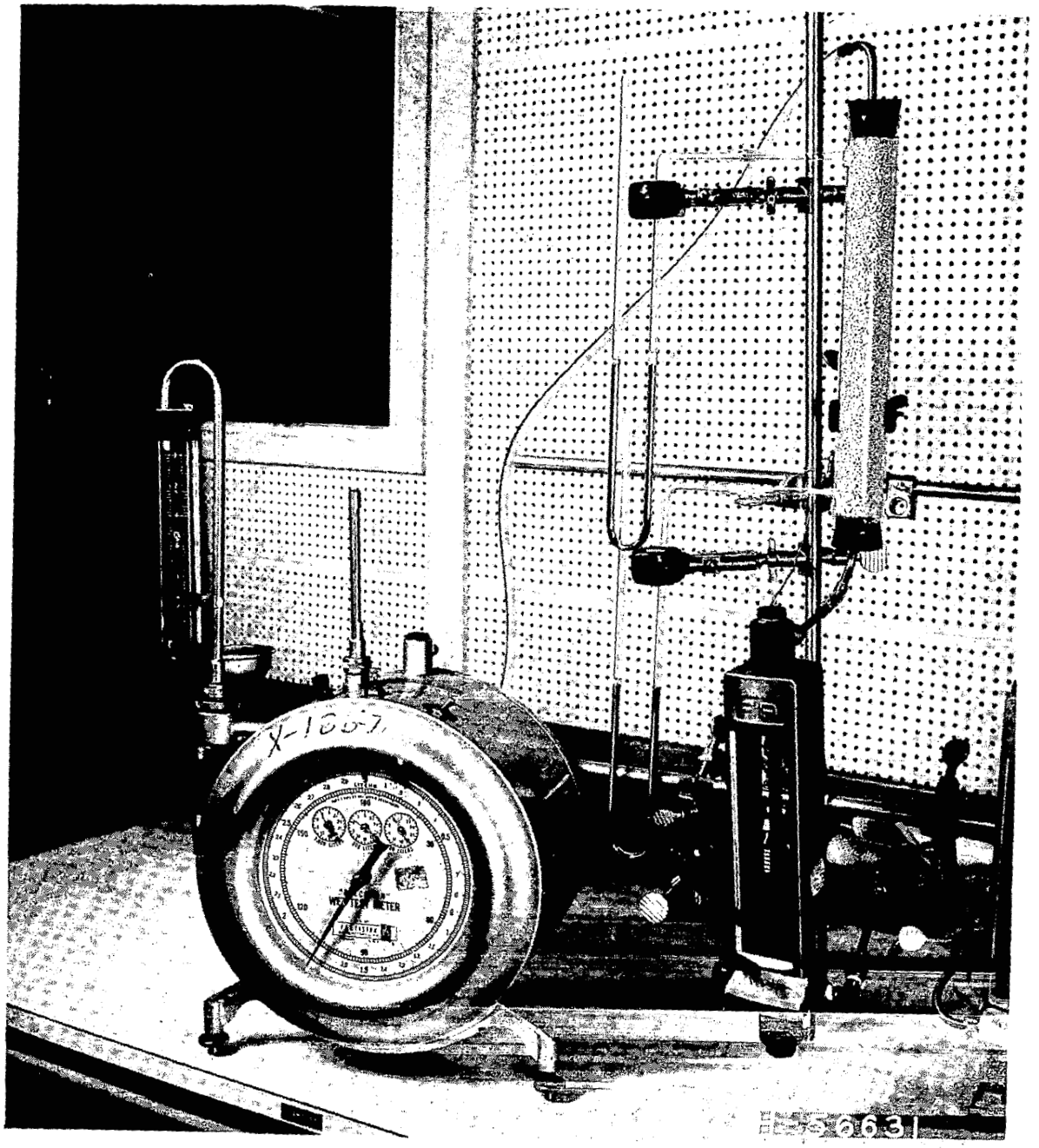

Figure 157 Pressure-Drop Test Rig H-56631

Tube No.	Inside Diameter of Tube, Inch.	Molecular Sieve Form	Pressure Drop, psi
1	0.41	1/16-inch dia. 13X pellets	0.018
2	0.87	1/16-inch dia. 13X pellets	0.010
3	1.34	1/16-inch dia. 13X pellets	0.001
1	0.41	60-80 mesh 13X power	1.5

No unusual phenomena were observed during these tests. The pellet form of the adsorber material provides much lower pressure drops than the powder form.

Particle size measurements on Linde Types 4A and 13X molecular-sieve material in powdered form graded to 60 to 80 mesh size were performed. The results of these measurements are as follows:

Molecular Sieve Type	Size Range, microns
4A pretest	131 - 188
4A posttest	104 - 224
13X pretest	83 - 166

These data were obtained using the Coulter counter shown in Figure 158.

Since the Linde 13X material in pellet form exhibited satisfactory adsorption characteristics in the 100-hour tests and since it offers a significant pressure-drop advantage, this material was selected for further test. The diameter of the adsorber column for this test was increased over that of the 100-hour test column to provide a ratio of minimum bed diameter to pellet diameter of 20 to 1. A Pyrex tube having an inside diameter of 1.31 inch was selected for the adsorber bed container. The length of the column was also increased over that of the 100-hour test column to approximately 33 inches. Pressure taps were provided at the inlet, midpoint, and discharge of the bed so that pressure-drop measurements across the bed could be made during the test. The design flow of argon through the bed corresponded to the mass flow rate per unit cross-sectional area that was used in the 100-hour adsorber tests. Dual manifold vaporizer and swirl separators were incorporated into the test rig so that these units could be serviced without

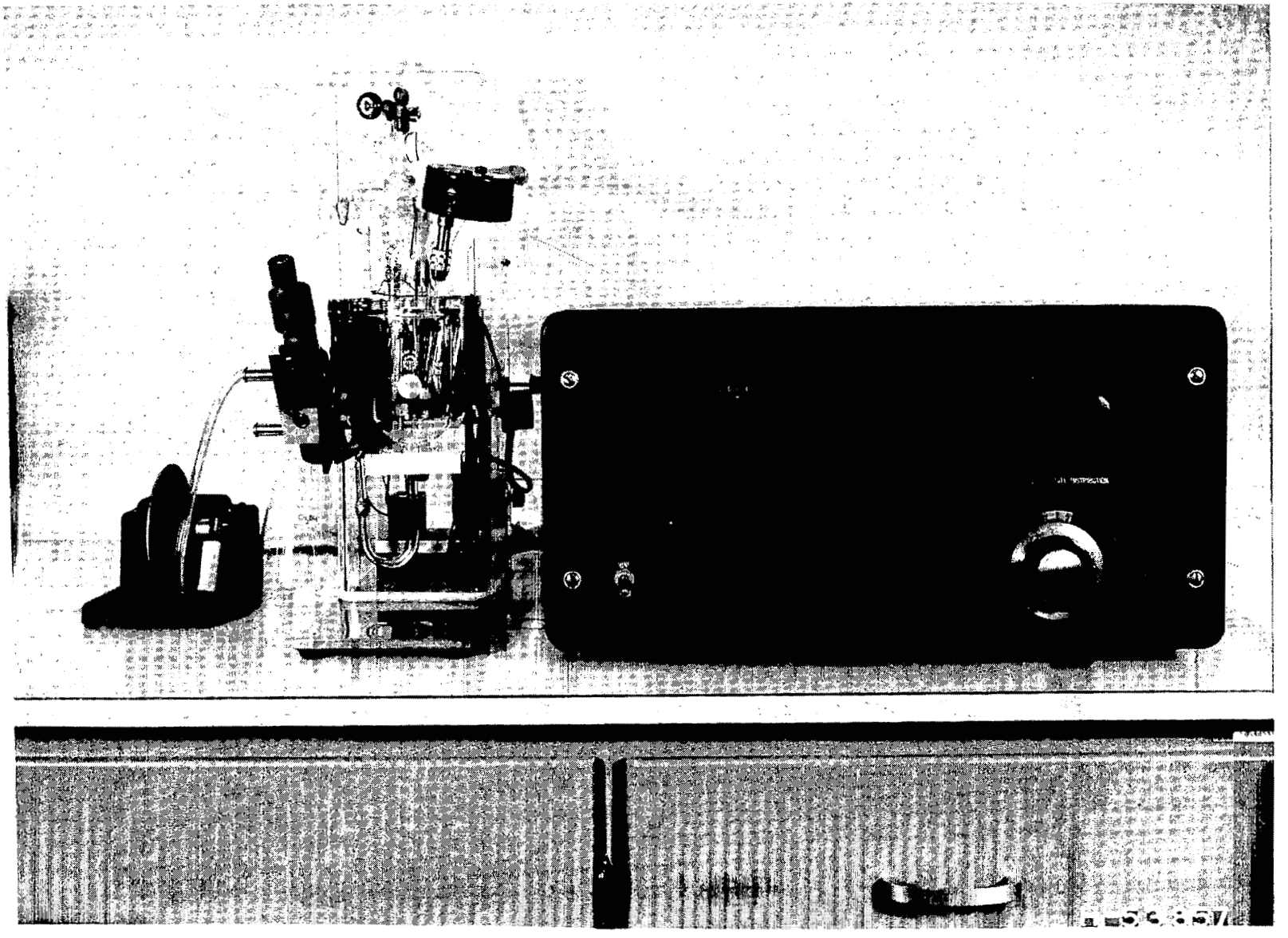

Figure 158 Coulter Counter for Determination of Adsorbate Particle Size H-53857

interrupting the test. In addition, the size of the swirl separator was increased to accommodate the increased argon flow rate. A total-hydrocarbon analyzer was incorporated in the test rig to monitor the argon flow for oil content leaving the adsorber bed. The argon leaving the adsorber column flowed through a scrubber column intended to collect all of the oil leaving the bed. A photograph of the adsorber test rig is presented in Figure 159.

The scrubber column was removed at 100-hour intervals and replaced with a new scrubber column containing new adsorber material. After removal, the contents of the scrubber column were analyzed by constant-temperature chromatography. The total contents of the column was immersed in benzene, extracted, and boiled down to 1 ml samples for chromatographic analysis.

The adsorber test rig was operated at the selected conditions for a total of 600 hours. Evidence of oil collecting in the glass wool packing at the column inlet was observed and the oil accumulation in this case continued to increase with test time (Figures 160 and 161). It extended almost completely around the tube when the test was terminated as shown in Figure 161. Some adsorber pellets adjacent to this zone showed a brown coloration similar to that of pellets saturated with lubricant in previous saturation capacity tests. Pressure measurements were taken every 24 hours at the four locations on the column and the results are presented in Figure 162. The pressure drop across the whole adsorber including the glass wool increased about 0.04 psi. This pressure loss occurred primarily across the glass wool and can be attributed to the increase in resistance due to the oil collecting in the glass wool.

Visual inspection of the Pyrex glass container indicated the formation of a very thin film on the inner wall at the top of the adsorber bed. Figure 163 shows the film after 600 hours, when a swab sample of the film was identified as lubricant.

For the duration of the test, the hydrocarbon content of argon discharged from the adsorber column was monitored by means of a total-hydrocarbon analyzer one minute out of every hour. All results indicated that the discharged argon contained less than 3 microliters of oil per liter of argon. Analysis of a standard methane gas mixture at regular periods throughout the test period verified that instrument calibration and response were satisfactory.

The test was interrupted at 500 hours when the pressure measurements suggested a flow resistance in the exit plumbing. Also, some pellets at the exit

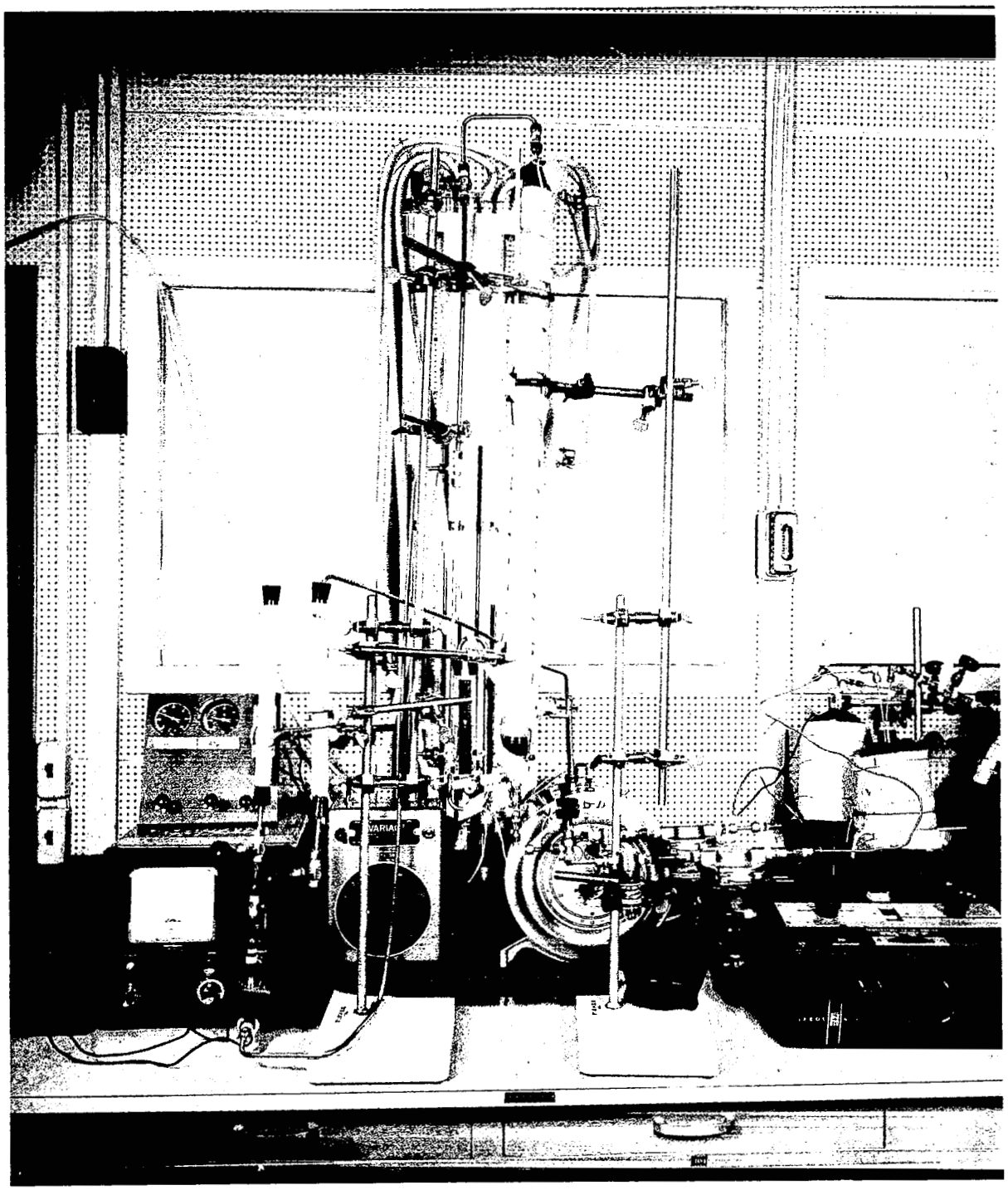

Figure 159 Apparatus for Adsorber Test H-58136

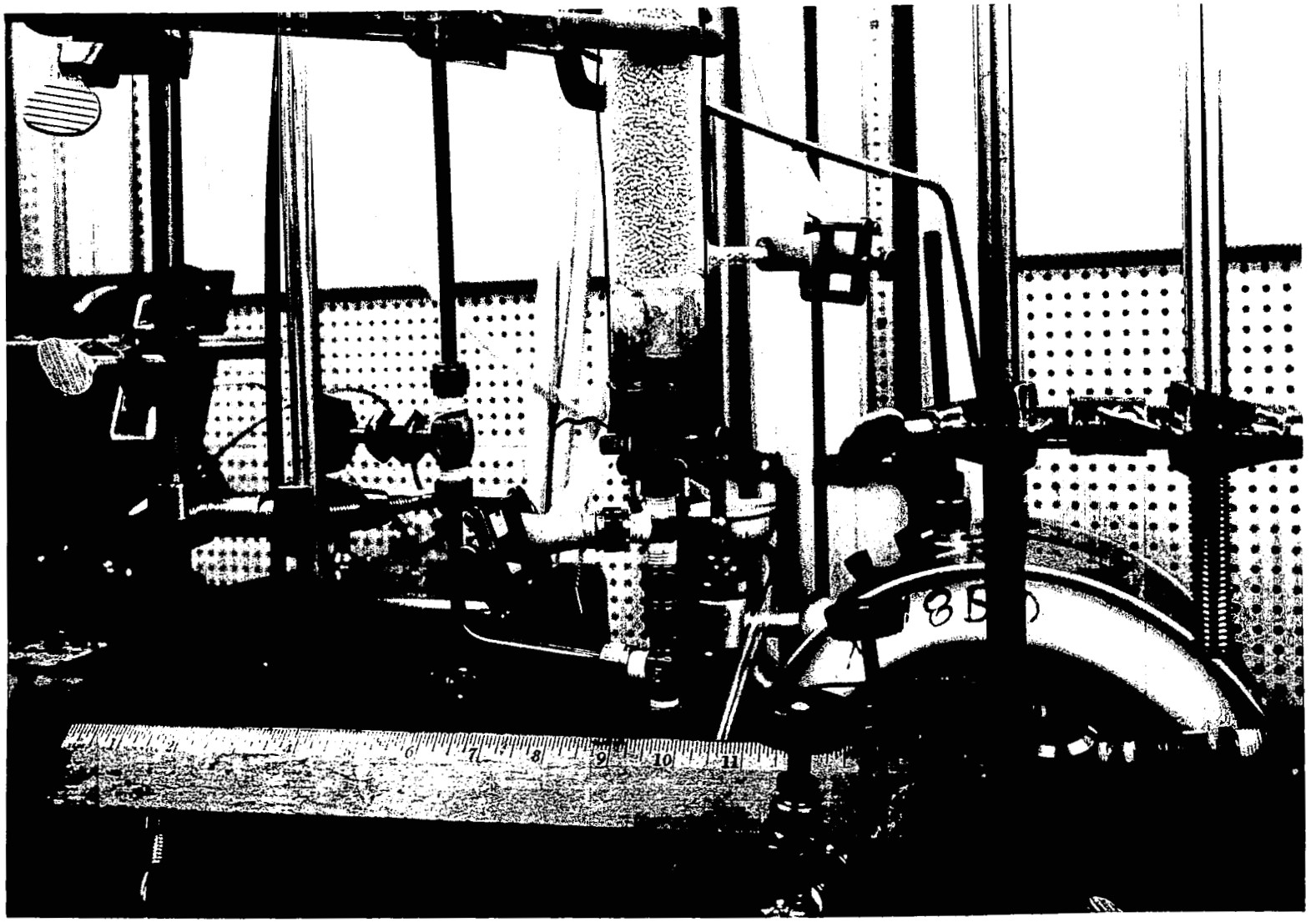

Figure 160 Inlet Section of Adsorber Column at 370 Hours H-58570

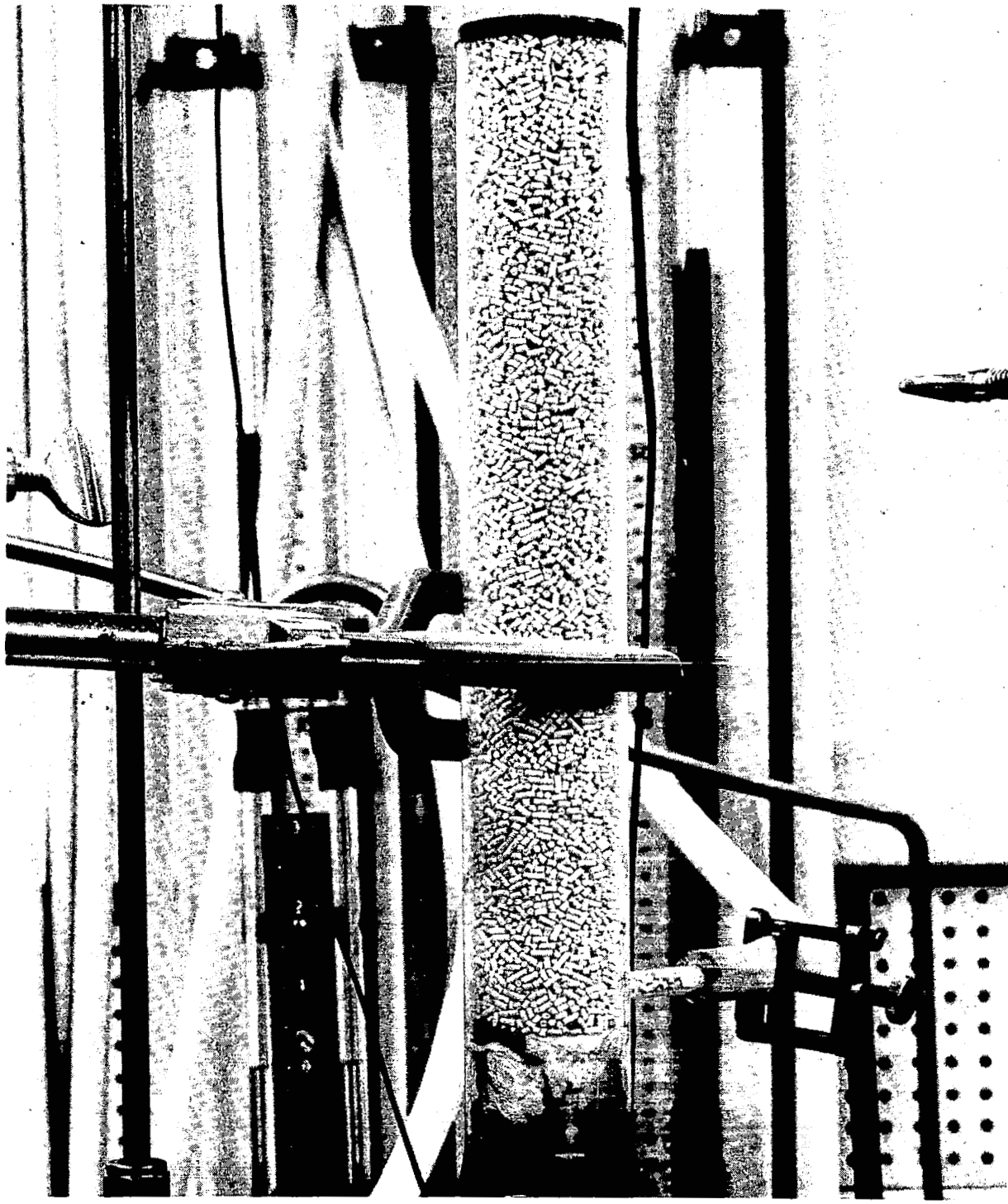

Figure 161 Closeup of Adsorber Inlet Section at 600 Hours H-58784

of the adsorber bed showed a brown color which is indicative of oil saturation of the pellets (the pellets are normally white). The first discoloration was observed after 370 hours of operation. The exit tubing was removed and the glass wool located at the exit of the bed was found to contain a significant quantity of oil, 0.46 gram. Visual observation of this oil accumulation was not possible since the glass wool was located in the metal tube at the exit. The top layer of pellets was removed and the discolored pellets were analyzed and found to contain 0.367 gram of oil per gram of pellets. This concentration indicates that the discolored pellets were saturated with oil. No discolored pellets were observed in the adsorber bed except at the inlet and exit ends where pellets were in contact with the glass wool.

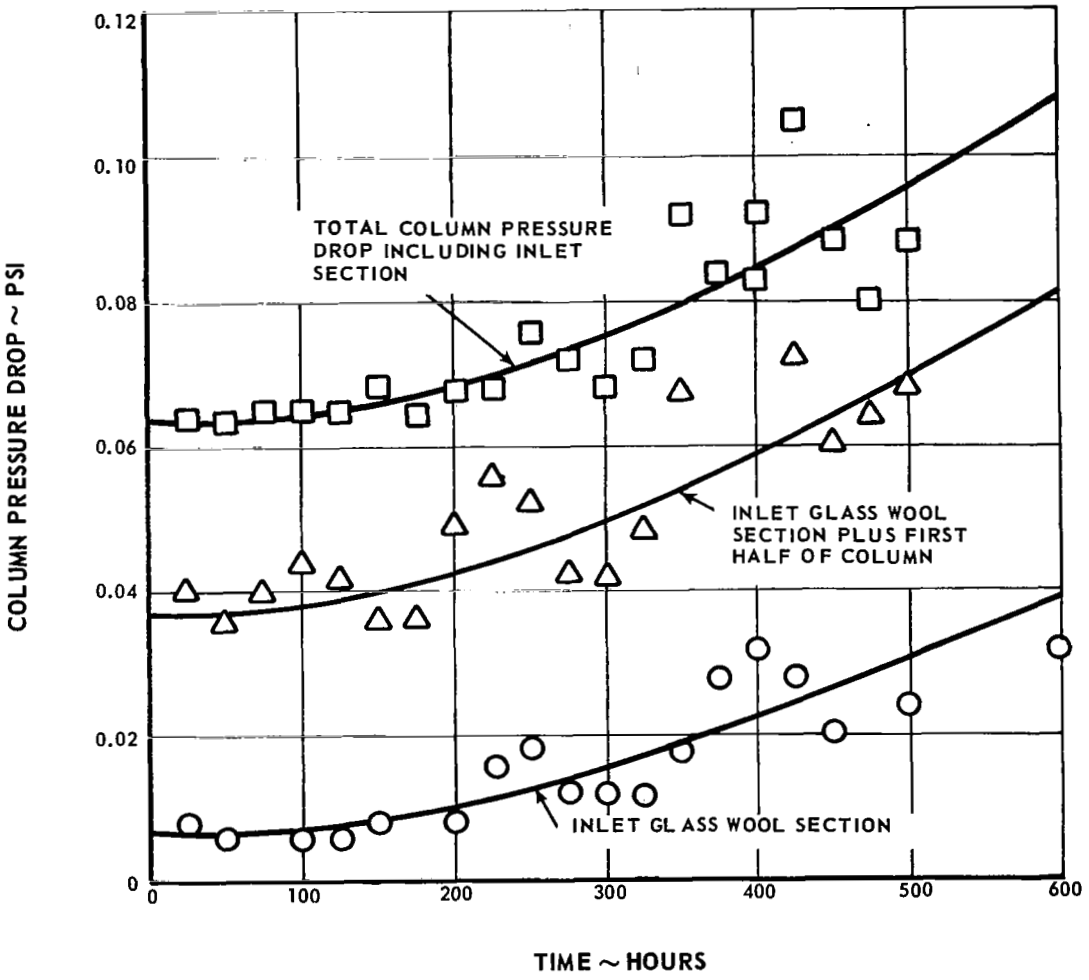

Figure 162 Pressure-Drop Characteristics of Adsorber Column

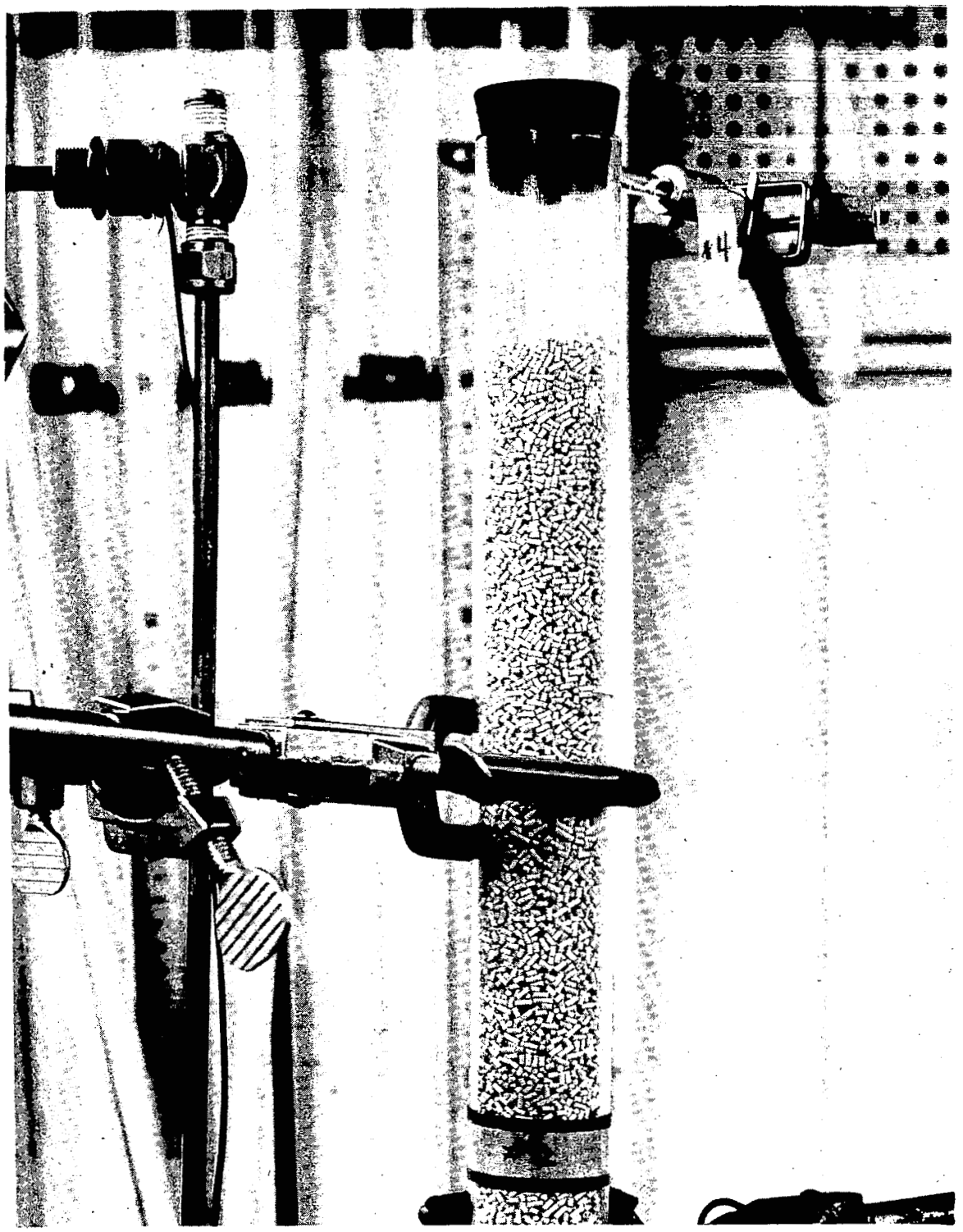

Figure 163 Exit End of Adsorber Column at 600 Hours H-58783

Although precautions were taken to thoroughly clean the exit tubing prior to the test, the possibility of oil contamination due to improper cleaning could not be completely eliminated. Therefore, the exit tubing was removed, cleaned, and reassembled. A clean glass wool packing was installed and the test was restarted.

The scrubber at the exit of the rig was analyzed to determine the quantity of oil in the discharge argon. 0.014 gram of oil accumulated in the scrubber in the 100 hours prior to the interruption at 500 hours, indicating a small breakthrough. Figure 164 presents a plot of the total oil that entered the rig and the total oil leaving the adsorber. The breakthrough of a small amount of oil between 400 and 500 hours is evident in this figure. The oil flow entering the rig was determined by periodically bypassing the adsorber and measuring the oil content of the flow out of the swirl separator using the total-hydrocarbon analyzer. This measurement is subject to some error. The measurement of the oil leaving the adsorber was a result of measuring the contents of the scrubber beds.

While the scrubber contents were being analyzed, the adsorber test was continued to 600 hours with the new glass wool in the exit section. The adsorber bed was not disturbed during the interruption at 500 hours, except to remove a small layer of pellets from the top of the bed as shown in Figure 163. At 600 hours the test was interrupted again and the glass wool in the exit section was examined and found to contain 0.075 gram of oil. This oil was collected between 500 and 600 hours. No oil was detected in the exit tubing which had been cleaned at 500 hours when the new exit glass wool was installed. At the 600-hour point, the contents of the scrubber used between 400 and 500 hours had been analyzed and the small oil breakthrough shown on Figure 164 was found. Therefore, the test was terminated at 600 hours to permit analysis of the oil content in the adsorber bed and the inlet glass wool section.

The glass wool packing at the inlet of the adsorber bed contained 13.20 grams of oil located primarily near the outer diameter. This constituted the majority of the oil entering the adsorber. The inlet tubing between the separators and the adsorber contained 3.30 grams of oil which could have run back from the inlet glass wool section. The exhaust scrubber used between 500 and 600 hours contained 0.0002 gram of oil.

The oil content in the adsorber bed was measured and a total of 0.5856 gram was found. The Linde 13X pellets were removed in layers of approximately 1/2-inch near the inlet of the column and in 1-inch layers for the remainder of the tower. The oil content of each layer was determined using the chromato-

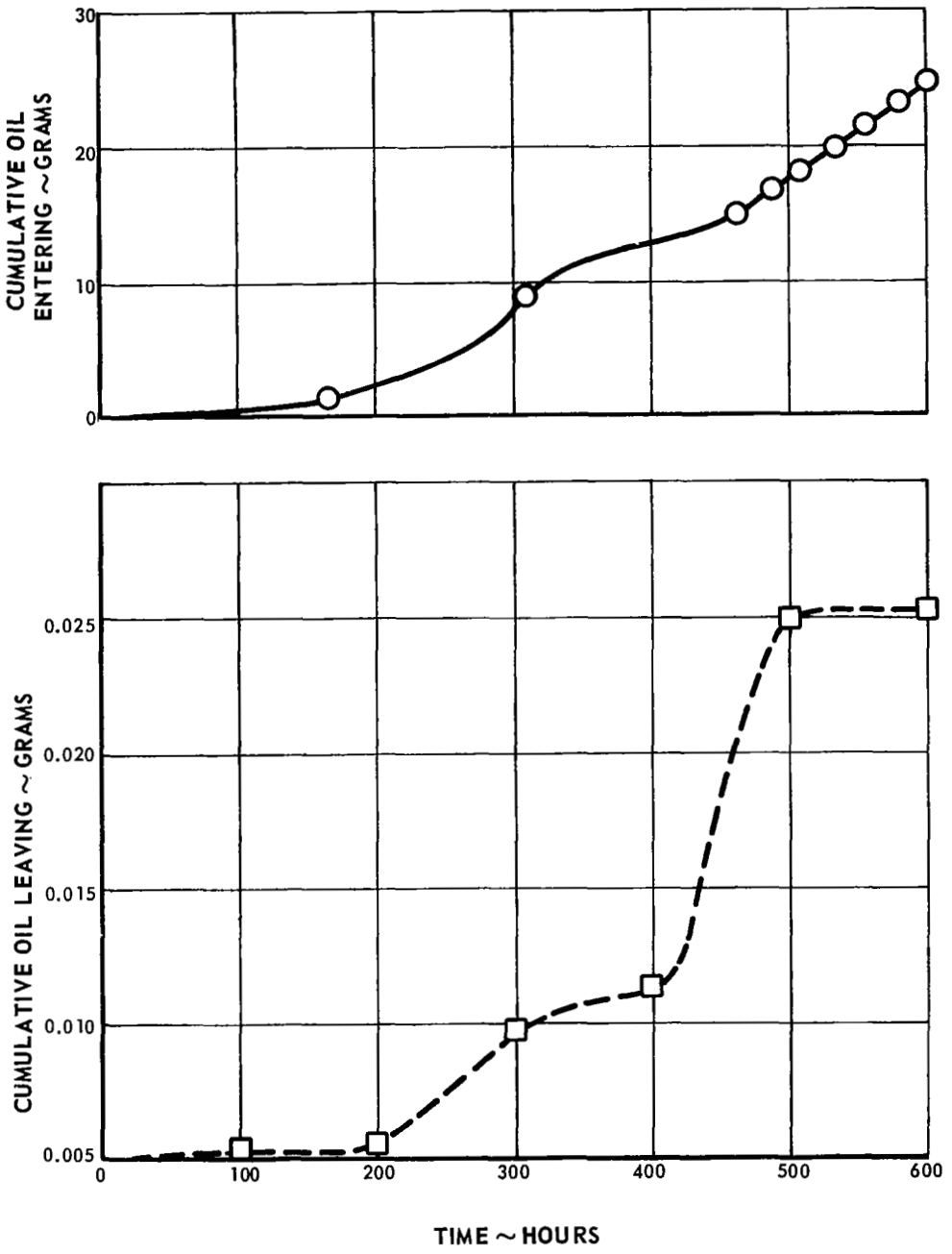

Figure 164 Cumulative Oil Flow in Adsorber Endurance Test

graph. Also the weight of each layer of pellets was determined. The oil distribution measured in the adsorber bed is presented in Figure 165. As this figure indicates, the bulk of the oil adsorbed in the bed is contained in the first inch of material. 90.3 per cent (0.5285 gram) of the oil was contained in the first 1.06 inch of the bed. The inlet section contained small pellets that were discolored, indicating saturation. The normal saturation level determined previously is 0.3305 gram of oil per gram of pellets. Some of the saturated pellets are visible in Figure 161. These pellets appear to be in contact with the glass wool and may have acquired oil by wicking. The bulk of the bed adsorbed 0.0001 to 0.0002 gram of oil per gram of adsorber, and this level is fairly constant throughout the length of the bed. This result was not expected since the concentration of oil is decreasing as the oil-gas mixture proceeds through the column. A decreasing amount of oil adsorbed might be expected. The 100-hour test indicates such a reduction. The results of the 100-hour test with Linde 13X pellets are also presented on Figure 165. The column length of the 100-hour test was 10 inches. Evidently the first inch or two of the column produced essentially the same performance in both the 100-hour and 600-hour tests. Apparently the 100-hour test was not of long enough duration to show a low level of adsorption for the bulk of the column as was found in the 600-hour test.

A second unexpected result in comparing the 100-hour test with the 600-hour test is the fact that the first inch or so of the bed did not adsorb more oil in the long term test than in the short. Since the adsorption level is approximately one order of magnitude less than saturation, the longer test was expected to adsorb more oil as a result of the longer exposure. Actually, the oil adsorption in the long and short tests are quite similar as shown in Figure 165.

The third unexpected result was the oil breakthrough. In the 100-hour test, benzene scrubbers were employed and no oil was detected downstream of the adsorber. In the 600-hour test a total of 0.0202 gram of oil was found in the exit scrubbers. Also, 0.6269 gram total was found in the exit glass wool, exit stopper and exit tube in the 600 hours of testing. While the quantity of oil transmitted through the column was small it is roughly the same magnitude as the oil adsorbed in the pellets. Evidently, the Linde 13X pellets did not adsorb the combination oil vapor and aerosol leaving the glass wool as effectively as desired.

Some other mechanism of oil transport through the bed could have been of importance. The length of the adsorber column and the previous tests indicated that channeling was not a factor, but capillary action might have been a factor. Capillary activity which might not be of importance in 100 hours could be a factor for extended periods such as 600 hours. A very thin film was observed

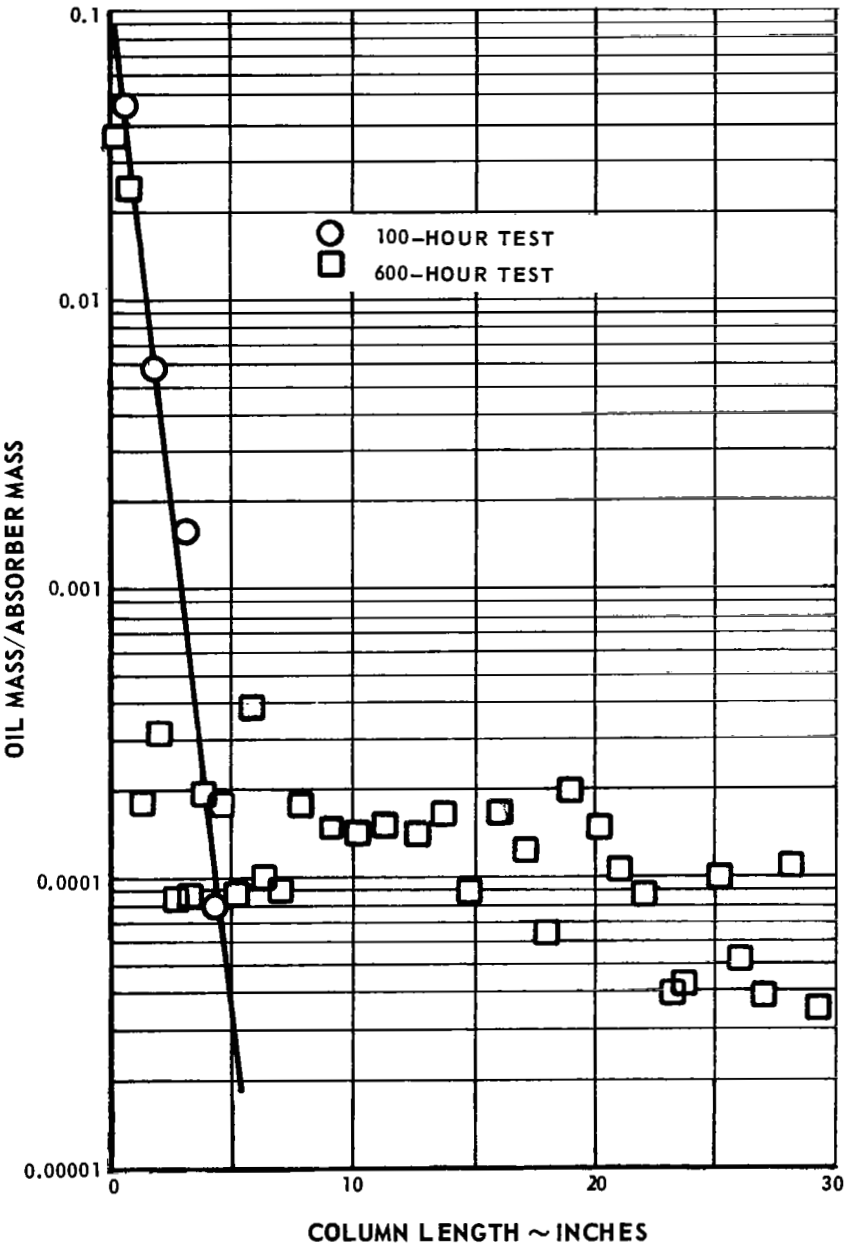

Figure 165 Adsorber Performance with Linde 13X Pellets

on the glass wall at the top of the column, which may be seen in Figure 163. A swab of this film was analyzed and found to contain oil.

A major discovery in the 600-hour test was the effectiveness of the glass wool in collecting the aerosol. The glass wool could not adsorb oil vapor but oil droplets could be entrained in the wool. A test was conducted to determine the potential saturation of the glass wool by immersing glass wool in oil and measuring the weight of the glass wool before and after immersion. The wool contained oil amounting to 27.2 times it own weight. The tentative conclusion from the 600-hour test is that the adsorber should be designed with a combination of glass wool to collect the oil particles and Linde 13X molecular sieve material to adsorb the oil vapor.

Although the long time adsorber test did not attain the goal of 1000 hours of operation, the results obtained during 600 hours of running were excellent until the outlet glass wool section became overloaded. Since installation of a new glass wool section restored the performance, it was decided that modified designs incorporating more glass wool and larger flow areas should be evaluated. Accordingly three additional long-term tests were undertaken. The additional work is presented below.

B. Phase 2 - Adsorber Evaluation

The Phase 2 adsorber program was formulated to continue the investigations started in Phase 1. In Phase 1 it was demonstrated that Pyrex glass wool was very effective in removing an oil aerosol and that the molecular sieve materials would apparently remove only oil vapor. It was learned that large amounts of oil were carried over from the oil-gas mixture generator as an aerosol. The five-ring polyphenyl ether oil used on the program has an extremely low vapor pressure, hence relatively small amounts were carried in the vapor phase. Further, it was learned that Pyrex glass wool would hold several times its own weight of oil.

1. Spiral Adsorber With Mixed Materials

In view of the above findings it was decided that the gas cleanup system should include several stages of removal with materials having specific characteristics for each stage. The first stage should have the capability to remove large oil droplets with succeeding stages separating finer droplets and vapor. Hence a spiral flow design was evolved that provided this capability, as well as having long flow paths with large flow areas. The arrangement is shown in photographs Figures 166, 167, and 168.

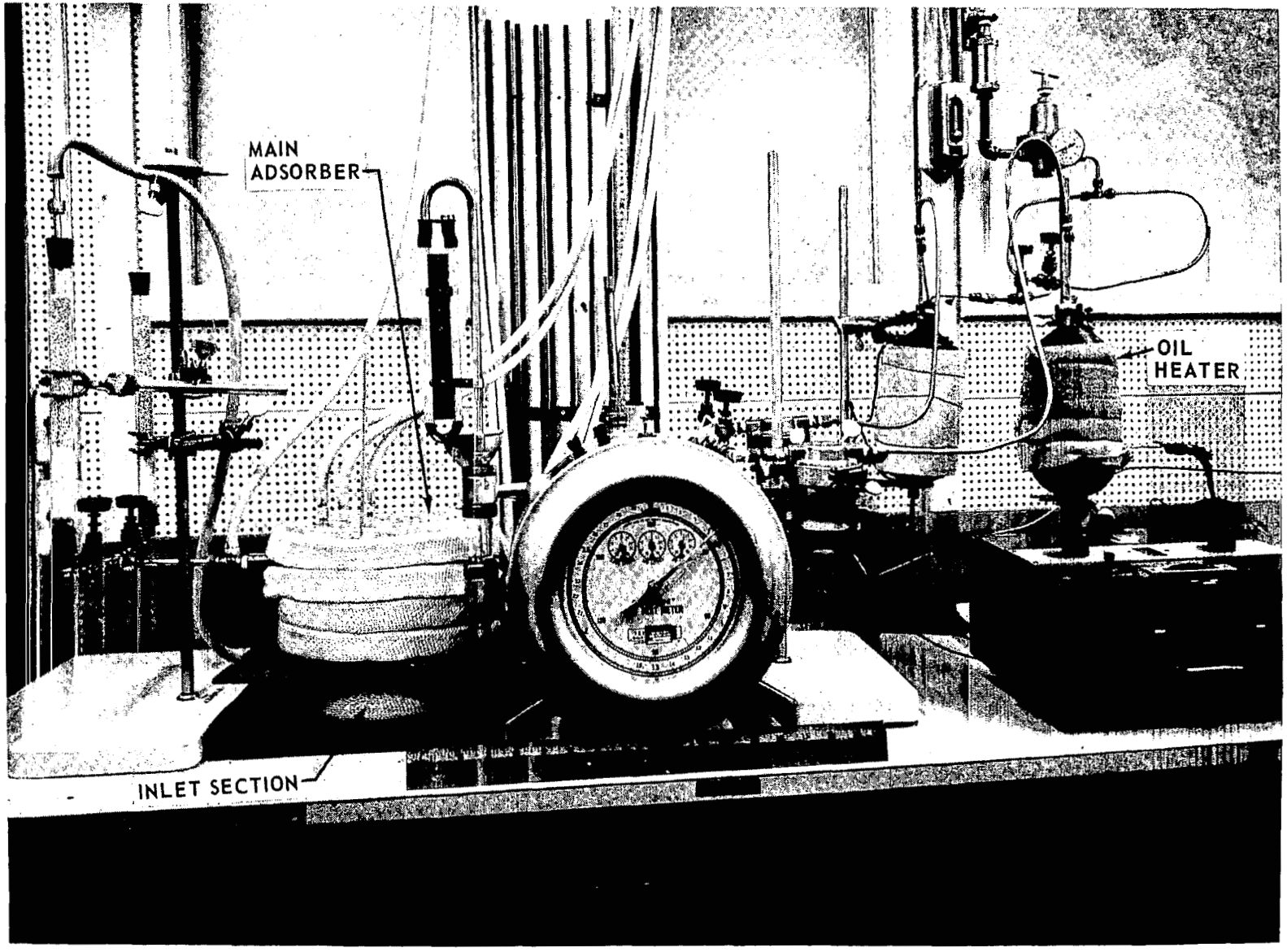

Figure 166 Spiral Adsorber Test Installation H-64261

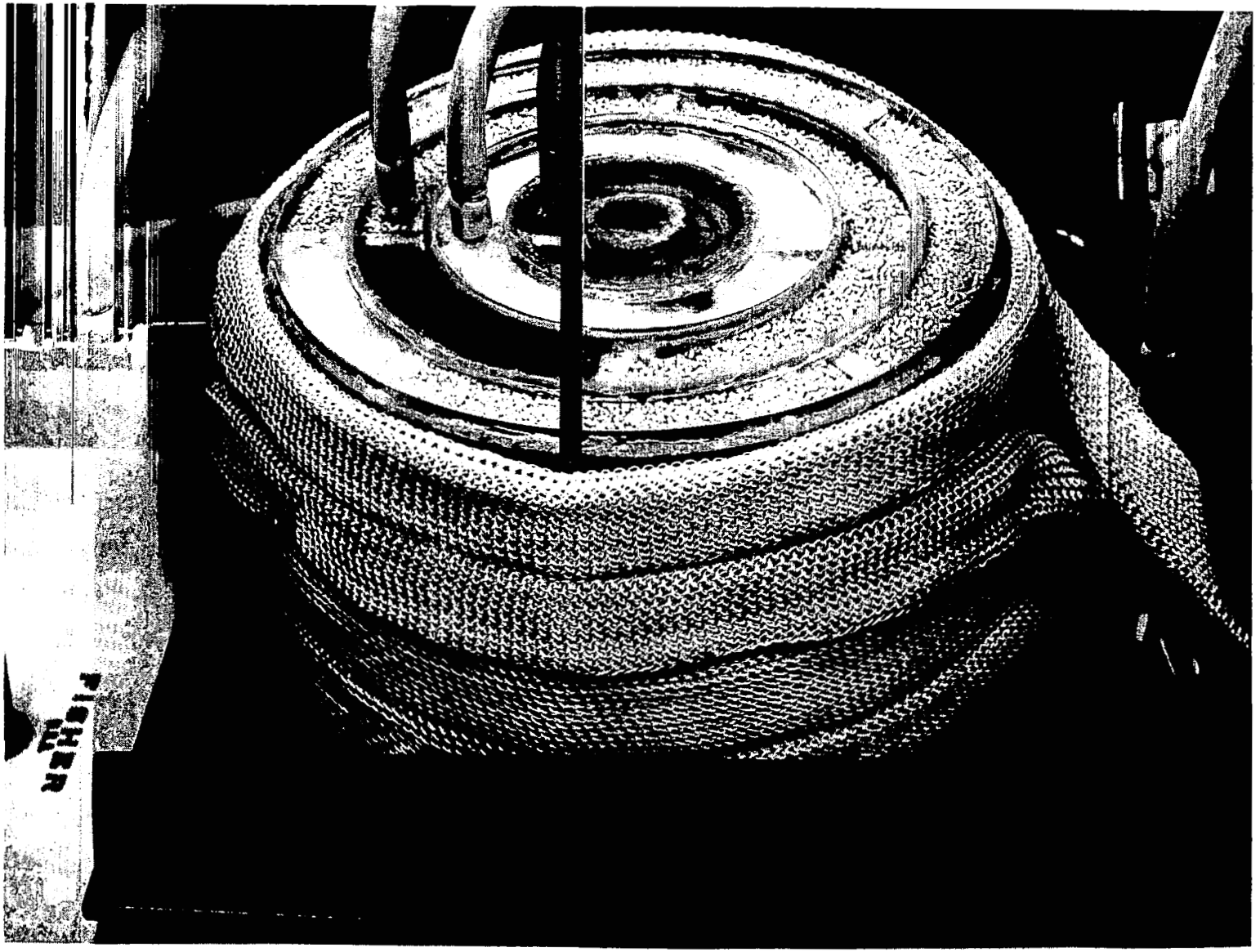

Figure 167 Spiral Adsorber Test H-64260

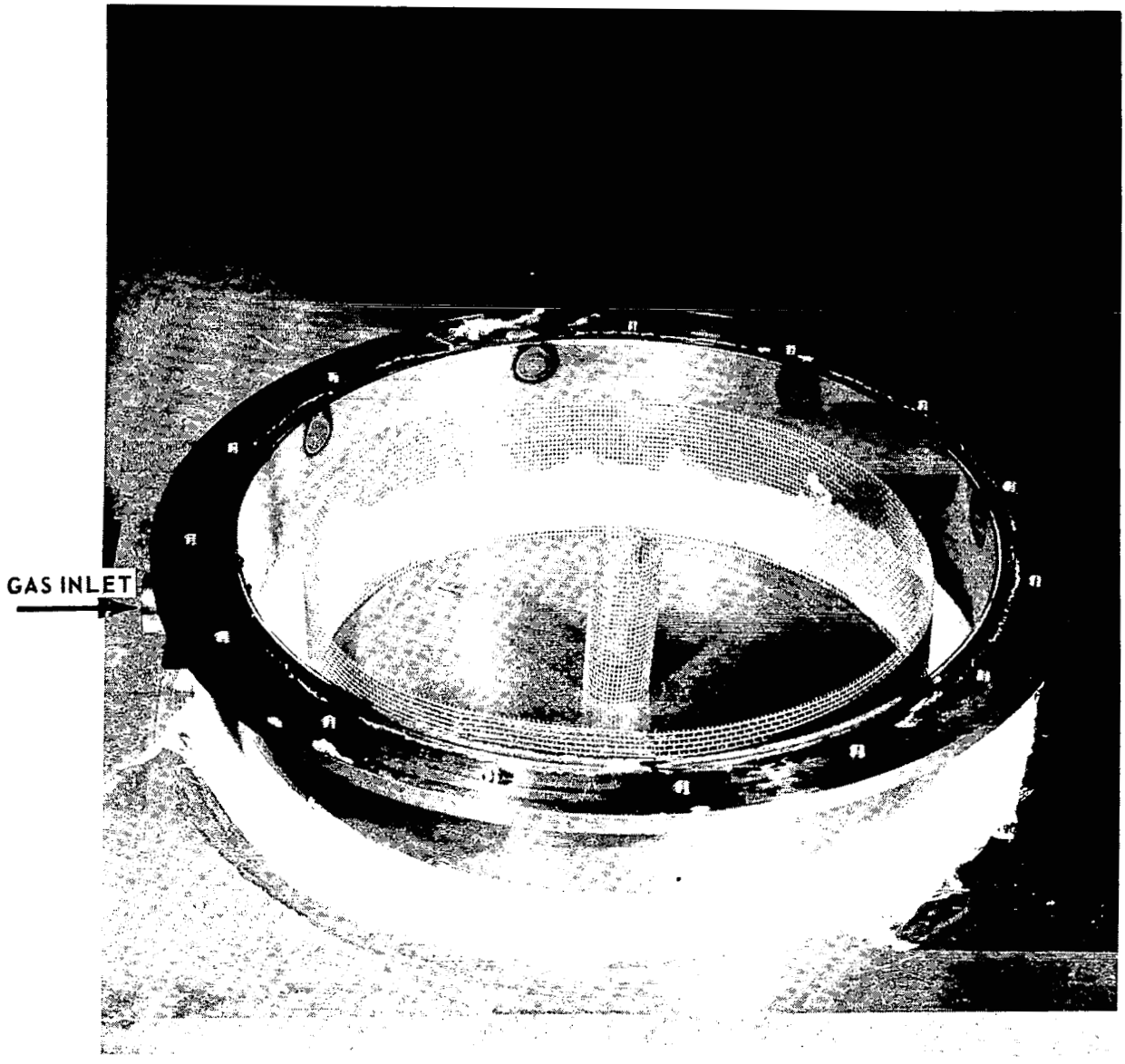

Figure 168 First-Stage Adsorber Container H-64094

Figure 166 shows the completed assembly ready for test, with two distinct sections shown, the inlet section and the main adsorber. The inlet section container, Figure 168, is used to contain the first stage for aerosol removal. Polyurethane foam of 60 pores per inch was selected as the material for this stage, based upon several screening tests. In this stage, the flow entered the circumferential manifold and passed radially inward to the standpipe screen which directed the flow into the main adsorber. The main adsorber shown in Figure 167 contains circular sections of material. Figure 169 shows the main adsorber container before loading. The gas-oil mixture entered the main adsorber at the center from the inlet section. At this point, the mixture flowed radially and circumferentially through another stage of polyurethane. This stage was followed by a complete circular pass which contained Pyrex glass wool. The flow then passed radially outward to a partial circular path which contained activated charcoal and was designed to be the first stage of vapor removal. This stage was followed by two nearly complete circular paths of Linde 13X molecular-sieve pellets. These two paths completed the vapor-removal section. Finally the last stage of cleanup was a partial ring of Pyrex glass wool intended to remove material that might have passed through the other stages.

In order to provide a baseline for comparison, the test methods selected for the Phase 2 test were the same as the Phase 1 methods. Instrumentation, operating procedures and performance analysis were all maintained as in the first test. Figure 166 shows the oil heaters, adsorber assembly, effluent monitor columns and other necessary apparatus. The Phase 2 test of the spiral adsorber also had a test goal of 1000 hours of operation. Operation of the test was performed on an essentially continuous basis with but few interruptions. Each time the oil heaters were recharged with oil, the units were operated for twenty-four hours to boil off the high-vapor-pressure ends. The measure of performance for this test was the same as in the Phase 1 test, by monitor columns. At the end of each 100 hours of operation, the monitor column was analyzed for oil content. Figure 170 displays the oil content at each 100-hour interval extrapolated to 10,000 hours at that interval. Upon completion of 1000 hours of operation, the unit was disassembled for analysis. Sectioning and analysis results are shown in Figures 171 and 172. These two figures have the same basic format. The whole numbers identify the section and the rectangular blocks identify the horizontal and vertical subdivisions of the section. The arrows indicate gas flow path. The analysis results are written in each rectangular block using decimal numbers. In Figure 171, the grams of the oil per gram of adsorbent are shown. Pre-test calibrations determined the ultimate holding capability of each constituent as follows:

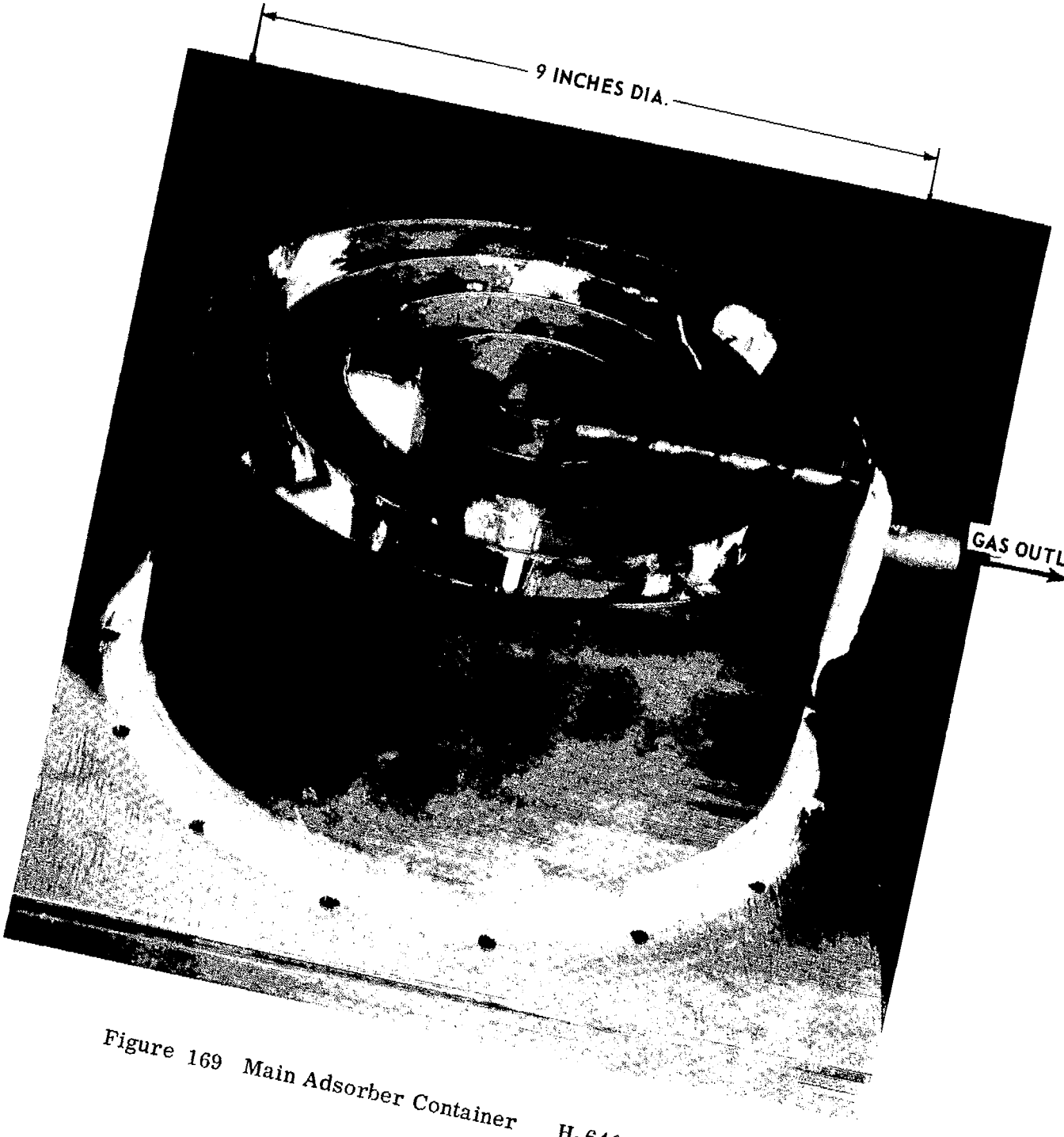

Figure 169 Main Adsorber Container H-64093

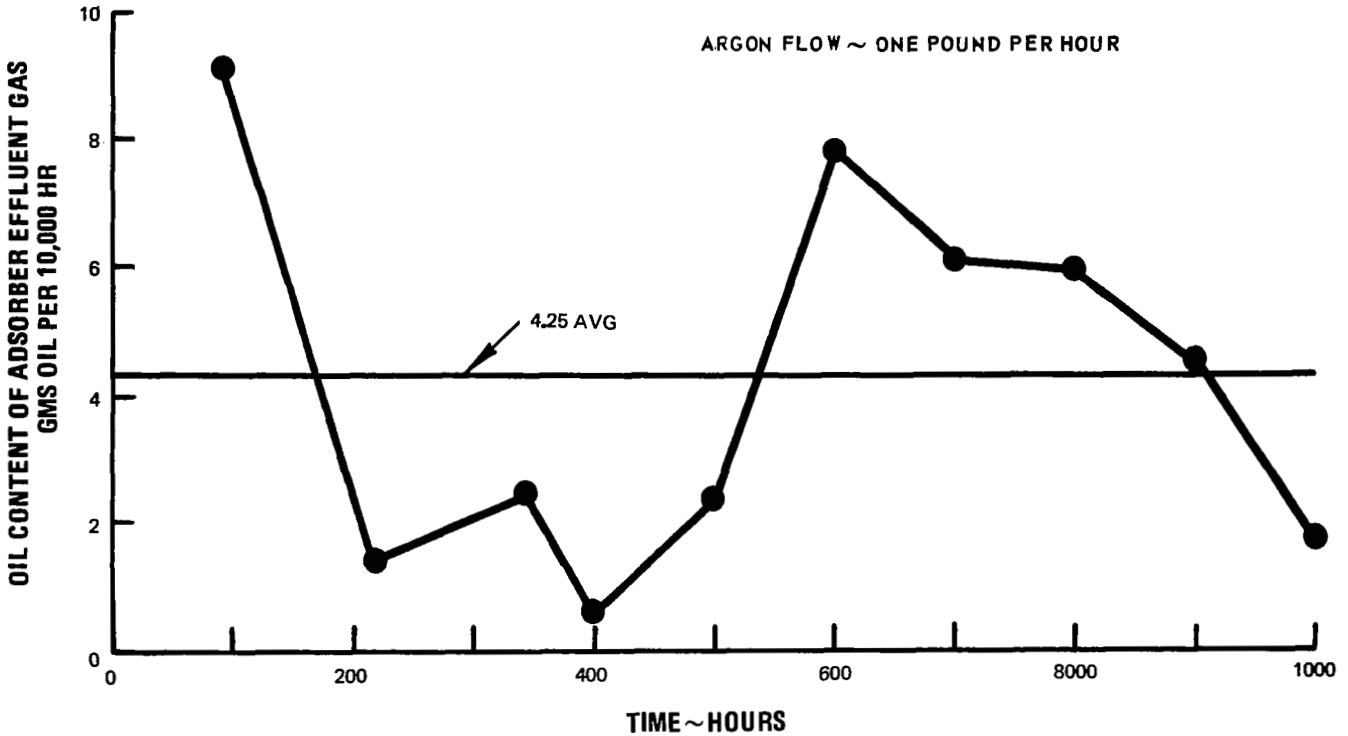

Figure 170 Performance of Spiral Adsorber with Mixed Materials M-49233

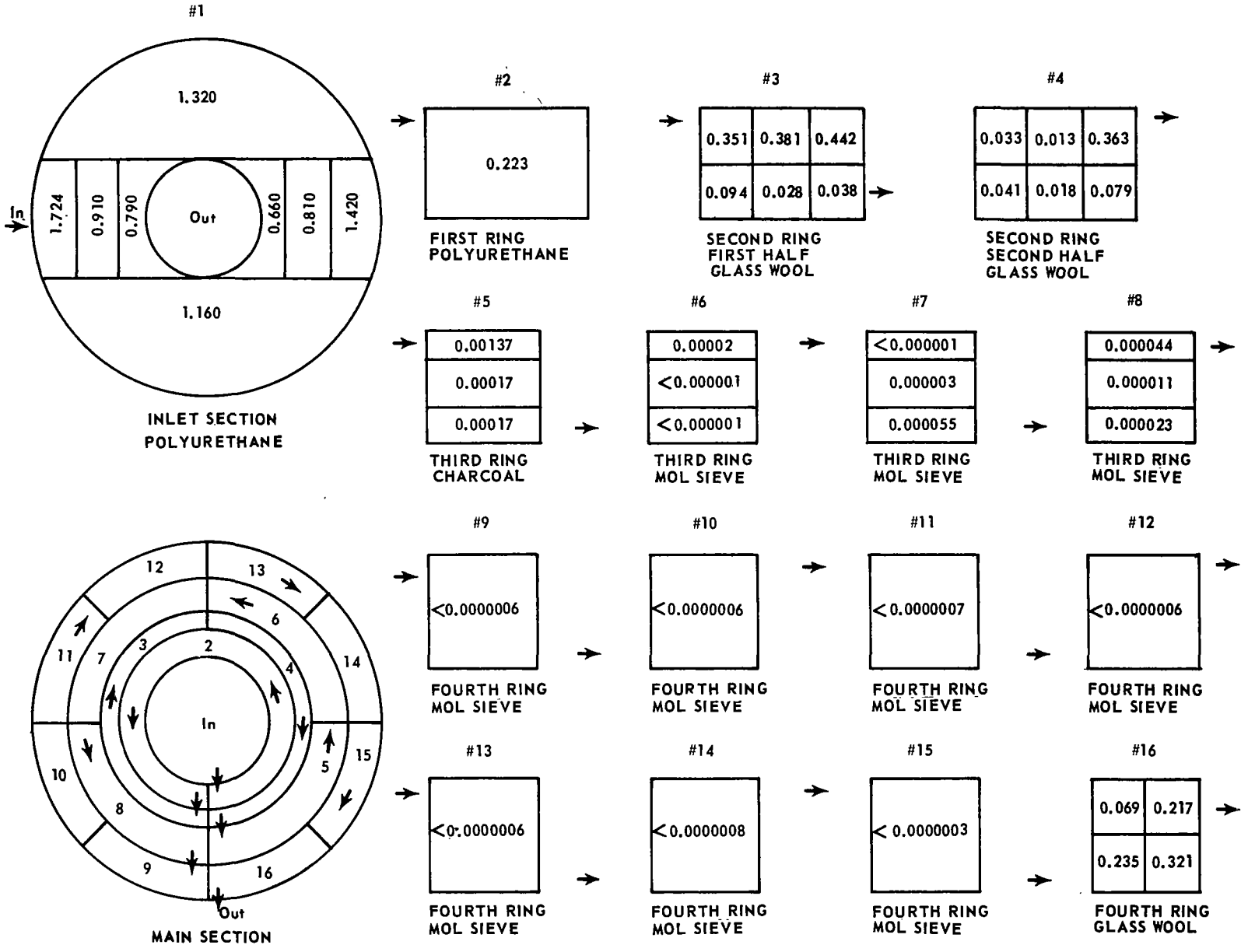

Figure 171 Profile of 1000-Hour Spiral Adsorber. Grams of Oil/Gram of Adsorbent

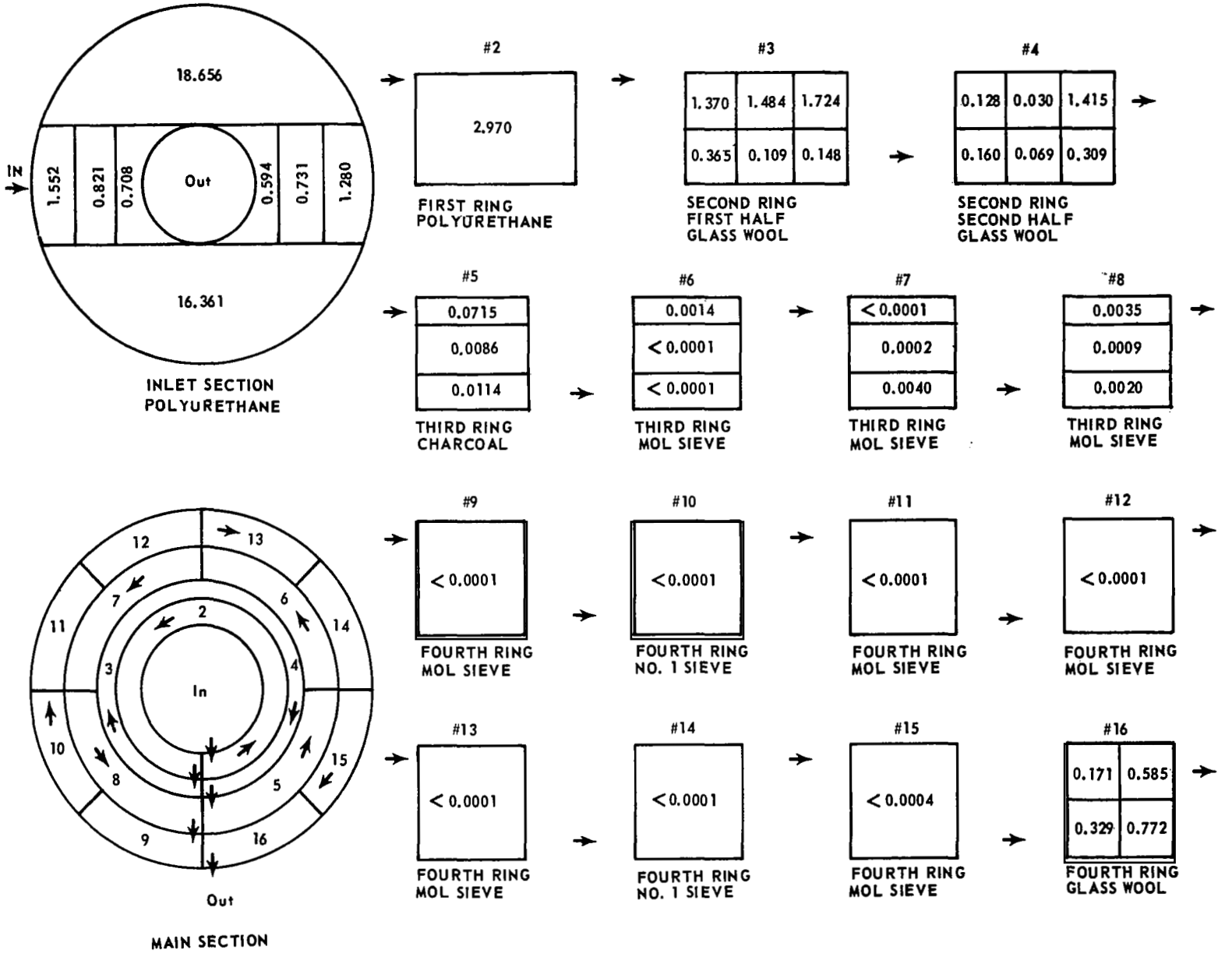

Figure 172 Profile of 1000-Hour Spiral Adsorber. Total Grams of PWA 524 Oil Retained

molecular-sieve 13X pellets	0.331 gram oil/gram pellet
activated charcoal	0.647 gram oil/gram charcoal
Pyrex glass wool	27.00 gram oil/gram glass wool
polyurethane, 60 pores per inch	32.00 gram oil/gram polyurethane

The total amount of oil held in each section is shown in Figure 172. Examination of these two figures will show two outstanding results. First, the polyurethane inlet section was very effective in removing incoming oil with essentially no pressure-drop change. Secondly, the glass wool removed more oil than the molecular-sieve pellets and charcoal combined.

2. Spiral Adsorber With All Glass Wool

Although the performance of the spiral adsorber with mixed materials was well within acceptable limits for powerplant gas cleanup purposes, efforts to improve the performance to increase design margin was continued. Another test using the same spiral-shaped container more densely packed with glass wool in all sections was initiated. The inlet filter section was retained without any change in the 60-pore per inch polyurethane filter. Closer controls were imposed upon the cleanliness and packing techniques for the glass wool section. In addition the glass wool was packed more densely to minimize chances of having small bypass flow paths. The repacked container prior to test is shown in Figure 173.

In order to minimize the number of variables entering the evaluation, all test parameters were maintained as in the previous spiral test. The major parameters were 1) boiler temperature 350°F, 2) gas flow rate one pound per hour, 3) adsorber temperature 100°F, 4) monitor sampling period 100 hours, and 5) test duration 1500 hours. The test was operated on a nearly continuous basis for the scheduled 1500 hours. A carbon dioxide dry ice cold trap was attached to the monitor column discharge for the last 700 hours of the test to act as a final trap for oil and oil vapor. The results of the monitor column analysis determined every 100 hours are plotted in Figure 174. Comparison of this curve with the mixed-material spiral results, Figure 170, shows two significant trends. The first is that the average oil content of the effluent gas was reduced from 4.25 grams per 10,000 hours to 2.3 grams per 10,000 hours. The second trend is that the spread in the analysis band was reduced from about 8 to 1 for the mixed spiral to about 4 to 1 for the all glass wool unit. The amount of oil retained in the adsorber glass wool as a function of flow path length is shown in Figure 175. A study of this curve shows that most of the oil was retained in the polyurethane inlet filter and the first sections of the adsorber. As noted on the curve, the polyurethane filter retained more than 65 percent of the oil for the 1500-hour test.

Figure 173 . Spiral Adsorber with Glass Wool M-49731

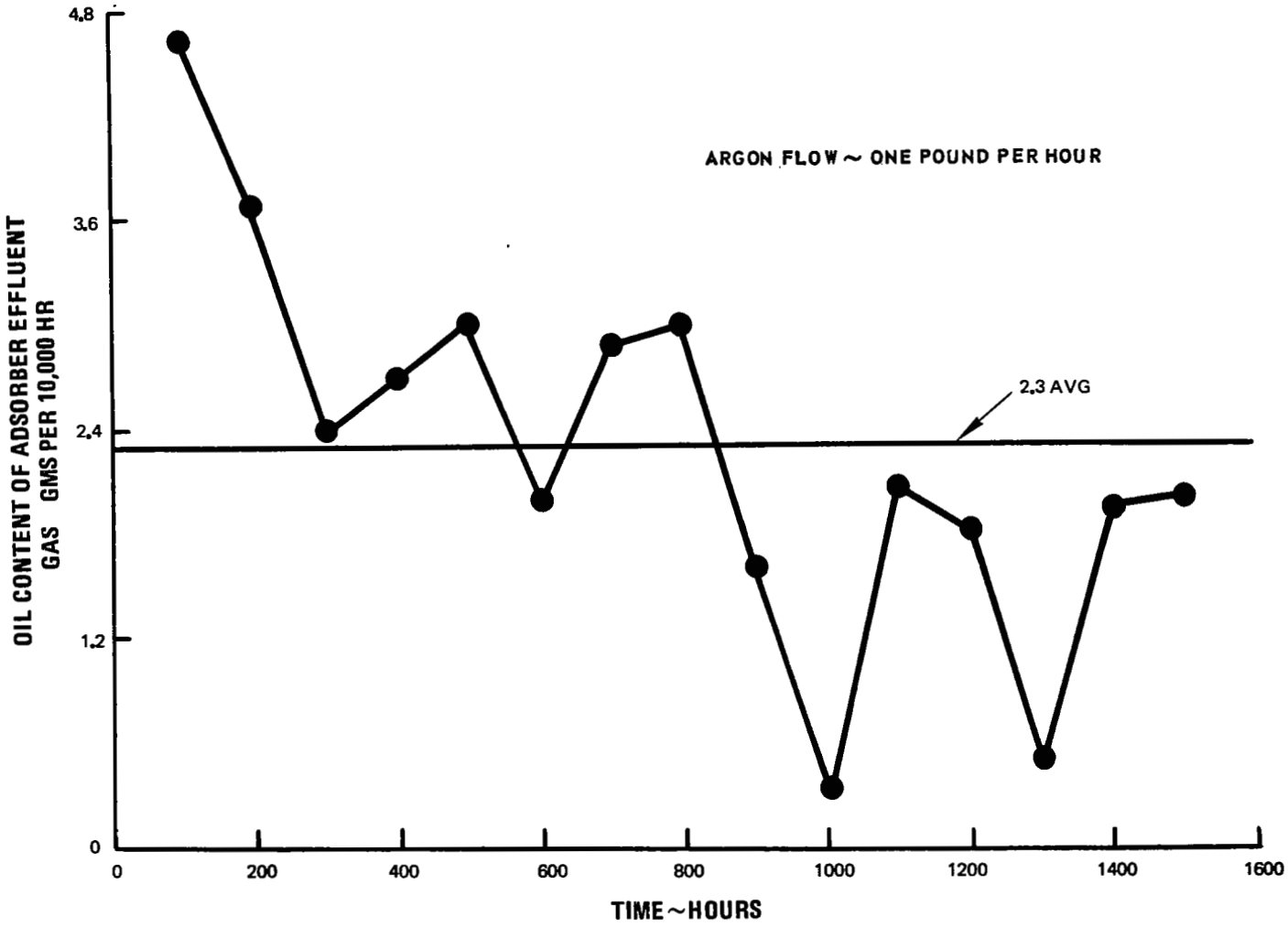

Figure 174 Performance of Spiral Adsorber. All Glass Wool plus Polyurethane Inlet Filter M-49225

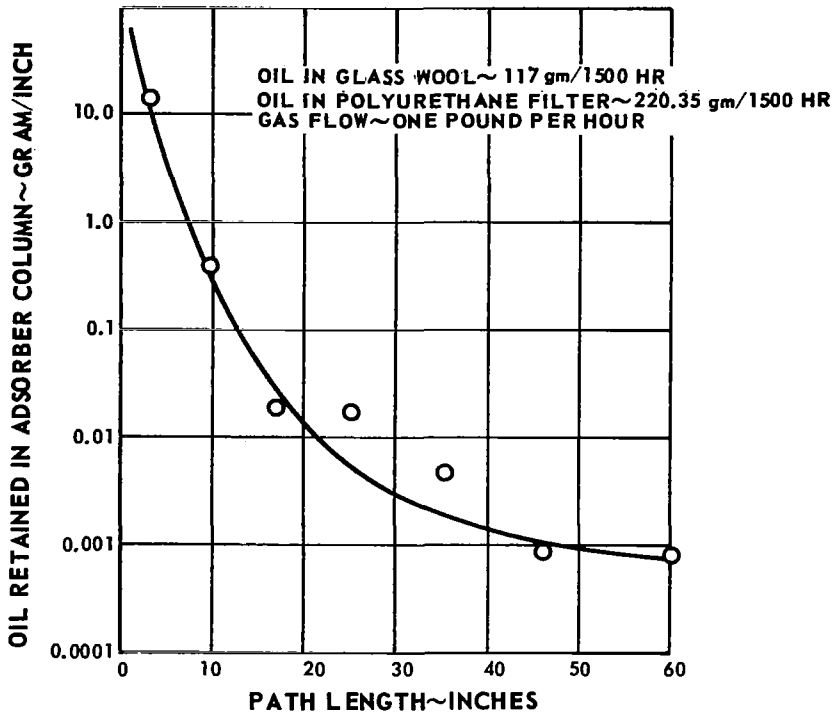

Figure 175 Performance of Spiral Adsorber Filled with Glass Wool. 1500-hr Test

3. Long Cylindrical Adsorber with All Glass Wool

The test results on the spiral adsorber with a dense packing of glass wool did indeed show a marked improvement in performance over the previous mixed spiral test. In view of this improvement it was felt that still further improvement could be attained by using a cylindrical adsorber. A cylinder provides better shape for packing control. Results from the pilot system test adsorber column also indicated that excellent results should be attainable from a cylindrical design.

In order to confirm this and to expand the range of adsorber design data it was decided to run a test incorporating a glass wool-filled cylindrical column with the same radial polyurethane prefilter used in the previous tests. Figure 176 shows the arrangement for this test setup. The prefilter is shown in Figure 177. In order to maintain a common baseline for comparison the test parameters were maintained as in previous tests. A carbon dioxide ice cold trap was attached to the monitor column discharge as in the later part of the previous test. The test

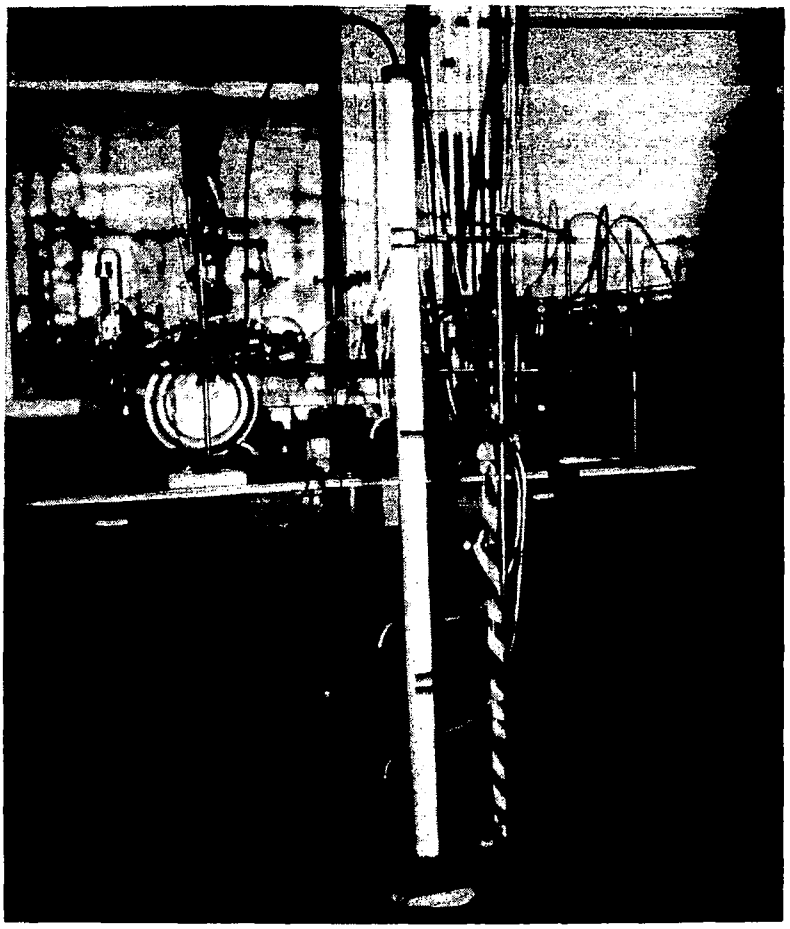

Figure 176 Cylindrical Adsorber with Glass Wool M-49733

was operated for 1000 hours. Figure 178 depicts the column performance with respect to test time. The monitor column contents, the cold-trapped oil and the sum of both are plotted. The amount of oil extracted from the monitor columns was reduced from 2.3 gms per 10,000 hours (all glass wool spiral) to 0.029 gram per 10,000 hours. Also the spread in data points was reduced from 4 to 1 in the previous test to about 2 to 1. The amount of oil retained in the adsorber column glass wool as a function of column length is shown in

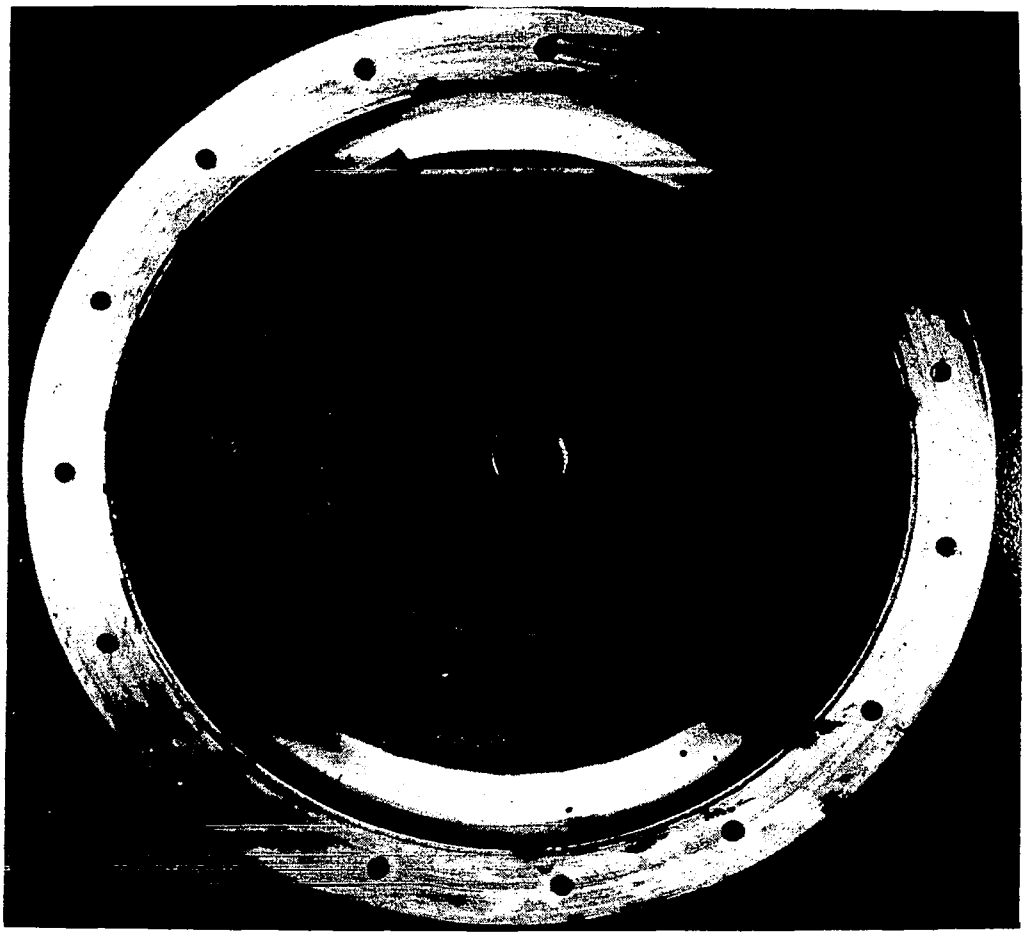

Figure 177 Adsorber Prefilter M-49732

Figure 179 and 180. In Figure 179 the overall column length is shown and in Figure 180 only the first four inches from the inlet are plotted. The significant point is that for a test of this duration (1000 hours) most of the oil was retained in the first 4 inches of the 60-inch length of glass wool. The prefilter still retained a significant fraction of the total oil adsorbed, 74 percent. Examination of the oil vapor pressure curve revealed that the amount of oil held in the cold trap was approximately the amount of vapor-phase oil that would be transported through the 100°F system in 1000 hours for the gas flow rate used. Hence the adsorber column removed essentially 100 percent of the liquid-phase oil.

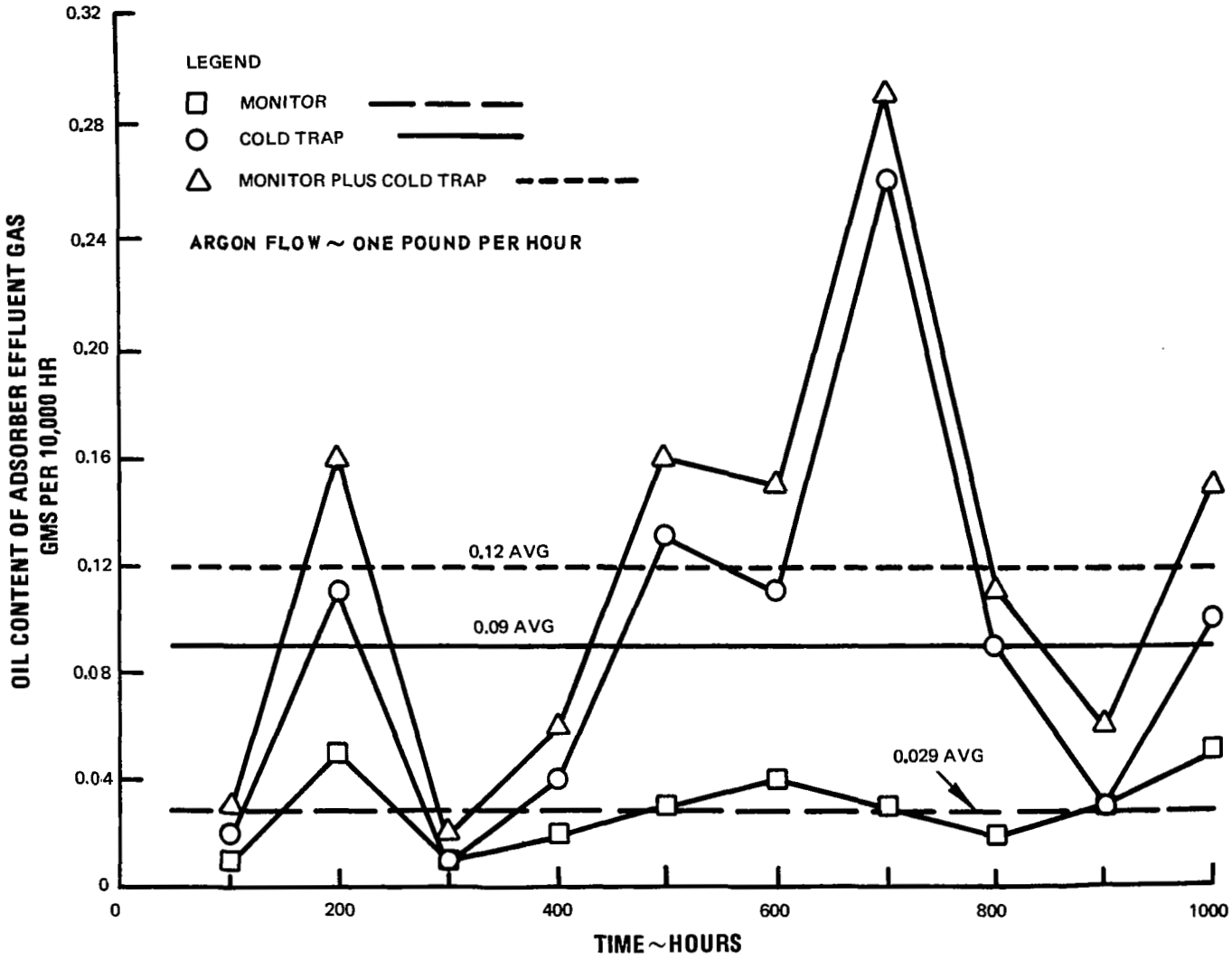

Figure 178 Performance of Long Cylindrical Adsorber plus Radial Inflow Prefilter

M-49224

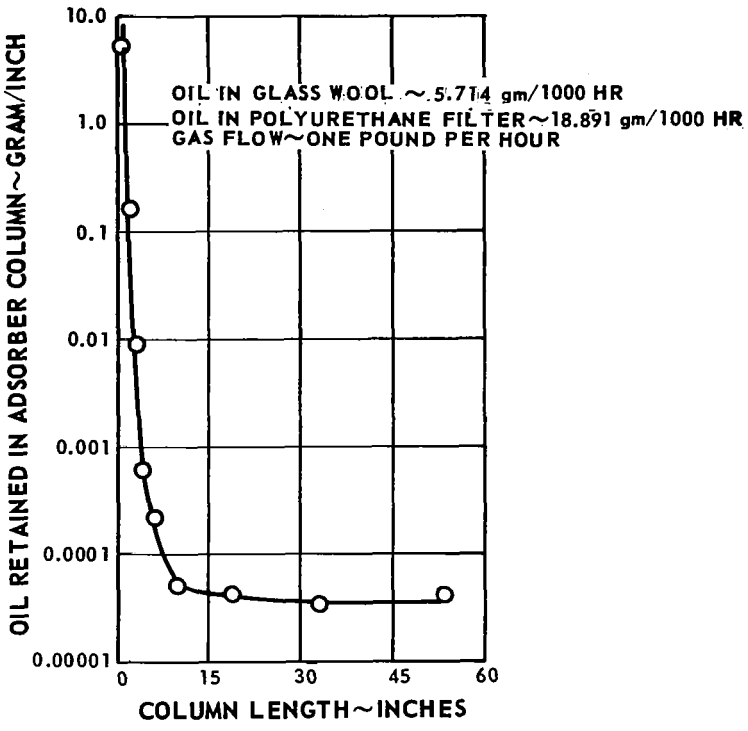

Figure 179 Performance of Cylindrical Adsorber Filled with Glass Wool. 1000-hr Test

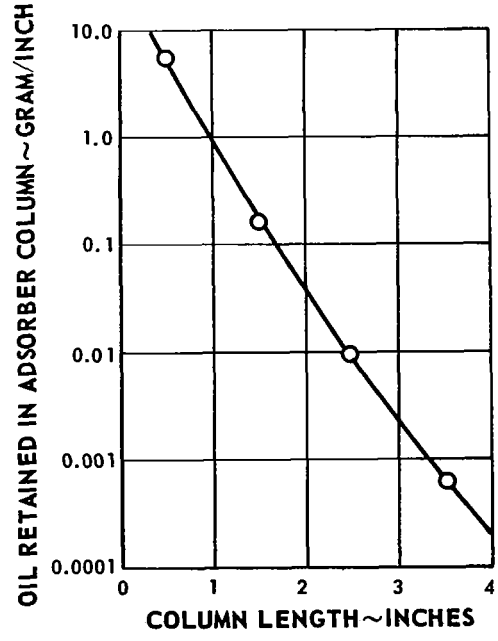

Figure 180 Performance of Inlet Section of Cylindrical Adsorber Filled with Glass Wool. 1000-hr Test

4. Adsorber Endurance Test Summary

A summary comparing the performance of the spiral adsorber with mixed materials, the spiral adsorber with glass wool and the long cylindrical adsorber with glass wool as well as the pilot system adsorber is given below in Table 14. The pilot system adsorber was a long cylinder filled with glass wool and molecular sieve pellets, see Section IX.

TABLE 14

Adsorber Performance Comparison
(Gas Flow - One Pound Per Hour)

	Pilot System	Mixed Spiral	Glass Spiral	Glass Cylinder
Test Hours	2500	1000	1500	1000
Oil Extracted From Adsorber Assembly, grams (1)	59.740	52.966	337.366	24.605
Oil Extracted From Monitor Columns, grams (2)	0.1317	0.4249	0.3498	0.0029
Efficiency $\frac{(1)}{(1)+(2)}$ percent	99.780	99.204	99.896	99.988
Effectiveness Ratio $\frac{(1)+(2)}{(2)}$	455	126	966	8486
Oil Collected in Adsorber, gm/hr	0.02389	0.05297	0.2249	0.02461
Oil Leaving Adsorber, gm/yr	0.526	4.249	2.33	0.029
Monitor Column Oil/Cold Trap Oil	–	–	147/4	29/90

The effectiveness ratio is considered the best measure of performance for comparison purposes. As shown in the table, the effectiveness ratio is the sum of the oil extracted from the adsorber column and monitor column divided by the amount of oil extracted from the monitor column. The higher the effectiveness ratio the better the performance. Using this criterion, the long glass cylinder with effectiveness ratio of 8486 performed much better than the nearest competitor, the spiral adsorber filled with glass wool whose effectiveness ratio was 966.

The last line of the table shows the ratio of monitor column oil to cold trap oil for the period the cold trap was used. The oil collected in the cold trap consisted of oil which had passed through the adsorber and monitor columns as well as condensed oil vapor. Since the adsorber and monitor columns were operating at 100°F and the cold trap at carbon dioxide ice temperature, an appreciable temperature difference existed for condensation. Adding the oil collected in the cold trap to that collected in the monitor column in the long cylindrical adsorber would reduce the effectiveness ratio by a factor of four. However, since the cold trap was not used on all the adsorber tests, a valid comparison incorporating cold-trap data is not possible. The results obtained indicate the importance of using an oil of low vapor pressure, and of maintaining the adsorber column at as low a temperature as practical.

IX. PILOT LUBRICATION SYSTEM

The purpose of the pilot lubrication system test was to demonstrate closed-loop operation of a complete lubrication system for 2500 hours, and to obtain long-time performance data on the test items.

A schematic diagram of the pilot lubrication system is shown in Figure 181. In the lower left, the 50,000 rpm turbine-compressor bearing compartment is represented. The dry-face seal was selected because of the low leakage and power consumption. The vaned scavenge impeller was selected because of superior performance.

The 12,000 rpm turboalternator separator is shown in the lower right section of the schematic. The redesigned scoop pump and the 10 percent density separator matrix were selected for test. The adsorber is shown directly above the separator. Linde 13X pellets and Pyrex glass wool were used as the matrix materials. These materials were selected as a result of many laboratory tests.

Argon was used as the gas in the system, the same as in the reference two-shaft design. The lubricant was PWA-524, a five-ring polyphenyl ether, the fluid used throughout the program.

The system operating point was as follows:

bearing compartment speed	50,000 rpm
pump-separator speed	12,000 rpm
adsorber argon flow	1 lb/hr
turbine-compressor bearing	
oil flow under race	70 lb/hr
oil flow through bearing	10 lb/hr
scavenge gas flow	8 lb/hr
bearing cavity pressure	11 psia
oil temperature into bearing	300°F

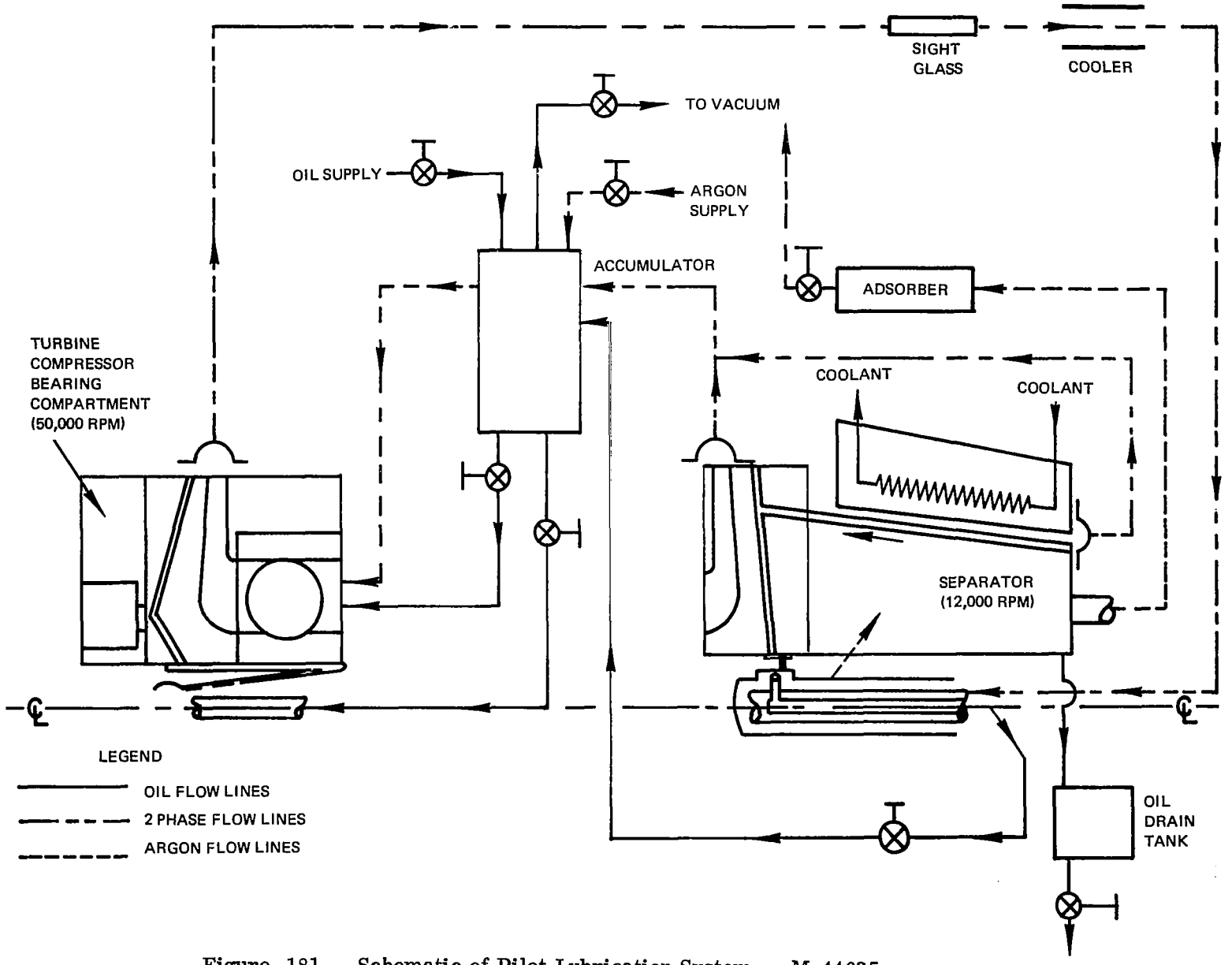

Figure 181 Schematic of Pilot Lubrication System M-44035

The major elements of the system are shown in Figures 182 through 188.

The adsorber column shown in Figure 186 contained glass wool at the inlet and outlet with a section of Linde 13X pellets in the middle. The two small monitor columns shown at the right had the same make-up. The basic oil circulation flow mode is shown in Figure 187. A mixture of gas and oil was circulated by the gas pressure developed in the bearing-compartment impeller. The clean gas-out line leading from the mechanical separator to the adsorber is shown in Figure 188. The glass section was used to aid in visually monitoring the separator operation.

System operation was essentially trouble-free with no detectable change in performance throughout the test. Shutdowns were experienced due to stand equipment failures, power outages and holidays. After accumulating 500 hours of test an inspection was made to ascertain the condition of the test items. The disassembly and cleaning were held to a minimum so that the test could be resumed with as few changes as possible. The results of the inspection are given below along with the inspection results obtained at 2500 hours. Photographs of the test parts at 500 hours are shown in Figures 189 through 202. A similar presentation of the parts after 2500 hours of test is shown in Figures 203 through 216. A comparison of these two series of photographs shows very little difference in the condition of the parts. The 2500-hour views contain more deposits in some cases. In spite of these deposits there was no detectable change in performance. The gas side of the turbine-compressor seal cavity was dry at the end of 2500 hours of running as evidenced by the photographs of Figures 203 and 204. This indicates that the seal did not leak any significant amount of oil and/or that the sweep gas that passed through this cavity was effective in removing the oil. In any event the dry condition of the cavity indicates a very effective seal-sweep gas combination.

Carbon wear measurements for the 2500-hour pilot endurance test turbine-compressor seal were as follows:

Test Period, Hours	Carbon Wear, Inch
0 - 500	0.0007
500 - 2500	0.0032
0 - 2500	0.0039

Projecting the wear rate in the period from 0 to 500 hours to 10,000 hours

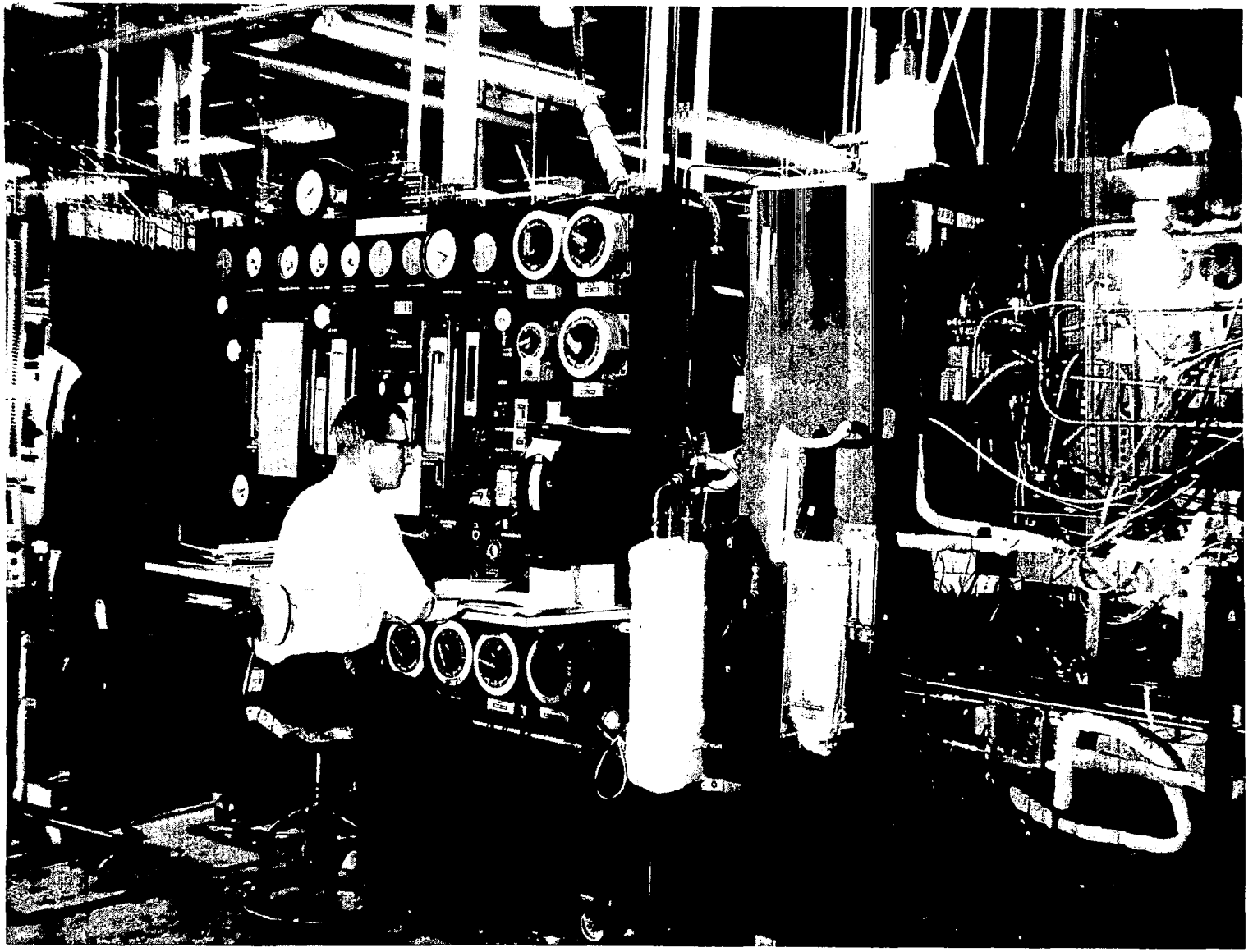

Figure 182 Pilot Lubrication System Separator Control Panel at Left and Bearing Compartment Rig at Right X-25060

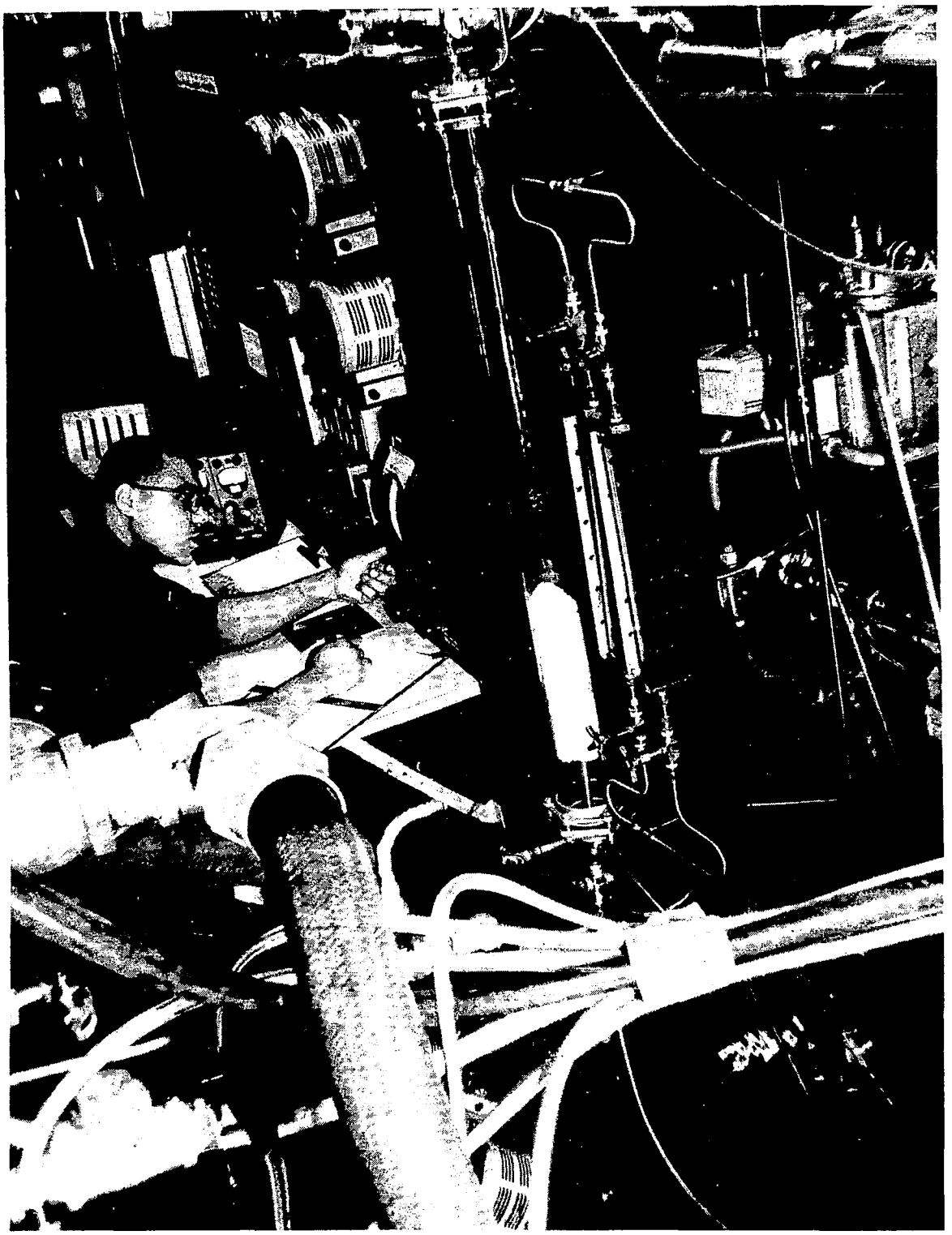

Figure 183 Pilot Lubrication System Control Panel for Bearing Compartment Rig X-25058

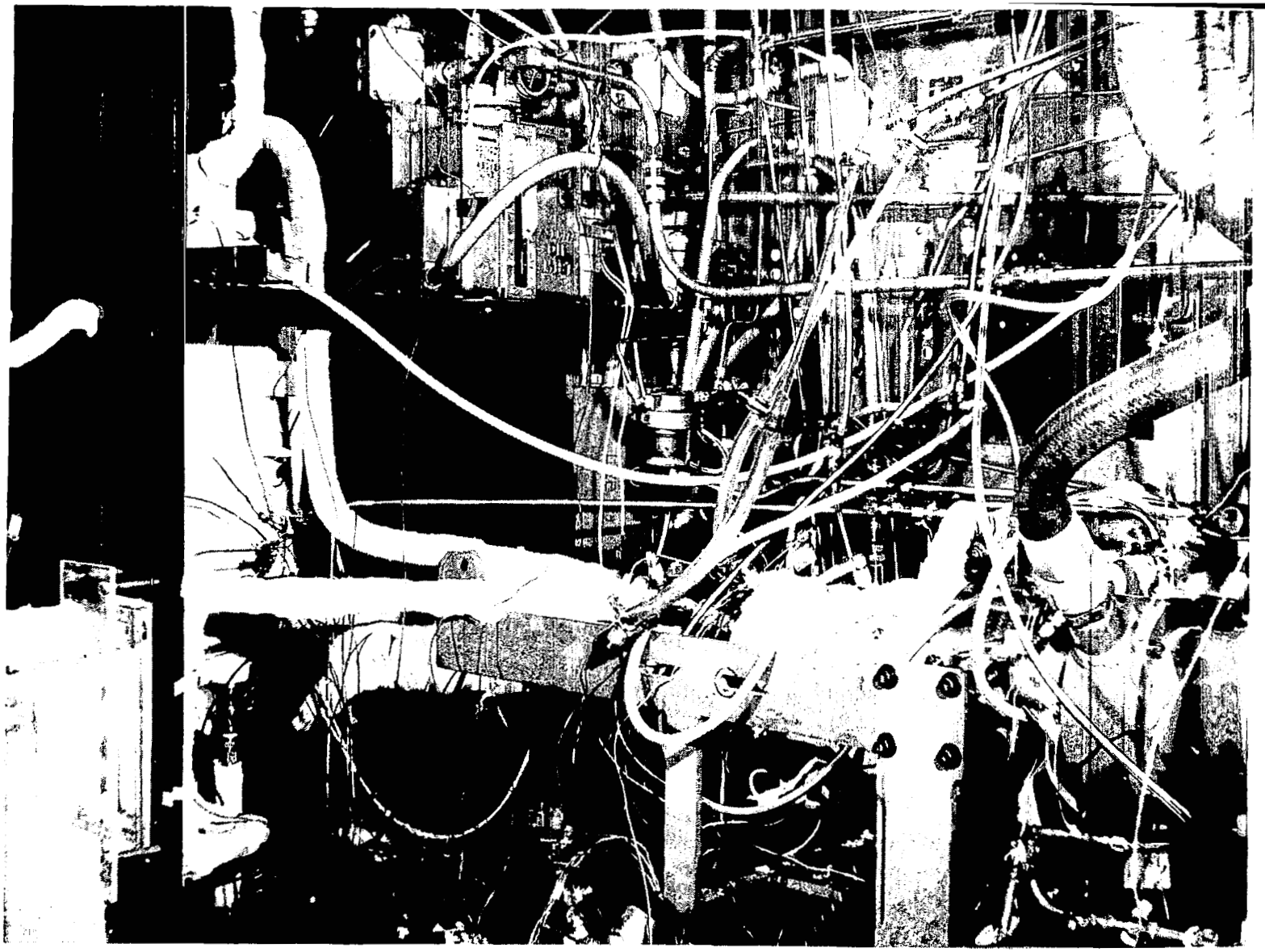

Figure 184 Pilot Lubrication System Bearing Compartment Rig X-25061

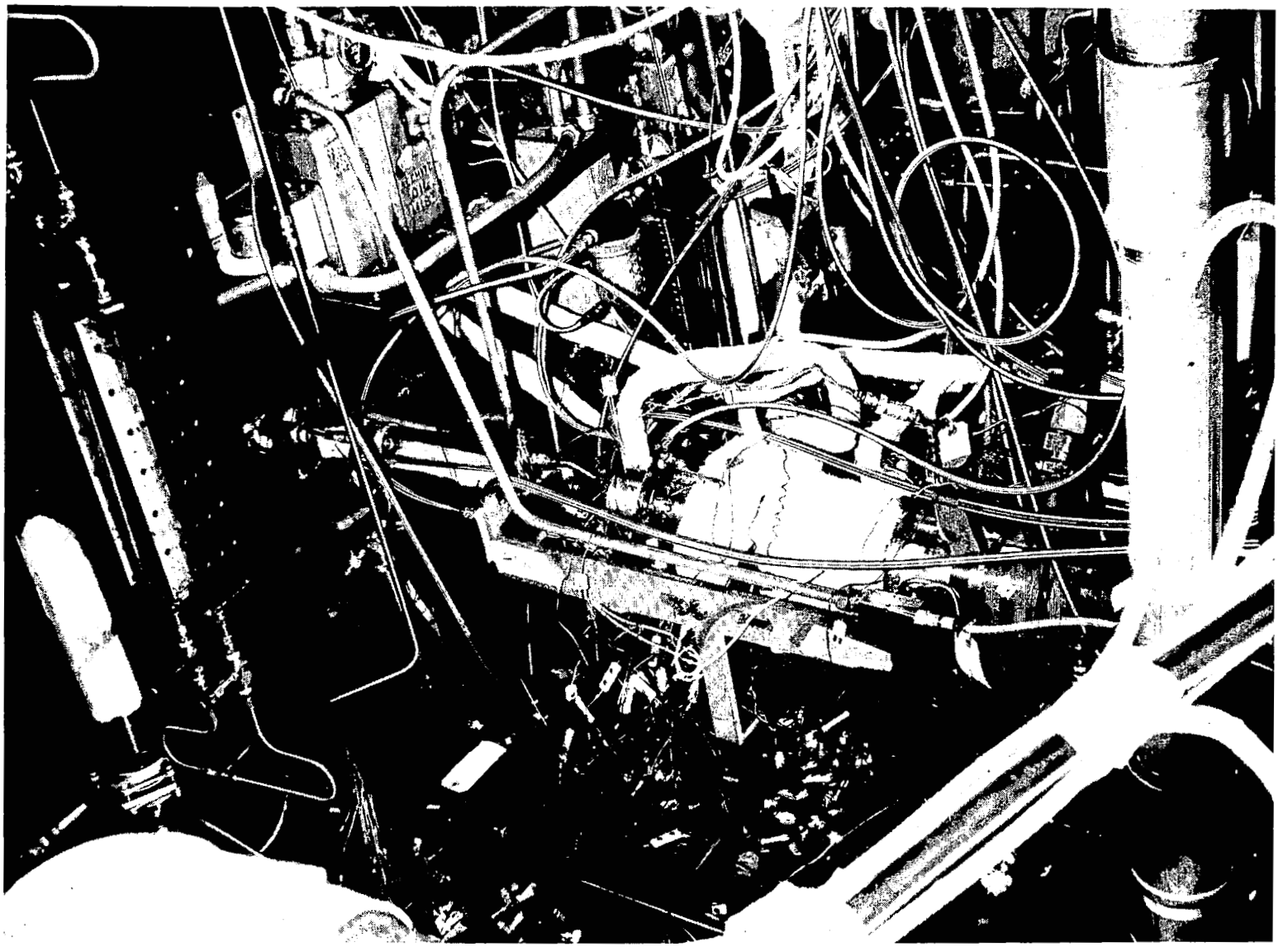

Figure 185 Pilot Lubrication System Separator Rig X-25059

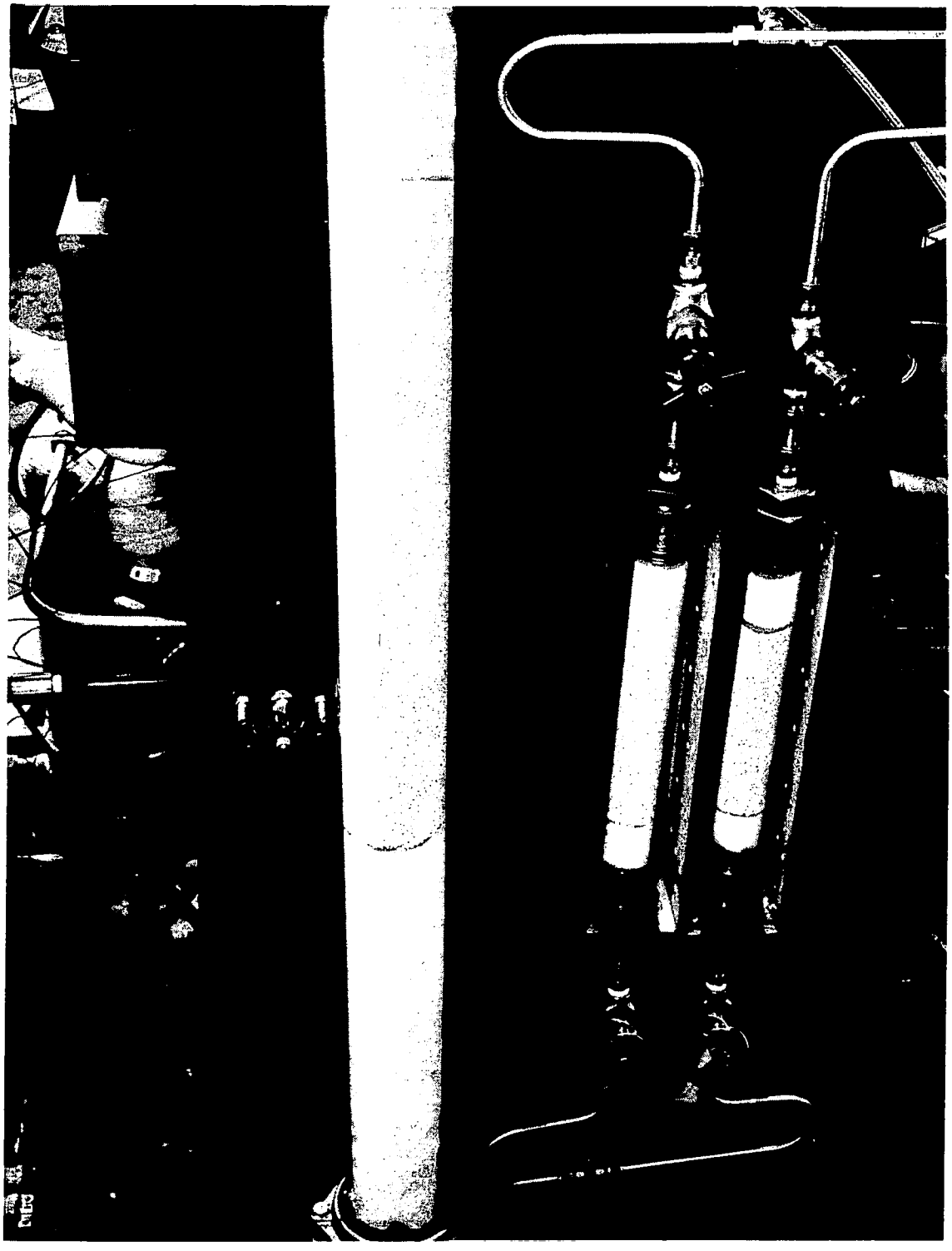

Figure 186 Pilot Lubrication System Adsorber and Monitor Columns X-25148

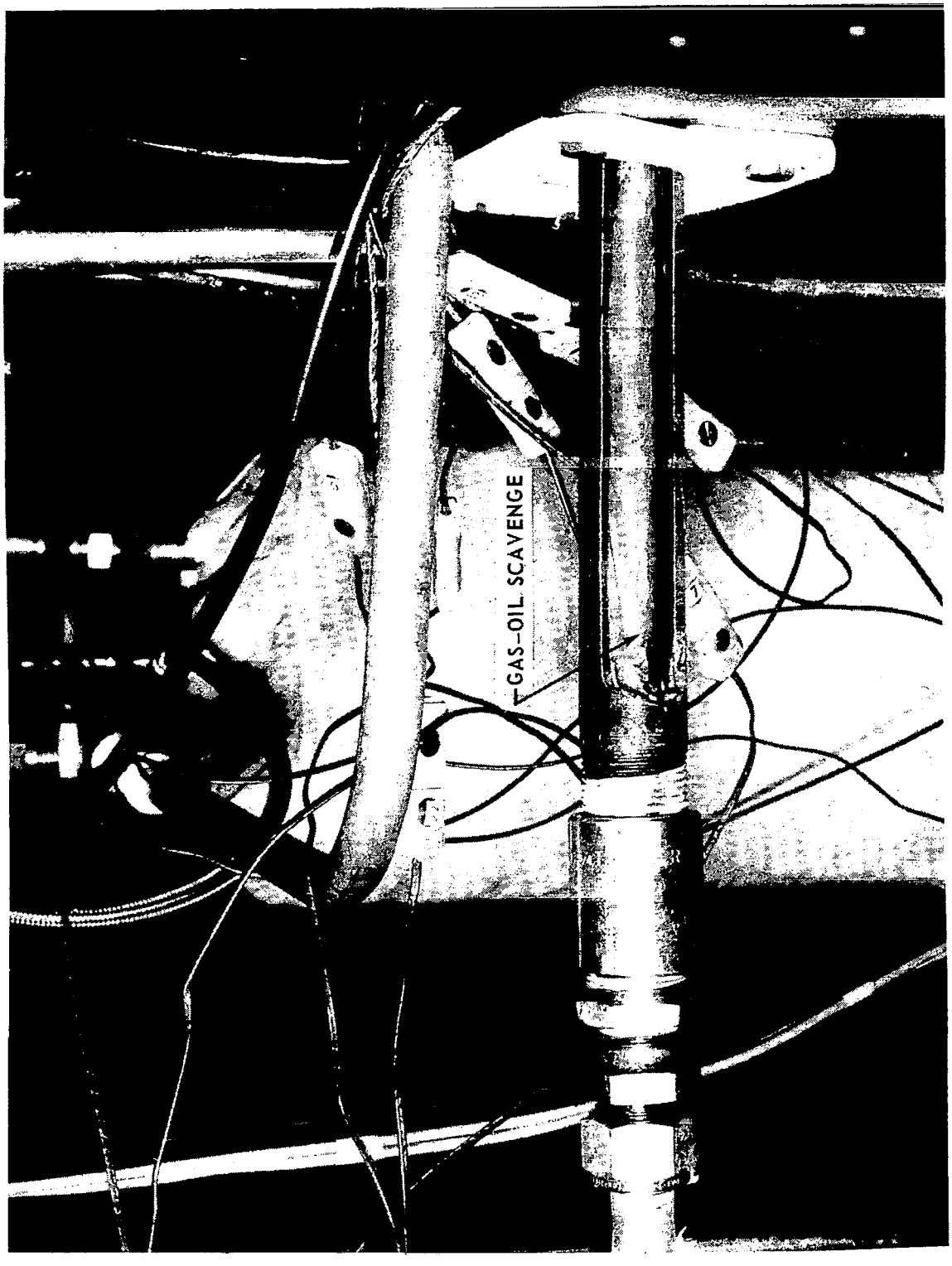

Figure 187 Pilot Lubrication System. Two-Phase Flow in Bearing-Compartment Scavenge Line Sight Glass X-25147

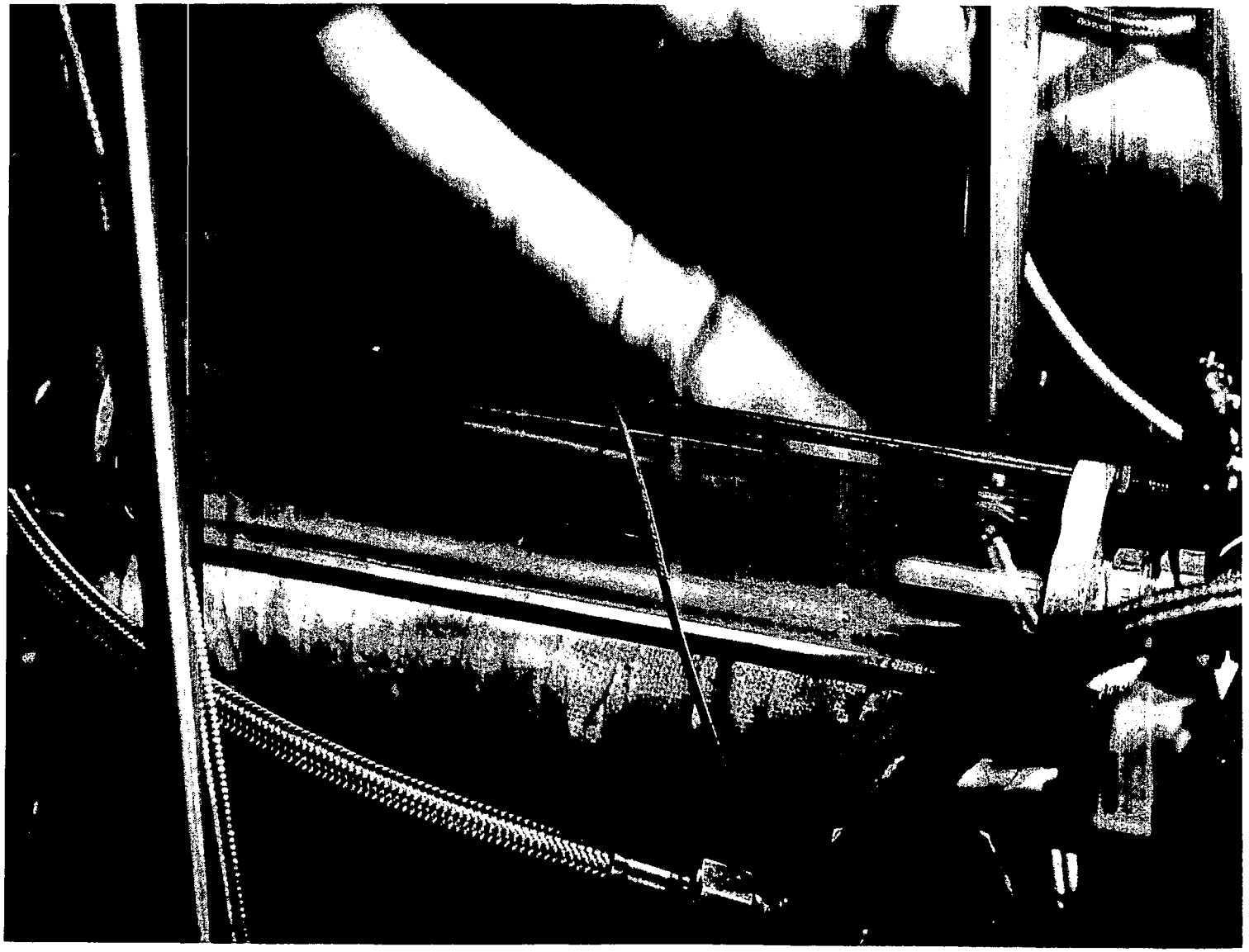

Figure 188 Pilot Lubrication System. Clean Argon from Separator to Adsorber Viewed through Sight Glass X-25149

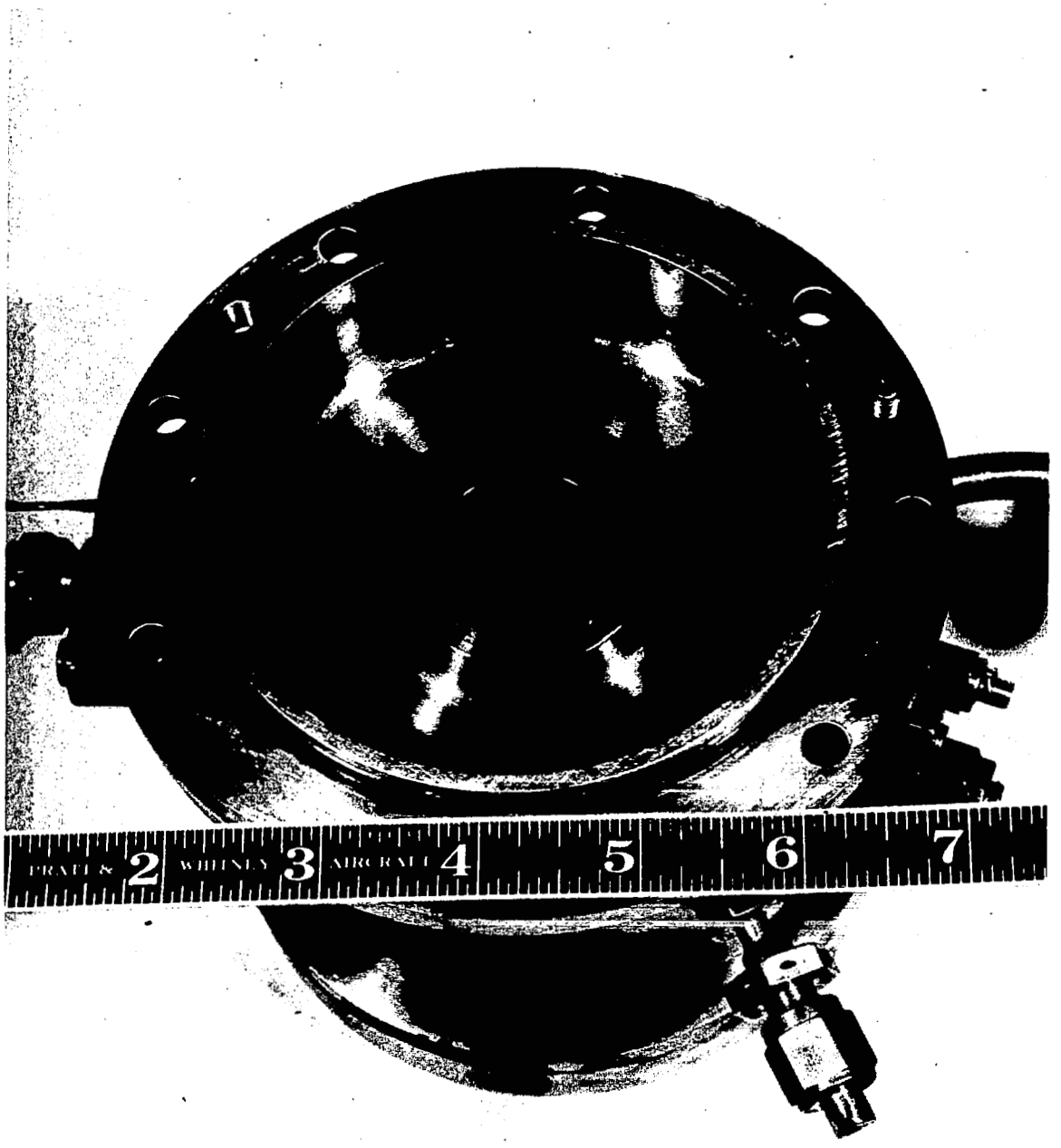

Figure 189 Powerplant Side of Turbine-Compressor Bearing Compartment after 500 Hours of Test CN-8883

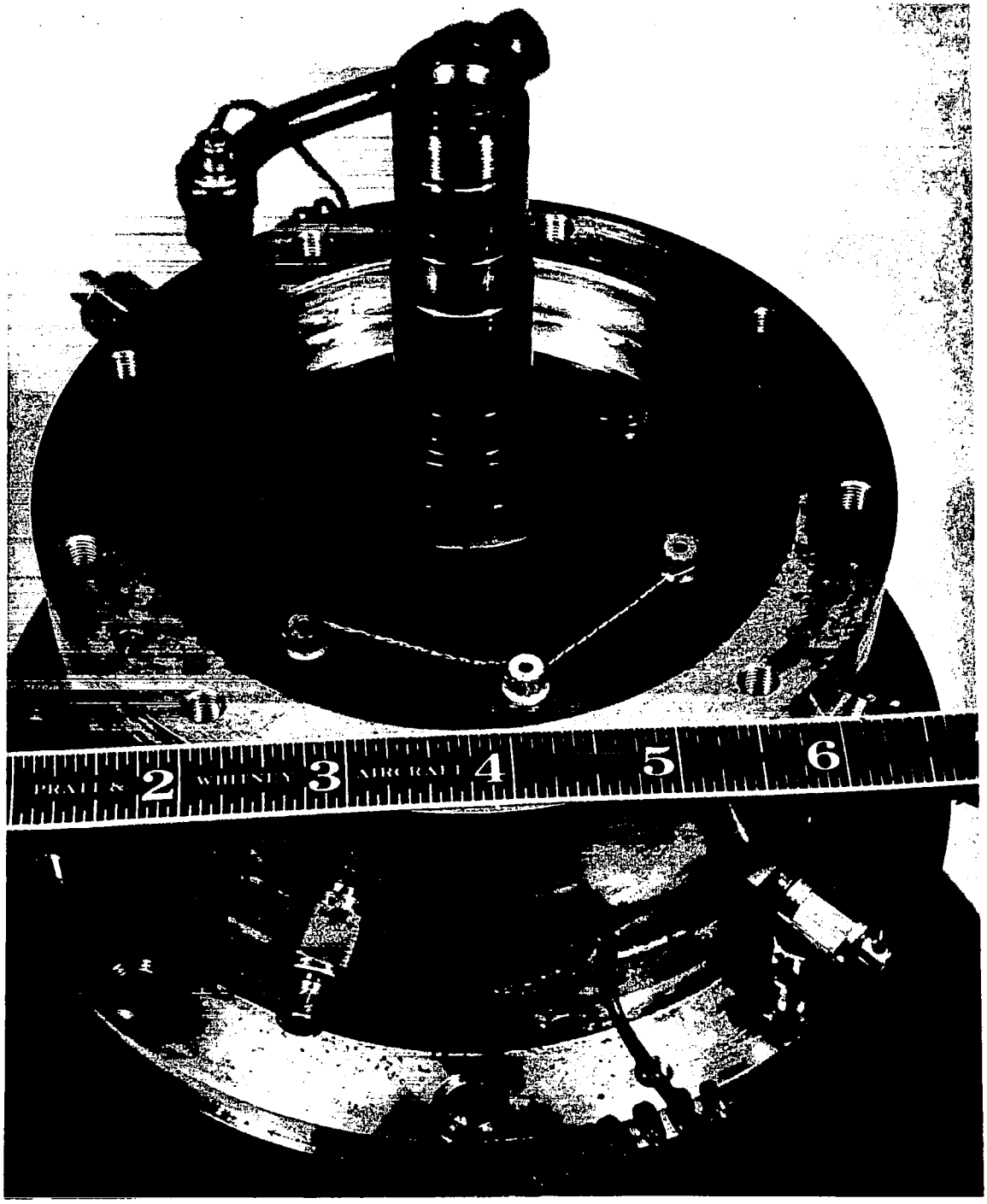

Figure 190 Powerplant Side of Turbine-Compressor Bearing Compartment (Drive End) after 500 Hours of Test CN-8893

Figure 191 Turbine-Compressor Seal and Sealplate after 500 Hours of Test CN-8890

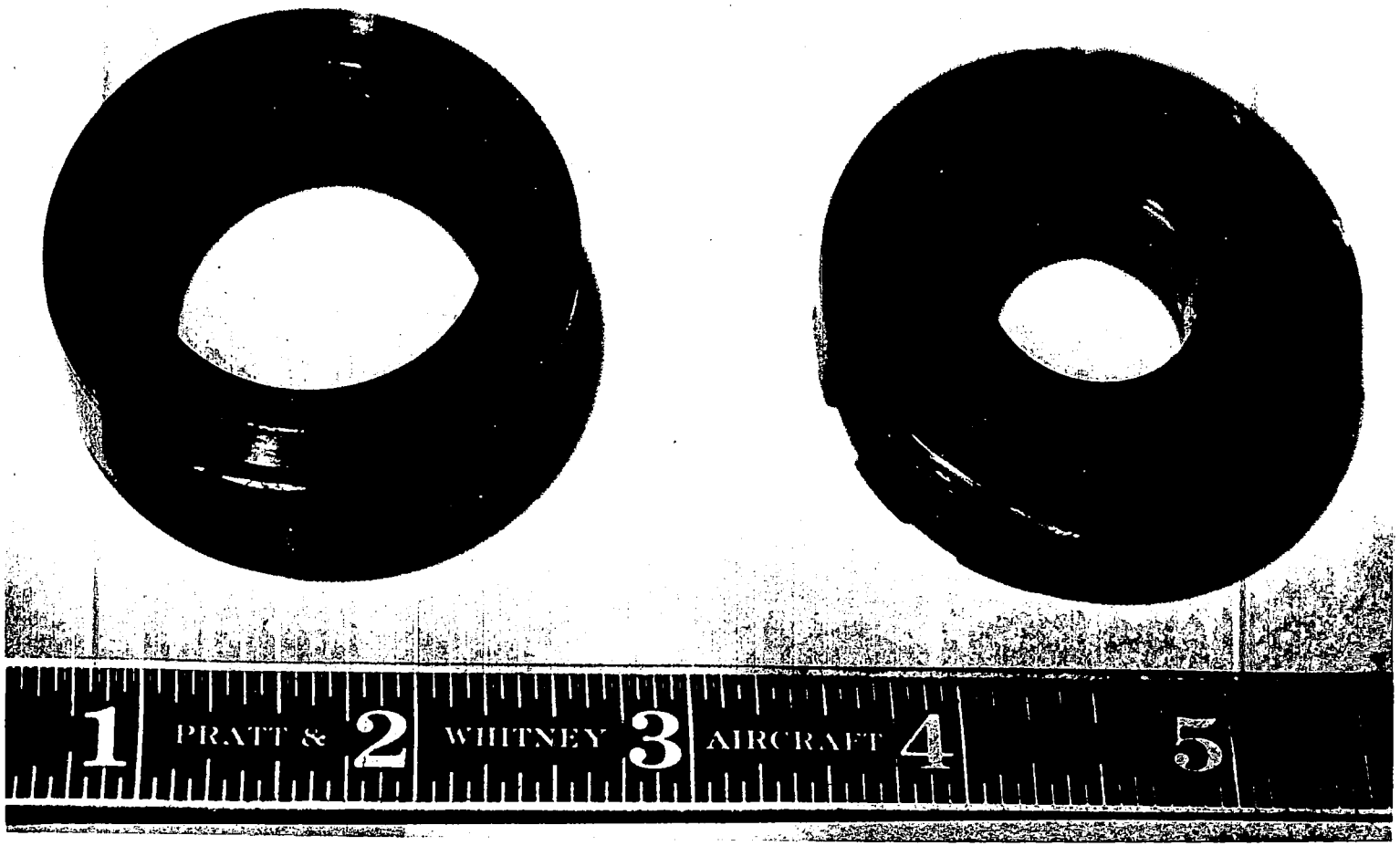

Figure 192 Turbine-Compressor Seal and Sealplate after 500 Hours of Test and Cleaning CN-8895

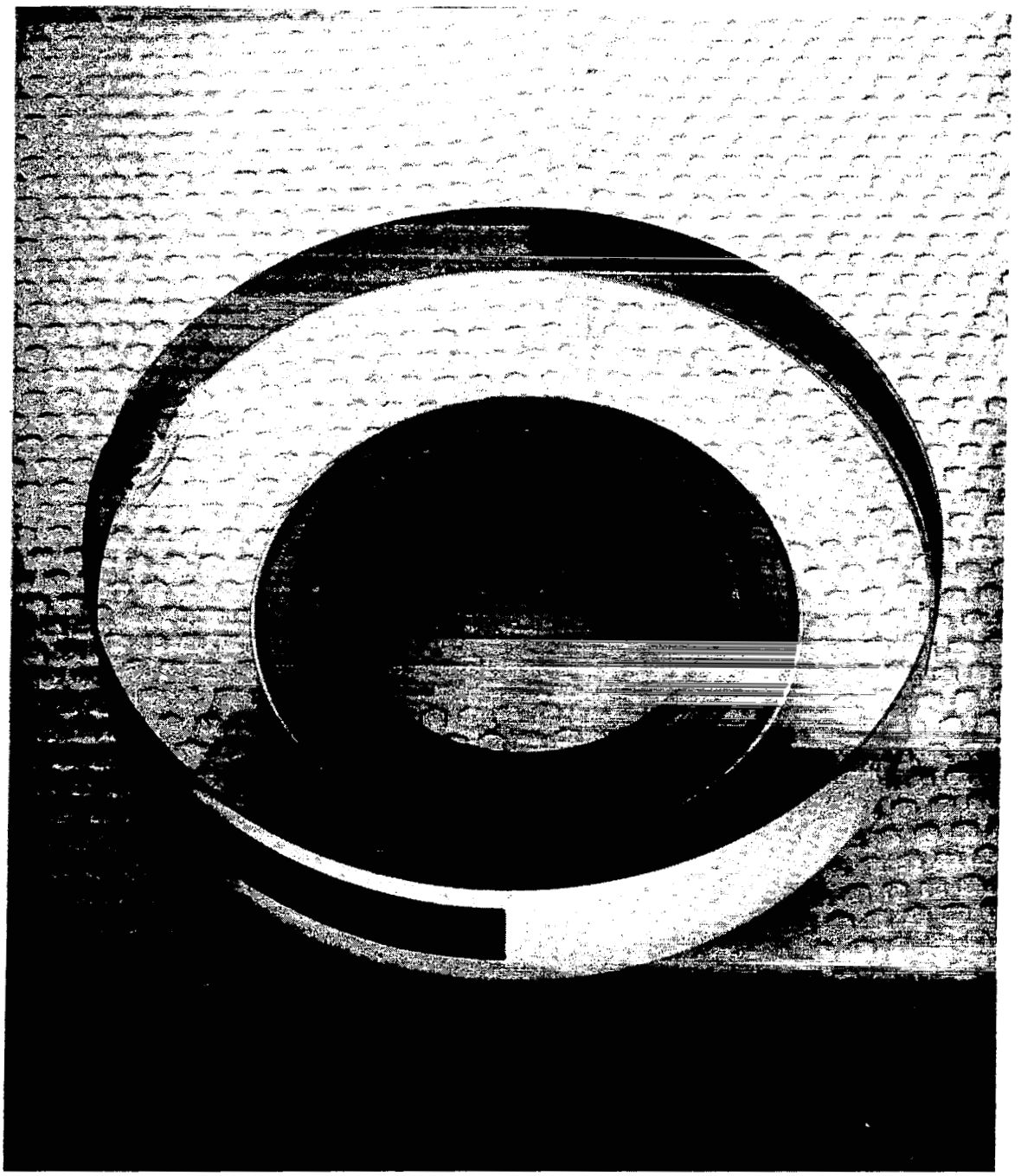

Figure 193 Turbine-Compressor Seal under Optical Flat after 500 Hours of Test
X-25372

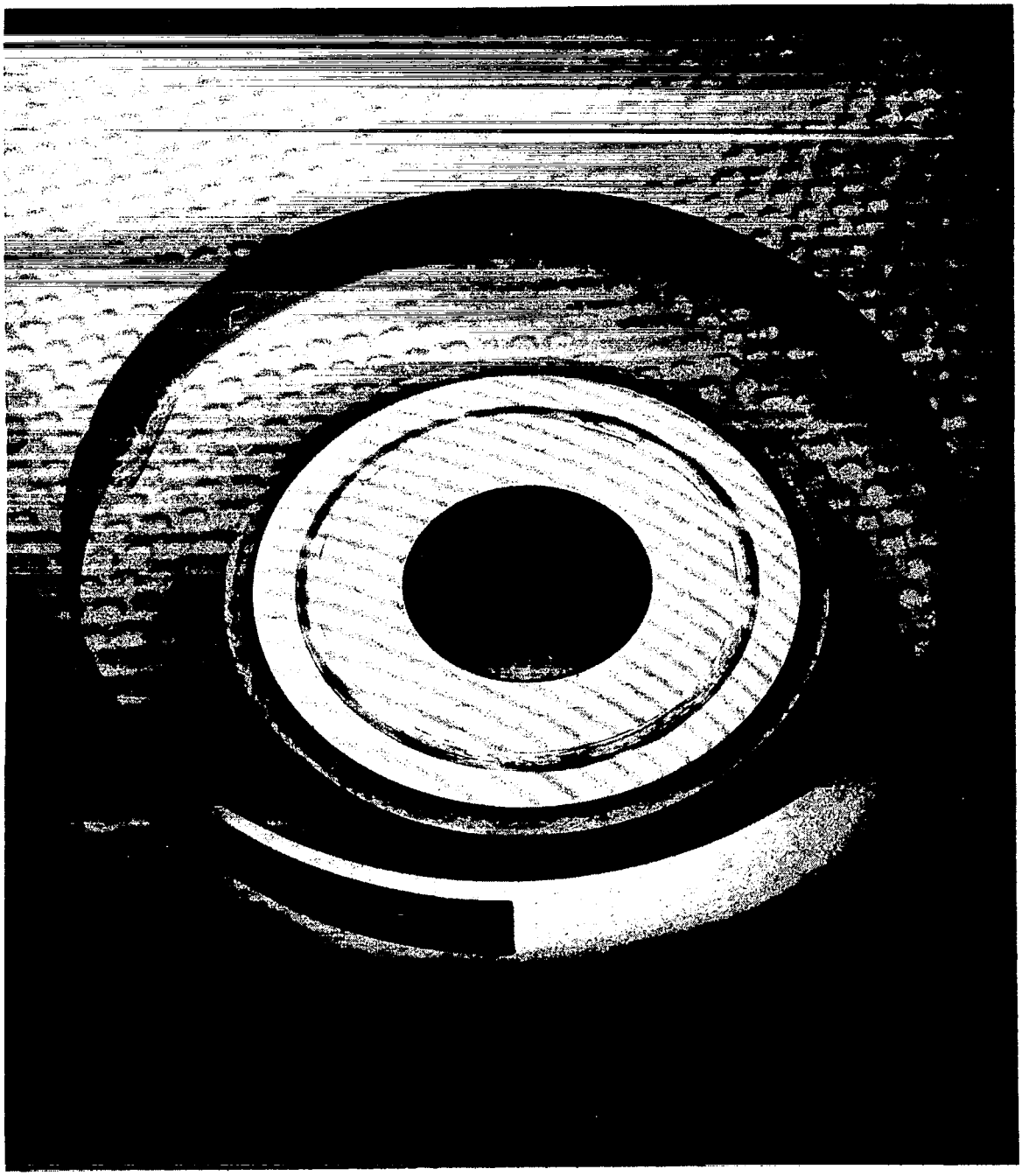

Figure 194 Turbine-Compressor Sealplate under Optical Flat after 500 Hours of Test X-25373

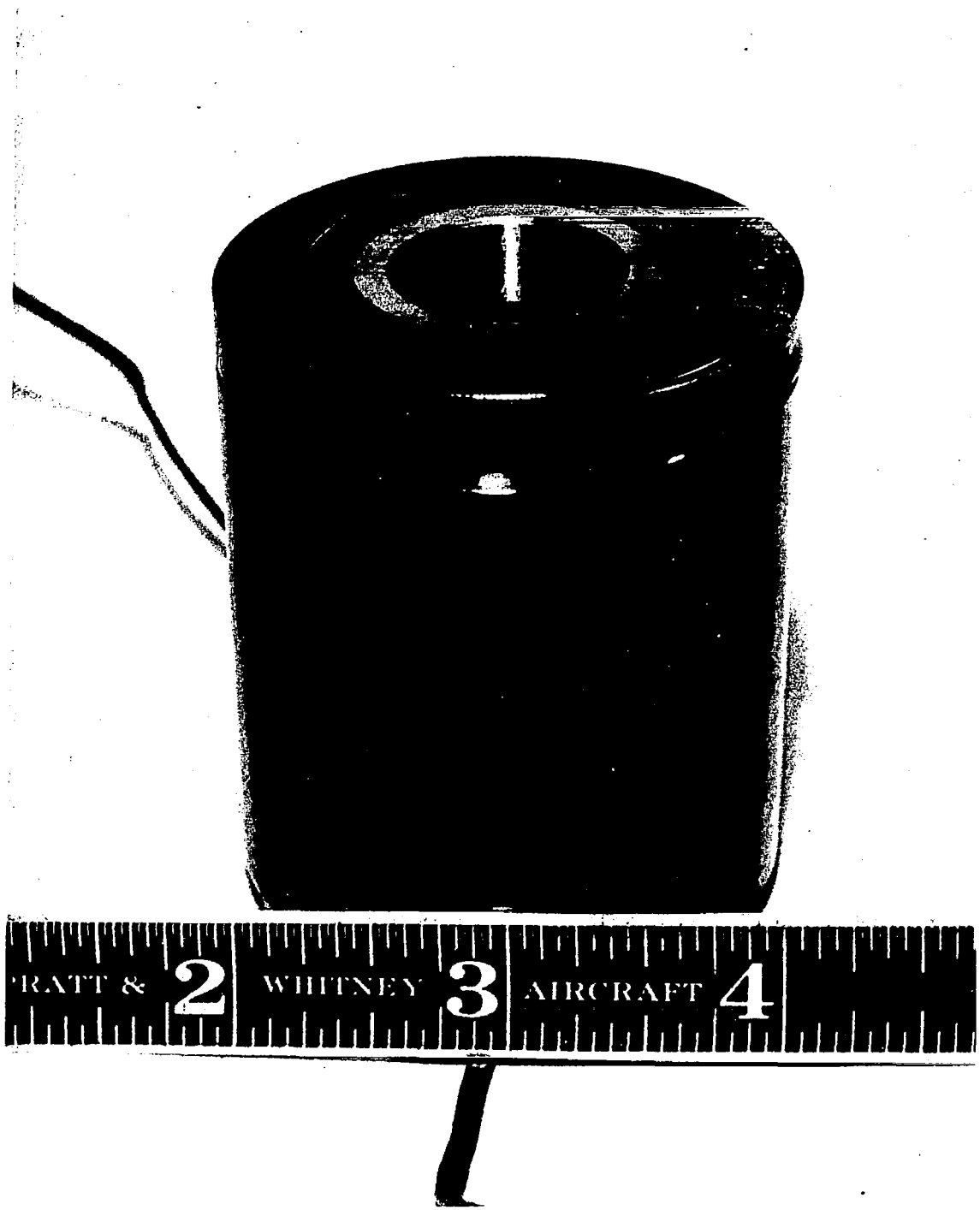

Figure 195 Sleeve Mount and Sealplate of Turbine-Compressor after 500 Hours of Test CN-8889

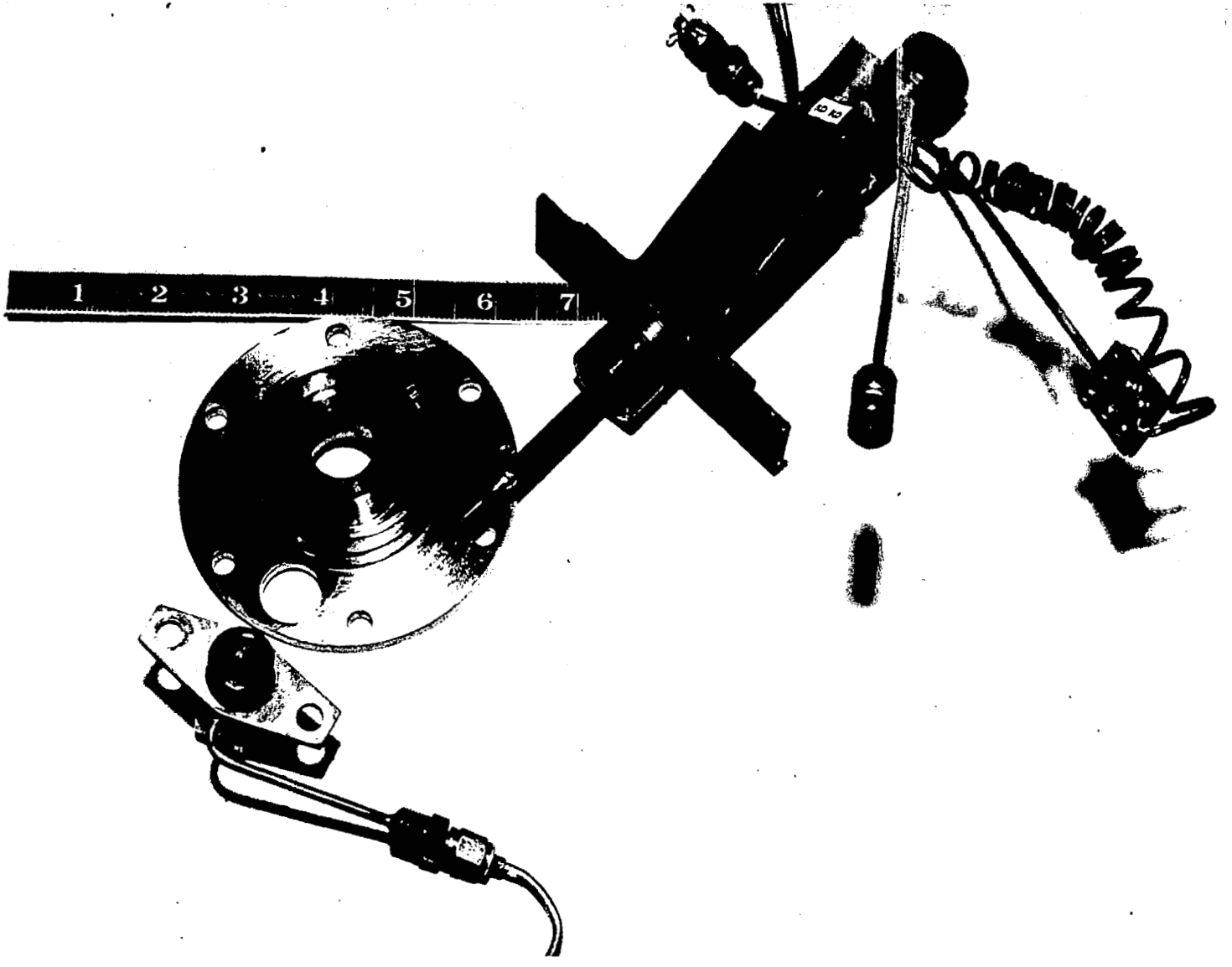

Figure 196 Oil and Gas Inlets for Turbine-Compressor Bearing after 500 Hours of Test CN-8894

Figure 197 Turbine-Compressor Bearing Cavity after 500 Hours of Test
CN-8887

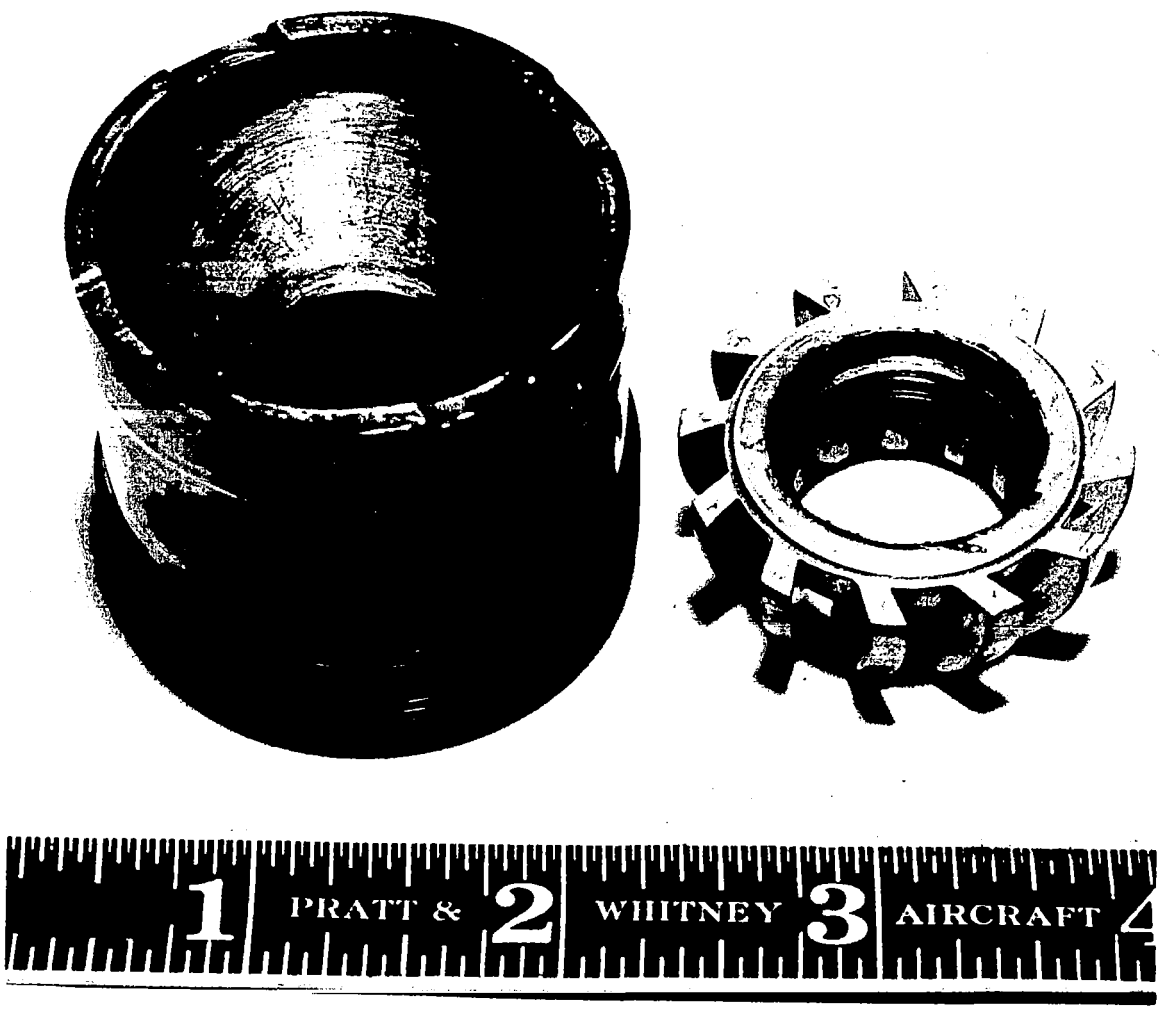

Figure 198 Locking Nut and Inlet Housing of Turbine-Compressor after 500 Hours of Test

CN-8884

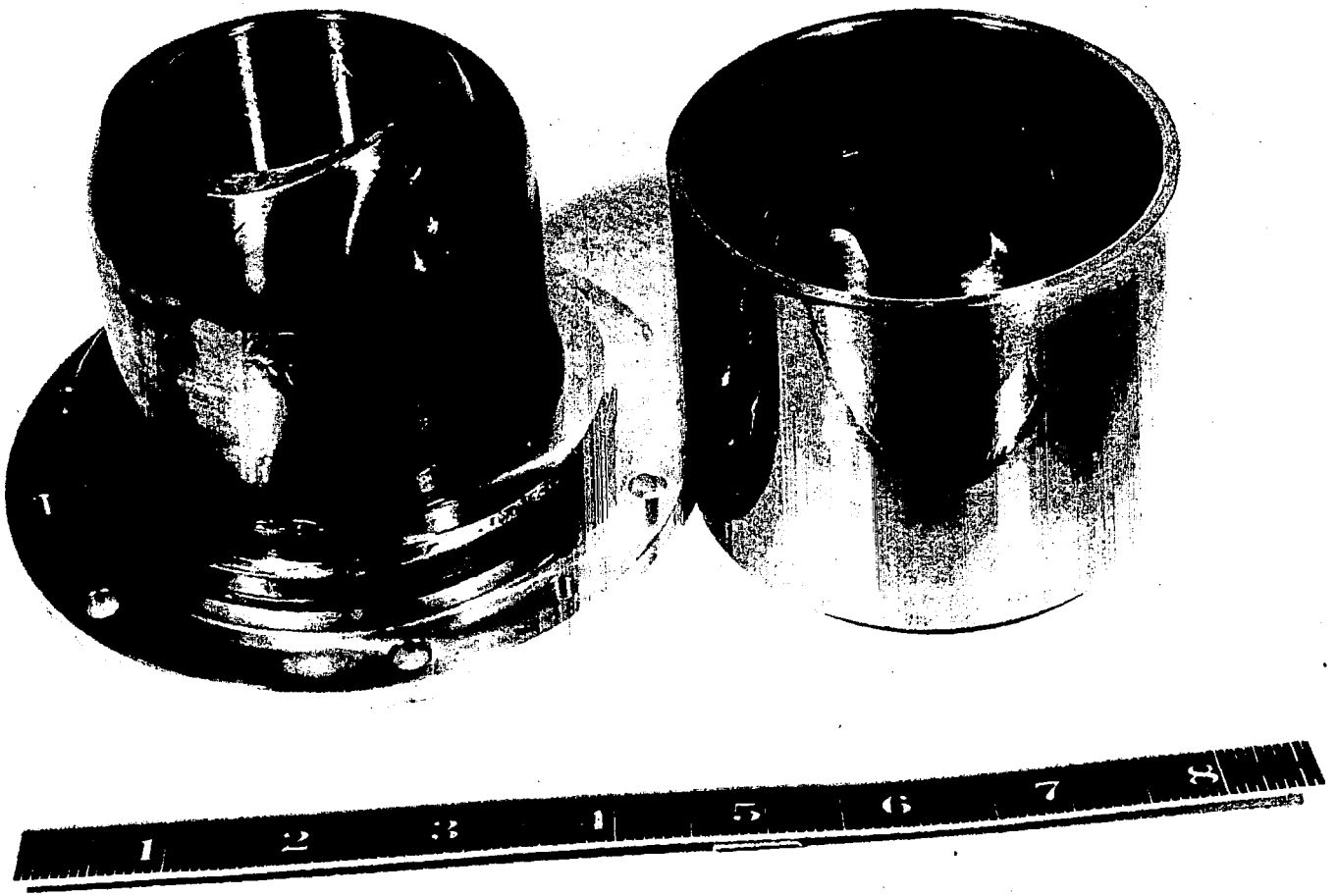

Housing of Turbine-Compressor after 500 Hours of Test CN-8885

Figure 200 Middle and Outlet Sections of Separator Mesh after 500 Hours of Test
CN-8902

Figure 201 Inlet Section of Separator Mesh after 500 Hours of Test CN-8897

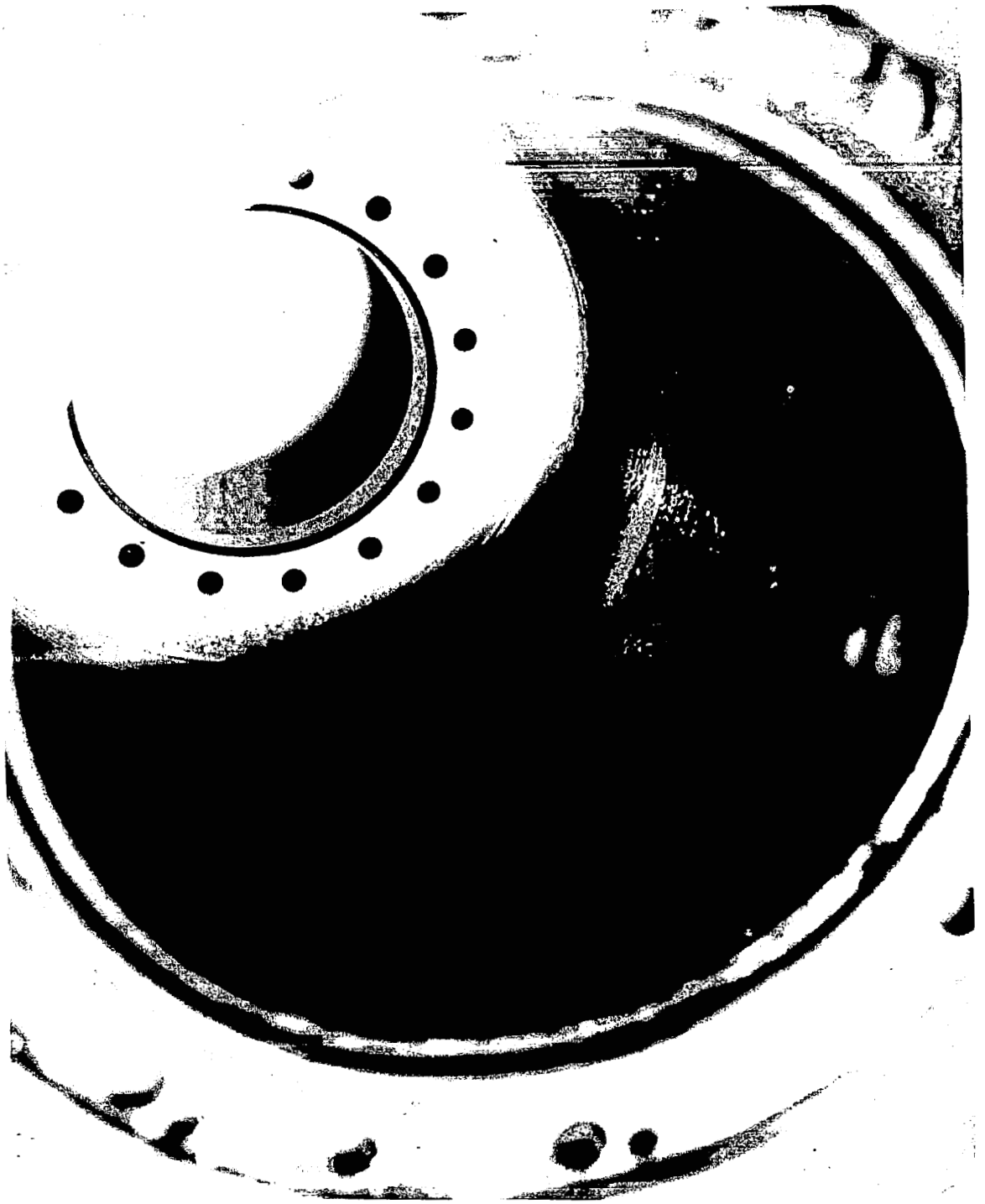

Figure 202 Separator Housing after 500 Hours of Test CN-8904

Figure 203 Powerplant Side of Seal Cavity after 2500 Hours of Test CN-10418

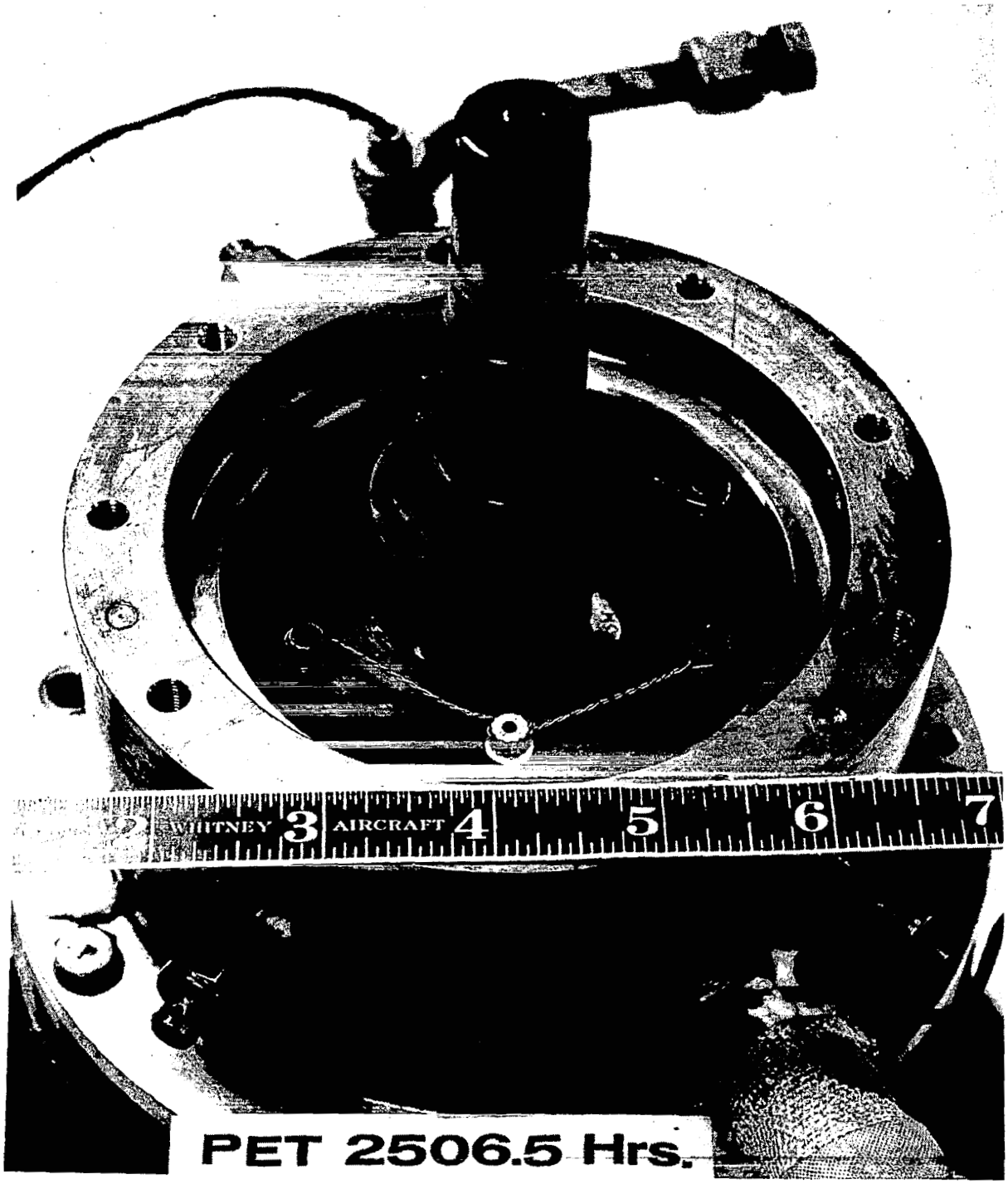

Figure 204 Powerplant Side of Seal Cavity after 2500 Hours of Test CN-10417

Figure 205 Sealplate before Cleaning and after 2500 Hours of Test CN-10429

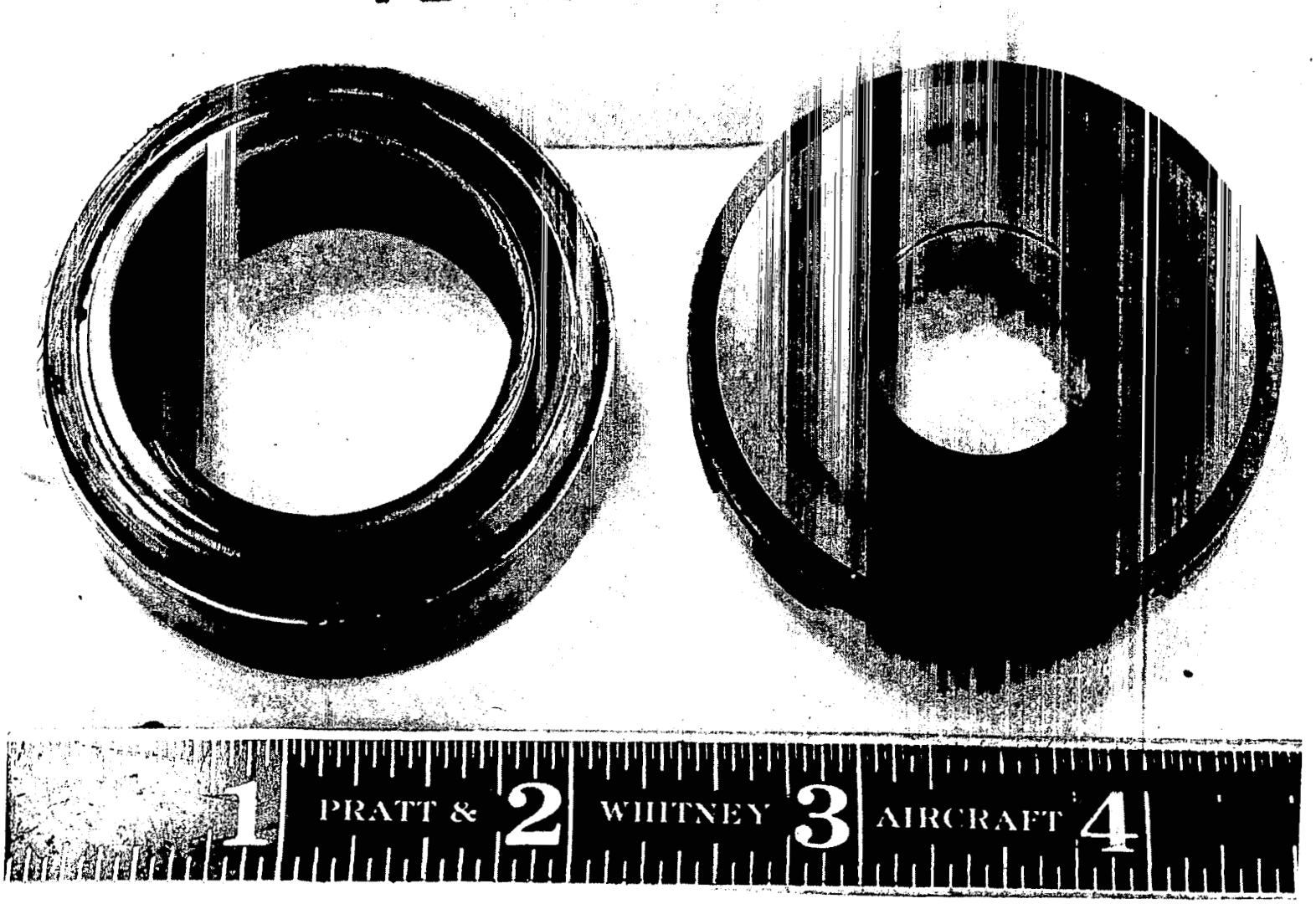

Figure 206 Sealplate after Cleaning and after 2500 Hours of Test CN-10437

Figure 207 Optical Flat on Seal after 2500 Hours of Test X-26488

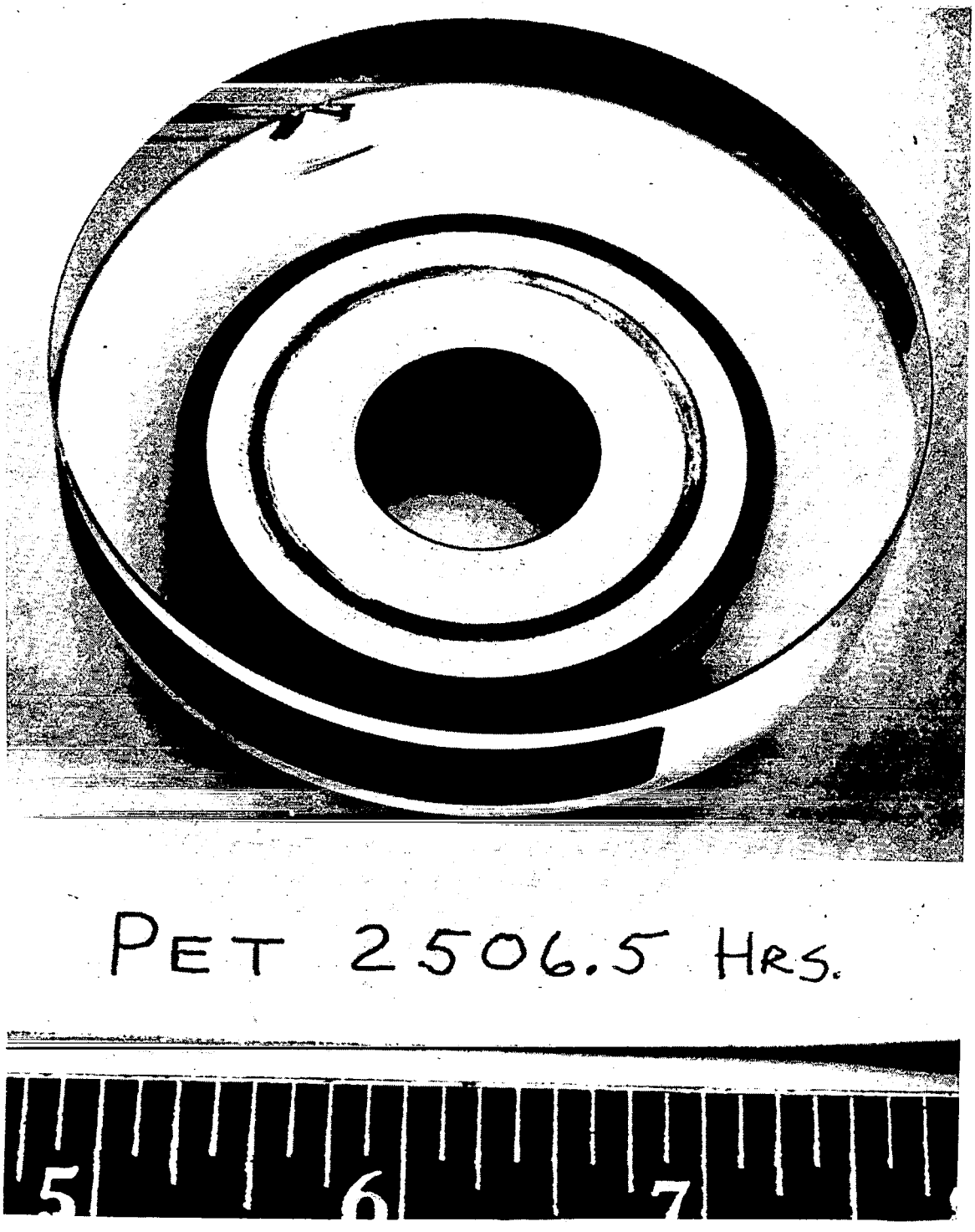

Figure 208 Optical Flat on Sealplate after 2500 Hours of Test X-26487

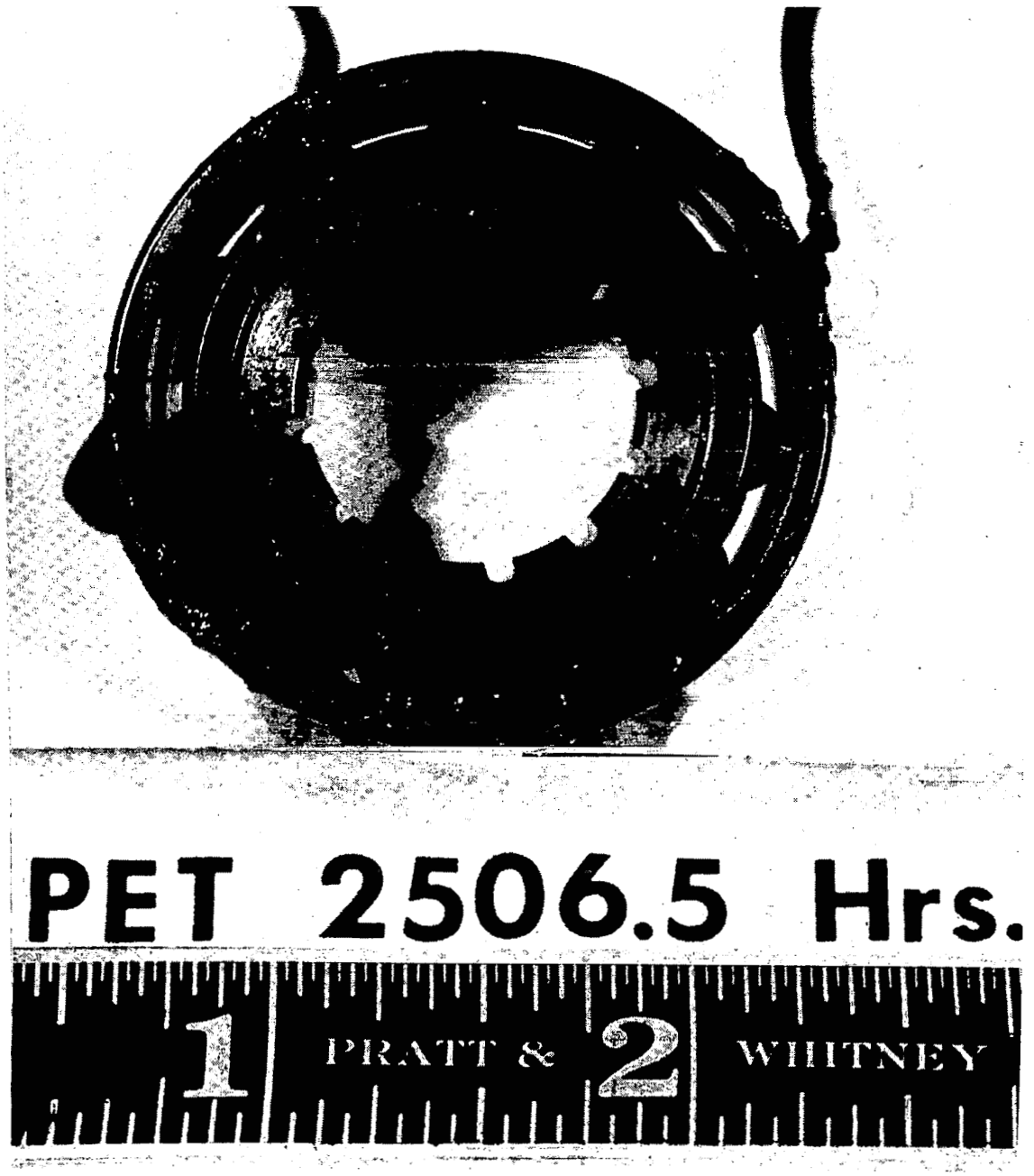

Figure 209 Turbine-Compressor Bearing before Cleaning and after 2500 Hours of Test_ CN-10329

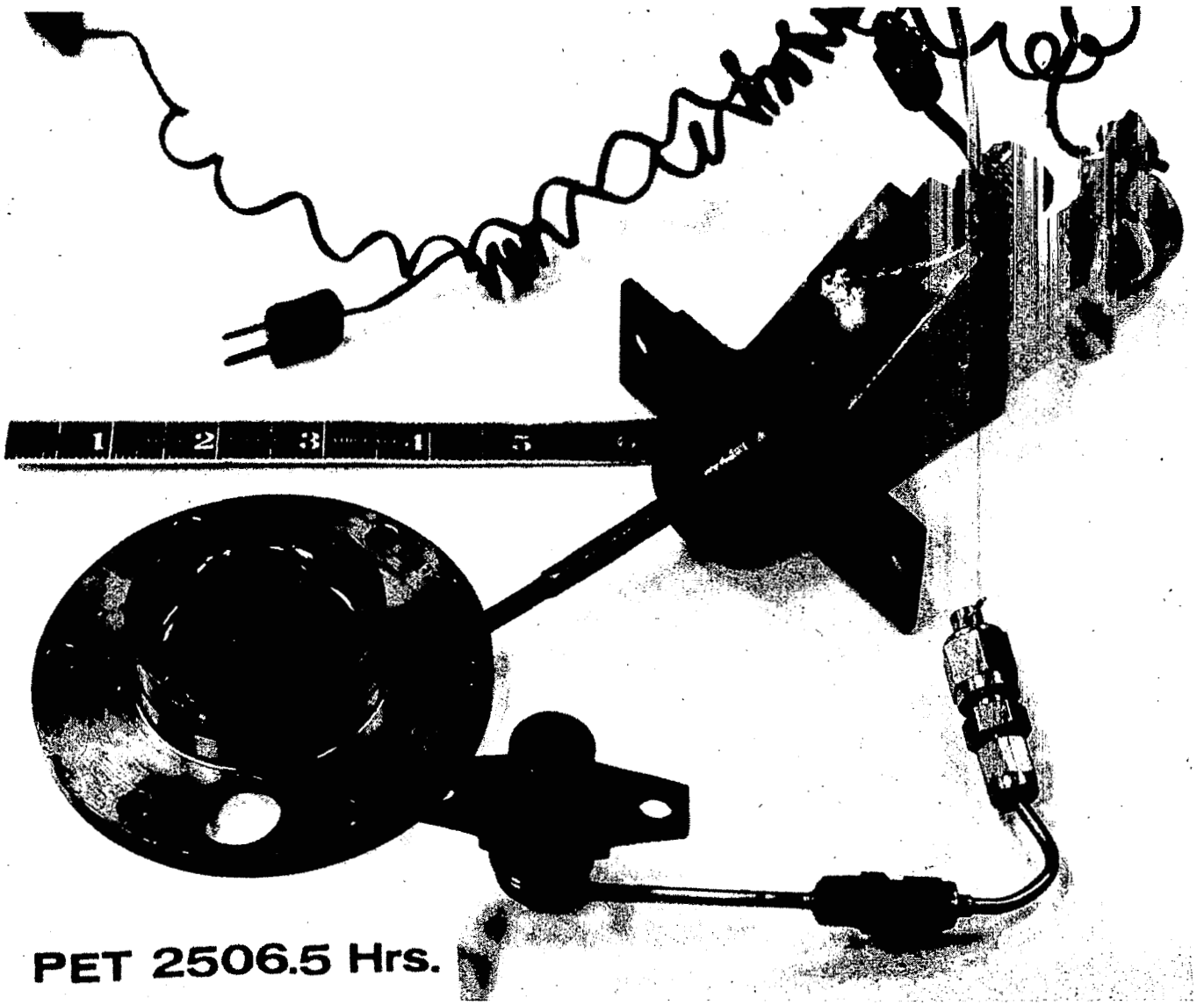

Figure 210 Oil and Gas Inlets for Turbine-Compressor Bearing after 2500 Hours of Test CN-10420

Figure 211 Turbine-Compressor Bearing Cavity after 2500 Hours of Test
CN-10414

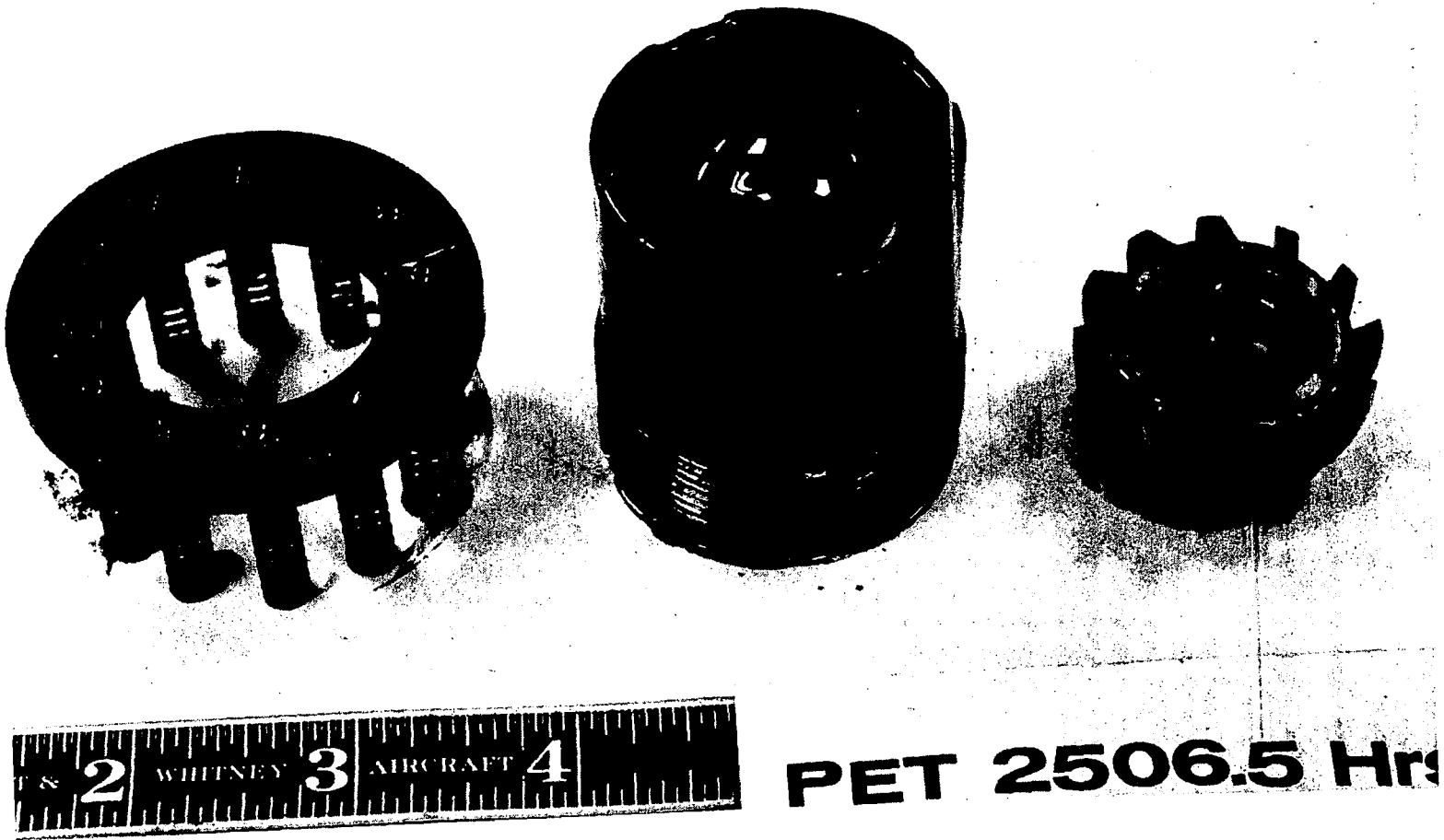

Figure 212 Locking Nut and Inlet Housing of Turbine-Compressor Bearing after 2500 Hours of Test
CN-10410

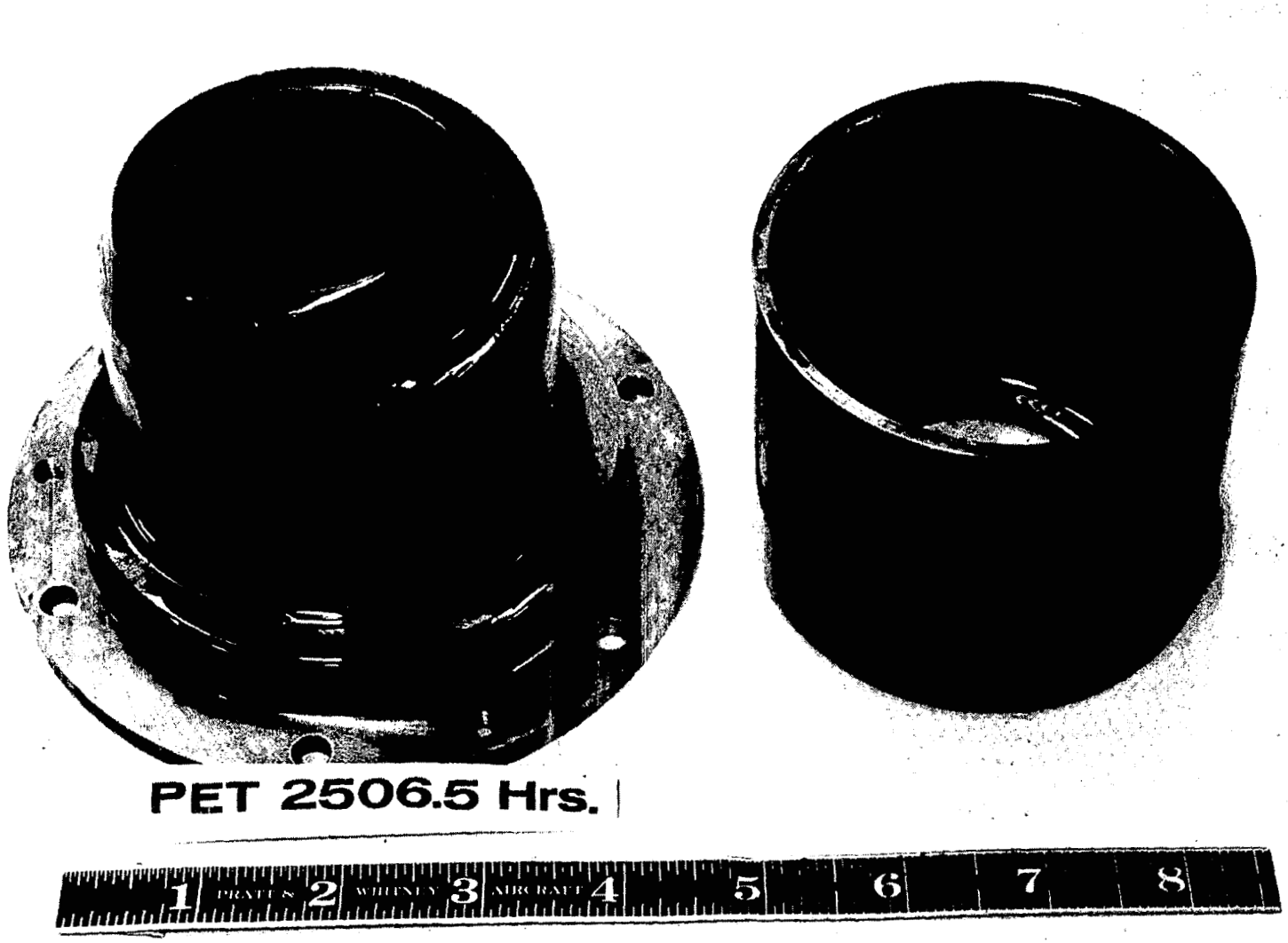

Figure 213 Oil-Gas Outlet Housing of Turbine-Compressor after 2500 Hours of Test CN-10433

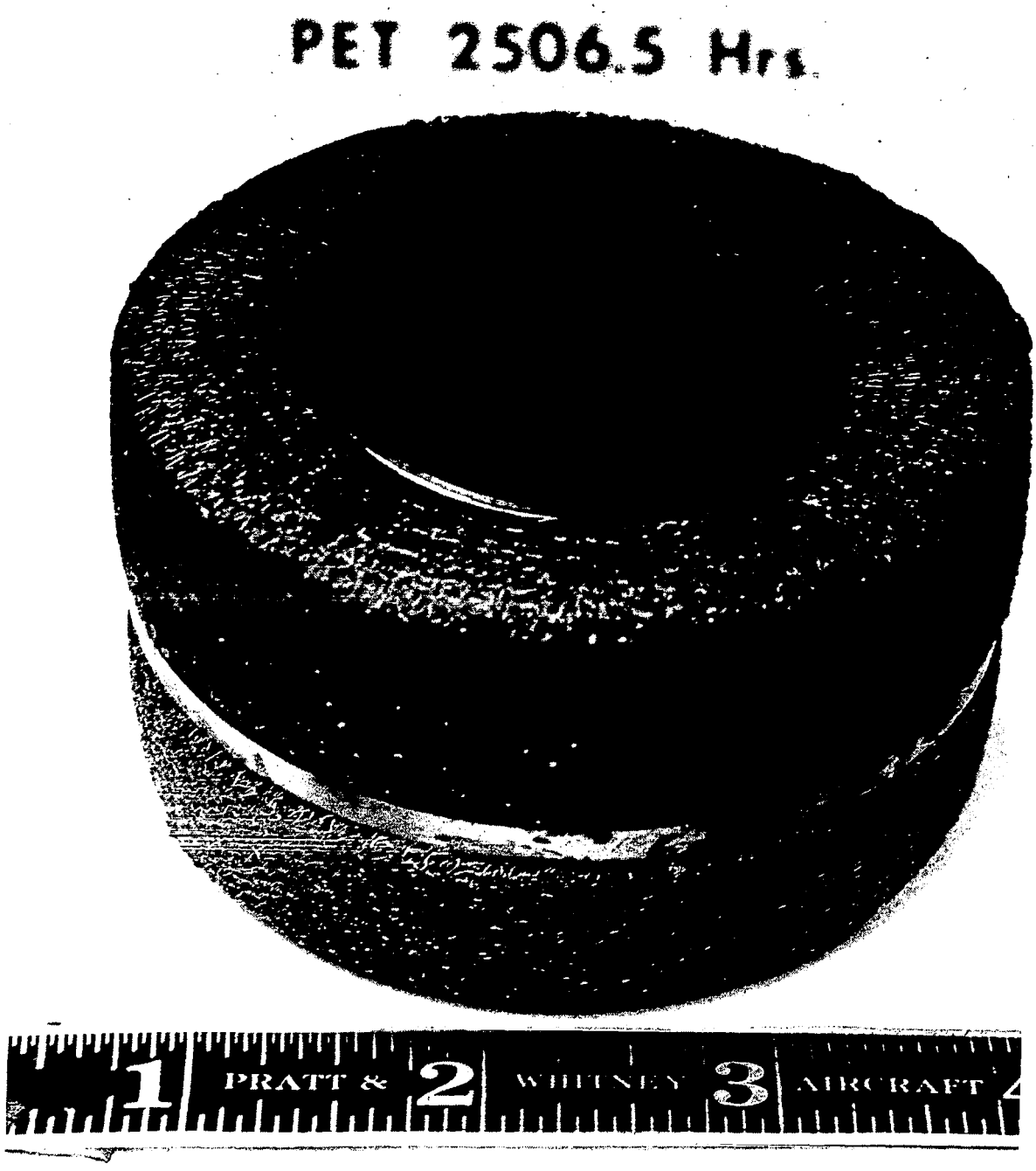

Figure 214 Middle and Outlet Sections of Separator Mesh after 2500 Hours of Test
CN-10332

Figure 215 Inlet Section of Separator Mesh after 2500 Hours of Test CN-10333

Figure 216 Separator Housing after 2500 Hours of Test CN-10424

would result in a total carbon wear of 0.014 inch. Similarly projecting the 500 to 2500-hour wear rate would result in a total carbon wear of 0.016 inch. A total carbon wear allowance of 0.035 inch was provided in the seal design.

Some wear was measured on the pilot endurance test sealplate. The maximum amount that occurred at one location was 0.0002 inch for the 2500 hours of test.

Critical measurements on the turbine-compressor bearing are given below:

	As Built	Post-Test
bore of inner ring, inch	0.78735	0.7873
	0.7873	0.7874
outside diameter of outer ring, inch	1.7323	1.7323
	1.73225	1.7325
diametral cage clearance, inch		0.006
	0.0065	0.0065
contact angle		
	16°37'	16°37'
radial play, inch		0.0011
	0.00105	0.00115

These results show no significant change as a result of the 2500-hour run.

Two views of the adsorber column at the completion of the test are shown in Figures 214 and 218. The oil concentration is in the inlet zone.

Figure 219 displays the performance of the pilot system adsorber column for the 2500-hour test. The ordinate of the graph is the amount of oil found in the monitor column attached to the main column discharge. The determination was made at 100-hour intervals and projected to 10,000 hours.

Extractions of the main adsorber column yielded the following quantities of lubricant for the 2500-hour run.

inlet gas wool section	59.7 grams
Linde 13X pellet section	0.0128 gram
outlet glass wool section	0.0305 gram

Figure 217 Right-Side View of Pilot Lubrication System Adsorber Column
CN-9945

Figure 218 Left-Side View of Pilot Lubrication System Adsorber Column
CN-9942

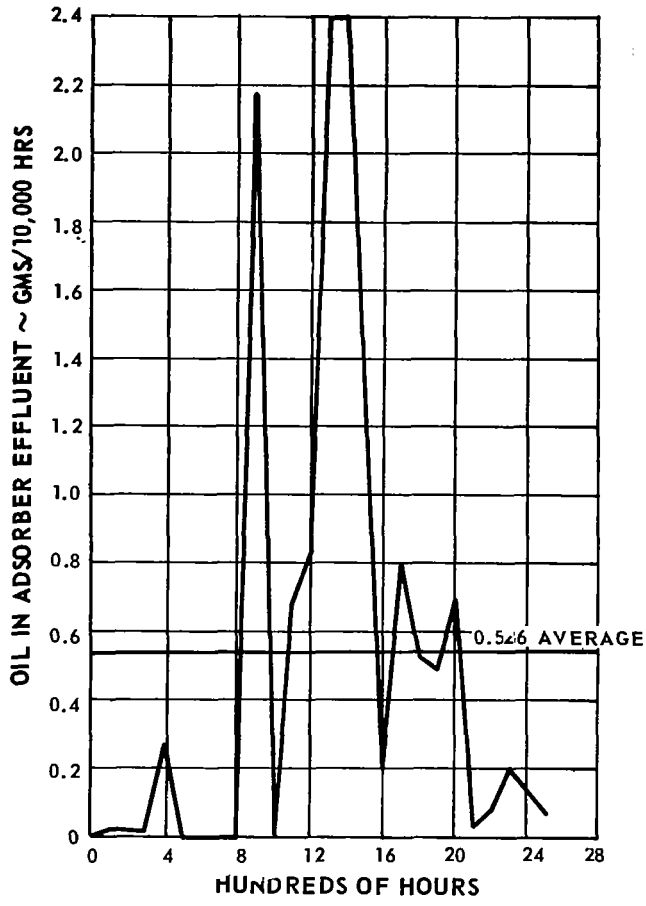

Figure 219 Adsorber Performance during Pilot System Test

These results indicate that the mechanical separator performed efficiently during the test, and that the outlet glass wool section had unused reserve capacity at the end of the test.

The post-test condition of the polyphenyl ether lubricant is summarized in Tables 15 and 16. Two conditions are apparent from an examination of these tables:

1) The oil viscosity changed a small amount, probably due to fluid-composition change resulting from the low boiler A, 3-ring ether, intermediate and 4-ring ether decreases.

2) The deposits removed from the system were composed of a high percentage of additive. Other tests have shown similar results.

Although these two changes did occur, no system performance degradation was observed. Both of these conditions can be reduced. The first by modifying the fluid distillation techniques, and the second by leaving out the additive which is not considered necessary for this application.

TABLE 15

Analysis of Lubricant for Pilot Endurance Test

	New Fluid Lot QE-1	Fluid Sample After Test
viscosity (cs)		
at 100°F	363	391
at 210°F	13.1	14.7
specific gravity, 25/25	1.203	1.1995
fluid composition (GLC)		
low boiler A	0.0640	0.0015
3-ring ether	0.0370	0.0076
intermediate	0.0005	0.0133
4-ring ether	0.6097	0.213

TABLE 16

Analysis of Deposits from Pilot Lubrication System

	Bearing Area Deposit	Separator End Deposit	Separator Housing ID Deposit
benzene solubles, %	84	33	13
additive concentration, % (550 ppm new, 128 ppm end of test)	40.1*	43*	55.3*
emission analysis, %			
aluminum	0.002 -0.8	-0	0.002 -0.8
calcium	<0.003	<0.003	<0.003
chromium	0.01 -0.05	0.002 -0.01	0.002 -0.01
cobalt	<0.001	<0.001	0.001
copper	0.002 -0.07	0.002 -0.07	0.002 -0.07
iron	0.01 -0.6	0.01 -0.6	0.01 -0.6
magnesium	0.03 -0.1	0.03 -0.1	0.03 -0.1
manganese	0.0006-0.001	0.0006-0.001	0.0006-0.001
nickel	0.003 -0.08	0.003 -0.08	0.003 -0.08
silicon	0.01 -0.15	0.01 -0.15	0.01 -0.15
tin	major	major	major

* Percent of benzene insolubles

The 2500-hour pilot system test demonstrated that the test hardware performed exceptionally well and is suitable for longer periods of operation. It confirmed many of the basic concepts used in the overall design, in particular the two-phase zero-gravity scavenge and circulation concept, and the separator-adsorber gas cleanup combination.

Gas and oil leakage characteristics on a powerplant system basis projected from the 2500-hour test results are shown in Figure 220. The powerplant contains two turbine-compressor bearing compartments and one turboalternator bearing compartment which constitute the gas and oil leakage paths between the power-conversion system and the lubrication system. The gas and oil leakage rates were measured on the 2500-hour seal test, the separator and adsorber performance was obtained from the 2500-hour pilot system test, and the sweep gas flow rates were obtained from the powerplant design. All of these parameters were extrapolated to a yearly basis from the 2500-hour results. Examination of Figure 220 shows that 0.0725 + 0.0003 or 0.0728 grams of oil would enter the power-conversion system in one year with the return leakage and buffer sweep gas. This amount of oil offers no significant contamination problem.

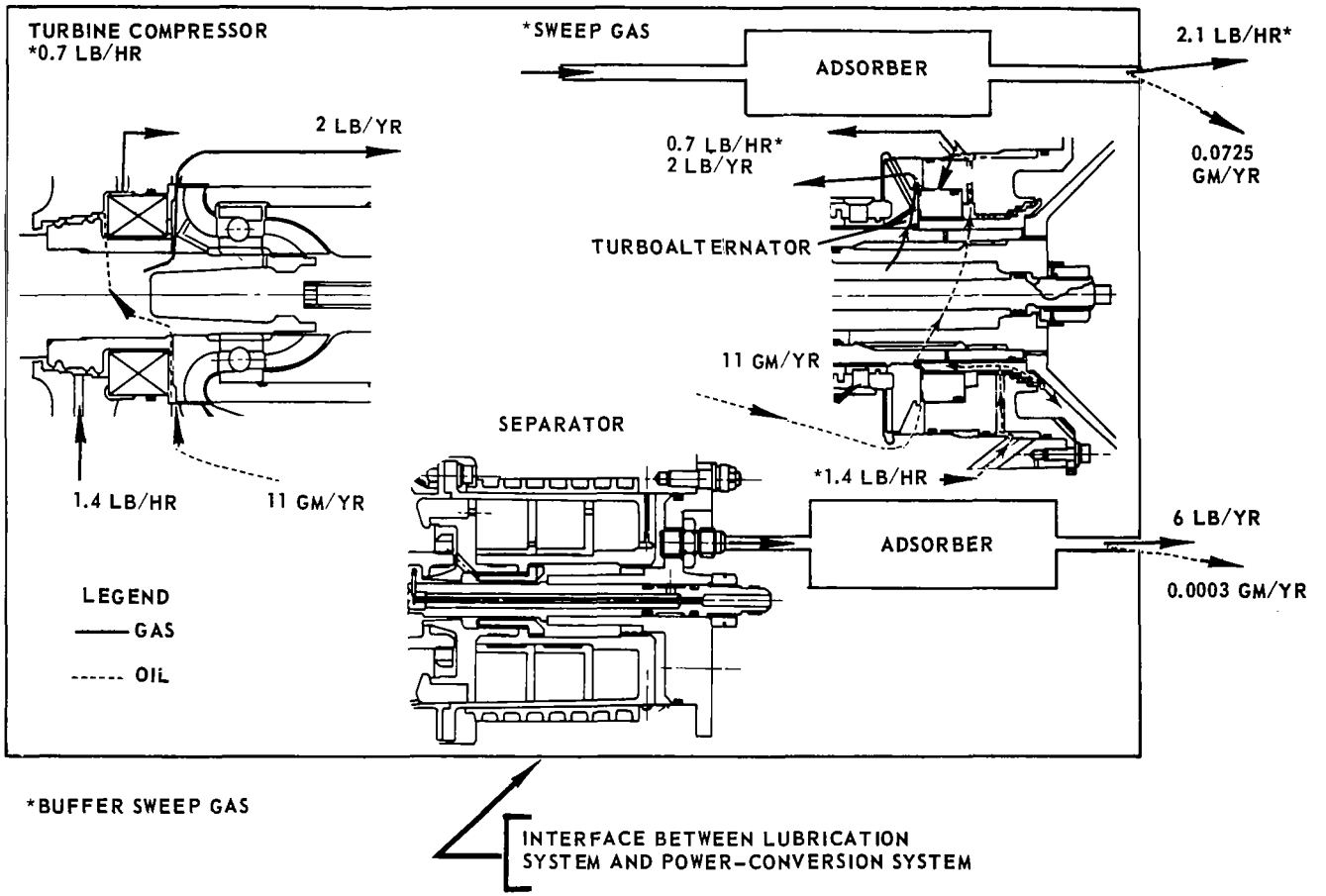

Figure 220 Brayton-Cycle Oil and Gas Leakage M-47264

X. RECOMMENDATIONS

The material presented in the preceding sections validates the basic design. Further, the test results obtained in every area of investigation indicate that only refinement-type optimizations are necessary as a part of a continuing development program. These optimizations would include further seal work to reduce power consumption without significantly increasing gas and oil leakage. Similarly, bearing work should be continued to simplify the gas and oil flow paths in the bearing compartment and to decrease power consumption. Minor design changes should be made in the separator to reduce the interaction between the gas and oil flows in the scoop-pump region. Although the long-time adsorber test results were excellent, still longer-term tests should be undertaken to establish the ultimate endurance life. A multiple bearing-compartment test should be made to investigate the interaction between compartments, mainly from the two-phase zero-gravity flow and scavenging viewpoints. Although realistic system performance projections were made from the component tests, a full-scale lubrication-system simulator test should be made. This effort would duplicate as nearly as possible all aspects of the complete lubrication system and would be operated for long periods of time to determine actual performance parameters such as rotor system dynamic behavior, system gas and oil leakage, adsorber effectiveness, and bearing and seal wear. A complete realistic development program must include a complete system test. In this effort all systems should be included and operated over a wide spectrum of conditions.

REFERENCES

1. Lockhart, R. W. and R. C. Martinelli, Proposed Correlation of Data for Isothermal Two-Phase Two-Component Flow in Pipes, Chemical Engineering Progress, January 1949, Vol. 45, No. 1,pages 39-48

2. Baker, Ovid, New Pipeline Techniques. Designing for the Simultaneous Flow of Oil and Gas, Oil and Gas Journal, July 26, 1954, pg 185-190, 192, 195

3. Griffith, P. and G. B. Wallis, Two-Phase Flow Phenomena II, Chemical Engineering Service, 1960, Vol. 12, No. 4, pp 233-242

4. Anderson, R. J. and T. W. F. Russell, Designing for Two-Phase Flow (3parts) Chemical Engineering; 12-6-65, p. 139; 12-20-65, p. 99; 1-3-66, p. 87

5. Quandt, Earl, Analysis of Gas-Liquid Flow Patterns, Preprint No. 47 Sixth National Heat Transfer Conference, AI Ch E - ASME, Boston, 1963 (Also printed as WAPD-T-1547)

6. Martinelli, R. C., L.M.K. Boelter, T.H.M. Taylor, E.G. Thomsen, and E.H. Morrin, Isothermal Pressure Drop for Two-Phase Two-Component Flow in a Horizontal Pipe, Transactions of ASME, February 1944, 139-151

7. McMillan, H.K., W.E. Fontaine, J.B. Chaddock, Pressure Drop in Isothermal Two-Phase Flow, Fluids Eng. Division, ASME, Annual Meeting, No. 29-Dec. 4, 1964, Paper 64-WA/FE-4

8. Ros, N.C.J., Simultaneous Flow of Gas and Liquid as Encountered in Well Tubine, Journal of Petroleum Technology, October 1961, pp. 1037-1049

9. Govier, G. W., B. A. Radford, J.S.C. Dunn, The Upward Vertical Flow of Air-Water Mixture, Canadian Journal of Chemical Engineering, August 1957, pp 58-70

10. Anderson, G.H. and B.G. Mantzouranis, Two-Phase Flow Phenomena I, Chemical Engineering Science, 1960, Vol. 12, pp 109-126

11. Calvert, S. and B. Williams, Upward Concurrent Annular Flow of Air and Water in Smooth Tubes, A.I. Ch. E. Journal, March 1955, pp 78-86

12. Nicklin, D. J., J.D. Wilkes, J.F. Davidson, Two-Phase Flow in Vertical Tubes, Trans. Instr. Chem. Engrs. Vol. 40, 1962 pp 60-68

13. Symposium on Two-Phase Flow, 7 Feb. 1962, Institution of Mechanical Engineers, Thermodynamics and Fluid Mechanics Group, Papers 4 and 11

14. Ambrose, T. W. Literature Survey of Flow Patterns Associated with Two-Phase Flow, HW-52927, General Electric, October 8, 1957

15. Vohr, J. H., Flow Patterns of Two-Phase Flow, A Survey of the Literature, TID-11514 Physics, Columbia University, December 15, 1960

16. Rohsenow, W. M., Developments in Heat Transfer, The M.I.T. Press, Press, 1964, Chapter 9, P. Griffith, pp 261-291

17. Montross, C. F., Entrainment Separation, Chemical Engineering, October 1953

18. Kannel, J., J. C. Bell and J. A. Walowit, Battelle Memorial Institue, Rept. ASD TDR 61-643, Part V, A Study of the Influence of Lubricants on High-Speed Rolling-Contact Bearing Performance

19. Adamczak, R. L., R. J. Benzing, and H. Schwenker, Advanced Lubricants and Lubrication Techniques, Ind. and Eng. Chem., Vol. 56, No. 1, 1964

20. Bisson, E. E., and W. J. Anderson, (eds), Advanced Bearing Technology, NASA SP-38

21. Blake, E. S., et al, Thermal Stability as a Function of Chemical Structure, Journal of Chem. and Engr. Data, Vol. 6, No. 1, 1961

22. Bolt and Carroll, Radiation Effects on Organic Materials, Academic Press

23. Gunderson and Hart (eds), Synthetic Lubricants, Reinhold Publishing Company

24. Larsen, R. G. and A. Bondi, Functional Selection of Synthetic Lubricants, Ind. and Eng. Chem., Vol. 42, No. 12, 1950

25. McTurk, W. E., et al, Synthetic Lubricants, WADC, AF Tech. Report 6663, 1951

26. Boeing Report, Document D-14766-8, 1953

27. Super-Refined Hydraulic Oils, Bulleting D237-E, Humble Oil and Refining Company

28. Groth, R. H., Polyphenyl Ethers, PWA memo, 12/17/63

29. Mahoney, C. L., et al, Engine Oil Developement, WADC TR-57-177, Part II

30. Mahoney, C. L., et al, Nuclear Radiation Resistant High Temperature Lubricants, WADC TR 59-173

31. Mohoney, C. L., et al, Polyphenyl Ethers as High-Temperature Radiation-Resistant Lubricants, Journal of Chem. and Engr. Data, Vol. 5, No. 2 1960

32. Rice, W. L. R., D. A. Kirk, and W. B. Cheney, Radiation-Resistant Fluids and Lubricants, Nucleonics, Vol. 18, No. 2, 1960

33. Schmidt-Collerus, and Bohner, Determination of the Relation Between Structure and Radiation Stability of Aryl Ether Fluids,WADD TR 60-282

34. Frost and Pearson, Kinetics and Mechanism, 2nd ed., John Wiley and Sons

35. Johns, I. B., E. A. McElhill, and S. O. Smith, Thermal Stability of Organic Compounds, I and EC Product Reasearch and Dev., Vol. 1, No. 1 1962

36. Fuchs, W., and A. G. Sandhoff, Theory of Coal Pyrolysis, Ind. and Eng. Chem,. Vol. 34, No. 5, 1942

37. Fieser and Fieser, Organic Chemistry, 3rd ed., Reinhold Publishing Company

38. Othmer, Encyclopedia of Chemical Technology

39. Weiss, Jr., et al, Radiolysis and Pyrolysis of Polyaromatic Compounds, I & EC Product Research and Dev., Vol. 3, No. 2, 1964

40. Davies, C. M., Aerosol Science, Academic Press, London and New York, 1966

41. Gill, S., Proceedings of Cambridge Philosophical Society, Vol 47, p. 96, 1951

42. Flugel, G., NACA tech. Memo. No. 982, July 1941

43. Schlicting, H., Boundary Langer Theory, McGraw - Hill Book Co., New York, p. 466, 1960

NASA-Langley, 1969 — 15 E-4649